Scuola Internazionale Superiore di Studi Avanzati - SISSA

Trieste, Italy

ROLE OF CELLULAR PRION PROTEIN IN CENTRAL NERVOUS SYSTEM MYELINATION

Thesis submitted for the degree of "Philosophiae Doctor"

CANDIDATE

Elisa Meneghetti

SUPERVISORS

Prof. Giuseppe Legname, Ph.D.

Dr.Federico Benetti, Ph.D.

Academic year 2014/2015

DECLARATION

The work described in this thesis has been carried out at Scuola Internazionale Superiore di Studi Avanzati (SISSA), Trieste, Italy, from November 2011 to October 2015.

During my Ph.D. course I contributed to two research articles:

- Gasperini, L., E. Meneghetti, B. Pastore, F. Benetti and G. Legname (2015). "Prion Protein and Copper Cooperatively Protect Neurons by Modulating NMDA Receptor Through S-nitrosylation." Antioxidants & Redox Signaling **22**(9): 772-784. Included in the “APPENDIX” section.

- Gasperini, L., Meneghetti, E., Legname, G. and Benetti, F. “The Absence of the Cellular Prion Protein Impairs Copper Metabolism and Copper-Dependent Ferroxidase Activity, Thus Affecting Iron Mobilization.” To be submitted.

INDEX

LIST OF ABBREVIATIONS

AD: Alzheimer's disease

AMPA: α-amino-3-hydroxy-5-methyl-4-isoxazolepropionate

ATP: adenosine triphosphate

Atp7a: ATPase 1

BACE1: β-secretase 1

BCA: bicinchoninic acid

BrdU: 5'-bromo-2'-deoxyuridine

BSA: bovine serum albumin

BSE: bovine spongiform encephalopathy

CaM: calmodulin

CaMKII: Ca^{2+}/calmodulin-dependent protein kinase II

CC: charged cluster

CD: central domain

CDP: chronic demyelinating polyneuropathy

CJD: Creutzfeldt-Jakob disease

CNS: central nervous system

CTR1: copper transporter 1

CWD: chronic wasting disease

CZ: cuprizone

DAPI: 4',6-diamidino-2-phenylindole

DIV: days *in vitro*

Dpl: Doppel

EAE: experimental allergic encephalitis

ER: endoplasmic reticulum

fALS: familial amyotrophic lateral sclerosis

fALS: familial amyotrophic lateral sclerosis

FFI: fatal familial insomnia

Gapdh: glyceraldehyde 3-phosphate dehydrogenase

GluN(1, 2A-D, 3A-B): NMDAR subunit (1, 2A-D, 3A-B)

GPI: glycosylphosphatidylinositol

GSS: Gerstmann, Sträussler and Scheinker syndrome

HC: hydrophobic core

HRP: horseradish peroxidase

KO: knock-out

L-MAG: long myelin-associated glycoprotein

L-MPZ: large-myelin protein zero

LPC: lysolecithin, lysophosphatidylcholine

MAG: myelin-associated glycoprotein

MBP: myelin basic protein

MOG: myelin oligodendrocyte glycoprotein

MPZ: myelin protein zero

MS: multiple sclerosis

MTS: 3-(4,5-dimethylthiazol-2-yl)-5-(3-carboxymethoxyphenyl)-2-(4-sulfophenyl)-2H-tetrazolium

NeuN: neuronal nuclei

NG2: neural/glial antigen 2

NMDA: N-methyl-D-aspartate

NMDAR: N-methyl-D-aspartate receptor

nNOS: neuronal nitric oxide synthase

NO: nitric oxide

NRG: neuregulin

NTC: non-template control

OHC: organotypic hippocampal cultures

OPC: oligodendrocyte precursor cells

OR: octapeptide repeat

P: postnatal day

PBS: phosphate-buffered saline

PD: Parkinson's disease

PES: phenazine ethosulfate

PFA: paraformaldehyde

PKA: protein kinase A

PKC: protein kinase C

PLP: proteolipid protein

PNS: periferal nervous system

PrP^{C}: cellular prion protein

PrP^{Sc}: scrapie prion protein

ROS: reactive oxygen species

RT: room temperature

S-MAG: short myelin-associated glycoprotein

SN: sciatic nerve

SNO: S-nitrosylation

SOD: superoxide dismutase

Sox10: (sex determining region Y)-box 10

TBST: Tris-Buffered Saline plus Tween 20

TGN: *trans*-Golgi network

TSE: transmissible spongiform encephalopathies

Tubb3: βIII-tubulin

WB: Western blot

WT: wild-type

ABSTRACT

The cellular form of the prion protein (PrP^C) has been widely investigated since its alternative folded isoform is the causative agent of prion disorders. PrP^C is highly expressed in the nervous system, where it is involved in many physiological processes such as the maintenance of peripheral nervous system (PNS) myelination. A similar role in the central nervous system (CNS) is still controversial, since PrP^C absence affects proliferation and maturation of oligodendrocyte precursor cells without affecting myelination. On the other hand, PrP^C is involved in metal homeostasis and modulates oxidative stress, two processes influencing myelin formation and maintenance. In light of these considerations, we took advantage of wild-type (WT, *Prnp*$^{+/+}$) and PrP^C knock-out (KO, *Prnp*$^{0/0}$) mice to investigate PrP^C role in CNS myelination. Myelin composition was examined in mouse brains at different developmental stages, from early postnatal days to aging, through cholesterol content measurement and through myelin protein and gene expression evaluation. Furthermore, peripheral myelin status was also investigated in the sciatic nerve (SN) in order to have a comparative analysis between the CNS and PNS myelin. Finally, an *ex vivo* model based on organotypic hippocampal cultures (OHC) was established to better investigate PrP^C role in CNS myelin.

Concerning the PNS, most of our results are consistent with the PNS myelin degeneration observed in literature. Accordingly, results show a 50% decrease in SN cholesterol content, a strong reduction of myelin genes transcription and an altered expression level of some myelin proteins during *Prnp*$^{0/0}$ mouse aging. Moreover, some changes in the early postnatal period were also detected. Focusing on the CNS, a small reduction in cholesterol content was observed at postnatal day 1 and in aging brains of *Prnp*$^{0/0}$ mice, suggesting an alteration in CNS myelin status. Differently from PNS, CNS myelin proteins are slightly upregulated in *Prnp*$^{0/0}$ brains during the whole life. In particular, in *Prnp*$^{0/0}$ brains a higher amount of myelin proteolipid protein, myelin basic protein, myelin oligodendrocyte glycoprotein and the glycosylated form of myelin associated glycoprotein was detected. This myelin protein upregulation correlates with a higher gene expression in *Prnp*$^{0/0}$ mouse brains. To better investigate PrP^C role in CNS myelination, an *ex vivo* model based on OHC was established. In accordance with *in vivo* experiments, after 28 days *in vitro* the amount of myelin proteins and myelin gene expression is higher in *Prnp*$^{0/0}$ than in *Prnp*$^{+/+}$ OHC. Furthermore, the copper chelator cuprizone (CZ) was administered to OHC to investigate its effect in PrP^C presence or absence. CZ treatment did not trigger the expected myelin degeneration.

Differently it induced an increase in myelin protein percentage particularly in $Prnp^{+/+}$ OHC, while the effect on $Prnp^{0/0}$ OHC was milder. Thus, different response of $Prnp^{+/+}$ and $Prnp^{0/0}$ OHC to CZ exposure denotes a distinct CNS susceptibility to this kind of stimulus in the presence or absence of PrP^{C}.

Altogether, these results support the hypothesis that PrP^{C} is involved in CNS myelination, although in a different manner compared to the PNS. In fact, the differences observed in CNS lipid composition, protein expression and gene transcription are less pronounced compared to PNS, but are extended for the whole lifetime. Since electron microscopy on CNS myelinated regions did not show gross morphological changes between $Prnp^{+/+}$ and $Prnp^{0/0}$ mice, it is possible that myelin protein overexpression could be the result of a compensatory mechanism to prevent functional abnormalities. Furthermore, since PrP^{C} plays neuroprotective roles, it is possible that it could protect myelin under stress conditions.

INTRODUCTION

Neurodegenerative diseases are incurable and debilitating conditions leading to progressive loss of nerve cells and affecting movement (ataxia) or mental functions (dementia). With the global population aging, an ever-increasing number of people will be afflicted with neurodegenerative diseases. The World Health Organization predicted that neurodegenerative diseases will overtake cancer and become the second leading cause of death after cardiovascular disease by 2040. Because of their enormous social and economic implications, neurodegenerative diseases are considered a public health priority. Despite many efforts, the molecular mechanisms responsible for the pathophysiology of these disorders are still elusive. Several neurodegenerative diseases share common features, such as aberrant protein folding and aggregation, alterations in protein degradation pathways, mitochondrial dysfunction, compromised axonal transport processes and induction of cell death mechanisms (Jellinger 2010). Among them, oxidative or metabolic stress has an important role in the pathogenesis of neurodegenerative diseases (Bush 2000, Singh, Singh et al. 2010). Altered metal-protein interactions were proposed to be the causative mechanism for certain disorders like Alzheimer's disease (AD), familial amyotrophic lateral sclerosis (fALS) Creutzfeldt-Jakob disease (CJD) (Bush 2000) (Table 1). These aberrant metal-protein interactions likely generate microanatomical stress, thus damaging the cell site where this event occurs.

Cu/Fe-mediated degenerative diseases*.

Specific protein	Adverse metal	Specific tissue	Specific disease
Aβ	Cu, Fe, possible loss of Zn	Neocortex	AD
PrP^c	Cu	Neocortex	CJD
SOD1	Cu, loss of Zn	Motor neuron	FALS
α-Crystallin	Cu, Fe	Lens	Cataracts

Table 1. List of the neurodegenerative diseases that share the same molecular pathogenic mechanism, where the abnormal metal ion interaction with a protein target is the common neurochemical denominator (Bush 2000).

PRION DISEASES

Among neurodegenerative diseases, prion disorders are biologically and pathologically interesting since they manifest as sporadic, genetic and infective diseases (Prusiner 2001). Prion diseases, also called

transmissible spongiform encephalopathies (TSE), are a group of rare, progressive and fatal neurodegenerative disorders affecting both humans and animals. TSE include bovine spongiform encephalopathy (BSE) in cattle, scrapie in ovine, chronic wasting disease (CWD) in deer, moose and elk, and Kuru, Creutzfeldt-Jakob disease (CJD), fatal familial insomnia (FFI) and Gerstmann, Sträussler and Scheinker syndrome (GSS) in humans (Table 2) (Aguzzi, Heikenwalder et al. 2004).

Spectrum of prion diseases of humans and animals

Prion disease	Natural host species	Etiology
sCJD	Humans	Unknown (somatic *PRNP* mutation?)
Familial Creutzfeldt-Jakob disease (fCJD)	Humans	Familial (germ line *PRNP* mutation)
Iatrogenic Creutzfeldt-Jakob disease (iCJD)	Humans	Surgical procedures (infection)
vCJD	Humans	Ingestion of BSE-contaminated food; transfusion medicine (infection)
Kuru	Humans	Ingestion, ritualistic cannibalism (infection)
Fatal Familial Insomnia (FFI)	Humans	Familial (germ line *PRNP* mutation)
Gerstmann-Sträussler-Scheinker Syndrome	Humans	Familial (germ line *PRNP* mutation)
Scrapie	Sheep, goats	Infection, natural; mode of transmission unclear
Chronic Wasting Disease (CWD)	Deer, Elk	Infection; mode of transmission unclear
BSE	Cattle	Ingestion of BSE-contaminated feed (infection)
Transmissible mink encephalopathy	Mink	Ingestion (infection); Origin unclear
Feline spongiform encephalopathy	Cats	Ingestion of BSE-contaminated feed (infection)
Spongiform encephalopathy of zoo animals	Zoologic bovids, primates	Ingestion of BSE-contaminated feed (infection)

Table 2. List of prion diseases of human and animals (Aguzzi, Heikenwalder et al. 2004)

Although TSE affect primarily the nervous system, the clinical features can vary according to the different TSE forms. These differences regard the etiology, the incidence of the disease, the brain region affected by replicating prion deposits, the manifested clinical symptoms and the disease time-course (Prusiner 1992, Prusiner and DeArmond 1994). Despite these differences, all TSE share some pathological traits such as scrapie prion protein (PrP^{Sc}) deposition, synapse and dendritic spine loss, spongiform vacuolation, brain inflammation with diffused astrocytic gliosis and neuronal death (Figure 1) (Soto and Satani 2011).

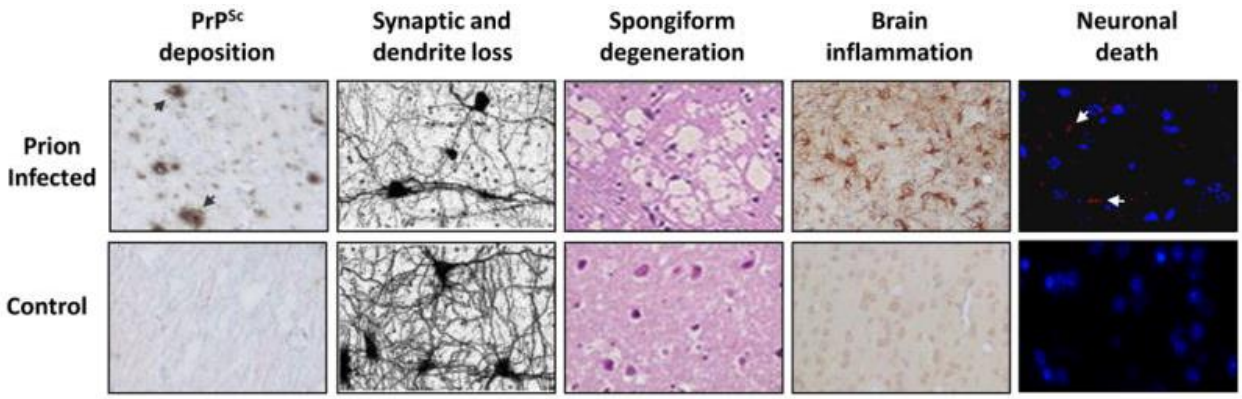

Figure 1. Multiple neurodegenerative pathways are implicated in TSEs (Soto and Satani 2011). Abnormalities in the brain of infected individuals include the accumulation of PrP^{Sc} deposits, synaptic damage and dendrite loss, spongiform degeneration, brain inflammation and neuronal death.

PRION PARADIGM

The term "prion" was introduced by Stanley B. Prusiner in 1982 and stands for "proteinaceous infectious particle", to underline the exclusively proteinaceous property of this infective agent causing prion diseases (Prusiner 1982). While the scrapie agent was resistant to nucleic acid inactivation (Alper, Cramp et al. 1967), the infectivity of inoculated brain extracts was reduced after proteolytic treatments. Therefore, prion transmission and propagation occur without requiring nucleic acids. The so-called "protein-only hypothesis" challenged the central dogma of biology: even proteins and not only DNA and RNA could store and propagate biological information. The identification of the protein responsible for TSE revealed that this protein was encoded by an endogenous cellular gene (*Prnp* in mouse chromosome 2 or *PRNP* in human chromosome 20), whose translational product was called cellular prion protein (PrP^{C}) (Oesch, Westaway et al. 1985). Prions are the product of posttranslational conformational changes converting PrP^{C} into the disease-associated infectious form PrP^{Sc}. The two isoforms, PrP^{C} and PrP^{Sc}, show different biochemical properties. While PrP^{C} is mainly α-helical folded (40% α-helix, 3% β-sheet), PrP^{Sc} is highly enriched in β-sheet structures (30% α-helix, 45% β-sheet) (Caughey, Dong et al. 1991, Gasset, Baldwin et al. 1993). Genetic forms of TSE depend on mutations occurring in PrP encoding gene, which alter protein folding and stability promoting its conversion to the scrapie form. In infective forms of TSE, a preformed PrP^{Sc}-aggregate directly triggers the conversion of endogenous PrP^{C}. In sporadic disease, PrP^{C} tertiary structure is likely perturbed by environmental conditions favoring PrP^{Sc} formation. However, the biochemical and environmental events responsible

for sporadic TSE are still unclear (Prusiner 1991, Prusiner 1994, Caughey 2003, Budka, Head et al. 2011, Benetti and Legname 2015).

PRION NEUROTOXICITY

The mechanism underlying prions damage on CNS remains unknown. Given its accumulation in the brain and its ability to transmit fatal neurodegenerative conditions, PrP^{Sc} was generally assumed to be the neurotoxic specie, proposing a gain-of-toxic-function mechanism. However, PrP^{Sc} itself is not sufficient for the disease progression, but the presence of the cellular prion protein is also required. Accordingly, PrP KO mice inoculated with PrP^{Sc} did not show any neurotoxic effect (Bueler, Aguzzi et al. 1993). Besides, the accumulation of PrP^{Sc} within PrP^{C}-expressing tissue grafted into the brains of PrP^{C}-null mice does not damage the neighboring PrP^{C}-null tissue (Brandner, Isenmann et al. 1996). It was observed that PrP^{C} removal from cell membrane inhibited neurotoxicity (Chesebro, Trifilo et al. 2005). Interestingly, *in vivo* PrP^{C} ablation during the neurotoxic phase of prion replication reversed prion pathology leading to a hypothetical switch off of PrP^{C} expression as a cure of prion diseases (Mallucci, Dickinson et al. 2003). Recently, it has been suggested that prion replication is dissociated from neurotoxicity (Halliday, Radford et al. 2014). This hypothesis is supported by the discovery of subclinical states of prion infection, characterized by experimental animals that were asymptomatic carriers of infectivity, but never develop clinical disease throughout their lifespan (Hill and Collinge 2003). On the other hand, the lack of striking phenotypes and the absence of neurodegeneration and spongiform changes in the brain of PrP KO mice argue the loss-of-function hypothesis (Bueler, Fischer et al. 1992, Mallucci, Ratte et al. 2002). Therefore, it is still under debate whether prion toxicity is due to a gain-of-function of oligomeric species, to a loss-of-function of PrP^{C} or to a combination of the two. To answer these questions, PrP^{C} physiological function needs to be understood.

THE CELLULAR PRION PROTEIN

The cellular prion protein, PrP^C, is an endogenously encoded protein with a molecular weight of 35-36 kDa. As described in Figure 2, it is a sialoglycoprotein attached to the outer leaflet of the plasma membrane via a C-terminal GPI anchor (Stahl, Borchelt et al. 1990, Caughey and Baron 2006).

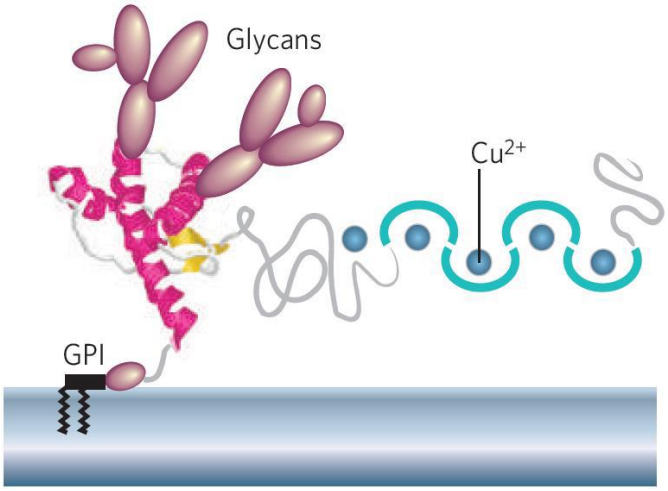

Figure 2. Mature form of the cellular prion protein, PrP^C. PrP^C is a GPI-anchored membrane protein, with a flexible, random coil N-terminus and a globular C-terminal domain. The N-terminal domain of PrP^C contains octapeptide repeats (in light blue), which can bind divalent cations such as copper ions. The C-terminal domain of PrP^C contains three alpha-helices (in pink) and an antiparallel β-pleated sheet formed by two β-strands (in yellow). PrP^C can be found non-, mono-, or diglycosylated forms (Caughey and Baron 2006).

PrP^C precursor protein contains two signal peptides: the N-terminal targets the protein to the endoplasmic reticulum (ER), while the C-terminal sequence is essential for the addition of the GPI moiety (Figure 3). Following the precursor protein proteolytic processing in the ER and Golgi, most of mammalian PrP^C is exported to the cell surface as a mature protein of 208-209 amino acids (Stahl, Borchelt et al. 1987). Mature PrP^C contains two domains: the unfolded N-terminal domain and the folded C-terminal domain. The N-terminal domain is unstructured and contains charateristic octapeptide repeats (OR) and two positively charged clusters, CC_1 and CC_2. The C-terminal domain presents three α-helices and two β-sheets. It contains a disulfide bridge linking Cys178 and Cys213 (mouse numbering) and two glycosylation sites. PrP^C can be expressed as un-, mono- or di-glycosylated form, depending on glycosylation level at Asn180 and Asn196 residues (Haraguchi, Fisher et al. 1989). N- and the C-terminal

domains are linked by a hydrophobic amino acidic stretch, also named hydrophobic core (HC) (Zahn, Liu et al. 2000) (Figure 3).

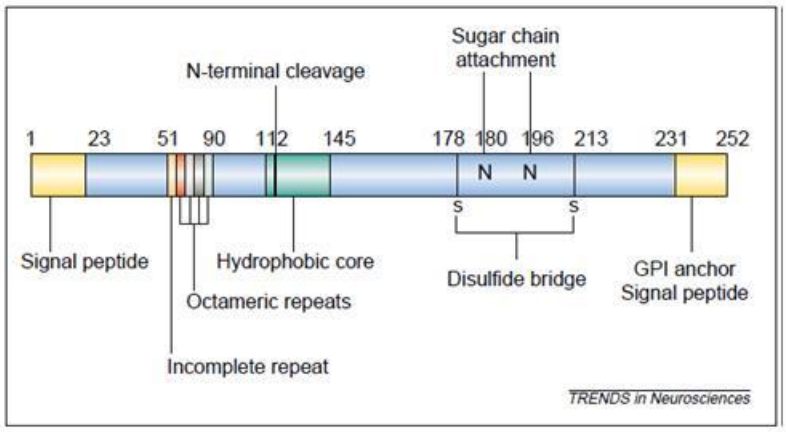

Figure 3. Mouse prion protein scheme. This protein is anchored to the cell membrane by a glycosylphosphatidylinositol (GPI) anchor. The signal peptide for entry into the endoplasmic reticulum and the GPI signal peptide are cleaved before the protein reaches the cell surface. Glycosylation can occur on one, two or none of the Asn residues indicated. A hydrophobic region envelops a cleavage point (N-terminal cleavage) where the protein is cleaved during normal metabolic breakdown. A disulfide bridge links two regions of the protein that form separate α-helices in the three dimensional structure of the protein. The complete octameric repeats can bind up to four copper atoms, most mammals also have an incomplete repeat located upstream of this (Brown 2001).

The OR region confers to PrP^C one of its most salient feature that is the ability to bind divalent cations as copper, zinc, nickel, iron and manganese (Stockel, Safar et al. 1998, Jackson, Murray et al. 2001, Singh, Das et al. 2010, Arena, La Mendola et al. 2012). The OR region is composed of four sequential repeats (PHGGGWGQ) between residues 59-90. Residues 51-58 constitute a nonarepeat lacking the histidine residue (PQGGGTWGQ) (Hornshaw, McDermott et al. 1995, Brown, Qin et al. 1997). The importance of copper binding for PrP^C physiological function is supported by the high OR homology among different species (Vassallo and Herms 2003). Depending on copper concentration, PrP^C binds copper differently, passing from a multi-His binding mode at low copper levels to a single-His, amide nitrogen bond at high copper levels (Chattopadhyay, Walter et al. 2005, Liu, Jiang et al. 2011). The OR region cooperatively binds up to four copper ions with affinity of 5-8 μM (Whittal, Ball et al. 2000, Kramer, Kratzin et al. 2001). These values are compatible with the physiological copper concentration released in the synaptic cleft during synaptic vesicle release (15 μM) and during neuronal depolarization (100-300 μM) (Hartter and Barnea 1988). Moreover, histidines at positions 96 and 111 create a fifth high affinity copper binding site (10^{-14} M), the so called “non-OR copper-binding site” (Jackson, Murray et al. 2001, Jones,

Abdelraheim et al. 2004). Both the low and high occupancy copper binding mode support the reduction of Cu(II) to Cu(I), thus conferring PrP^C the important function in protecting neurons from oxidative stress (Liu, Jiang et al. 2011). Despite many studies trying to understand the physiological relevance of PrP^C-Cu binding, a defined consensus is still elusive.

PrP^C EXPRESSION AND SUBCELLULAR LOCALIZATION

PrP^C is mostly expressed in the developing and in the mature nervous system, indicating a special relevance of this protein for neurons. However, PrP^C is also present in many non-neuronal tissues, such as blood lymphocytes, gastro-epithelial cells, heart, kidney and muscles (Horiuchi, Yamazaki et al. 1995, Fournier, Escaig-Haye et al. 1998). According to this expression pattern, PrP^C function is not limited to the nervous tissue. In the CNS, PrP^C expression has been described in postmitotic neurons and glial cells (Ford, Burton et al. 2002, Steele, Emsley et al. 2006), including oligodendrocyte precursor cells (OPC), mature oligodendrocytes and myelin (Radovanovic, Braun et al. 2005, Bribián, Fontana et al. 2012). PrP^C expression starts from early embryonic stages and is developmentally regulated (Mobley, Neve et al. 1988, Lazarini, Deslys et al. 1991, Manson, West et al. 1992, Sales, Hassig et al. 2002, Benvegnu, Poggiolini et al. 2010). In the mouse brain, PrP^C expression increases from the initial postnatal weeks till the end the synaptogenesis and it reaches a plateau during adulthood. The protein levels may decrease with aging. The distribution and the expression level vary among distinct brain regions, cell types and neurochemical phenotypes (Linden, Martins et al. 2008, Benvegnu, Poggiolini et al. 2010). A detailed analysis of PrP^C expression pattern revealed that the olfactory bulb and the hippocampus, which are both characterized by neuronal renewal also during adulthood, show the highest PrP^C expression levels (Sales, Hassig et al. 2002). Starting from embryonic day 18.5 (E18.5) to adult life, the hippocampus is the region with the earliest and highest expression of PrP^C. In particular, it is highly expressed in the stratum lacunosum moleculare, which contains a large number of synapses and afferent fibers (Figure 4) (Benvegnu, Poggiolini et al. 2010). High PrP^C expression was also detected in specific white matter fiber tracts as the hippocampal fimbria and its anatomical continuation, the fornix, the stria terminalis and the fasciculus retroflexus.

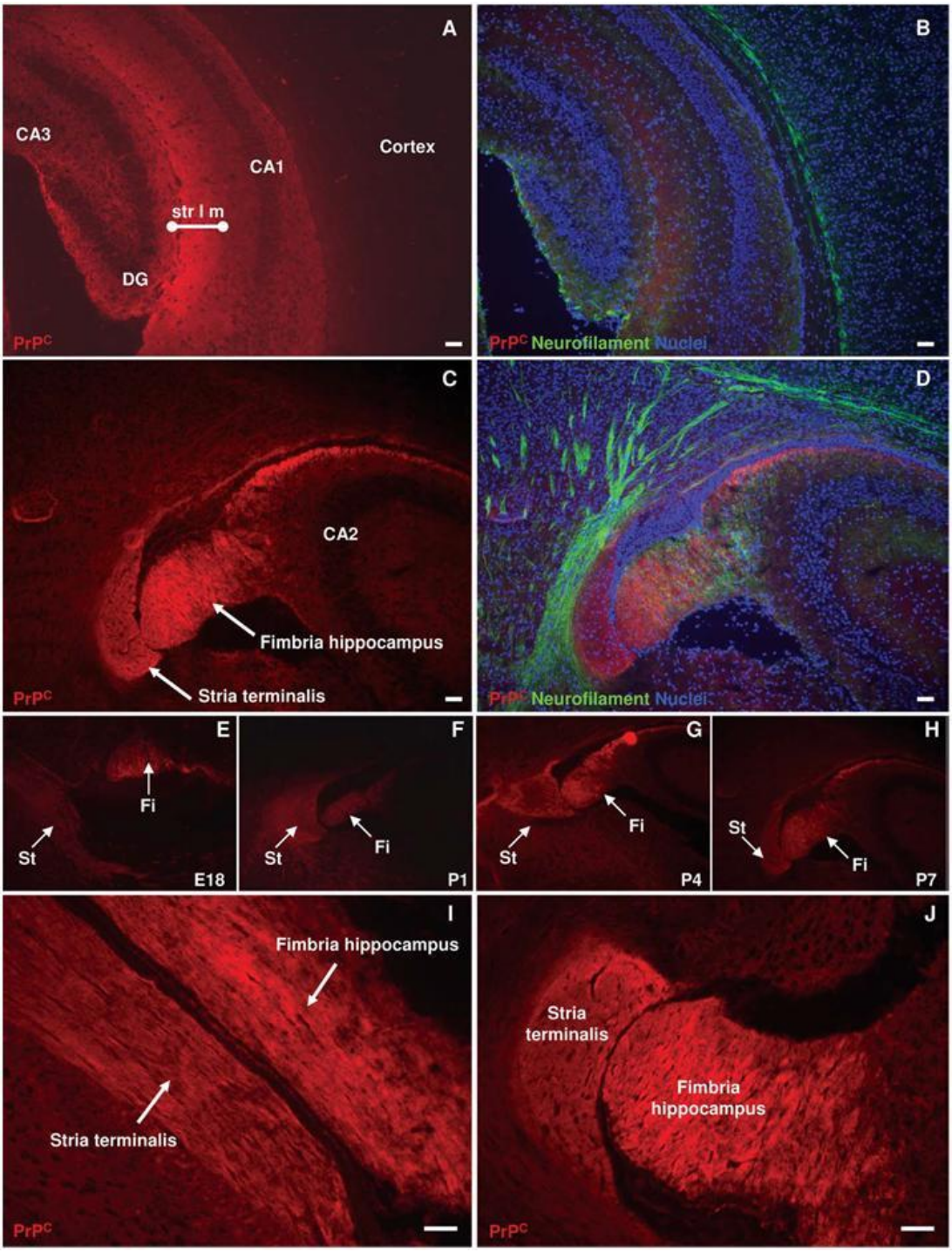

Figure 4. PrP^C expression in the hippocampus during development. A,B: At P7 PrP^C (in red; A) is detected throughout the hippocampus, and in particular at high levels in the stratum lacunosum-molecolare (str l m), a synapse-dense region. No signal for PrPC is yet detected in the cortex. A merged image is shown in B (PrP^C, in red; neurofilament, in green; nuclei signals in blue). C–H: PrP^C is specifically and highly expressed by the fimbria of the hippocampus and the stria terminalis at P7 (C,D). The fimbria of the hippocampus (Fi) and the stria terminalis (St) express high level of PrP^C also at embryonic stages (E18.5), and progressively increase the level of expression during postnatal development: P1 (F), P4 (G), and P7 (H). I,J: Higher magnification

of longitudinal (I) and coronal (J) section of the fimbria of the hippocampus and the stria terminalis, highlighting the net boundaries of PrP^C -expression between other brain regions and these structures. Scale bars ¼ 50 lm (Benvegnu, Poggiolini et al. 2010).

Concerning PrP^C subcellular localization, it is widely accepted that its expression is concentrated at synapses, both presynaptically and postsynaptically (Fournier, Escaig-Haye et al. 1998, Sales, Rodolfo et al. 1998, Herms, Tings et al. 1999, Haeberle, Ribaut-Barassin et al. 2000, Moya, Sales et al. 2000, Linden, Martins et al. 2008). Many lines of evidence suggest that different glycoforms of the prion protein determine its transport along the axon to the synaptic compartment (Rodolfo, Hassig et al. 1999). Diglycosylated PrP^C is associated to detergent insoluble rafts (Naslavsky, Stein et al. 1997). These are specialized plasma membrane areas enriched in cholesterol, sphingolipids and proteins, functioning in membrane trafficking and signalling (Simons and Ikonen 1997). Both the presynaptic and postsynaptic sites are enriched in lipid rafts, which are likely to organize and maintain a precise localization of synaptic proteins, as for example ionotropic and metabotropic glutamate receptors (Sebastiao, Colino-Oliveira et al. 2013).

PrP KNOCK-OUT AND TRANSGENIC MICE

To shed light on the physiological function of PrP^C, an astonishing number of KO and transgenic mouse lines for the *Prnp* gene has been generated. The first generation of KO mice with disruptive modifications restricted to the open reading frame, namely $Prnp^{0/0}$ (Zurich I) and $Prnp^{-/-}$ (Edimburgh) showed normal development as well as no pathological signs during their lifespan (Bueler, Fischer et al. 1992, Manson, Clarke et al. 1994). Subsequently, another three KO lines were created, namely Ngsk$Prnp^{-/-}$ (Nagasaki), Rcm0 and $Prnp^{-/-}$(Zurich II), which revealed ataxia, loss of Purkinje cells and cerebellar degeneration (Sakaguchi, Katamine et al. 1996, Moore, Lee et al. 1999, Rossi, Cozzio et al. 2001). This discrepancy between the first and second generation lines of PrP KO mice was explained with the discovery of a novel gene, *Prnd*, encoding a protein called Doppel (Dpl), which is not usually expressed in the brain. Prnd gene, located 16 kb downstream to *Prnp*, resulted to be overexpressed in Ngsk, Rcm0 and ZurichII, but not in ZurichI and Edimburgh (Moore, Lee et al. 1999). The accidental deletion of a splice acceptor site to the third exon of *Prnp* led to the formation of chimeric *Prnp-Prnd* transcripts, with Prnd under the transcriptional control of *Prnp* promoter. Thus, Dpl ectopic expression in the brain caused cerebellar granule ataxia and degeneration that could be rescued by *Prnp* gene re-

introduction (Nishida, Tremblay et al. 1999). This latter result showed PrP^C acting as an antagonist of Dpl, counteracting its neurotoxic effects *in vivo* and *in vitro* (Didonna, Sussman et al. 2012).

Additionally, murine models carrying PrP^C deletion mutants have been created aiming at identifying functionally relevant domains within the protein (Figure 5).

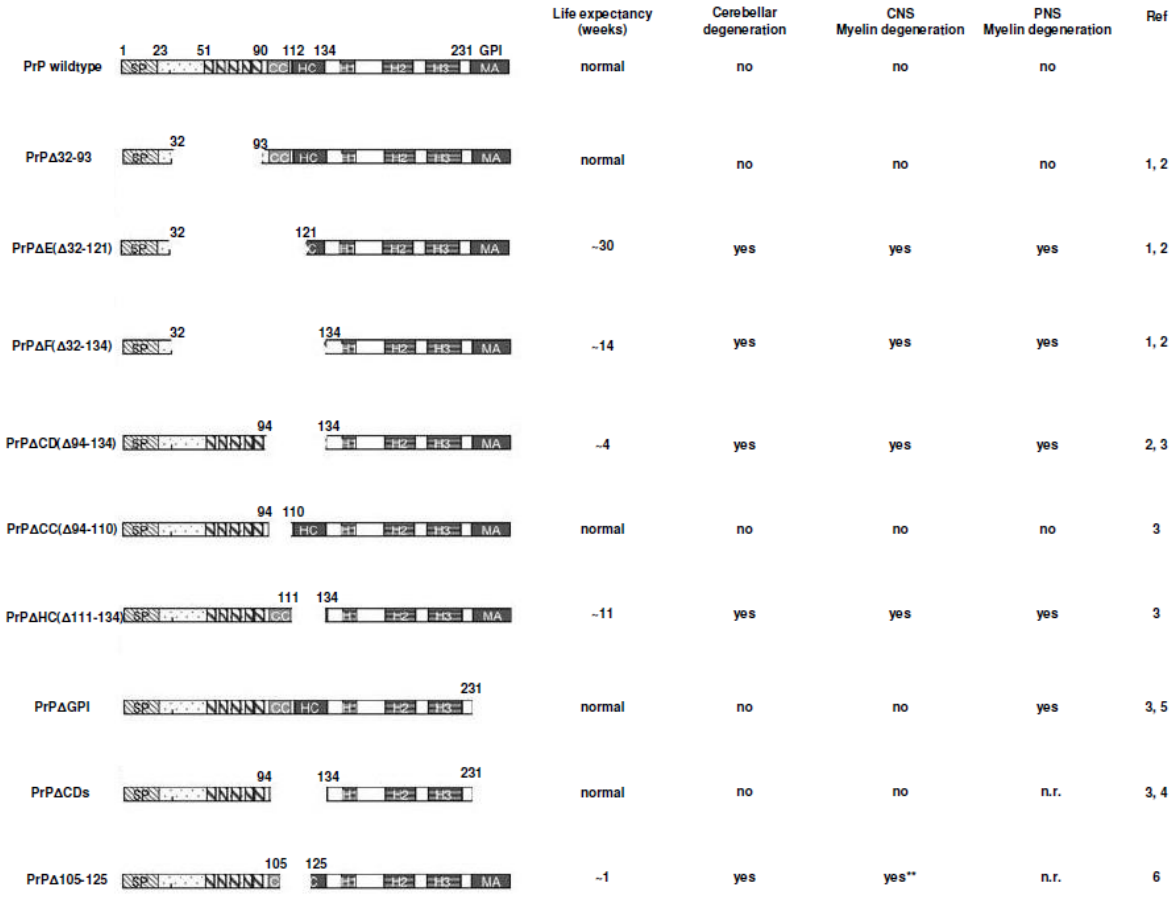

Figure 5. Murine PrP^C protein and transgenic mutant PrP. Schematic drawing of full-length murine PrP^C, with sequence for the signal peptide (SP) and for the GPI anchor (MA). The left column denotes the individual mutants described in this thesis. The right columns indicate life expectancy of the animals, presence of cerebellar neurodegeneration, CNS demyelination, PNS demyelination, and references. All the mutants are to be intended as expressed in a $Prnp^{0/0}$ genetic background. n.r. = not reported; ** = CNS demyelination of PrPΔ105-125 mice was revealed in a $Prnp^{+/0}$ genetic background, due to the neonatal lethality of the mice expressing the transgene in a $Prnp^{0/0}$ genetic background. 1 = (Shmerling, Hegyi et al. 1998); 2 = (Bremer, Baumann et al. 2010); 3 = (Baumann, Tolnay et al. 2007); 4 = (Baumann, Pahnke et al. 2009); 5 = (Chesebro, Trifilo et al. 2005); 6 = (Li, Christensen et al. 2007). Modified from (Baumann, Tolnay et al. 2007).

Among these transgenic mutants, *Prnp*$^{0/0}$ mice expressing PrP^{C} lacking amino acid residues 32-121 or 32-134 (PrPΔ32-121 and PrPΔ32-134) suffer from ataxia and cerebellar granule cell loss, as well as widespread gliosis and demyelination in the brain stem (Shmerling, Hegyi et al. 1998). Only gliosis and demyelination could be rescued by oligodendrocyte-specific PrP^{C} expression, while neuron-specific PrP^{C} expression could partially rescue cerebellar granule cell degeneration, but not demyelination (Radovanovic, Braun et al. 2005). Thus, PrP^{C} expression is required in both neurons and glia to completely revert the degenerative phenotype. Additional observations showed that *Prnp*$^{0/0}$ mice expressing PrP^{C} lacking amino acid residues 32-93 (PrPΔ32-93) within the OR region did not present pathological phenotypes. This fact hints at the central domain (CD, residues 94-134) as a key functional domain. The CD domain includes the positively charged CC2 cluster (residues 95-110) and the HC core (residues 112-134), (Figure 3, Figure 5). Therefore, other *Prnp* transgenic models have been created to analyze the different contributions of these two domains to the pathological phenotype. Mice entirely lacking the CD (PrPΔ94-134) showed a drastic neuropathological phenotype with vacuolar degeneration, astrogliosis, extensive central and peripheral nervous system demyelination and death within 20-30 days (Baumann, Tolnay et al. 2007). Despite the similar myelin damage, this model did not present the same cerebellar degeneration observed in PrPΔ32-121 and PrPΔ32-134 expressing mice. Furthermore, mice lacking residues 105-125 (referred to as ΔCR) develop an even more dramatic phenotype, with severe neurodegeneration becoming lethal within the first post-natal week (Krebs, Wiebelitz et al. 2007). Each of these phenotypes can be rescued co-expressing the WT PrP^{C} in a dose-dependent manner according to the mutant PrP expression level and the severity of the pathology elicited (Baumann, Tolnay et al. 2007, Krebs, Wiebelitz et al. 2007). Moreover, other transgenic mice have been used to shed light on PrP^{C} involvement in myelin homeostasis. Bremer et al. showed that *Prnp*$^{0/0}$ mice display a late-onset chronic demyelinating polyneuropathy (CDP) in their PNS, (Bremer, Baumann et al. 2010). Interestingly, mice expressing mutant PrP lacking the CC2 domain (PrPΔ94-110) did not develop CDP, while on the contrary mice expressing mutant PrP lacking the hydrophobic core (PrPΔHC) showed a reduced life expectancy (survival 80 ± 3.5 days), white-matter vacuolation and astrogliosis in cerebellum, brain stem and corpus callosum, and showed CDP (Bremer, Baumann et al. 2010). Thus, the hydrophobic core (HC), but not the charge cluster (CC2), of the central domain of PrP^{C} is essential for myelin maintenance. However, the demyelinating phenotype in *Prnp*$^{0/0}$ mice is mild and less severe than the demyelination-affecting mice expressing PrP mutants lacking the central domain. Indeed, while *Prnp*$^{0/0}$ mice show only PNS demyelination during aging, *Prnp*$^{0/0}$ mice expressing the mutant with deletion of the central domain of PrP, *i.e.* PrPΔHC, PrPΔ32-121, PrPΔ32-134, show a more dramatic and lethal

demyelinating phenotype, with both central and peripheral demyelination, clinical manifestations ranging from partial hind limb paresis to ataxia, full tetraplegia, and reduced life expectancy (Shmerling, Hegyi et al. 1998, Baumann, Tolnay et al. 2007, Bremer, Baumann et al. 2010). Trying to explain the great phenotypical difference between demyelination in *Prnp*$^{0/0}$ and PrPΔCD-expressing mice, Baumann and colleagues proposed a model in which PrP^{C} and its deletion mutants can compete for a common ligand, maybe a receptor that regulates signal transduction. According to this scenario, a residual, basal activity of this receptor in *Prnp*$^{0/0}$ mice may exist, whereas disruption of the CD may sequester the receptor in a dominant-negative state (Figure 6) (Steele, Lindquist et al. 2007).

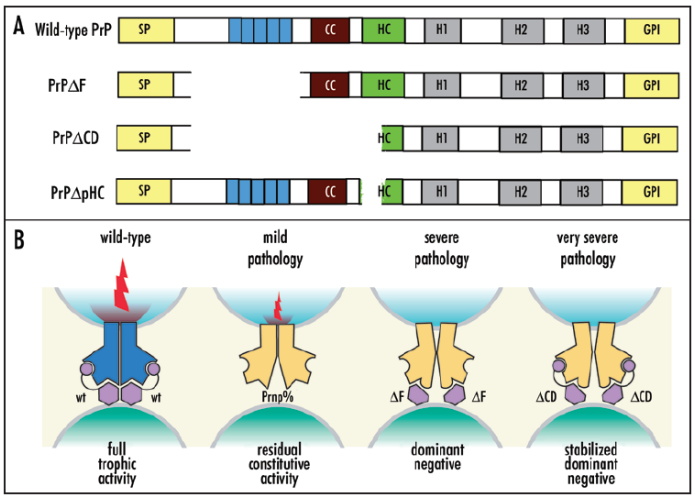

Figure 6. A model showing the effects of PrP^{C} deletion mutants. (A) Schematic diagram of WT PrP^{C} and its several deletion mutants. SP, signal peptide; octarepeats are indicated in blue; CC, charged cluster; HC, hydrophobic core; H1, H2, H3 Helix 1, 2 and 3, respectively; GPI, GPI-anchor addition sequence **(B)**. PrP (purple) consists of a globular C-terminal domain (hexagon) and a N-terminal flexible tail (arch) encompassing the octapeptide repeats (circle). The model rests on the following assumptions: (1) PrP activates a hitherto unidentified receptor (PrP_R) which transmits myelin maintenance signal (flashes); (2) in the absence of PrP, PrP_R exerts some residual activity, either constitutively or by recruiting a surrogate ligand; (3) the activity of PrP and its mutants requires homo- or heterodimerization, and induces dimerization of PrP_R; and (4) PrP dimers containing PrPΔCD or PrPΔCD trap PrP_R in an inactive dominant-negative state (from (Steele, Lindquist et al. 2007)).

Finally, experiments on mice lacking the GPI anchor (PrPΔGPI and PrPΔCDs) revealed that the proper expression and membrane anchoring of PrP^{C} is necessary for both beneficial and deleterious effects elicited by PrP^{C} and its variants, including the neurodegenerative effect of PrP^{Sc}. Despite the generation of all these KO and transgenic mice for PrP^{C}, a general consensus on PrP^{C} physiological function and mechanism of action is still missing.

PHYSIOLOGICAL FUNCTION OF PrP^C

The high *Prnp* sequence conservation between the mammalian species suggests that PrP^C may retain some important physiological functions during evolution (Colby and Prusiner 2011). Even though *PrnP*$^{0/0}$ mice have normal lifespans without gross disturbancies under standard laboratory conditions, upon a deeper analysis many subtle phenotypic changes have been reported. PrP^C has been implicated in oxidative stress potection, stress response, circadian rhythm, hippocampal neuronal function, spatial learning, synapse formation and functionality, brain copper and cuproenzyme level regulation, neurite outgrowth, maintenance of myelinated axons, phagocytosis and inflammatory response, haematopoietic-stem-cell renewal and neural-stem-cell differentiation (Caughey and Baron 2006, Aguzzi, Baumann et al. 2008). Figure 6 and Table 3 summarize some of the cellular processes in which PrP^C is involved.

Hereafter, some of the proposed PrP^C functions will be described in detail, in accordance with the topic and the aim of this thesis.

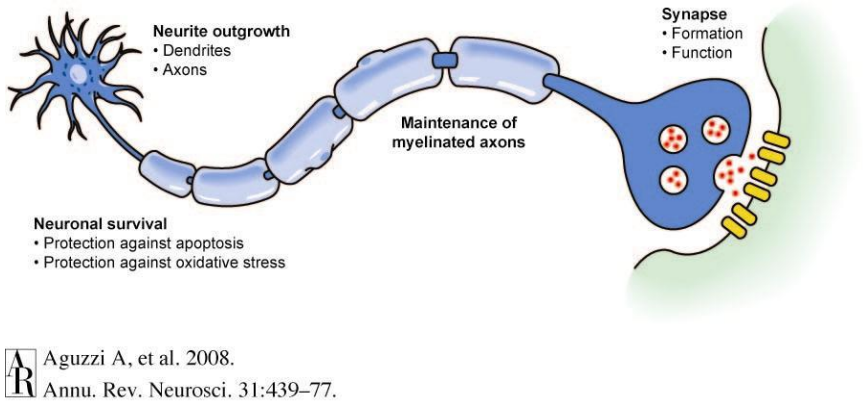

Figure 5. Physiological processes involving PrP^C. Several processes in the nervous system have been influenced by PrP^C. Neurite outgrowth, including growth of axons and dendrites, was observed to be reduced in neurons lacking PrP^C. PrP^C has often been reported to promote neuronal survival, in particular following apoptotic or oxidative stress. Cerebellar granule cell apoptosis was observed in mice expressing toxic N-terminal deletion mutants of PrP. In addition, the latter transgenic mice show an impaired maintenance of myelinated axons in the white matter. Another site of PrP^C action might be the synapse, which is often affected in the first stage of prion diseases and whose formation was found to be reduced in neuronal cultures devoid of PrP^C. Furthermore, electrophysiological studies indicate a role of PrP^C in synapse function, especially in neurotransmitter release (Aguzzi, Baumann et al. 2008).

Table 1 | The cellular distribution and activities of PrP^C in cell types in which known or putative functions have been described

Cell type	Process	Function	Mechanisms, ligands and pathways
Neuron	Neuritogenesis	Adhesion, signalling	Recruits NCAM into rafts to allow it to activate Fyn kinase[35], which mediates intracellular signalling pathways
			STI-1 binding induces activation of mitogen-activated protein kinase[36]
			Binds LRP/LR and HSPG by means of separate sites[60]
			Binds laminin[74]
	Synaptogenesis, polarization	Signalling	PrP^C acts as a growth factor, activating multiple pathways[38]
	Survival, trophic effects	Anti-apoptotic	Interacts with BAX[31], STI1 (ref. 36) and NCAM[75]
		Pro-apoptotic	Binds to anti-apoptotic Bcl-2 (for a review, see ref. 31)
			Crosslinks with anti-PrP antibody[76]
			Increases levels of p53 (reviewed in ref. 31)
	Copper binding	Copper endocytosis	Induces PrP^C to aggregate, exit from rafts and undergo clathrin-dependent endocytosis[77]
		Copper homeostasis	Maintains appropriate copper levels at the presynaptic membrane and during conditions of oxidative stress (reviewed in ref. 34)
		SOD activity*	Copper-bound PrP^C has SOD activity (reviewed in ref. 34)
	Redox homeostasis	Signalling	Induces NADPH-oxidase dependent ROS through Fyn activation[78]
Neural stem cells	Neurogenesis	Unknown	Increases cell proliferation in neurogenic regions[46]
	Differentiation	Unknown	PrP^C levels positively influence differentiation[46]
Haematopoietic stem cells	Long-term renewal	Anti-apoptotic? Homing?	Possible mechanisms: transduce cell survival signals; cell-adhesion activity targets cells to appropriate environment; or function as co-receptors for hormones affecting HSC activity[45]
T cells	Activation	Signalling?	PrP^C upregulation upon mitogen-induced activation[79]
	Development	Antioxidant	Copper binding in thymus[80]
Leukocytes	Differentiation	Unknown	PrP^C expression by lymphocyte/monocyte lineage[81]
	Phagocytosis	Unknown	PrP^C modulates phagocytosis[44]
	Inflammatory response	Homing	PrP^C alters leukocyte recruitment to site of inflammation[44]

*Some argue that PrP does not exhibit SOD activity.

Table 3. The cellular distribution and activities of PrP^C in cell types in which known or putative functions have been described (Caughey and Baron 2006).

PrP^C ROLE IN METAL HOMEOSTASIS

As already mentioned, one of the most salient features of PrP^C relies on its ability to bind divalent cations (in particular copper with the highest affinity, zinc, nickel, iron and manganese to a lesser extent) and to participate in their homeostasis.

Biometals are essential for a wide range of functions in living organism, such as enzyme active site formation, electrochemical gradient formation, DNA replication, oxygen transport and oxidative/nitrosative stress regulation. Metal homeostasis is tightly regulated by highly interconnected and interdependent cellular pathways involving ion-specific transporters and metal-binding proteins. Hence, the impairment of an essential metal homeostasis may affect the metabolism of other species. Because of their chemistry, the distribution of physiological transition metals needs to be finely regulated to avoid dangerous effects, such as oxidative/nitrosative stress generation and abnormal

metal-protein interaction (Bush 2000, Valko, Morris et al. 2005, Bolognin, Messori et al. 2009, Rivera-Mancia, Perez-Neri et al. 2010).

It has been largely demonstrated that the brain requires high metal ion concentration because of its elevated oxidative metabolic rate (Bush 2000). Therefore, the brain must efficiently regulate metal amount, distribution and buffering system for its proper functioning. Metal ion deficiency and accumulation can both lead to neurological diseases (Lovell 2009). Importantly, the relative impermeability of the blood-brain barrier to fluctuating levels of plasma metal ions together with a proper energy production for the functioning of metal regulatory transport systems generally prevent detrimental effects of metal dysregulation in the CNS (Bush 2000). Many reports show the link between altered biometal homeostasis, especially copper, zinc, iron and manganese, and neurodegenerative pathologies, such as ALS, AD, Parkinson's disease (PD) and prion diseases. Metals dysmetabolism can lead to protein aggregation, altering enzymatic activity, or catalyzing protein oxidation followed by protein damage and denaturation (Bush 2000). Despite many efforts have been done to disclose the role of metal homeostasis in neurodegeneration, it is not clear whether metal impairment could be an initiating/aggravating factor or a consequence of the neurodegenerative progression (Bolognin, Messori et al. 2009). Noteworthy, the aging is the dominant risk factor associated with neurodegeneration and it is characterized by an alteration of brain metal content and their topographical distribution (Tarohda, Yamamoto et al. 2004). Moreover, different neurodegenerative disorders are triggered by mutations in metal ion metabolism proteins. Two examples are Menkes' and Wilson's diseases that are caused by loss-of-function mutations in two copper transporters, affecting the proper distribution of this redox-active metal ion (Dening 1991, Oder, Grimm et al. 1991, Vulpe, Levinson et al. 1993, Madsen and Gitlin 2007).

Besides its role in neurodegeneration, metal homeostasis has been implicated also in myelin formation and maintenance. In particular, copper and iron dysmetabolism may affect proper myelination (Morelli, Ravera et al. 2012, Aspli, Flaten et al. 2015). It has been observed that copper deficiency induced by a low copper diet in rats is associated with a substantial reduction in myelin content, suggesting that copper is essential for myelin formation and growth during critical periods in development (Zimmerman, Matthieu et al. 1976). Moreover, demyelination has been proven to occur in Menkes' disease patients and in mice exposed to the copper chelator cuprizone (CZ) (Matsushima and Morell 2001, Liu, Chen et al. 2005, Skjørringe, Møller et al. 2012). Oligodendrocytes contain a huge amount of iron (Connor and Fine 1987). Since these cells are responsible for CNS myelin production, alterations in their functioning

are associated with hypomyelination (Beard and Connor 2003). Iron is directly involved in myelin production as a co-factor for cholesterol and lipid biosynthesis, and indirectly because of its requirement for oxidative metabolism (which occurs in oligodendrocytes at a higher rate than other brain cells) (Connor and Menzies 1996). A lack of iron bioavailability is associated with decreased amount and altered composition of myelin, together with oligodendrocyte maturation impairment. Given this strict connection between iron and myelination rate, a relationship between iron and multiple sclerosis (MS) was also hypothesized (Abo-Krysha and Rashed 2008).

Considering the importance of metal-mediated molecular mechanisms, PrP^{C} could be implied in some of these processes due to its ability to interact with biometals. In normal conditions, PrP^{C} mediates copper and iron uptake (Brown 2003, Singh, Kong et al. 2009). PrP^{Sc} has a higher affinity for nickel, decreasing the binding of zinc and manganese (Jackson, Murray et al. 2001). Considering the strict interconnection among all metal metabolic pathways, it is likely that copper and iron uptake is impaired in prion diseases due to this shift in metal binding affinity of PrP^{Sc}.

Since PrP^{C} is implicated in the regulation of two important metals for myelination, its role in copper and iron regulation is described.

As mentioned, PrP^{C}-Cu interaction is well-known. Studies on neuroblastoma cells suggested that PrP^{C} contributes to copper uptake since it binds extracellular copper ions and delivers them to the endocytic compartment, increasing antioxidant enzymes activity (Pauly and Harris 1998, Brown and Harris 2003, Rachidi, Vilette et al. 2003). The OR region plays a role in the reduction of Cu(II) to Cu(I) before transporting the metal across the endosomal membrane to the cytosol (Miura, Sasaki et al. 2005). PrP^{C} may act as a copper uptake and delivery protein, although published results on copper content in the brain of WT, PrP^{C}-null, PrP^{C} overexpressing and scrapie infected mice are discordant (Singh, Das et al. 2010). While some results showed no differences in copper content upon PrP^{C} ablation (Waggoner, Drisaldi et al. 2000, Giese, Buchholz et al. 2005), others highlighted a reduced copper amount in the CNS of PrP^{C}-null mice (Brown, Qin et al. 1997, Brown, Schmidt et al. 1998, Kralovicova, Fontaine et al. 2009, Singh, Kong et al. 2009). It has been proposed that PrP^{C} acts as a buffer of Cu^{2+} ions released into synaptic cleft, protecting synapses from copper-dependent Fenton redox reactions (Vassallo and Herms 2003). In the presynaptic bouton, PrP^{C} has a role in the redistribution of released copper ions, contributing to synaptosomal copper concentration maintenance. This likely occurs by transferring copper to membrane transporters such as copper transporter 1 (CTR1), having higher affinity than PrP^{C}. A similar mechanism may occur in the postsynaptic bouton where PrP^{C} is also expressed (Moya, Sales et

al. 2000) and copper ions are released from the *trans*-Golgi network (TGN) upon activation of glutamate ionotropic receptors (Schlief, Craig et al. 2005, Schlief, West et al. 2006). According to this hypothesis, copper content in *Prnp*$^{0/0}$ mice may be unchanged since PrP^{C} absence affects copper distribution without changing its overall content (Vassallo and Herms 2003).

Conversely from PrP^{C}-Cu interaction, no direct PrP^{C}-Fe binding has been yet observed (Singh, Das et al. 2010). By using both *in vitro* models expressing PrP^{C} mutants and *Prnp*$^{0/0}$ mice, it has been shown that the prion protein has a fundamental role in iron metabolism (Singh, Kong et al. 2009, Singh, Mohan et al. 2009). PrP^{C}-null cells have a lower iron content as well as a lower saturation level of ferritin, the major iron storage protein. PrP^{C} ablation prevents iron upatake as shown using *in vitro* cell models. On the contrary, cells overexpressing PrP^{C} increase the intracellular iron pool, saturating ferritin molecules. In addition, *Prnp*$^{0/0}$ mice showed a lower iron content in the brain, probably due to an impaired intestinal absorption. Re-establishing PrP^{C} expression in PrP^{C}-null mice the phenotype is reversed, indicating the specificity of PrP^{C} functional role in iron homeostasis (Singh, Kong et al. 2009, Pushie, Pickering et al. 2011). To date, it is not clear whether PrP^{C} mediates iron uptake by using a novel pathway or by interacting with conventional iron uptake and transport pathways (Singh, Das et al. 2010). It has been proposed that it could interact with transferrin/transferrin receptor pathway or act as a ferric reductase, facilitating the transport of Fe(III) from endosomes to cytosolic ferritin (Singh, Mohan et al. 2009).

Considering the important role of PrP^{C} in modulating content and distribution of specific metals within the CNS, PrP^{C} can regulate neurodegenerative disease progression (Pushie, Pickering et al. 2011).

PrP^{C} PROTECTIVE ROLE IN OXIDATIVE STRESS

The protective role of PrP^{C} against oxidative damages is widely accepted. Oxidative stress depends on alterations in reactive oxygen/nitrogen species formation and in antioxidant defenses. It leads to mitochondrial impairments, defects in the ubiquitin-proteasome system, protein oxidation and aggregation, lipid peroxidation and DNA damages (Milhavet and Lehmann 2002, Aguzzi, Baumann et al. 2008, Didonna and Benetti 2015) (Figure 7).

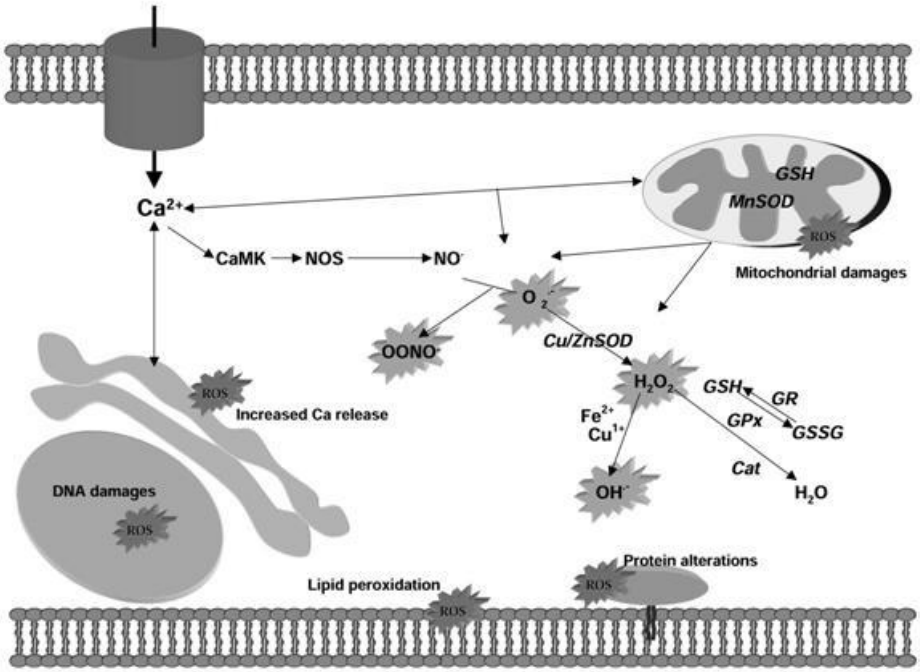

Figure 7. Main intracellular pathways of oxidative stress. Increased production of ROS ($O_2^{\cdot-}$, $OONO^-$, $OH^\cdot$) leads to alterations of proteins, lipids, DNA and organelles. Calcium ions play an important role by regulating various enzymes such as protein kinase, phospholipases, proteases and endonucleases. The main anti-oxidant systems which tightly regulate the intracellular levels of ROS are represented by SODs and the glutathione system. ER, endoplasmic reticulum; Ca^{2+}, calcium ions; CaMK, calmodulin kinase; NO, nitric oxide; NOS, nitric oxide synthase; $O_2^{\cdot-}$, superoxide ions; $OONO^-$, peroxynitrite; Cu/ZnSOD, copper–zinc-dependent superoxide dismutase; MnSOD, manganese-dependent superoxide dismutase; H_2O_2, hydrogen peroxide; Fe^{2+}, iron ions; Cu^{1+}, copper ions; $OH^\cdot$, hydroxyl radical; GSH, glutathione; GSSG, disulfide glutathione; GPx, glutathione peroxidase; GR, glutathione reductase; Cat, catalase; ROS, reactive oxygen species (Milhavet and Lehmann 2002).

The high presence of redox-active metals is one of the causes of oxidative stress in the brain (Avery 2001). Increasing evidence suggested that PrP^C improves resistance to oxidative stress, chelating free copper ions responsible for ROS generation (Brown, Clive et al. 2001). *In vitro* studies demonstrated that primary neuronal cells lacking PrP^C were more susceptible to oxidative stress than WT cells (Brown, Schulz-Schaeffer et al. 1997, White, Collins et al. 1999, Rachidi, Vilette et al. 2003). *In vivo* observations reported reduced Cu/Zn superoxide dismutase (SOD) activity and high levels of oxidative damage to proteins and lipids in PrP^C-deficient mice (Wong, Liu et al. 2001, Brown, Nicholas et al. 2002). Moreover, PrP^C expression is increased in a variety of stress related conditions, including heat shock, hypoxia, ischemia and hypoglycemia, as well as in stroke models (Shyu, Kao et al. 2000, McLennan, Brennan et al. 2004, Shyu, Lin et al. 2004, Shyu, Chen et al. 2005, Mitsios, Saka et al. 2007). While a knock-down of any SOD proteins triggers PrP^C expression, shutting down PrP^C increases extracellular-SOD expression and

SOD2 activity (Brown and Besinger 1998, Kralovicova, Fontaine et al. 2009). This connection between PrP^C and SOD proteins indicates a common cell protection pathway. *In vitro* experiments revealed that PrP^C has SOD-like activity with a dismutation constant rate similar to SOD2 (Brown, Wong et al. 1999, Brown, Clive et al. 2001, Cui, Daniels et al. 2003, Treiber, Pipkorn et al. 2007). SOD activity is dependent on Cu(II) incorporation and it probably involves Cu(II) reduction (Brown, Clive et al. 2001). Given its localization at synapses, PrP^C has been proposed to buffer Cu(II) ions in the synaptic cleft protecting neurons against toxic levels of this metal and acting as a synaptic SOD (Vassallo and Herms 2003). It should be also noted that PrP^C is cleaved at the end of its Cu-binding OR through the action of ROS, a process termed β-cleavage. β-cleavage is considered an early and critical event in the mechanism by which PrP^C protects cells against oxidative stress. PrP constructs lacking the OR fail the ROS-mediated β-cleavage, as occurs with PG14 and A116V mutations that are associated with human prion diseases (Watt, Taylor et al. 2005).

In their review, Vassallo and Hermes proposed the activation of redox signaling upon Cu(II)-PrP^C complex formation, modulating intracellular calcium content as secondary messenger (Vassallo and Herms 2003). Intracellular calcium is a critical component of the signaling pathways responsible for neuron structural and functional changes. The calcium signal usually corresponds to an elevation of the intracellular calcium concentration as a consequence of synaptic activity-induced depolarization. Indeed, in PrP^C-null conditions, neuron calcium homeostasis is impaired (Krebs, Wiebelitz et al. 2007). Hence, PrP^C may influence both neuron survival and synaptic physiology regulating calcium homeostasis (Vassallo and Herms 2003). The model proposed is reported in Figure 8.

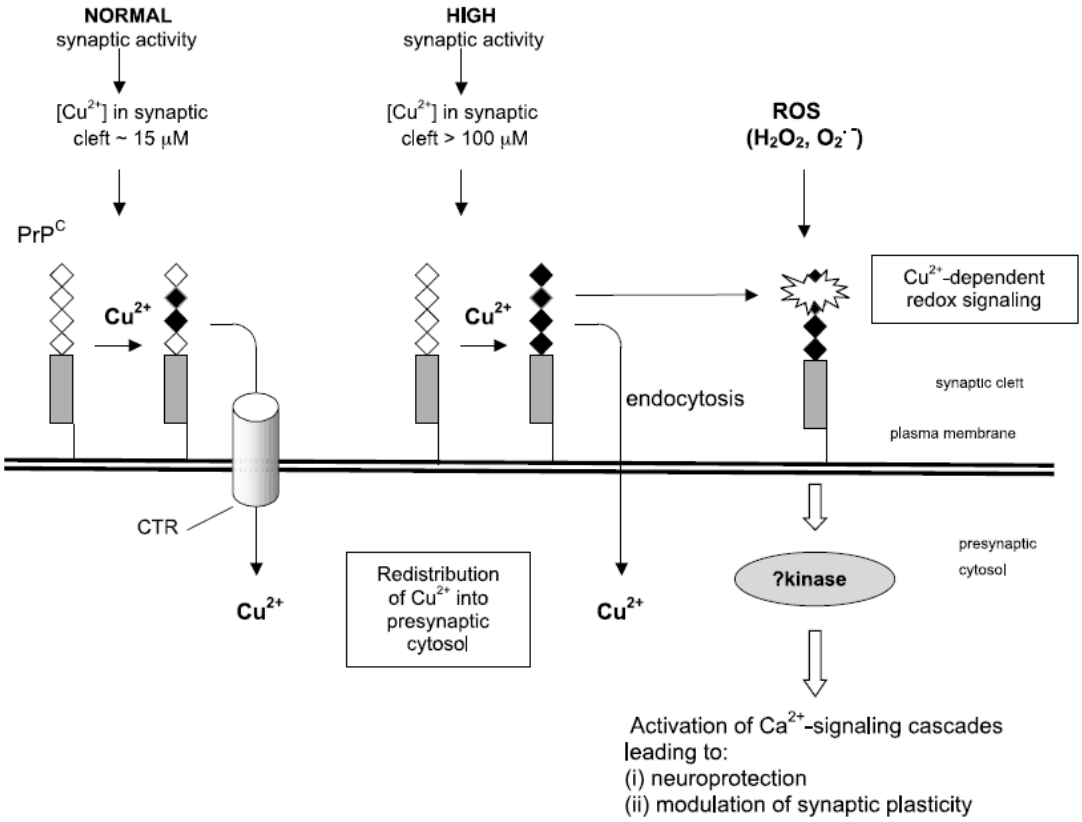

Figure 8. Schematic representation of the physiological role of prion protein (PrP^C) in copper homeostasis and redox signalling. Cu^{2+} ions released during neurotransmitter vesicles exocytosis are buffered by PrP^C, and subsequently returned to the pre-synaptic cytosol. This can occur either by the transfer of copper to copper transporter proteins (CTR) within the membrane, or in case of high copper concentrations in the synaptic cleft, via PrP^C-mediated endocytosis (◇represent an octarepeat; ◆represent an octarepeat bound to copper(II) ion). Further, copper-loaded PrP^C may interact with ROS, including H_2O_2 and $O_2^{\bullet-}$, triggering redox signalling and subsequently activation of Ca^{2+}-dependent signalling cascade. Changes in the intracellular Ca^{2+} levels lead to a modulation of synaptic activity and neuroprotection. (from (Vassallo and Herms 2003)).

PrP^C AND SYNAPTIC FUNCTIONALITY

PrP^C localizes at synapses together with a plethora of ion channels, supporting the hypothesis that it is important for normal synaptic development and functionality (Moya, Sales et al. 2000, Kanaani, Prusiner et al. 2005). Some features of PrP^C deficient mice such as alteration in circadian rhythm and impairment in spatial learning can be related to synaptic dysfunctions (Tobler, Gaus et al. 1996, Criado, Sanchez-Alavez et al. 2005). Electrophysiology studies suggest a role for PrP^C in the regulation of ion channels and neuronal excitability. A variety of abnormalities have been observed in the cerebellum and the

hippocampus of PrP^C-null mice (Collinge, Whittington et al. 1994, Manson, Hope et al. 1995, Colling, Collinge et al. 1996, Carleton, Tremblay et al. 2001, Herms, Tings et al. 2001, Mallucci, Ratte et al. 2002, Maglio, Perez et al. 2004, Fuhrmann, Bittner et al. 2006, Prestori, Rossi et al. 2008, Lazzari, Peggion et al. 2011, Caiati, Safiulina et al. 2013). Particular attention has been paied to PrP^C modulation of glutamate excitatory receptors, as N-methyl-D-aspartate receptors (NMDARs) (Mallucci, Ratte et al. 2002, Khosravani, Zhang et al. 2008, You, Tsutsui et al. 2012). PrP^C modulation of neuronal excitability has been shown to exert neuroprotection by preventing excitotoxicity (Spudich, Frigg et al. 2005, Rangel, Burgaya et al. 2007, Khosravani, Zhang et al. 2008). Excitotoxicity is a neuronal cell death pathway activated by the overactivation of glutamate receptors leading to massive calcium influx into cells (Dong, Saikumar et al. 2006). Calcium overload may increase the production of reactive oxigen and nitrogen species leading to cell death or damage (Nakamura and Lipton 2011). NMDARs overactivation is one of the mechanisms inducing excitotoxicity. For this reason, a precise modulation of NMDARs activity is essential for normal brain function. NMDARs are one of the major classes of ionotropic glutamate receptors mediating the excitatory synaptic transmission, plasticity and excitotoxicity in the brain. These glutamate-gated cation channels convert a chemical signal (glutamate released from presynaptic terminals) into an electric signal (excitatory post-synaptic potential) (Yashiro and Philpot 2008). These receptors are characterized by a voltage-sensitive block *via* extracellular Mg^{2+}, a high Ca^{2+} permeability and an unusually slow activation/deactivation kinetics. NMDARs work as heteromers composed of two GluN1 subunits, retaining the binding of the co-agonist glycine required for NMDAR activation (Cull-Candy, Brickley et al. 2001), and two other subunits among GluN2A-D and GluN3A-B (Moriyoshi, Masu et al. 1991, Sugihara, Moriyoshi et al. 1992, Das, Sasaki et al. 1998). The variety is also increased by the different splicing isoforms each subunit presents (Dingledine, Borges et al. 1999). According to the receptor composition, NMDARs differ in their localization, sensitivity to endogenous and exogenous ligands, permeation and block by divalent ions, kinetic properties, and interaction with intracellular proteins (Cull-Candy, Brickley et al. 2001). At least one type of GluN2 subunit retaining the glutamate binding site is required to form a functional receptor, while the GluN3 subunit does not form functional receptors alone, but can co-assemble with GluN1/GluN2 complexes (Das, Sasaki et al. 1998, Perez-Otano, Schulteis et al. 2001). NMDARs are found both at synaptic and extrasynaptic sites including cell soma and dendritic shaft. The possibility that NMDARs subunit composition differs between synaptic and extrasynaptic sites is still controversial. It has been proposed that GluN2A-containing NMDARs occupy the central portion of synapses, while GluN2B-containing ones are preferentially targeted to peripheral portions of synapses or to extrasynaptic sites where they are activated by glutamate spillover

(Cull-Candy, Brickley et al. 2001). Since NMDAR modulation plays crucial roles in physiological processes (learning and memory) and in pathological conditions (ischemia, epilepsy, neurodegenerative diseases and neuropsychiatric disorders), several regulatory mechanisms have been identified (Collingridge 1987, Lipton and Rosenberg 1994, Aarts, Liu et al. 2002, Loftis and Janowsky 2003). Binding of the co-agonist glycine is responsible for NMDAR activation. High glycine concentrations with subsequent NMDAR overactivation lead to a dramatic slowing of receptor desensitization kinetics, with consequent toxic calcium overload into cells and excitotoxicity (Mayer, Vyklicky et al. 1989, Vyklický, Benveniste et al. 1990). Activating phosphorylation can occur on serine and threonine residues by means of protein kinase A (PKA), protein kinase C (PKC) and Ca^{2+}/calmodulin-dependent protein kinase II (CaMKII), while deactivating dephosphorylation occurs via Ca^{2+}/calmodulin-dependent phosphatase calcineurin. Src and Fyn kinases can also activate NMDARs phosphorylating tyrosine residues (Dingledine, Borges et al. 1999). Other regulatory mechanisms involve glycosylation, covalent bound to lipids, as well as proteolytic degradation mainly mediated by calpain (Dingledine, Borges et al. 1999). Besides magnesium ions responsible for NMDAR voltage sensitivity, zinc ions modulate receptor activity by binding NMDAR outside the pore (Peters, Koh et al. 1987). Interestingly, copper released at the synaptic cleft emerged to be an important NMDAR modulator (Vlachova, Zemkova et al. 1996). Taking together these observations and searching for a possible mechanism of NMDAR modulation by PrP^C, it has been proposed that PrP^C protects neurons from excitotoxicity by inhibiting NMDAR currents in a copper dependent manner (Khosravani, Zhang et al. 2008, You, Tsutsui et al. 2012). Although researchers suggested that PrP^C may regulate NMDARs decreasing glycine affinity (You, Tsutsui et al. 2012), favoring desensitization and avoiding calcium overload, others affirmed that copper-mediated regulation of NMDARs depends on nitric oxide (NO) (Schlief and Gitlin 2006). To this regard, NMDAR S-nitrosylation provides a link between copper and NO inhibitory roles (Lipton, Choi et al. 2002). S-nitrosylation is a chemical post-translational modification targeting protein cysteines. In NMDARs, S-nitrosylation is inhibitory and addresses two residues on GluN1 and three residues on GluN2A, including Cys399, which mediates the predominant inhibitory effect. Cysteine free thiols are subjected to electrophilic attack by NO^+. Therefore, an electron acceptor, such as copper, is required for NO oxidation (Hess, Matsumoto et al. 2005). Copper released in the synaptic cleft is bound by metal-binding proteins such as PrP^C, which binds copper with high affinity and sustains Cu(II) redox cycling (Brown, Qin et al. 1997, Liu, Jiang et al. 2011). *In vitro* results have shown that PrP^C-bound Cu(II) promotes NO oxidation and it is consequently reduced to Cu(I) (Bonomo, Pappalardo et al. 2008). Me and my colleagues proposed and demonstrated that PrP^C exerts copper-dependent neuroprotection by mediating NMDAR S-nitrosylation (Gasperini,

Meneghetti et al. 2015). As shown in Figure 9, glutamate released from the presynaptic terminal activates NMDARs on the postsynaptic terminal. NMDAR activation triggers Na^+ and Ca^{2+} influx, together with K^+ efflux. In the intracellular compartment, Ca^{2+} activates different signaling cascades and, among these, it activates calmodulin (CaM). The Ca^{2+}/CaM complex activates neuronal nitric oxide synthase (nNOS) resulting in NO release in the synaptic cleft. Ca^{2+}/CaM activates also the copper-transporting ATPase 1 (Atp7a) in the TGN permitting Cu^{2+} release into synaptic cleft. Released Cu^{2+} ions are bound by copper-binding proteins such as PrP^C, highly expressed in lipid raft domains with NMDARs, and having high affinity for both Cu^{2+} and Cu^+. Released NO can be oxidized by Cu-PrP^C complex and react with extracellular cysteine thiols of NMDAR subunits GluN1 and GluN2A, leading to cysteine S-nitrosylation (SNO-Cys). Cu^{2+} bound to PrP^C acts as electron acceptor allowing the S-nitrosylation reaction, thus inhibiting NMDAR activation by closing the channel and preventing excitotoxic effects.

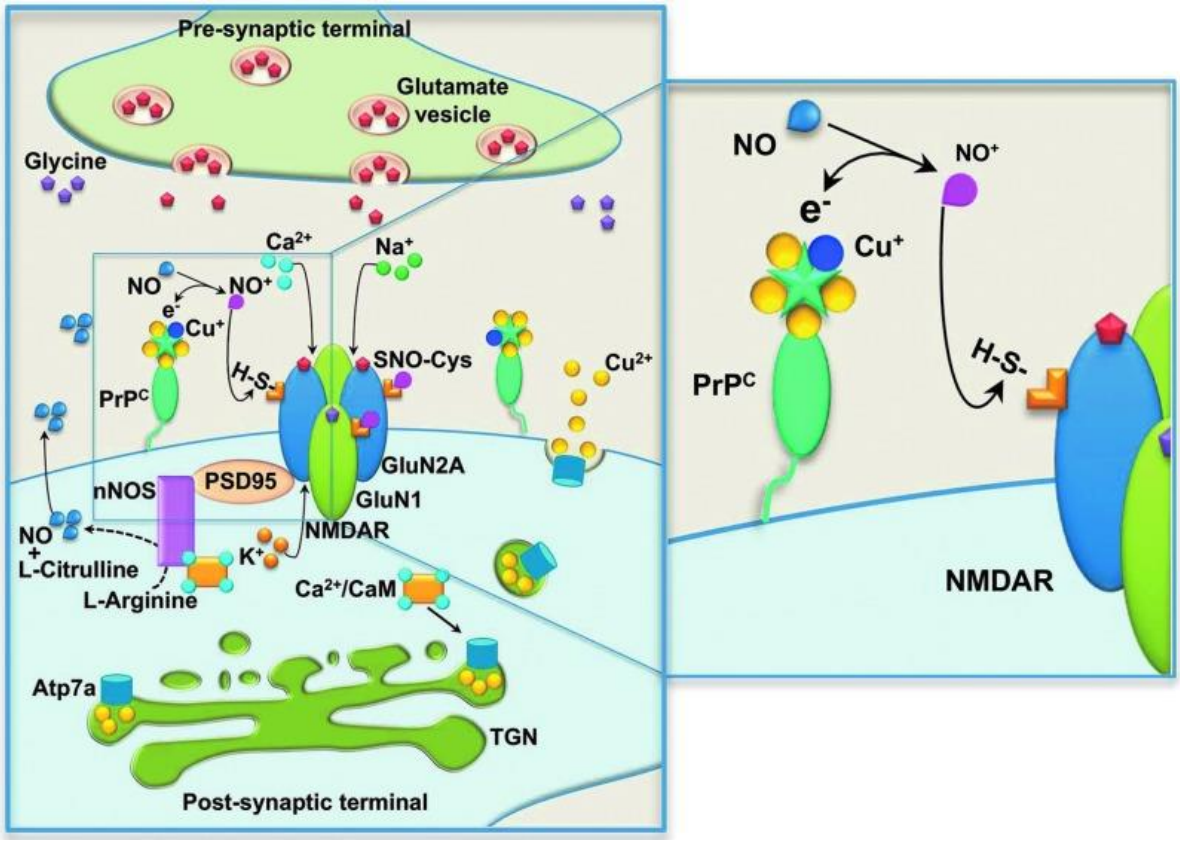

Figure 9. Mechanism of PrP^C-mediated S-nitrosylation of NMDAR. Glutamate released from the presynaptic terminal activates NMDAR on the postsynaptic terminal. NMDAR activation triggers Na^+ and Ca^{2+} influx, together with K^+ efflux. In the intracellular compartment, Ca^{2+} ions bind different proteins, including calmodulin (CaM). The Ca^{2+}/CaM complex activates, among others, neuronal nitric oxide synthase (nNOS) and copper-transporting ATPase 1 (Atp7a): nNOS activation results in NO release in the

synaptic cleft; Atp7a activation in the *trans*-Golgi network (TGN) results in Cu^{2+} release in the synaptic cleft. Released Cu^{2+} ions are immediately bound by copper-binding proteins: PrP^C is highly expressed in both presynaptic and postsynaptic terminals, and it can be included in lipid raft domains that also contain NMDARs, and it has high affinity for both Cu^{2+} and Cu^{+}. Released NO can react with extracellular cysteines thiols of NMDAR subunits GluN1 and GluN2A, leading to cysteine S-nitrosylation (SNO-Cys). The S-nitrosylation inhibits NMDAR activation by closing the channel. The chemical reaction between NO and the cysteine thiol requires the presence of an electron acceptor, often represented by Cu^{2+}. According to this model, PrP^Cbrings the Cu^{2+} ions that support the reaction of NO with thiols, leading to the S-nitrosylation of GluN1 and GluN2A, thus inhibiting NMDAR (Gasperini, Meneghetti et al. 2015).

PrP^C ROLE IN MYELINATION

One of the most debated roles of PrP^C concerns its involvement in CNS myelination. CNS white matter is mainly composed of myelinated axons. In some GSS cases, cerebellar and frontal white matter degeneration has been reported (Itoh, Yamada et al. 1994). Walis and colleagues showed vacuolation of myelinated fibers with splitting of myelin lamellae in myelin sheaths of rodents infected with human TSE (Walić, Bratosiewicz et al. 2003). However, it was not investigated whether myelin degeneration was due to PrP^C loss-of-function or it was a consequence of the pathological process. As already reported in the PrP KO and transgenic mice section, central and peripheral nervous system demyelination was observed in transgenic mice expressing the PrP^C truncated Δ32-121, Δ32-134, Δ94-134, Δ111-134 and Δ105-125, hinting at the HC as essential for myelin maintenance (Shmerling, Hegyi et al. 1998, Baumann, Tolnay et al. 2007, Li, Christensen et al. 2007, Bremer, Baumann et al. 2010). Vacuolation and degeneration of CNS myelinated fibers was also described in Dpl overexpressing mice (Nishida, Tremblay et al. 1999). These degenerating phenotypes are fully reverted co-expressing full-length PrP^C. It has been reported that PrP^C is present in purified myelin fractions derived from brain homogenates and that oligodendrocytes-specific full length PrP^C expression is necessary for CNS myelin maintenance (Radovanovic, Braun et al. 2005). Same authors hypothesized that oligodendrocyte-restricted PrP^C may repress *in trans* the axonal pathology elicited by PrP mutants. A cellular signal might be transduced through PrP^C from oligodendrocytes to axons, analogously to other GPI-anchored proteins playing a role in axon-myelin interactions. Alternatively, PrP^C may instruct oligodendrocytes to release factors necessary for axonal survival (Wilkins, Majed et al. 2003). Surprisingly, *Prnp*$^{0/0}$ mice presented a milder phenotype than PrP-mutant expressing mice, showing only PNS demyelination (Bremer, Baumann et al. 2010). In the absence of PrP^C there is an initial formation of morphologically normal PNS myelin followed by myelin disruption (Figure 10).

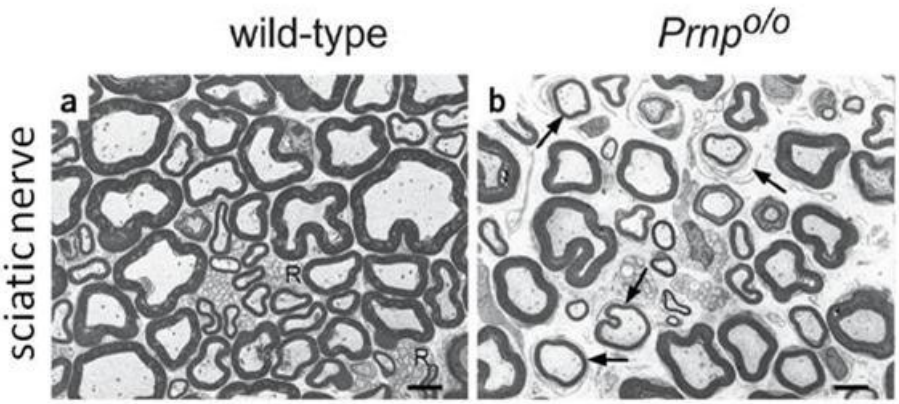

Figure 10. Ultrastructural alterations in *Prnp*$^{0/0}$ SNs. Electron microscopy of SNs of 60-week-old WT **(a)** and *Prnp*$^{0/0}$ **(b)** mice (both Balb/c). Cross-sections of WT nerves show normally myelinated nerve fibers and regular unmyelinated axons in Remak bundles (R). Cross-sections of *Prnp*$^{0/0}$ nerves show thinly myelinated axons, surrounded by onion bulb formations (arrows). Modified from (Bremer, Baumann et al. 2010).

PrP^{C} expression in neurons, but not in Schwann cells, is required to prevent CDP in the PNS. Thus, neuronal PrP^{C} *in trans* expression is required for the axon to Schwann cells communication (Bremer, Baumann et al. 2010). Bremer and colleagues suggested that PrP^{C} cleavage may be linked to its myelinotrophic function. Indeed, PrP^{C} is subjected to regulated proteolysis in late secretory compartments (Sunyach, Cisse et al. 2007), thus generating two distinct fragments, namely C1 and C2. C1 is generated by α-cleavage at amino acids 110–112, whereas C2 is derived by β-cleavage in the octarepeat region at position 96 (Mange, Beranger et al. 2004, Watt, Taylor et al. 2005). Bremer and colleagues evidenced an association between the presence of CDP and lack of the C1 fragment in SNs, suggesting that alpha-cleavage is important for PrP^{C} function in myelin physiology.

The importance of PrP^{C} in peripheral myelin maintenance during aging processes was also confirmed by a study by our group showing that PrP^{C} positively influence the processing of neuregulin-1 and 3 (NRG1 and NRG3) in the PNS of aged mice (Benvegnu, Gasperini et al. 2011). NRG proteolytic cleavage by different membrane proteases is crucial for myelin maintenance in the PNS. According to these findings, PrP^{C} may exert its protective function through the modulation of β-secretase 1 (BACE1) (Parkin, Watt et al. 2007). Interestingly, correct PNS myelination was compromised in PrP^{C} overexpressing mice (Westaway, DeArmond et al. 1994).

Despite the expectations concerning PrP^{C} involvement in CNS myelin maintenance, different studies failed to observe CNS myelin differences between WT and PrP^{C}-null mice. Accordingly, Bremer and

colleagues did not detect myelin degeneration in optic nerve, corpus callosum or spinal cord of 60-week-old *Prnp*$^{0/0}$ mice (Figure 11) (Bremer, Baumann et al. 2010).

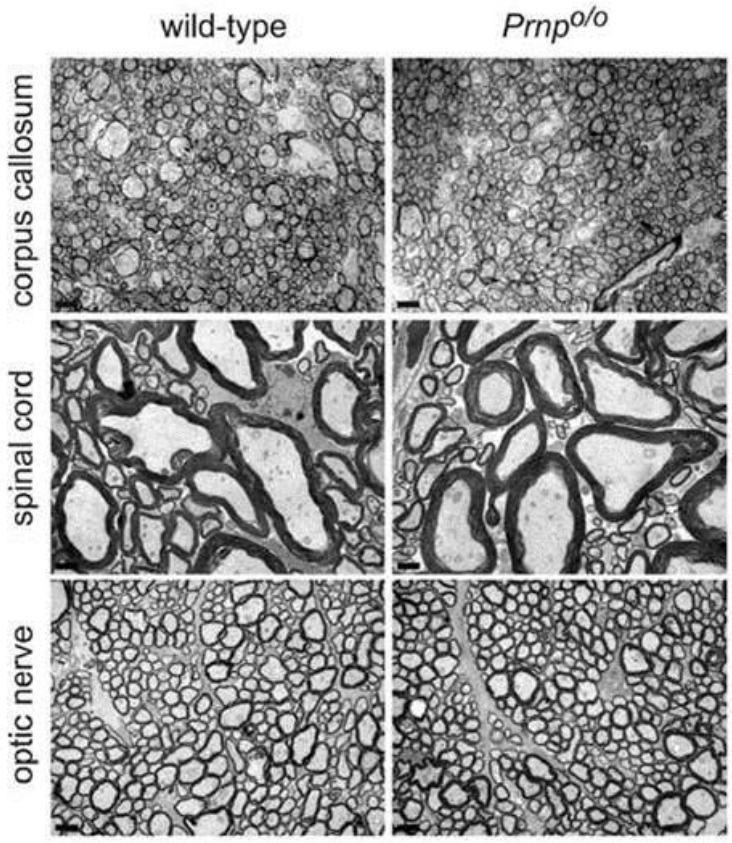

Figure 11. Normal ultrastructure of *Prnp*$^{0/0}$ CNS white matter at 60 weeks of age. Sixty-week old *Prnp*$^{0/0}$ compared to WT mice were analyzed by electron microscopy. No morphological abnormalities were observed in *corpus callosum*, spinal cord white matter and optic nerve. Scale bar = 2 µm. *Corpora callosa* were analyzed in mixed B6/129Sv mice whereas spinal cords and optic nerves belonged to Balb/c mice (Bremer, Baumann et al. 2010).

However, the authors did not exclude the possibility that subliminal myelin alterations might extend to central myelin in Prnp$^{0/0}$ mice. In fact, motor deficits were detected in 3 to 8 months old Prnp$^{0/0}$ mice, together with spongiform pathology in different CNS regions at 6 months of age (Nazor, Seward et al. 2007). Vacuolar lesions were detected in particular in the corpus callosum, at the level of the hippocampus, in the medial globus pallidus, in the cerebellum and the inferior cerebellar peduncle and finally in the spinal trigeminal tract. Furthermore, no differences in the processing of NRG in the hippocampus of 1-year-old Prnp$^{0/0}$ mice were observed (Benvegnu, Gasperini et al. 2011). Thus NRG cleavage modulation mediated by PrP^{C} is important only for PNS myelin maintenance, but not for the CNS. In addition, it has been reported that PrP^{C} absence increases OPC proliferation and delays their

maturation without affecting the final amount or quality of myelin (Bribián, Fontana et al. 2012). The expression of the myelin-associated glycoprotein (MAG), identifying mature myelinating oligodendrocytes, revealed no significant changes in the white matter of *Prnp*$^{0/0}$ mice (Figure12). Accordingly, myelination was not affected and no significant differences were detected between the two genotypes in terms of the amount of total MAG or myelin basic protein (MBP) in adult cortical and spinal cord extracts. In agreement with previous findings by Bremer and colleagues, electron microscopy revealed no alterations to the myelin sheaths in the cortical white matter due to the loss of *Prnp*. On the basis of their observations, authors proposed that the increase in the OPC proliferation observed in the absence of PrP^{C} may be compensated by extrinsic factors able to regulate the proper timing of OPC differentiation, ensuring adequate myelination and maintenance. Surplus OPC may be counterbalanced by cell death. In light of these controversial findings, PrP^{C} role in CNS myelin formation and maintenance has not been clarified yet.

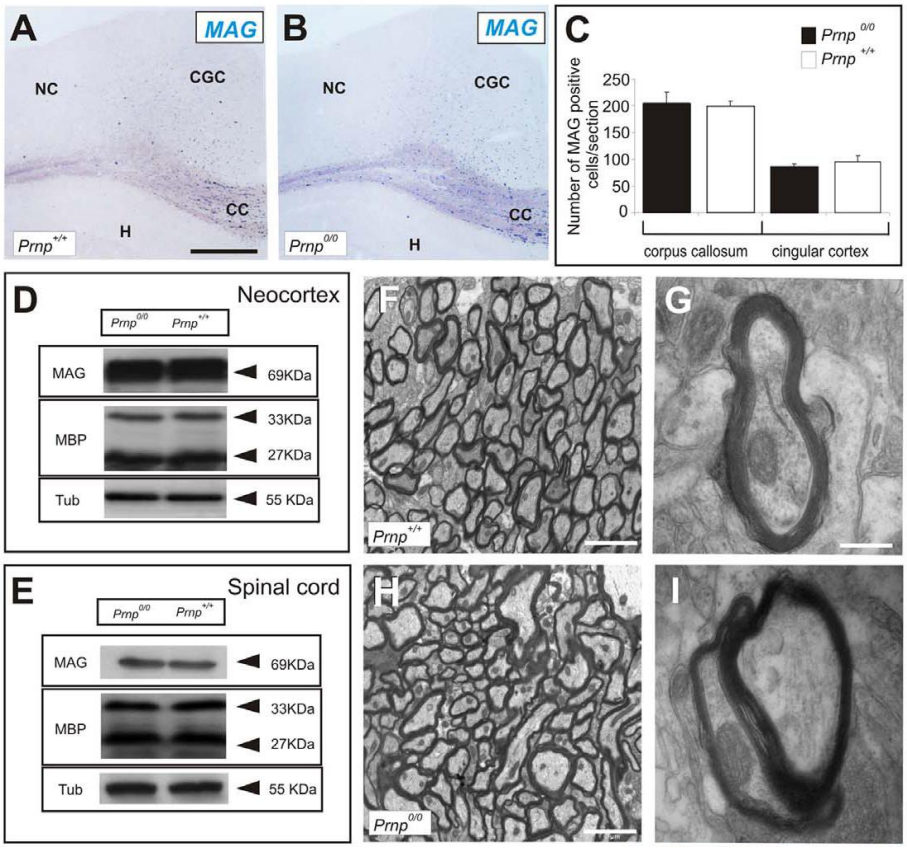

Figure 12. Adult *Prnp*$^{0/0}$ mice exhibit normal myelination in the CNS. (A-B) *In situ* hybridization of MAG in coronal sections from the brains of adult *Prnp*$^{+/+}$ and *Prnp*$^{0/0}$ mice. **(C)** Quantification of MAG-positive cells revealed no differences between genotypes in the *corpus callosum* or cingular cortex. Values represent the mean ± standard deviation and were analyzed using

the Student's t test. **(D-E)** Western blots of brain extracts from *Prnp*$^{+/+}$ and *Prnp*$^{0/0}$ mice showing no differences in the expression of the MAG and MBP myelin proteins between genotypes in neocortex **(D)** and spinal cord **(E). (F, H)** Lower magnification electron microscopy photomicrograph of *Prnp*$^{+/+}$ and *Prnp*$^{0/0}$ mice. **(G, I)** Higher magnification of F and H, respectively, show no gross ultrastructural differences in the myelin sheaths of the *corpus callosum*. Abbreviations: CC: corpus *callosum*; CGC: cingulate cortex; NC: neocortex. H: hippocampus; Scale bars: A = 300 µm also applies to B; F: 2 µm also applies to H; G = 0.5 µm also applies to I. (Bribián, Fontana et al. 2012).

MYELIN BIOLOGY

Myelin is a spiral structure constituted by a greatly extended and modified plasma membrane enwrapping nerve axons (Baumann and Pham-Dinh 2001). Myelin membrane derives from Schwann cells in the PNS and from oligodendrocytes in the CNS. Its unique lipid-enriched composition makes the electrical insulation of axons possible. Myelin segmental structure allows the saltatory propagation of axon potentials and therefore the high-speed conduction and synchronization of afferent nerve impulses (Waxman 1997). Myelin maintains axon integrity by providing glial support, including glycolytic energy metabolites, neurotrophic factors and cargo-containing vesicles termed exosomes (Figure 13) (Nave 2010, Funfschilling, Supplie et al. 2012, Beirowski 2013, Fruhbeis, Frohlich et al. 2013, White and Krämer-Albers 2013). On the other hand, axonal contact, diameter, electrical activity and signaling are essential for a correct myelination, as reviewed in (Taveggia, Feltri et al. 2010, Hines, Ravanelli et al. 2015).

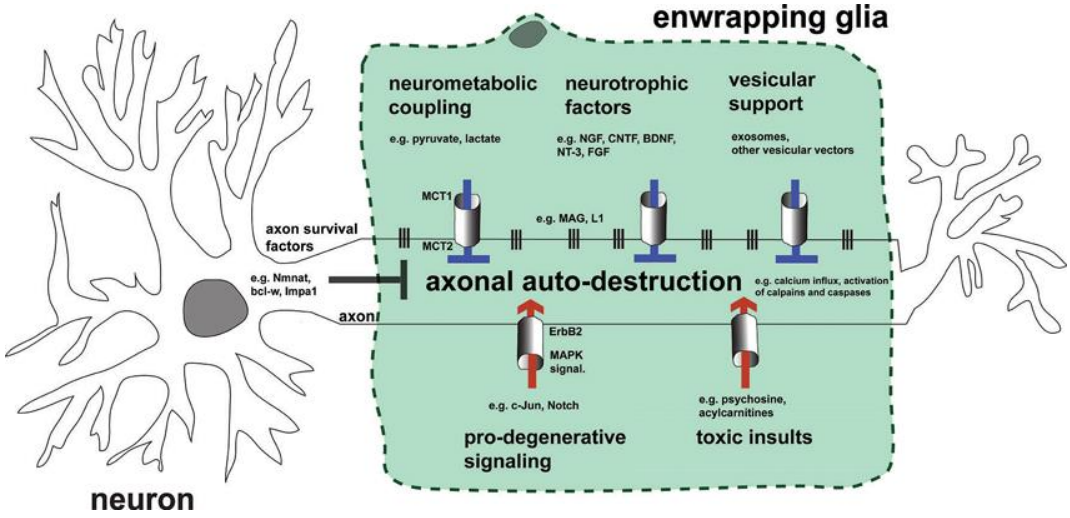

Figure 13. Hypothetical model summarizing impact of EG on axonal integrity by the mechanistic themes discussed. Preservation of healthy axons is controlled by the cooperative action of both the neuron and adjacent glia by

blocking endogenous axonal auto-destruction. Examples of neuronal mechanisms blocking this program(s) include somatic delivery of the putative axonal survival molecule Nmnat2 into axons, or the local translation of axonal maintenance factors such as Bcl-w. On the other hand, glia inhibit axonal death by transfer of metabolic substrates, neurotrophic factors, and vesicular shuttles (upper glia portion). This transfer is mediated by specific transport mechanisms represented by columns between glia and axon. Vertical lines embody adhesion mechanisms that ensure correct apposition and formation of nutritive channels between glia and axon. Under pathological conditions glia may also contribute to axonal auto-destruction by activating pro-degenerative signaling, releasing toxic substances, and loosening contact to axons (lower glia portion). Note that the myelin membrane of EG is uncoiled in the illustration and myelination thus not represented (Beirowski 2013).

Myelin presents a characteristic periodic structure of alternating electron-dense and -light layers, named major dense line and intraperiod line respectively. The major dense line is formed by the close apposition of the cytoplasmic surfaces of myelin membranes, while the apposition of the two outer leaflets forms the intraperiod line (Figure 14). Myelinated segments are separated by small unmyelinated gaps, Ranvier nodes, where sodium channels are highly concentrated and the membrane depolarization occurs. Within myelin segments, there are small regions of uncompacted membranes retaining small amount of cytoplasm (Schmidt-Lanterman clefts and paranodal loops). Myelin sheath is separated from the axonal membrane by an extracellular cleft, called periaxonal space. While in the PNS one myelinating Schwann cell forms only one myelin segment, in the CNS one oligodendrocyte can myelinate as many as 40 or more separate axons (Baumann and Pham-Dinh 2001, Hartline 2008, Aggarwal, Yurlova et al. 2011).

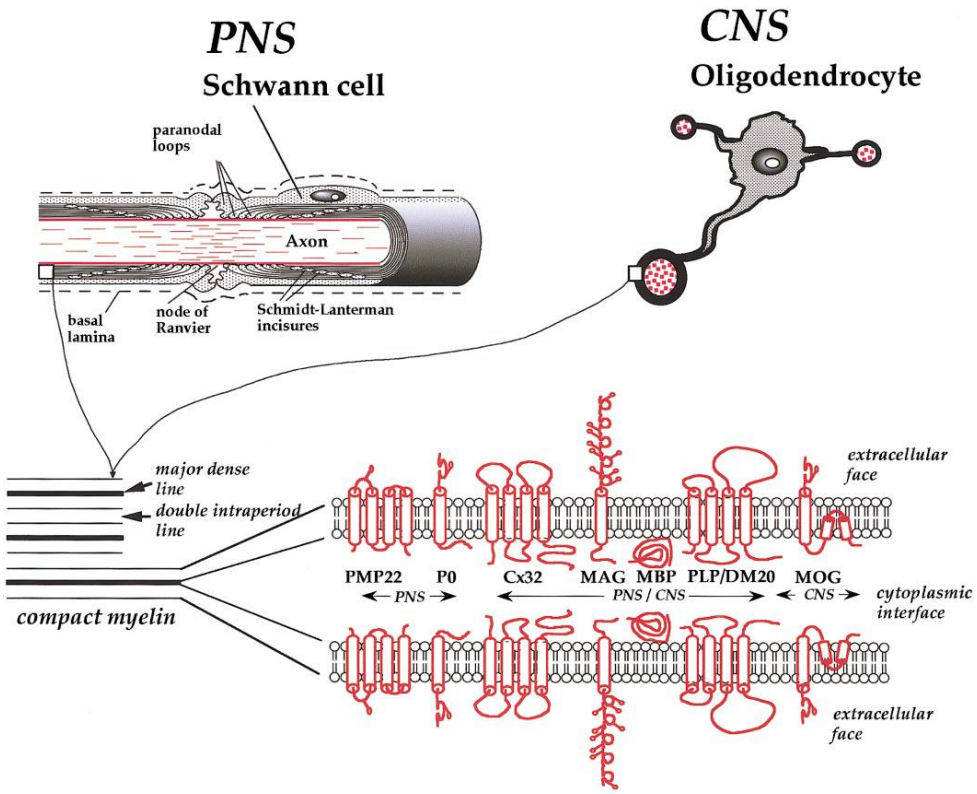

Figure 14. Myelinating glial cells, myelin structure, and composition in the peripheral nervous system (PNS) and in the CNS. In the PNS, the myelinating Schwann cell myelinates only one segment of axon (top left corner), whereas in the CNS (top right corner), the oligodendrocyte is able to myelinate several axons. The compact myelin is formed by the apposition of the external faces of the membrane of the myelinating cell, forming the "double intraperiodic line"; the apposition of the internal faces followed by the extrusion of the cytoplasm, form the "major dense line." The myelin proteins are schematically described; they differ between PNS and CNS (Baumann and Pham-Dinh 2001).

Myelin is a poorly hydrated structure containing only 40% water, in contrast to 80% in gray matter. Conversely from other cellular membranes, it consists of 70-85% lipids and only 15-30% proteins. There are no myelin-specific lipids, though myelin contains cholesterol, phospholipids and glycolipids in molar ratios ranging from 4:3:2 to 4:4:2. Cholesterol constitutes about 30% of total myelin lipids and it is essential for membrane stability. Among the other lipids, cerebroside, sulfatide, lecithin and sphingomyelin are present in myelin. Peripheral and central nervous system myelin lipids are qualitatively similar, but some quantitative differences are present. PNS myelin has less cerebroside and sulfatide, but more sphingomyelin than CNS. Differently from lipid composition, CNS and PNS present similarities and peculiarities in protein composition, as described in Figure 14. Some myelin proteins important for this thesis are here described, referring to (Campagnoni 1988, Baumann and Pham-Dinh 2001, Aggarwal, Yurlova et al. 2011). Concerning CNS, myelin basic protein (MBP) and proteolipid

protein (PLP) represent the majority (80%) of the total myelin proteins. The Mbp gene, located on the mouse chromosome 18, is composed of 7 exons with at least 6 splice variants, encoding for 21.5, 18.5, 17 and 14 kDa proteins. MBP is an extrinsic protein, localized exclusively at the cytoplasmic surface of the major dense line where it plays a role in membrane stability. It alone constitutes the 30% of CNS myelin proteins, while in the PNS it varies from 5 to 18% of the total proteins and it does not seem essential for correct myelin structure. Plp gene, located on mouse chromosome X, is composed by 7 exons with 2 splice variants. PLP1 is a 30 kDa protein, while its isoform, DM20, present a 35 aminoacids deletion (Wight and Dobretsova 2004). The DM20 developmental expression precedes that of PLP1. Therefore, in adult brains DM20 is present at a much lower level compared to PLP1. In some reports, DM20 gene expression has been associated with remyelinating conditions in the adult brain (Mathisen, Kawczak et al. 2001). PLP is an integral membrane protein that stabilizes the intraperiod line. Both isoforms are highly acylated and extremely hydrophobic. PLP constitutes 50% of the total CNS myelin proteins, while in the PNS it is present in a small amount. Another protein that is shared between CNS and PNS is myelin associated glycoprotein (MAG). Its gene is located on mouse chromosome 7 and it is composed by 13 exons encoding two different splice variants: the 72 kDa long-MAG (L-MAG) and the 67 kDa short-MAG (S-MAG). These proteins are usually found in the heavily glycosylated form, with an apparent molecular mass of 100 kDa. These transmembrane proteins are located in the periaxonal membrane of myelin sheats, where they are supposed to play a role in neuron-glia adhesion and in bi-directional signaling. One of the CNS specific myelin proteins is myelin oligodendrocyte glycoprotein (MOG), encoded by a gene located on mouse chromosome 17. MOG is a 25 kDa protein presenting some glycosylation. It is a transmembrane protein localized in the outside surface of myelin sheats, where it may be involved in signal transduction. Differently from the CNS where the essential proteins are MBP and PLP, in the PNS myelin protein zero (MPZ or P0) constitutes more than 50% of the total myelin proteins. Mpz gene is located on mouse chromosome 1 and it encodes for a 30 kDa transmembrane protein that is subjected to post translational modifications, such as glycosylation, phosphorylation and acylation. MPZ stabilizes the intraperiod line, thus replacing the function of PLP which has very low expression levels in PNS. Expression of the correct amount of MPZ is apparently essential for normal myelin formation and maintenance. Recently, a novel 36 kDa isoform has been identified and named large-MPZ (L-MPZ) due to the presence of an additional domain at the C-terminus (Yamaguchi, Hayashi et al. 2012). This protein derives from the stop codon readthrough of MPZ mRNA and it has been identified both in physiological and pathological conditions. As MPZ, L-MPZ may retain a stuctural importance in myelin adhesion and compaction. Furthermore, many other proteins are

associated to myelin, such as enzymes and neurotransmitter receptors, making myelin a metabolically and signaling active structure.

CNS MYELINATION, DEMYELINATION AND REMYELINATION

In mouse, myelination predominantly occurs postnatally, starting at birth in the spinal cord and subsequently in the brain (Baumann and Pham-Dinh 2001). The process of myelin membrane formation and compaction is very rapid and many signaling mechanisms regulate the precise timing of oligodendrocyte differentiation and myelination, lipid and protein synthesis, displacement and organization (Baumann and Pham-Dinh 2001, Bradl and Lassmann 2010, Taveggia, Feltri et al. 2010). During development, myelinating glia and axons establish a continuous and reciprocal exchange of signals (Figure 15). While glial cells provide survival signals to neurons, define specific domains along the axon and determine the axon diameter, axons modulate proliferation, survival and differentiation of glia, thus controlling myelin formation (Bozzali and Wrabetz 2004, Simons and Trajkovic 2006, Salzer, Brophy et al. 2008). In addition, neuronal electrical activity promotes myelination, instructing nearby oligodendrocytes to initiate myelination (Malone, Gary et al. 2013, Hines, Ravanelli et al. 2015).

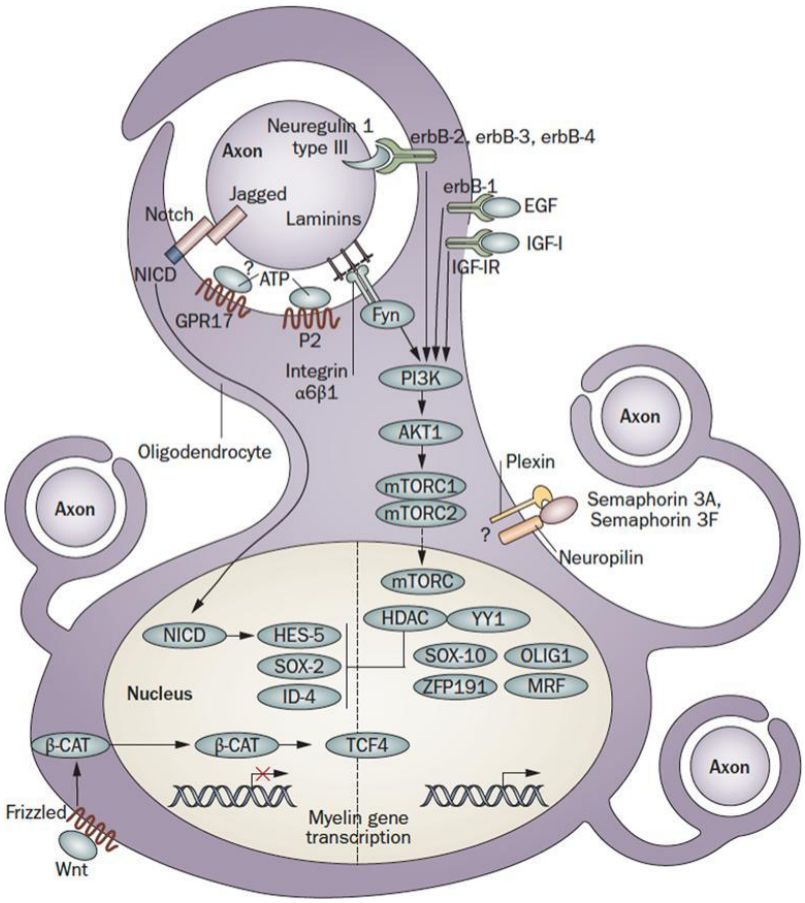

Figure 15. Axon to glia signaling pathways in myelination. Schematic representation of the main signaling pathways that regulate the onset of myelination during CNS development. The figure depicts an oligodendrocyte just before wrapping. The pathways shown are not comprehensive, but focus on signaling that converges on the glial cell nucleus. Regulatory feedback loops are not displayed. For some molecules, the localization shown is putative. Note that, as oligodendrocytes must integrate signals from multiple axons, with different calibers and electrical activities, a layer of local peri-axonal regulation is likely to be superimposed on nuclear regulation of myelination. Dashed lines indicate signals with uncertain targets. Abbreviations: Nrg: Neuregulin; EGF: Epidermal Growth Factor; IGF1: Insulin-like Growth Factor 1; Sema: Semaphorin; Fyn: Fyn kinase; GPR17: G protein-coupled receptor 17; P2: Purinergic Receptors 2; NICD: Notch-1 intracellular domain: PI3K: phosphatidylinositol-3 kinase; Akt: serine/threonine-specific protein kinaseAkt/PKB; mTOR: mammalian target of rapamycin (mTOR) signaling complexes; HDAC: Histone deacetylase; YY1: YIN-YANG-1; Sox: SRY-box containing transcription factor; Zfp: zinc finger protein; MRF: Myelin gene regulatory factor; Tcf: T-cell factor 4 transcription factor; Hes: hairy and enhancer of split 5 transcription factor; Id: Inhibitor of differentiation transcription factor; β-cat: β-catenin; Wnt: Wingle wingless-related mouse mammary tumor virus integration site protein (Taveggia, Feltri et al. 2010).

Once the myelinating phase is completed, the intricate signaling between enwrapping glia and axons continues in order to maintain a proper myelination. Observation that axonal damage follows myelin

damage in most myelin disorders, suggests that signals from myelin to axons might be altered by disease conditions (Beirowski 2013). In some cases, a simultaneous destruction of oligodendrocyte and myelin has been reported (Bradl and Lassmann 2010). Differently, in the Wallerian degeneration myelin degenerates as a consequence of primary axonal loss (Friese, Schattling et al. 2014). Thus, different degenerative mechanisms acting in pathological conditions may result in demyelination. Due to the combination of some peculiar features, oligodendrocytes and their myelin sheath are in general more susceptible to damage than other CNS cellular components. This peculiar vulnerability is due to the extremely high metabolic rate of oligodendrocytes. During myelination, oligodendrocytes consume large amounts of oxygen and adenosine triphosphate (ATP) in order to produce a large amount of membrane (McTigue and Tripathi 2008). This high cellular metabolism, together with accelerated ATP production, leads to ROS production that must be promptly metabolized to prevent cell damages. On the other hand, OPC and oligodendrocytes have the highest iron content among the cells of the brain (Thorburne and Juurlink 1996). Iron is directly involved in myelin production as a required co-factor for many myelin synthetic enzymes, as the ones involved in cholesterol and other lipid biosynthesis (Connor and Menzies 1996). Iron is a transition metal that may participate in redox reactions leading to ROS production. Therefore, both these conditions make oligodendrocytes and myelin highly susceptible to oxidative stress, which is a common feature of many neurodegenerative diseases associated with demyelination (Bongarzone, Pasquini et al. 1995, Bizzozero, DeJesus et al. 2004, Encinas, Manganas et al. 2005, Morelli, Ravera et al. 2012). Furthermore, oligodendrocytes have only low concentrations of the anti-oxidative enzyme glutathione (Connor and Menzies 1996). Several additional studies have shown that oligodendrocytes and myelin are vulnerable to glutamate excitotoxicity (Matute, Sanchez-Gomez et al. 1997, McDonald, Althomsons et al. 1998) since they express both α-amino-3-hydroxy-5-methyl-4-isoxazolepropionate (AMPA)/kainite mainly in the soma and NMDA receptors in the myelin sheath. While in physiological conditions oligodendrocytes respond to glutamate released by electrically active axons, in pathological conditions NMDAR contribute to oligodendrocyte toxicity (McTigue and Tripathi 2008, Wake, Lee et al. 2011). Finally, the capacity of endoplasmic reticulum (ER) to properly produce and fold proteins in a quick but precise manner is another factor influencing myelin amount and stability. Indeed, slight variations in the amount of one protein may result in the retention, misfolding and accumulation of many other proteins in the ER (Bauer, Bradl et al. 2002).

After initial myelin damage, a remyelinating process can initiate, trying to form new myelin sheaths around axons (Franklin and Ffrench-Constant 2008, Bradl and Lassmann 2010). CNS remyelination is possible thanks to the generation of new mature oligodendrocytes from the adult, quiescent OPC pools.

Initially, OPC must switch from a quiescent to a regenerative state and they are subsequently recruited to demyelinated areas. The differentiation of OPC to remyelinating oligodendrocytes starts, with the expression of myelin genes and proteins, membrane wrapping and compaction. Although these processes resemble developmental myelination, some differences exist: first, remyelination is a slower process compared to developmental myelination, since adult OPC have a longer cell cycle time and a slower rate of migration. Secondly, signaling molecules and transcription factors seem to be different in these two processes. Lastly, remyelination results in a thinner and shorter myelin sheath than would be expected for a given axon diameter, meaning that the developmental correlation between axon diameter and myelin sheath thickness and length is lost during remyelination. Remyelination is a promising topic, since it provides a possible therapeutic target for demyelinating diseases. However, at later stages of the disease progression, remyelination largely fails leading to progressive neurodegeneration and disability (Franklin and Ffrench-Constant 2008).

MODELS TO STUDY CNS MYELIN

In the past years, many models have been established to study CNS myelination, demyelnation and remyelination. *In vitro*, *in vivo* and *ex vivo* models have been set up, each of them presenting some peculiarities.

In vitro models based on OPC-neurons co-culture are simple, inexpensive and high throughput (Wang, Colognato et al. 2007, Watkins, Emery et al. 2008). However, they can only model myelination, but not remyelination (Zhang, Jarjour et al. 2011).

Differently, myelination, demyelination and remyelination can be studied by using *in vivo* models based on experimental allergic encephalitis (EAE), viral-induced myelin damages and administration of toxins, among which the most common are lysolecithin (Lysophosphatidylcholine, LPC) and CZ (Blakemore and Franklin 2008, Furlan, Cuomo et al. 2009, van der Star, Vogel et al. 2012). Even if LPC mode of action is still debated, this toxin disrupts membranes, including myelin, by inserting into lipid bilayers which then form micellas (Gregson 1989). A precise dosage of this toxin allows damage to be specific to myelinating cells, sparing other cell types. Remyelinating processes start some weeks after the toxin source removal (van der Star, Vogel et al. 2012). Concerning CZ, oral administration of this copper chelating agent was widely used in myelin research since the 1960s (Carlton 1967, Hoffmann, Lindner et al. 2008,

Koutsoudaki, Skripuletz et al. 2009, Zendedel, Beyer et al. 2013). In adult mice, the administration of 0.2-0.3% CZ containing diet for 5-6 weeks can induce an acute demyelination that may be reverted by a spontaneous and endogenous remyelination process once the normal diet is restored. Differently, CZ feeding for more than 12 weeks induces chronic demyelination with impaired spontaneous remyelinaion process (van der Star, Vogel et al. 2012). The way in which CZ induces demyelination is still unclear. However, it is known that CZ induces the death of mature myelinating oligodendrocytes, with concomitant microglia activation and astrocytosis (Norkute, Hieble et al. 2009, Bénardais, Kotsiari et al. 2013). Figure 16 shows the cellular and molecular response during CZ-induced acute demyelination (Gudi, Gingele et al. 2014). Since no traces of CZ have been found in the brain of CZ-fed mice, the decrease in brain copper content might be caused by CZ-mediated interference with the intestinal absorption of this metal (Venturini 1973, Benetti, Ventura et al. 2010). Even though *in vivo* experiments are largely used to study myelination, these models are very low-throughput and expensive in terms of animals, time and money.

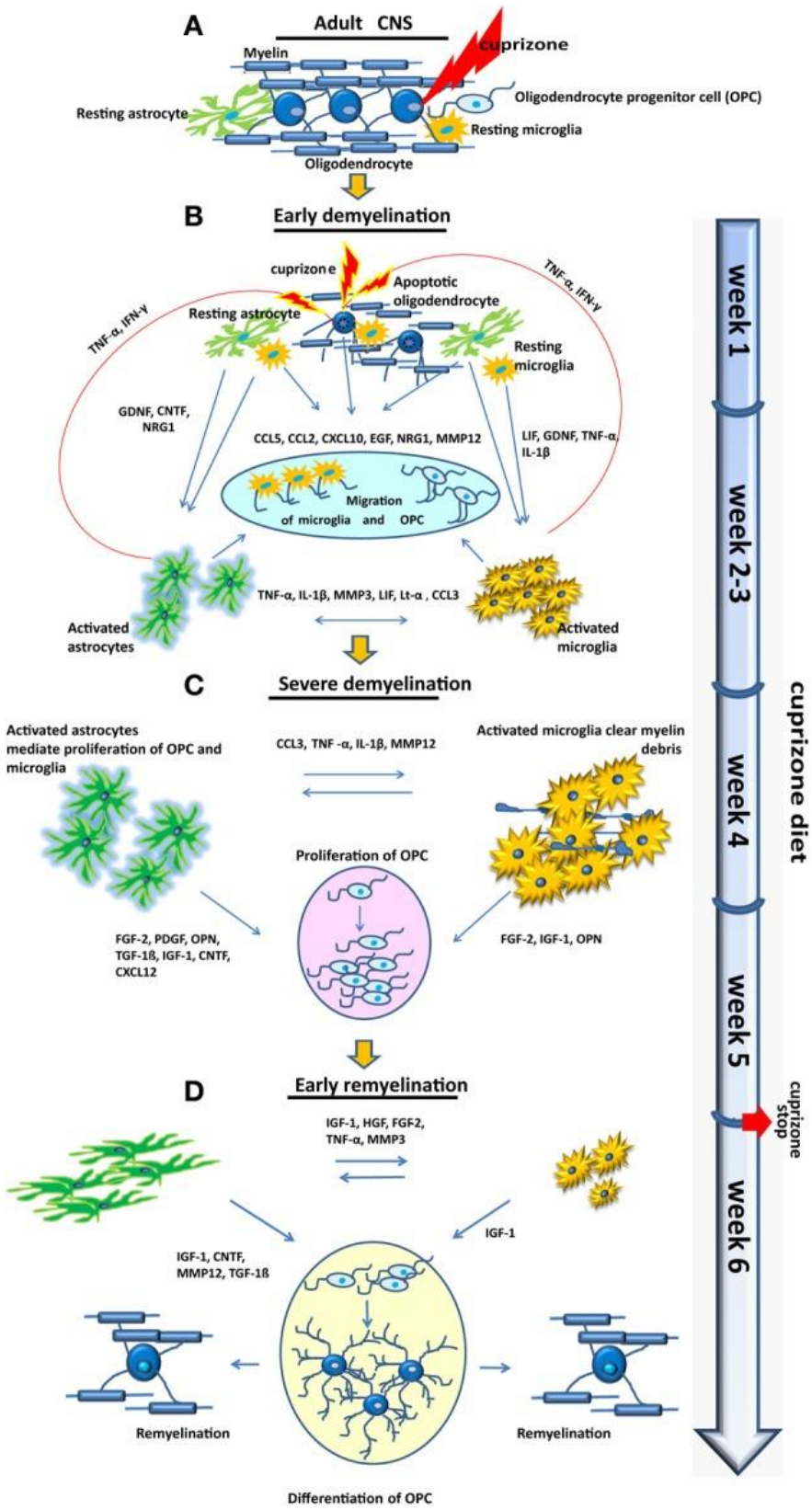
A
Adult CNS
Myelin
cuprizone
Oligodendrocyte progenitor cell (OPC)
Resting astrocyte
Resting microglia
Oligodendrocyte
B
Early demyelination
cuprizone
Apoptotic oligodendrocyte
TNF-α, IFN-γ
TNF-α, IFN-γ
Resting astrocyte
Resting microglia
GDNF, CNTF, NRG1
CCL5, CCL2, CXCL10, EGF, NRG1, MMP12
LIF, GDNF, TNF-α, IL-1β
Migration of microglia and OPC
TNF-α, IL-1β, MMP3, LIF, Lt-α , CCL3
Activated astrocytes
Activated microglia
C
Severe demyelination
Activated astrocytes mediate proliferation of OPC and microglia
CCL3, TNF -α, IL-1β, MMP12
Activated microglia clear myelin debris
Proliferation of OPC
FGF-2, PDGF, OPN, TGF-1ß, IGF-1, CNTF, CXCL12
FGF-2, IGF-1, OPN
D
Early remyelination
IGF-1, HGF, FGF2, TNF-α, MMP3
IGF-1
IGF-1, CNTF, MMP12, TGF-1ß
Remyelination
Remyelination
Differentiation of OPC
week 1
week 2-3
week 4
week 5
week 6
cuprizone diet
cuprizone stop

Figure 16. Cellular and molecular response in the medial corpus callosum during cuprizone-induced de- and remyelination. **(A)** Distribution of glial cells under normal conditions. **(B)** Weeks 1–3, "early demyelination." Mature oligodendrocytes begin to undergo apoptosis already during the first week of cuprizone feeding. Microglia are highly motile cells. They may detect apoptotic oligodendrocytes and initiate together with astrocytes numerous inflammatory and probably also reparative processes. Various chemokines, cytokines, and growth factors, promoting attraction and activation of microglia and astrocytes but also migration of OPC are produced during the first week of cuprizone treatment. In the next 2 weeks of the "early demyelination" period inflammatory cytokines are already slightly up-regulated and maintain the inflammatory cycle by further promoting activation and proliferation of astrocytes and microglia but probably harming oligodendrocytes as well. Oligodendrocytes are almost completely depleted at week 3 of cuprizone treatment. **(C)** Weeks 3.5–5, "severe demyelination." Activated microglia begin to clear myelin debris. Several matrix metalloproteinases (MMP), chemokines, cytokines, and growth factors produced by activated astrocytes and microglia are supporting phagocytosis and promoting proliferation of OPC. At week 5 nearly all axons in the medial corpus callosum are demyelinated. **(D)** Weeks 5–6 "early remyelination." In this week the amount of activated microglia begins to decline. Astrocytes are still activated but change their morphology. OPC differentiate and begin to remyelinate nude axons (Gudi, Gingele et al. 2014).

To overcome disadvantages of *in vitro* and *in vivo* models, *ex vivo* models based on organotypic cultures have been established. Myelination in such cultures was first examined in 1956 (Hild 1956). Since then, the technique was further developed to investigate different brain areas and organotypic cultures have been characterized and adapted to study myelination, demyelination and remyelination (Zhang, Jarjour et al. 2011). According to this characterization, organotypic culture myelination occurs readily and it is extensive by 10 days *in vitro* (DIV). After exposure to a demyelinating stimulus, remyelination process takes place since OPC are present in slice cultures. Thus organotypic cultures mimic *in vivo* processes and are a suitable model to study myelin status in different conditions.

AIM

Prion disorders are a group of rare, fatal and progressive neurodegenerative disorders affecting both humans and animals. Among all neurodegenerative diseases, prion disorders are of prominent biological and pathological interest since they have genetic, sporadic and infectious origin. The infectious agent derives from PrP^{C}, the endogenously encoded protein (Prusiner 2001). Upon conformational conversion, PrP^{C} gives rise to the prion, or PrP^{Sc}, enriched in β-sheets and prone to aggregate (Caughey and Raymond 1991, Gasset, Baldwin et al. 1993). There is an ongoing debate about the nature of the neurotoxicity observed in prion diseases. According to the gain of toxic function hypothesis, the prion pathology is attributable to novel toxic properties acquired by PrP^{Sc} (Harris and True 2006, Westergard, Christensen et al. 2007, Linden, Martins et al. 2008, Winklhofer, Tatzelt et al. 2008). However, PrP^{Sc} alone is not sufficient to induce prion disease (Bueler, Aguzzi et al. 1993, Brandner, Isenmann et al. 1996, Hill and Collinge 2003). Therefore, it has been proposed that PrP^{C} protective activity may be lost upon conversion to or contact with PrP^{Sc}. This PrP^{C} loss-of-function would then cause neurodegeneration. Arguing against this second hypothesis, genetic ablation of *Prnp* expression has relatively little phenotypic effect and does not induce prion disease by itself. Both gain-of-function and loss-of-function may act to cause the disease. PrP^{Sc} toxic function may perturb PrP^{C} protective function, exacerbating the pathology (Harris and True 2006, Westergard, Christensen et al. 2007, Linden, Martins et al. 2008, Winklhofer, Tatzelt et al. 2008). Understanding physiological function of PrP^{C} may help to disclose pathological and disease-related phenotypes, as well as to propose new curative strategies. Despite many efforts have been done in the past years, PrP^{C} physiological function has not been completely defined (Aguzzi, Baumann et al. 2008). To unveil PrP^{C} function, several KO and transgenic mouse models have been generated. At a first look, PrP^{c}-deficient mice develop normally but, at a deeper analysis, many subtle phenotypic changes have been reported. A striking property of PrP^{C} is its ability to bind divalent cations such as copper (Stockel, Safar et al. 1998, Jackson, Murray et al. 2001, Singh, Das et al. 2010). PrP^{C} is able to support copper reduction from Cu(II) to Cu(I) (Liu, Jiang et al. 2011) and it may have superoxide dismutase activity, protecting cells from oxidative damage (Brown, Wong et al. 1999, Brown, Clive et al. 2001). PrP^{c} and copper cooperatively protect neurons from excitotoxicity by mediating NMDAR inhibition through S-nitrosylation (Gasperini, Meneghetti et al. 2015). Other studies report a PrP^{c} protective role against programmed cell death (Kuwahara, Takeuchi et al. 1999) and Bax-mediated apoptosis (Bounhar, Zhang et al. 2001, Didonna, Sussman et al. 2012). PrP^{c} is also a cell-

surface receptor coupled to the tyrosine kinase Fyn for signal transduction (Mouillet-Richard, Ermonval et al. 2000, Aguzzi, Baumann et al. 2008), it plays a role in circadian rhythm, spatial learning, neurite outgrowth, phagocytosis and inflammatory response, hematopoietic-stem-cell renewal and neural-stem-cell differentiation (Caughey and Baron 2006, Aguzzi, Baumann et al. 2008). Besides, PrP^C is involved in the maintenance of PNS myelination as observed in PrP^C-null mice that, after an initial formation of morphologically normal PNS myelin, show a long-term myelin maintenance disruption (Bremer, Baumann et al. 2010, Benvegnu, Gasperini et al. 2011). Neuronal PrP^C expression is sufficient to prevent peripheral myelin degeneration, probably mediating axon to Schwann cells communication (Bremer, Baumann et al. 2010, Benvegnu, Gasperini et al. 2011). Differently, PrP^C absence does not affect CNS myelin maintenance. Only the expression of PrP^C mutants lacking the HC domain can trigger demyelination (Shmerling, Hegyi et al. 1998, Baumann, Tolnay et al. 2007, Li, Christensen et al. 2007, Bremer, Baumann et al. 2010). However, the possibility that subliminal myelin pathologies might extend to central myelin in *Prnp*$^{0/0}$ mice was not excluded. Indeed, PrP^C is involved in many processes that may influence myelin formation and maintenance. Firstly, its absence increases OPC proliferation and delays their maturation. Secondly, PrP^C is involved in metal homeostasis and modulates oxidative stress. Both processes must be tightly regulated to prevent myelin structural or functional impairments (Zimmerman, Matthieu et al. 1976, Bongarzone, Pasquini et al. 1995, Matsushima and Morell 2001, Beard and Connor 2003, Bizzozero, DeJesus et al. 2004, Encinas, Manganas et al. 2005, Liu, Chen et al. 2005, Morelli, Ravera et al. 2012, Skjørringe, Møller et al. 2012, Aspli, Flaten et al. 2015).

In light of these considerations, this thesis is aimed to deeper investigate the role of PrP^C in CNS myelination. Taking advantage from *Prnp*$^{+/+}$ and *Prnp*$^{0/0}$ mice, myelin composition was evaluated in mouse brains at different developmental stages, from early postnatal days to aging: neonatal (postnatal day 1 (P1)), early postnatal (P7), young (P14), end of the development-early adulthood (P30), adulthood (P90), late adulthood (P180), early aging (P365) and late aging (P450). In particular, cholesterol content and myelin-related proteins and genes were investigated in both *Prnp*$^{+/+}$ and *Prnp*$^{0/0}$ mice. Myelin morphology was investigated on *corpus callosum* by using transmission electron microscopy. The effects of PrP^C absence on CNS myelin formation and maintenance was compared with those identified in the SN. To better investigate PrP^C role in CNS myelin, an *ex vivo* model based on OHC was established and validated. This system showed a good correlation with *in vivo* observations for studying myelination-demyelination-remyelination.

MATERIALS AND METHODS

ANIMALS

Inbred FVB/N *Prnp*$^{+/+}$ and FVB *Prnp*$^{0/0}$ male mice were used in these experiments. The FVB *Prnp*$^{0/0}$ mice were obtained by backcrossing the original ZurichI *Prnp*$^{0/0}$ mice (Bueler, Fischer et al. 1992) to FVB/N inbred mice for more than 20 generations (Lledo, Tremblay et al. 1996). All experiments were performed in accordance with European regulations [European Community Council Directive, November 24, 1986 (86/609/EEC)] and were approved by the local authority veterinary service. All efforts were made to minimize animal suffering and to reduce the number of animals used. P1 to P14 animals were sacrificed by decapitation, while adult mice were killed by cervical dislocation. P180 and P365 mice used for electron microscopy studies were deeply anesthetized with CO2 and transcardially perfused. After the animal sacrifice, brains and SNs were extracted, immediately frozen in liquid nitrogen and stored at -80 °C. Samples were collected at the following developmental stages: P1, P7, P14, P30, P90, P180, P365 and P450. P1, P7 and P14 were considered developmental stages, P30 end of the development-early adulthood, P90 adulthood, P180 late adulthood, P365 early aging and P450 late aging.

TISSUE HOMOGENIZATION AND MEMBRANE PURIFICATION

Brains and SNs were homogenized in MES Buffer (25 mM pH 7.0, 2 mM EDTA, 5 mM NaF, 0.5 mM Na_3VO_4, proteases inhibitors cocktail (Inhibitor complete mini, Roche Diagnostics Corp., Mannheim, Germany)), (Sodero, Vriens et al. 2012). Samples were cleared by centrifugation (2000 g, 10 min, 4 °C) and supernatants were considered as total extracts. To purify the membrane fraction, part of the total extract was further centrifuged at 100000 g for 45 min at 4 °C (Optima Max Ultracentrifuge, Beckman Instruments). The resulting pellet was washed with MES Buffer and centrifuged again at 100000 g for 45 min at 4 °C. The membrane containing pellet was re-suspended in MES Buffer and briefly sonicated. As control, a different method for membrane purification was also used. P30 mouse brains were homogenized in Isotonic Buffer (0.32 M sucrose, 0.5 mM $MgSO_4$, 2 mM 2-Mercaptoethanol, 1 mM EDTA, 10 mM Hepes-KOH pH 7.4, proteases inhibitors cocktail, 5 mM NaF, 0.5 mM Na_3VO_4). Samples were

further processed as described for MES Buffer and membrane pellet was re-suspended in 10 mM Hepes-KOH pH 7.4, 1.5% SDS, proteases inhibitors cocktail, 5 mM NaF, 0,5 mM Na_3VO_4. Protein concentration was determined by bicinchoninic acid (BCA) assay (Sigma-Aldrich).

ENZYMATIC CHOLESTEROL

Brain and SN cholesterol level was assessed by fluorometric detection using a commercial available kit (Amplex Red Cholesterol Assay Kit, Molecular Probes, Invitrogen). Briefly, cholesteryl esters were hydrolyzed by cholesterol esterase into cholesterol, which was then oxidized using cholesterol oxidase to yield hydrogen peroxide and the corresponding ketone product. Hydrogen peroxide was then detected using 10-acetyl-3,7-dihydroxyphenoxazine. This compound, in the presence of horseradish peroxidase (HRP), reacts with hydrogen peroxide to produce highly fluorescent resorufin. Fluorescence was measured in a fluorescence microplate reader (SpectraMax M5, Molecular Devices) using excitation and emission wavelength of 544 nm and 590 nm respectively. The equivalent of 3 µg of total brain proteins and 0.5 µg of total SN proteins were loaded in the plate. As reference, a cholesterol standard curve was prepared with cholesterol concentration from 0 to 8 µg/ml. Background correction was applied by subtracting the value derived from the no-cholesterol control.

PROTEIN EXPRESSION ANALYSIS

Proteins expression was measured by Western blot (WB) in SN, brain and OHC. For each sample, the same protein amount (4-20 µg) was separated by SDS–PAGE in 12% polyacrylamide gels. On each gel, *Prnp*$^{+/+}$ and *Prnp*$^{0/0}$ samples were loaded, in order to compare them. Commonly, proteins were denaturated 15 min at 60 °C in loading buffer (10% glycerol, 50mM TrisHCl pH 6.8, 2% w/v SDS, 4M Urea, 0.005% bromophenol blue). Proteins were transferred on nitrocellulose and after 1h in blocking solution membranes were incubated overnight at 4°C with the primary antibody. After incubation with the secondary antibody, membranes were developed with ECL detection reagent (GE Healthcare, Waukesha, WI, USA) and recorded by the digital imaging system Alliance 4.7 (UVITEC, Cambridge, UK). Bands quantification was performed with Uviband 15.0 software (UVITEC, Cambridge, UK). Each protein signal

was normalized against β-Actin for total homogenate samples or against Flotillin-1 for membrane samples.

ANTIBODIES

The following primary antibodies were used in TBST (Tris-Buffered Saline plus Tween 20) + 5% milk: anti-β-Actin Peroxidase (AC-15) 1:10000 (A3854, Sigma-Aldrich); anti-Flotillin-1 (18) 1:1000 (610821, BD Biosciences), anti-Myelin PLP 1:1000 (AB28486, Abcam), anti-MAG 1:1000 (AB89780, Abcam), anti-MOG 1:1000 (AB32760), anti-MPZ 1:10000 (AB31851, Abcam). The following primary antibody was used in TBST + 5% bovine serum albumin (BSA): anti-MBP 1:500 (AB980, Millipore).

RNA EXTRACTION AND TEAL TIME PCR

To check the expression of myelin-related genes, mRNA was extracted from brains and SNs of four *Prnp*$^{+/+}$ and four *Prnp*$^{0/0}$ mice at P30, P180 and P365. Besides, mRNA was extracted from 4 independent sets of *Prnp*$^{+/+}$ and *Prnp*$^{0/0}$ OHC after 28 DIV, where each set was composed of around 20 or more hippocampal slices. Frozen samples were homogenized in TRIzol reagent (15596018, Invitrogen) and total RNA was extracted following the TRIzol reagent manufacturer's instructions. To limit genomic DNA contamination, samples were treated with RNase free DNase set (79254, Qiagen, Germantown, MD, USA) and purified using the RNeasy mini kit (74104, Qiagen). RNA quantification was performed using a NanoDrop 2000 spectrophotometer (Thermo Scientific). RNA quality was assessed by observing on 1% agarose gel the two characteristic bands corresponding respectively to 28S and 18S rRNA. RNA was retrotranscribed by using SuperScriptIII RT (18080, Invitrogen) and oligodT primer (5'-GCT GTC AAC GAT ACG CTA CGT AAC GGC ATG ACA GTG$(T)_{24}$-3'). In parallel, for each sample a negative control was carried along by omission of the reverse transcriptase (RT-) to check the presence of genomic contamination. All the primer sequences reported in Table 4 were tested by PCR and analyzed on a 2% agarose gel to verify their specificity for the genes of interest. Quantitative real time PCR was performed adding 2 ng RNA equivalent to the reaction mix including 2× iQ™ SYBR® Green Supermix (Bio-Rad Laboratories, Inc.) and 400 nM of the corresponding forward and reverse primer (Sigma) on an iQ5 Multicolor Real-Time PCR Detection System (Bio-Rad Laboratories, Inc.). After initial denaturation for 3 min at 95°C, 40 cycles were

performed at 95°C for 15 sec and 60°C for 1 min. The expression of the gene of interest was normalized to housekeeping gene glyceraldehyde 3-phosphate dehydrogenase (Gapdh) and β-actin, and the initial amount of the template of each sample was determined as relative expression *versus* housekeeping gene chosen as reference. The relative expression of each sample was calculated by the formula $2exp^{-\Delta\Delta Ct}$ (User Bulletin 2 of the ABI Prism 7700 Sequence Detection System) (Livak and Schmittgen 2001). Housekeeping gene expression is not modified under the present experimental conditions (data not shown).

Target	Primer name	Primer sequence (5'-3')	Amplicon size base pairs)	Accession number	Reference
Gapdh	Gapdh_fw	Forward TTCACCACCATGGAGAAGGC	237	NM_001289726.1	Chen et al., 2003
	Gapdh_rev	Reverse GGCATGGACTGTGGTCATGA			
Actb	βact_fw	Forward CACACCCGCCACCAGTTC	164	NM_007393.5	Grison et al., 2014
	βact_rev	Reverse CCCATTCCCACCATCACACC			
Plp (transcript variant 1-2-3)	Plp1DM20_wang_fw	Forward GGTACAGAAAAGCTAATTGAGACC	93	NM_011123.3 NM_001290561.1 NM_001290562.1	Wang et al., 2008
	Plp1DM20_wang_rev	Reverse GATGACATACTGGAAAGCATGA			
Plp (transcript variant 1-3)	Plp1_wang_fw	Forward GTTCCAGAGGCCAACATCAAGCTC	118	NM_011123.3 NM_001290562.1	Wang et al., 2008
	Plp1_wang_rev	Reverse AGCCATACAACAGTCAGGGCATAG			
Plp (transcript variant 2)	DM20_elisa_fw	Forward CTTCCTTTATGGGGCCCTCC	126	NM_001290561.1	Designed
	DM20_elisa_rev	Reverse GTGATGCCCACAAACGTTGC			
Mbp	MBP_fw	Forward CACACACGAGAACTACCCA	115	NM_001025251.2	Pernet at al., 2008
	MBP_rev	Reverse GGTGTTCGAGGTGTCACAA			
Mag short splice variant, S-Mag)	MAG_elisa_fw	Forward CTGAGAGCCCCAGGAGAGTGA	126	NM_010758.2	Designed
	MAG_elisa_rev	Reverse TTGGTGGGTCGTTTTCCCAG			
Mag (L-Mag)	LMAG_elisa_fw	Forward TCAGATCGTCCAACCTTCTGTG	117	NM_010758.2	Designed
	LMAG_elisa_rev	Reverse TCTCCCTGAGTTGGGGATGT			
Mog	MOG_elisa_fw	Forward TGCCCTGCTGGAAGATAACA	135	NM_010814.2	Designed
	MOG_elisa_rev	Reverse CTCAAAAGGGGTTTCTTAGCTCT			
Mpz	MPZ_fw	Forward CGGACAGGGAAATCTATGGTGC	106	NM_008623.5	Fontana et al., 2012
	MPZ_rev	Reverse TGGTAGCGCCAGGTAAAAGAG			
Cspg4 (NG2)	NG2_fw	Forward GCATCATCATTCCGGTGTGC	113	NM_139001.2	Designed
	NG2_rev	Reverse GGTCAACACCTGGACATCGT			
Sox10	Sox10_bank_fw	Forward AGGTTGCTGAACGAAAGTGAC	102	NM_011437.1	www.nature.com/nature/journal/v464/n7288/extref/nature08816-s3
	Sox10_bank_rev	Reverse CCGAGGTTGGTACTTGTAGTCC			
Tubb3	βIIITub_fw	Forward CGCCTTTGGACACCTATTC	240	NM_023279.2	Simonetti et al., 2008
	βIIITub_rev	Reverse TACTCCTCACGCACCTTG			
Rbfox3 (NeuN)	NeuNRbfox3_fw	Forward CCAGGCACTGAGGCCAGCACACAGC	111	NM_001039167.1	Kim et al., 2009
	NeuNRbfox3_rev	Reverse CTCCGTGGGGTCGGAAGGGTGG			

Table 4. Primer list for qRT-PCR experiments.

ELECTRON MICROSCOPY

P180 and P365 *Prnp*$^{+/+}$ and *Prnp*$^{0/0}$ mice were transcardially perfused with saline solution followed by 4% paraformaldehyde (PFA) in in 0.12 M phosphate buffer (PB). Brains were removed and fixed with 4% PFA and 2% glutaraldehyde in 0.12 M PB. Tissues were post-fixed with 1% osmium tetroxide and embedded in Epon (Fluka). Semithin and ultrathin sections were obtained as described in (Quattrini, Previtali et al. 1996). Ultrathin sections (70–90 nm thick) were stained with uranile acetate and lead citrate and examined by electron microscopy.

ORGANOTYPIC HIPPOCAMPAL CULTURES PREPARATION

As an *ex vivo* model of myelination, roller-tube OHC preparation protocol was set up based on Gahwiler's protocol (Gahwiler, Capogna et al. 1997). Briefly, P5 mice were sacrificed and hippocampi were dissected in aseptic condition in dissection medium (Gey's balanced salt solution, 5.6 mM D-Glucose (G8270, Sigma-Aldrich), 1 mM kynurenic acid (K3375, Sigma-Aldrich)). Hippocampi were sliced by means of a tissue chopper into 300 µm thick sections. After rinsing in dissection medium for 40 min at 4 °C, slices showing an intact hippocampal cytoarchitecture were selected and singularly attached to a coverslip by embedding in a chicken plasma (P3266, Sigma-Aldrich) and thrombin (112374, Merck KGaA, Darmstadt, Germany) cloth. After 45 min at room temperature (RT), coverslips were placed into flat-sided tubes (NUNC) with a medium composed by 50% basal medium Eagle (BME, 41010026, Gibco, Carlsbad, CA, U.S.), 25% horse serum (26050-088, Gibco), 25% Hank's balanced salt solution (24020141, Gibco), 5.6mM D-Glucose, 2mM L-Glutamine (25030-032, Gibco). OHC were maintained at 37 °C in slow rotation (ten revolutions per hour) up to 28 DIV, when they were collected, immediately frozen in liquid nitrogen and stored at -80 °C.

ORGANOTYPIC HIPPOCAMPAL CULTURES CUPRIZONE TREATMENT

The copper chelator CZ (14690, Sigma-Aldrich) was freshly dissolved 1 mM in OHC medium with 0.25% ethanol and filter-sterilized. The proper dissolution of CZ was monitored by adding copper sulfate (C2284, Sigma-Aldrich) to CZ-containing medium and recording the CZ[Cu(II)] complex absorption at

600 nm (Benetti, Ventura et al. 2010). After 14 DIV, OHC were exposed to CZ-containing medium or to control medium (OHC medium with 0.25% ethanol) for 7 days. At 21 DIV, the same treatment was repeated with freshly prepared CZ-containing or control medium. Control and CZ-treated OHC were collected at 28 DIV, immediately frozen in liquid nitrogen and stored at -80 °C.

MTS CELL VIABILITY ASSAY

To evaluate the effect of CZ treatment on cell viability, the MTS (3-(4,5-dimethylthiazol-2-yl)-5-(3-carboxymethoxyphenyl)-2-(4-sulfophenyl)-2H-tetrazolium) assay was performed on OHC after 14 days of 1 mM CZ exposure. The MTS assay was set up according to manufacturer instruction, with a few modifications necessary for roller-tube OHC. MTS powder was dissolved in phosphate-buffered saline (PBS) to 2 mg/ml to produce a clear golden-yellow solution. PES (phenazine ethosulfate) powder was dissolved in MTS solution to 0.21 mg/ml. Finally pH was adjusted to 6.0 to 6.5 using 1N HCl. The solution was filter-sterilized through a 0.2 µm filter into a sterile, light protected container. After 14 days of 1 mM CZ exposure, OHC were washed with PBS and incubated with 0.33 mg/ml MTS in OHC medium for 3 h at 37 °C. OHC medium containing the soluble formazan product produced by viable cells was collected and 200 µl were placed in a 96-well plate. Absorbance values were measured at 490 and 650 nm. The 650 nm absorbance value was used as background, hence subtracted to the 490 nm signal. Cell viability was expressed as percentage of the control OHC value that was considered to be 100% viable and compared by t-Test. After MTS assay, OHC were washed one time with PBS, collected and immediately frozen in liquid nitrogen. OHC were stored at -80 °C for further use.

STATISTICAL ANALYSES

All the results concerning mouse SN and brain were compared between *Prnp*$^{+/+}$ and *Prnp*$^{0/0}$ samples performing the Student's t-Test setting two-tailed distribution and two-sample unequal variance. For OHC experiments, 20 or more OHC slices of the same genotype and treatment were pulled together to be analyzed in one experimental replicate. Each pull was analyzed multiple times (technical replicates) during the same experimental replicate. The results of these technical replicates were compared between *Prnp*$^{+/+}$ and *Prnp*$^{0/0}$ samples performing the Student's t-Test setting two-tailed distribution and

two-sample unequal variance. Finally, the results of different experimental replicates were compared by performeing the paired Student's t-Test setting two-tailed distribution.

RESULTS

ANALYSIS OF PERIPHERAL NERVOUS SYSTEM MYELINATION IN *Prnp*$^{+/+}$ AND *Prnp*$^{0/0}$ MICE

PrP^C has been reported to be essential for the maintenance of peripheral nervous system myelination (Bremer, Baumann et al. 2010, Benvegnù, Gasperini et al. 2011). Therefore some experiments were performed in order to confirm the occurrence of peripheral demyelination in our aged *Prnp*$^{0/0}$ mice. Cholesterol quantification, myelin protein content and gene expression analysis were carried out in *Prnp*$^{+/+}$ and *Prnp*$^{0/0}$ mouse SN. Measurements were done at different developmental stages to monitor PNS myelin status from early postnatal days to aging.

SCIATIC NERVE CHOLESTEROL CONTENT

Cholesterol is the only integral myelin component essential for the development of both CNS and PNS myelin (Saher, Quintes et al. 2011). Considering this, cholesterol content was measured as a marker of myelin status in *Prnp*$^{+/+}$ and *Prnp*$^{0/0}$ mouse SN from early postnatal days to aging. Results are expressed as the ratio between *Prnp*$^{0/0}$ and *Prnp*$^{+/+}$ cholesterol content. In PrP^C-null SN, cholesterol is increased at P7 and P14 of about 20% and 10% respectively compared to WT animals (Figure 17). During aging (P365 and P450), cholesterol decreases in *Prnp*$^{0/0}$ SN of about 50% compared to *Prnp*$^{+/+}$ mice.

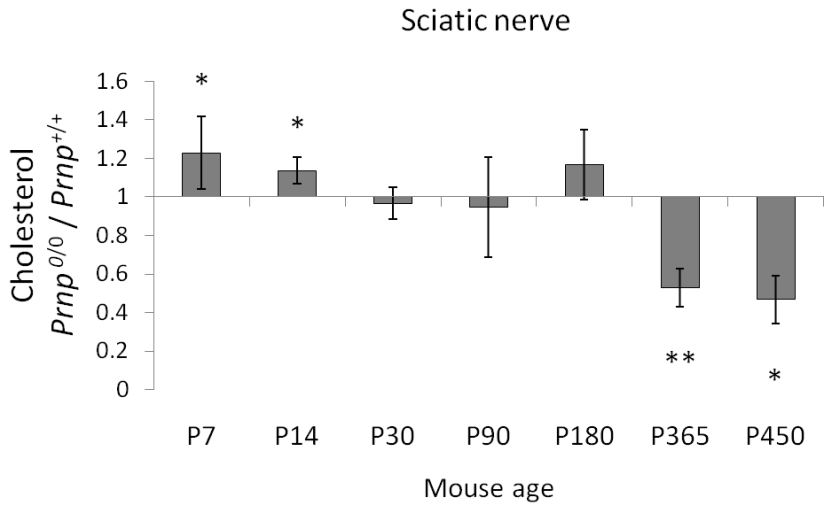

Figure 17. SN cholesterol content at different ages. The graph shows the ratio between *Prnp*$^{0/0}$ and *Prnp*$^{+/+}$ mice. All error bars indicate SD. Sample size: n=4; 3 right limb and 3 left limb SNs are considered n=1 at P7; right limb and left limb SNs are considered n=1 from P14 to P450; *p<0.05, **p<0.01.

MYELIN PROTEIN EXPRESSION ANALYSIS IN SCIATIC NERVES

Expression levels of myelin proteins were analyzed in PNS of both *Prnp*$^{+/+}$ and *Prnp*$^{0/0}$ mice at the different developmental stages. PLP, MBP, MAG and MPZ were analyzed in total SN homogenates. Representative images of bands obtained from WB experiments are shown in Figure 18. β-Actin was used as housekeeping protein for normalizing myelin protein contents. Results are expressed as the ratio between *Prnp*$^{0/0}$ and *Prnp*$^{+/+}$ protein content.

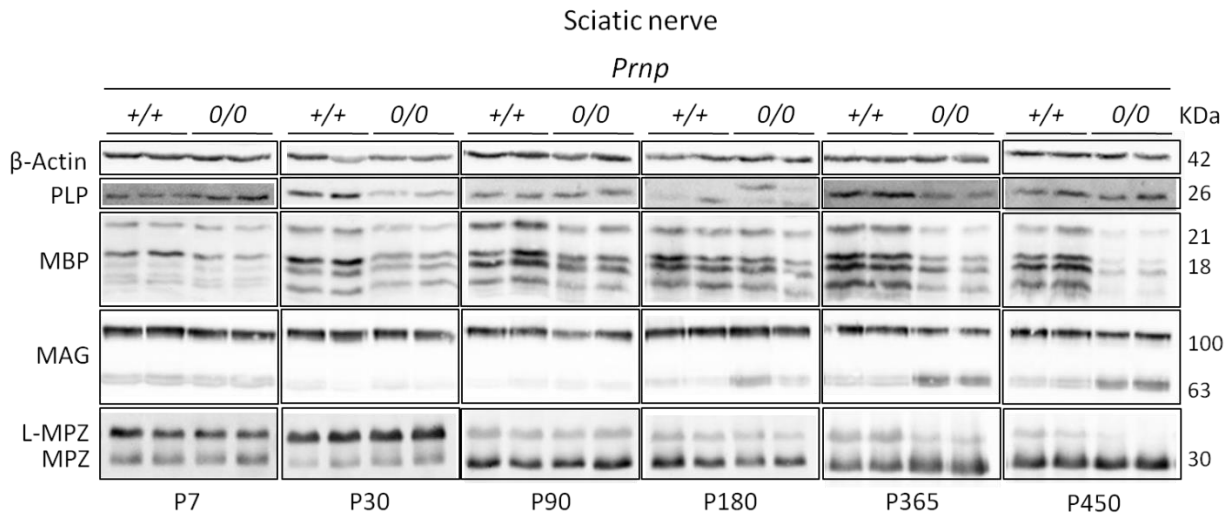

Figure 18. PNS myelin proteins. Representative WB images of PLP, MBP, MAG, MPZ and L-MPZ proteins from *Prnp*$^{+/+}$ and *Prnp*$^{0/0}$ total SN homogenates. The constant level of β-Actin is also shown.

Compared to *Prnp*$^{+/+}$ mice, in *Prnp*$^{0/0}$ SN PLP expression is lower at P30 and P365 (Figure19A), while MBP decreases in the early post-natal days till P30 and during aging (P365 and P450), (Figure 19B). In PrP^{C}-null SN, the expression level of glycosylated MAG is similar to WT SN at all developmental stages (Figure 19C). Differently, in the absence of PrP^{C}, non-glycosylated MAG is considerably increased starting from 3 months of age (Figure 19C). MPZ shows an increasing trend in aged *Prnp*$^{0/0}$ SN, with significant difference at P365 (Figure 19D). Its isoform L-MPZ is reduced in P7 *Prnp*$^{0/0}$ SN and it has a decreasing trend during aging, with significant difference at P450.

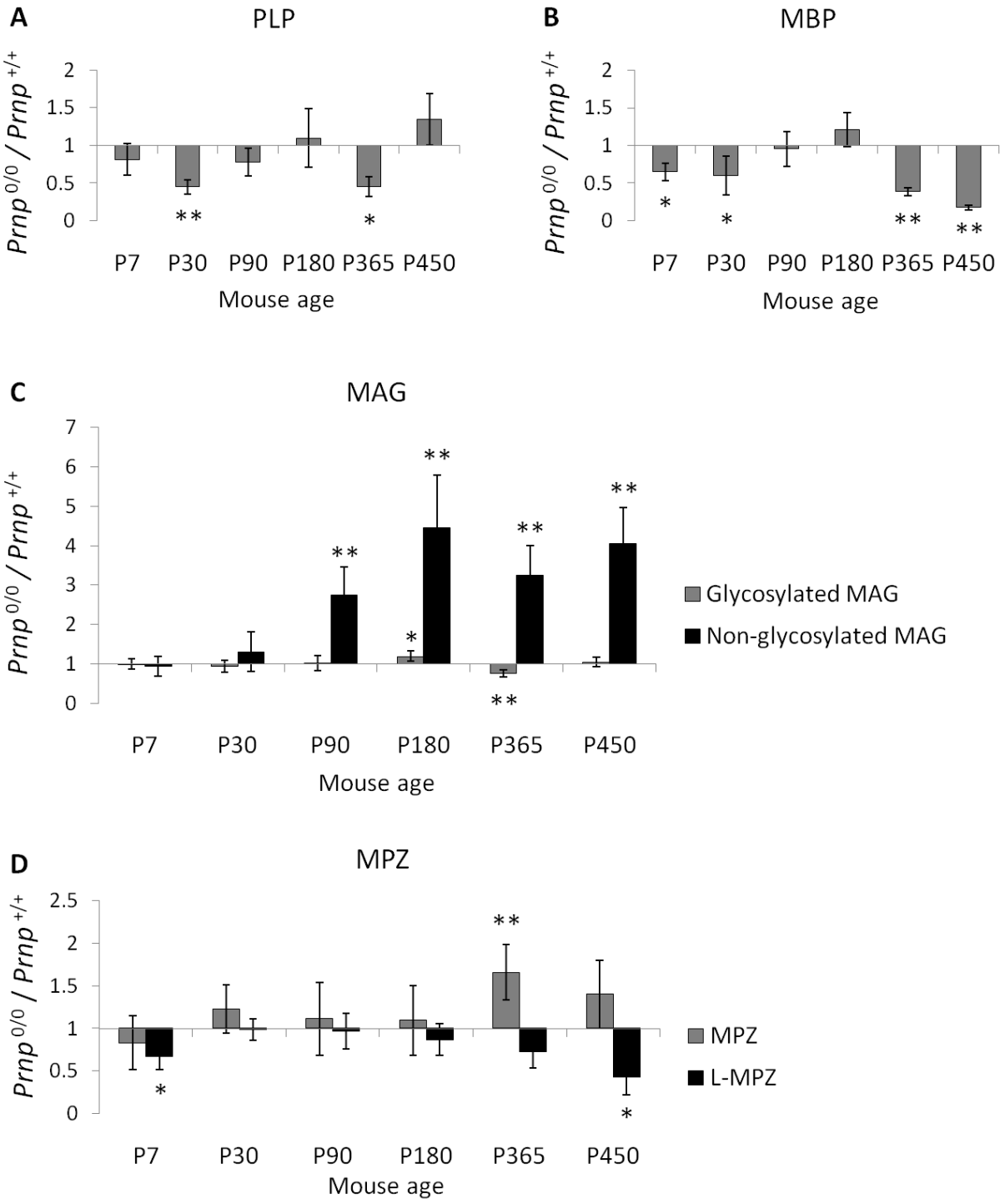

Figure 19. PNS myelin protein expression levels. The graphs show the ratio between *Prnp*$^{0/0}$ and *Prnp*$^{+/+}$ protein content. For each protein, the optical density value was normalized on the housekeeping protein β-Actin. All error bars indicate SD. **(A)** PLP. **(B)** MBP. **(C)** Glycosylated and non-glycosylated MAG. **(D)** MPZ and L-MPZ. Sample size: n=4, 3 right limb and 3 left limb SNs are considered n=1 at P7; right limb and left limb SNs are considered n=1 from P30 to P450; *p<0.05, **p<0.01.

TRANSCRIPTIONAL ANALYSIS OF MYELIN GENES IN THE PNS

To investigate the transcriptional regulation of myelin proteins, qRT-PCR experiments were performed on SN total RNA extracted from P30, P180 and P365 *Prnp*$^{+/+}$ and *Prnp*$^{0/0}$ mice. The following transcripts were analyzed: Plp1 and its splice variant Dm20, Mbp, S-Mag and L-Mag and finally Mpz. Results were normalized on the housekeeping gene β-actin whose expression level is not different in *Prnp*$^{+/+}$ and *Prnp*$^{0/0}$ samples (data not shown). The non-template control (NTC) did not give any amplification result, as well as the RT- reactions. Results are expressed as ΔΔCt relative quantification of *Prnp*$^{0/0}$ *versus* *Prnp*$^{+/+}$ samples and the fold change is reported. At P30, Plp1, S-Mag and Mpz do not present differences between *Prnp*$^{+/+}$ and *Prnp*$^{0/0}$ samples (Figure 20). On the contrary, Dm20, Mbp and L-Mag are significantly decreased in *Prnp*$^{0/0}$ SN. At P180, *Prnp*$^{0/0}$ SN shows a decreased transcription level of Plp1, Dm20 and Mbp. A decreasing trend is visible also for S-Mag, L-Mag and Mpz, though differences are not statistically significant due to the high sample variability. At P365, all analyzed genes present a decreased transcriptional level compared to WT samples, except for L-Mag which does not show any statistically significant difference.

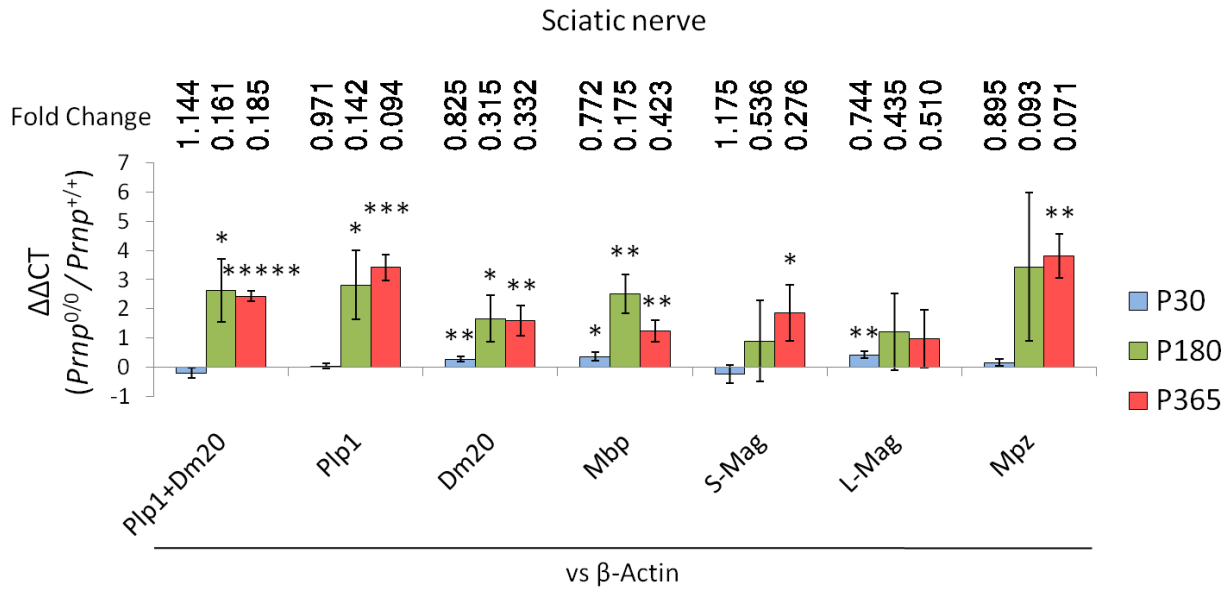

Figure 20. Myelin gene transcription in *Prnp*$^{0/0}$ and *Prnp*$^{+/+}$ SN measured by qRT-PCR. Plp1, Dm20, Mbp, S-Mag, L-Mag and Mpz transcripts were analyzed at P30, P180 and P365. The results were normalized on the housekeeping gene β-actin and are represented as ΔΔCt relative quantification of *Prnp*$^{0/0}$ *versus* *Prnp*$^{+/+}$ samples. All error bars indicate SD. The fold change values, calculated by the formula $2exp^{-\Delta\Delta Ct}$, are reported on the top of each column. Sample size: n=4, right limb and left limb SNs are

considered n=1 from P30 to P450; 3 right limb and 3 left limb SNs are considered n=1 at P7; *p<0.05, **p<0.01, ***p<0.001, *****p<0.00001.

ANALYSIS OF CENTRAL NERVOUS SYSTEM MYELINATION IN *Prnp*$^{+/+}$ AND *Prnp*$^{0/0}$ MICE

While the role of PrP^{C} in the maintenance of PNS myelination has already been proved, a similar role in the CNS is still controversial. *Prnp*$^{0/0}$ mice do not show any gross myelin disturbance, though PrP^{C} absence affects proliferation and maturation of oligodendrocyte precursor cells (Bribián, Fontana et al. 2012). PrP^{C} also modulates two important processes in myelin formation and maintenance as metal homeostasis and oxidative stress (Brown and Sassoon 2002). In this work the role of PrP^{C} in CNS myelination was investigated using *Prnp*$^{+/+}$ and *Prnp*$^{0/0}$ mouse brain. Similarly to PNS, cholesterol content, myelin protein and gene expression analysis were also carried out in the brain. To monitor CNS myelin status from early postnatal days to aging, measurements were done at the different developmental stages previously described.

BRAIN CHOLESTEROL MEASUREMENT

As for the PNS, cholesterol is essential for myelin membrane stability also in CNS. It represents about 30% of the total myelin lipids and approximately 70% of brain cholesterol is associated to myelin sheaths (Baumann and Pham-Dinh 2001). Therefore, cholesterol content was used as a marker of myelin status in *Prnp*$^{+/+}$ and *Prnp*$^{0/0}$ mouse brain from early postnatal days to aging. Results are expressed as the ratio between *Prnp*$^{0/0}$ and *Prnp*$^{+/+}$ cholesterol content. Figure 21 shows a 15% reduction in *Prnp*$^{0/0}$ brain cholesterol at P1 and a not significant slight reduction at P7. Starting from P180, a cholesterol decreasing trend is observed in *Prnp*$^{0/0}$ brains, with significant difference only at P365 (10% cholesterol reduction compared to *Prnp*$^{+/+}$ brains).

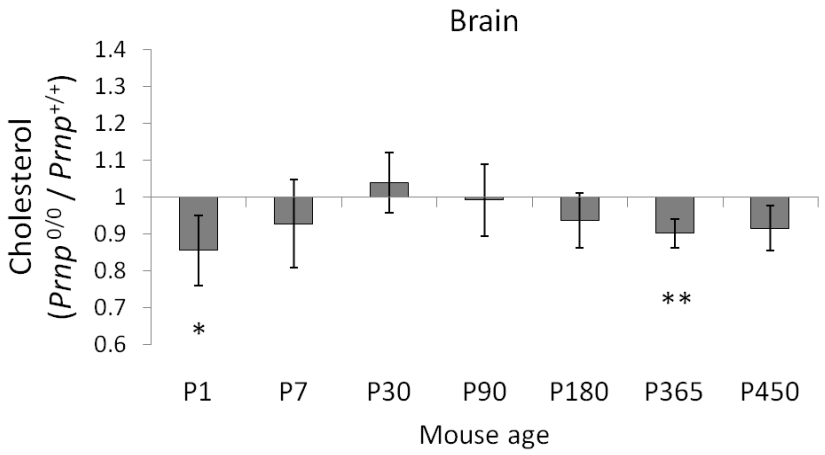

Figure 21. Brain cholesterol content at different ages. The graph shows the ratio between *Prnp*$^{0/0}$ and *Prnp*$^{+/+}$ mice. All error bars indicate SD. Sample size: n=6 at P1 and P7; n=4 from P30 to P450; *p<0.05, **p<0.01.

MYELIN PROTEIN EXPRESSION ANALYSIS IN THE BRAIN

The expression levels of the most important proteins for CNS myelination were analyzed in *Prnp*$^{+/+}$ and *Prnp*$^{0/0}$ brains at different ages. In particular the following proteins were investigated: PLP, MBP, MAG and MOG.

Noteworthy, protein expression analysis of total brain homogenates prepared in MES buffer did not reveal significant differences between *Prnp*$^{+/+}$ and *Prnp*$^{0/0}$ mice, showing high sample variability (data not shown).

Since myelin is composed of membranes enwrapping axons, membrane extracts were used for analyzing myelin proteins in *Prnp*$^{+/+}$ and *Prnp*$^{0/0}$ samples. Figure 22 shows representative images of bands obtained from WB experiments with membrane extracts, including the housekeeping protein Flotillin-1.

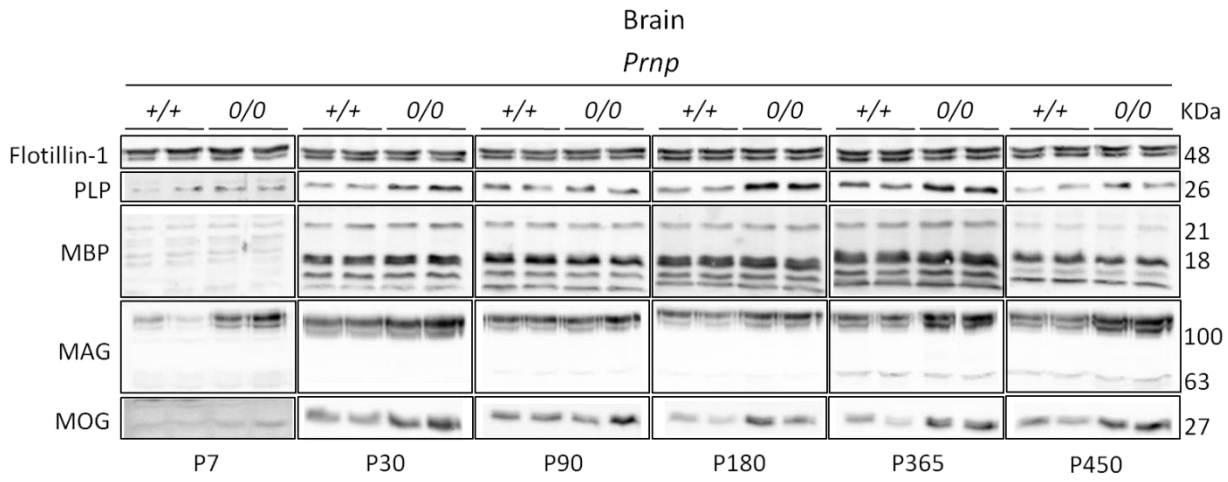

Figure 22. CNS myelin proteins. Representative WB images of PLP, MBP, MAG and MOG proteins from *Prnp*$^{+/+}$ and *Prnp*$^{0/0}$ brain membrane extracts. The constant level of Flotillin-1 is also represented.

In PrP^{C}-null membrane extracts, PLP is increased at all ages (Figure 23A) and MBP is increased at P1 and P365 (Figure 23B). In the absence of PrP^{C}, the level of MOG protein increases at all the ages except at P90 (Figure 23C). Conversely from PNS, non-glycosylated MAG is not altered in PrP^{C}-null brains, while the glycosylated form is increased at all ages except at P90 (Figure 23D). Although the non-glycosylated MAG has a low expression level, it is increased only in P7 *Prnp*$^{0/0}$ mice compared to WT controls (Figure 23D).

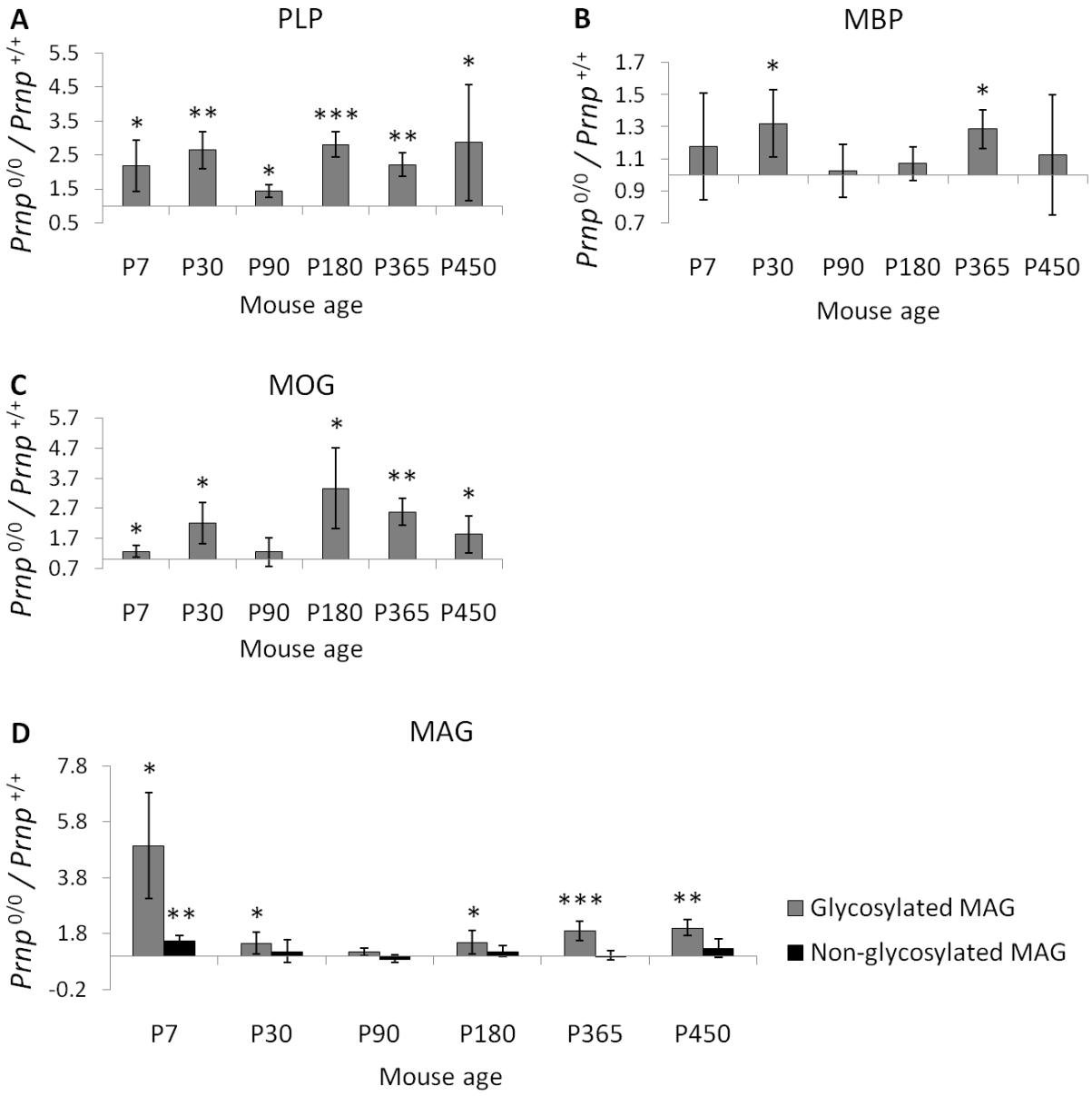

Figure 23. CNS myelin protein expression levels. The graphs show the ratio between *Prnp*$^{0/0}$ and *Prnp*$^{+/+}$ protein content measured in brain membrane-enriched fractions. For each protein, the optical density value was normalized on the housekeeping protein Flotillin-1. All error bars indicate SD. **(A)** PLP. **(B)** MBP. **(C)** MOG. **(D)** Glycosylated and non-glycosylated MAG. Sample size: n=4; *p<0.05, **p<0.01, ***p<0.001.

To exclude the dependence of these results on the membrane extraction protocol, another method based on Isotonic Buffer was applied. To reduce the number of required animals, this control experiment was performed only using P30 mice. PLP, MBP and MAG were measured and images of

bands obtained from WB experiments are shown in Figure 24A, including the housekeeping protein Flotillin-1. As previously described, PLP is higher in PrP^{C}-null brain than in WT mice (Figure 24B). MBP and MAG follow the same increasing trend, but the difference is not statistically significant due to the high sample variability (p=0.199 and p=0.066 respectively) (Figure 24B).

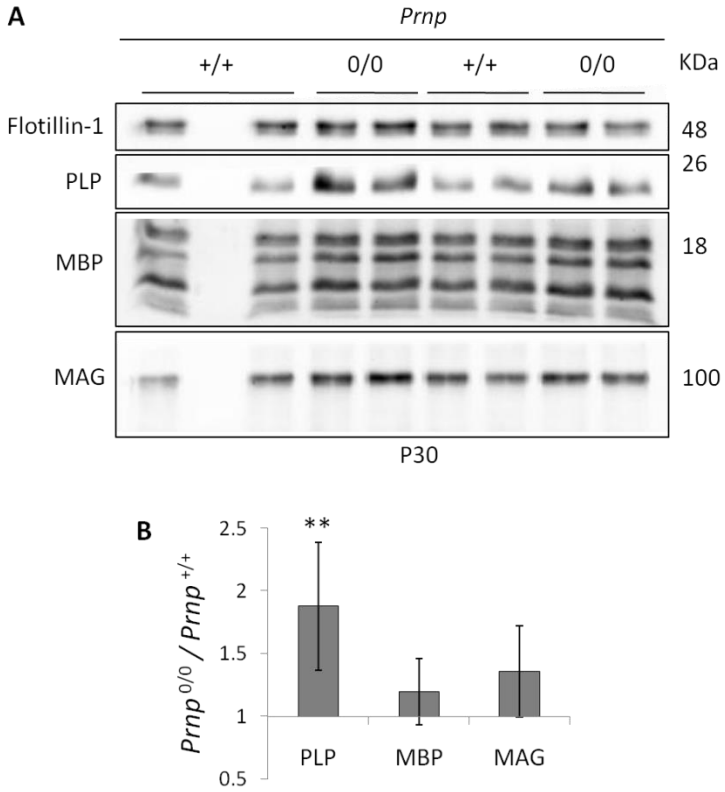

Figure 24. CNS myelin protein expression in P30 membrane fractions extracted in Isotonic Buffer. (A) Representative Western blot images of PLP, MBP and MAG in *Prnp*$^{+/+}$ and *Prnp*$^{0/0}$ brain membrane extracted in Isotonic Buffer. The housekeeping protein Flotillin-1 is also shown. **(B)** PLP, MBP and MAG quantification represented as a ratio between *Prnp*$^{0/0}$ and *Prnp*$^{+/+}$ protein content measured in Isotonic Buffer brain membrane-enriched fractions. For each protein, the optical density value was normalized on the housekeeping protein Flotillin-1. All error bars indicate SD. Sample size: n=4; **p<0.01.

TRANSCRIPTIONAL ANALYSIS OF GENES INVOLVED IN CNS MYELINATION

Prnp$^{0/0}$ mice showed a general myelin protein overexpression compared to *Prnp*$^{+/+}$. To investigate the role of transcription on myelin protein overexpression, qRT-PCR experiments were performed on total RNA extracted from P30, P180 and P365 *Prnp*$^{+/+}$ and *Prnp*$^{0/0}$ mouse brains. The following transcripts were analyzed: Plp1 and its splice variant Dm20, Mbp, Mog, S-Mag and L-Mag. Results were normalized on two housekeeping genes (β-actin and Gapdh) whose expression levels are not different in *Prnp*$^{+/+}$ and *Prnp*$^{0/0}$ samples (data not shown). The NTC did not give any amplification result, as well as the RT-reactions. Concerning P30 brains, all analyzed myelin-related genes are significantly increased in *Prnp*$^{0/0}$, normalizing *versus* either β-actin (Figure 25A) or Gapdh (Figure25B). Similar results were obtained at P180, though Plp1 shows significance only *versus* Gapdh (Figure 25B). At P365 all myelin-related genes are increased in their transcriptional level, except Mbp and L-Mag that show significance only *versus* β-actin (Figure 25A) but not Gapdh (Figure 25B). Interestingly, Dm20 has the highest fold change between *Prnp*$^{+/+}$ and *Prnp*$^{0/0}$ mice at all the ages (Figure 25A-B). Despite these results suggest that the myelin protein overexpression is due to transcriptional upregulation, they do not exclude an increase of oligodendrocytes population compared to WT.

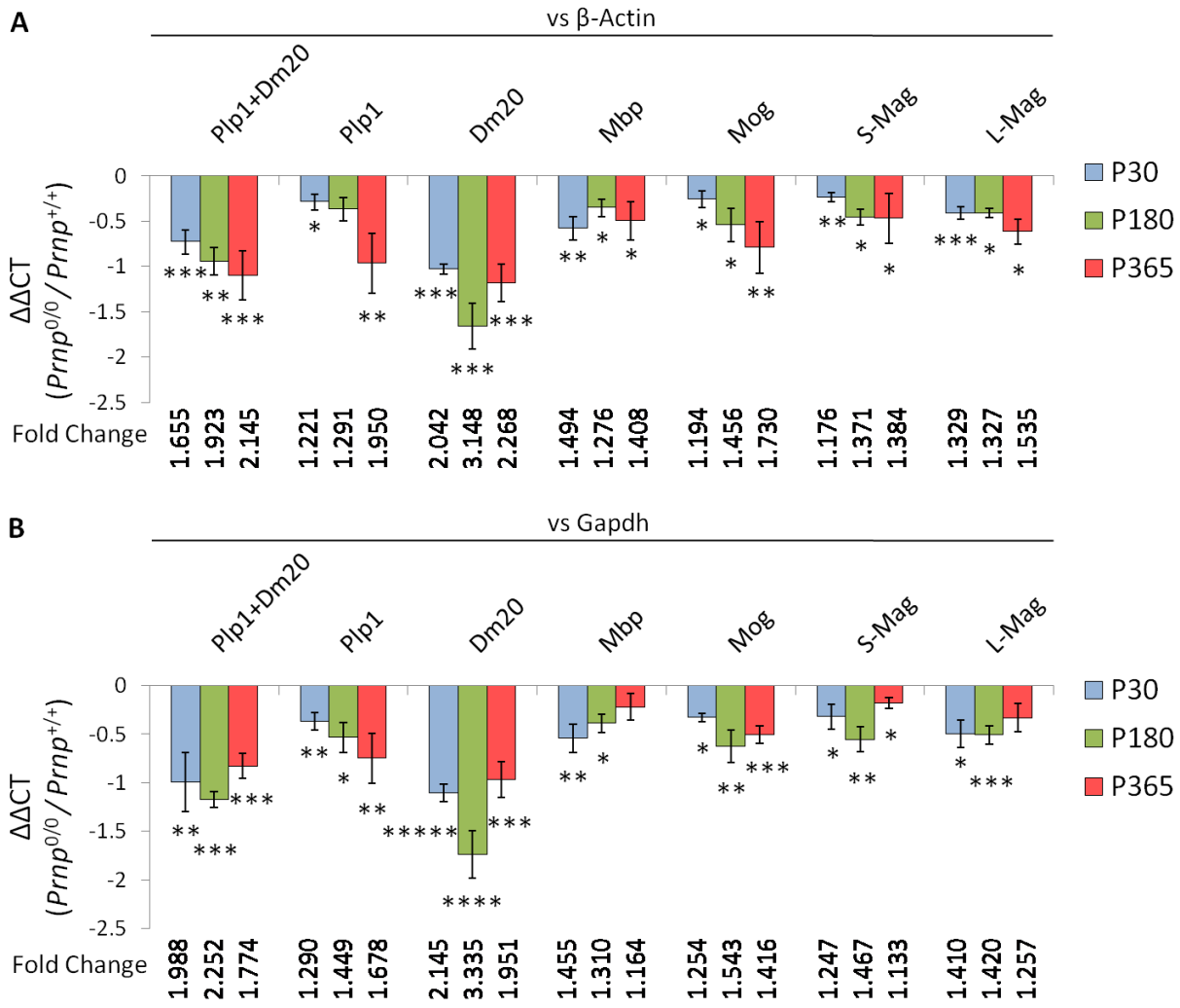

Figure 25. Myelin gene transcription in *Prnp*$^{0/0}$ and *Prnp*$^{+/+}$ brain measured by qRT-PCR. Plp1, Dm20, Mbp, Mog, S-Mag and L-Mag transcripts were analyzed at P30, P180 and P365. The results were normalized on the housekeeping gene β-actin **(A)** and Gapdh **(B)**. The graphs show the ΔΔCt relative quantification of *Prnp*$^{0/0}$ *versus* *Prnp*$^{+/+}$ samples. All error bars indicate SD. The fold change values, calculated by the formula $2exp^{-\Delta\Delta Ct}$, are reported in the lower part of each graph. Sample size: n=4; *p<0.05, **p<0.01, ***p<0.001, ****p<0.0001, *****p<0.00001.

To test this hypothesis, qRT-PCR experiments were performed on the same brain RNA samples in order to investigate the oligodendrocyte and neuronal population. The following transcripts were analyzed: NG2 (neural/glial antigen 2) as oligodendrocyte precursor cells indicator, Sox10 ((sex determining region Y)-box 10) as total oligodendrocyte marker, Tubb3 (βIII-tubulin) and NeuN (neuronal nuclei) as neuronal markers. At P30, no differences were detected between *Prnp*$^{+/+}$ and *Prnp*$^{0/0}$ brains, though NeuN presents a small increase in *Prnp*$^{0/0}$ samples when normalized with Gapdh (Figure 26B). Concerning P180

brains, NG2, Sox10 and Tubb3 are over-expressed in *Prnp*$^{0/0}$ brains only when normalized with Gapdh (Figure 26B). At P365, the only differentially transcribed gene is Tubb3 (Figure 26). These last results did not allow to clarify with certainty the influence of oligodendrocyte proliferation on myelin protein increase in PrP^{C}-null mice.

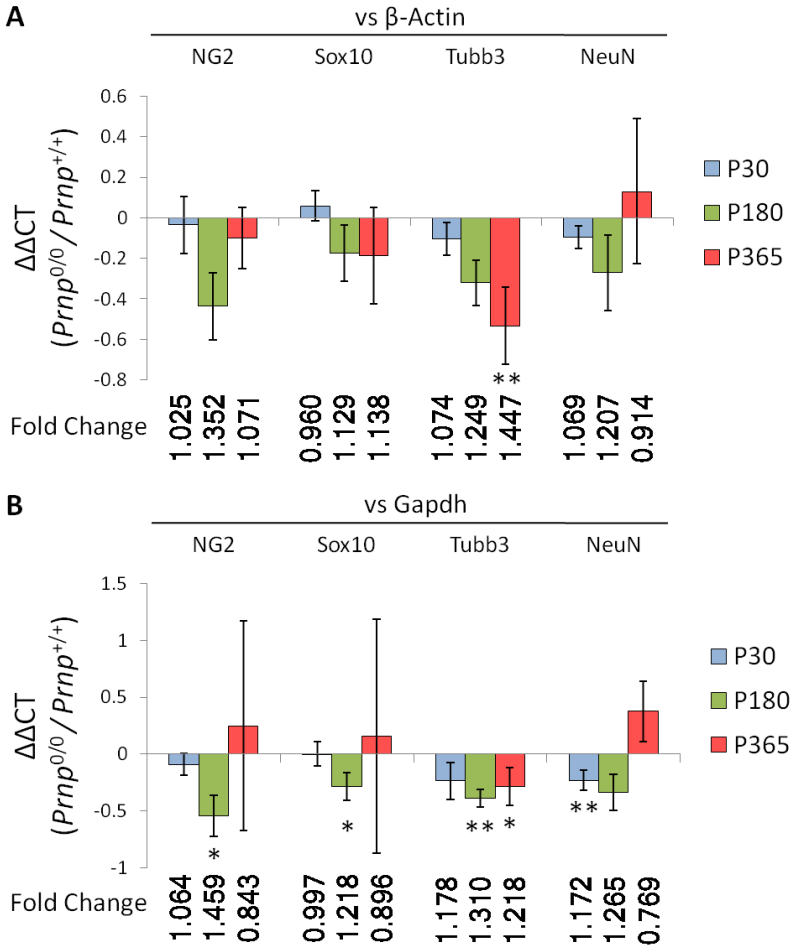

Figure 26. Oligodendrocyte and neuronal gene transcription in *Prnp*$^{0/0}$ and *Prnp*$^{+/+}$ brain measured by qRT-PCR. NG2, Sox10, Tubb3 and NeuN transcripts were analyzed at P30, P180 and P365. The results were normalized on the housekeeping gene β-actin **(A)** and Gapdh **(B)**. The graphs show the ΔΔCt relative quantification of *Prnp*$^{0/0}$ *versus Prnp*$^{+/+}$ samples. All error bars indicate SD. The fold change values, calculated by the formula 2exp$^{-\Delta\Delta Ct}$, are reported in the lower part of each graph. Sample size: n=4; *p<0.05, **p<0.01.

ELECTRON MICROSCOPY ANALYSIS OF CNS MYELIN

In the literature, no differences on CNS myelin structure and morphology have been associated to the absence of PrP^C (Bremer, Baumann et al. 2010, Bribián, Fontana et al. 2012). To further investigate the observed differences between PrP KO and WT brains, transmission electron microscopy was performed on P180 (Figure 27A-F) and P365 (Figure 27G-L) *Prnp*$^{+/+}$ and *Prnp*$^{0/0}$ *corpus callosum* samples. Micrographs revealed that *Prnp*$^{0/0}$ mice exhibit normal myelination in the CNS, inferring that the subtle changes observed in CNS myelin protein expression and gene transcription do not affect myelin structure.

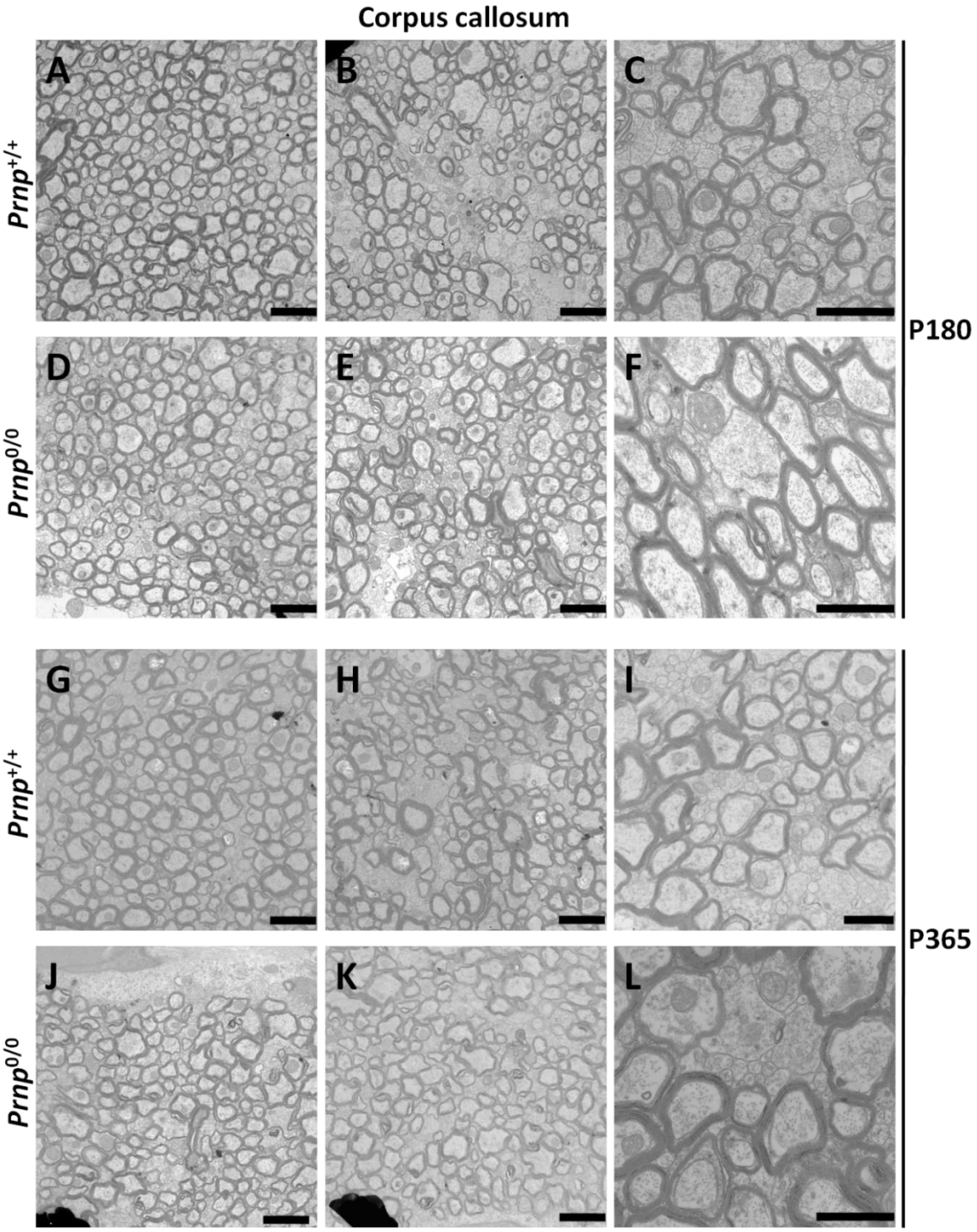

Figure 27. Adult *Prnp*$^{0/0}$ mice exhibit normal myelination in the CNS. Electron microscopy of P180 and P365 *Prnp*$^{+/+}$ and *Prnp*$^{0/0}$ *corpus callosum*. **(A, B, D, E, G, H, J, K)** Lower magnification electron microscopy photomicrograph of *Prnp*$^{+/+}$ and *Prnp*$^{0/0}$ mice. Scale bars: 2µm. **(C, F, I, L)** Higher magnification electron microscopy photomicrograph show no gross ultrastructural differences in the myelin sheaths of the *corpus callosum*. Scale bars: 1 µm.

ORGANOTYPIC HIPPOCAMPAL SLICE CULTURES AS AN *EX VIVO* MODEL FOR MYELINATION

To better investigate the role of PrP^C in CNS myelination, an *ex vivo* model based on OHC was established. Myelination of organotypic cultures was reported to occur readily and to be extensive by 10 DIV (Zhang, Jarjour et al. 2011). Therefore, $Prnp^{+/+}$ and $Prnp^{0/0}$ OHC were prepared and let in culture for up to 28 DIV to resemble the P30 mouse brain *in vivo*. To confirm the occurrence of myelination in OHC and validate the system, myelin protein and gene expression was evaluated.

MYELIN PROTEIN EXPRESSION ANALYSIS IN OHC

To analyze the OHC myelin protein expression, membrane proteins were purified from around 40-50 $Prnp^{+/+}$ and 40-50 $Prnp^{0/0}$ OHC slices. Membrane extraction was necessary for avoiding interferences with proteins composing the clot. OHC membrane proteins were analyzed by WB and three independent experimental replicates (Exp.1, Exp.2 and Exp.3) were performed. PLP, MBP and MAG expression levels were quantified and normalized *versus* Flotillin-1 and results are reported in Figure 28A. T-Test performed within each experimental replicate shows a significant increase in PLP, MBP and MAG expression levels in $Prnp^{0/0}$ OHC compared to $Prnp^{+/+}$ OHC (Figure 28A). A significant increase in the PLP expression level was also observed considering all the three experimental replicates. No statistical significance is observed for MBP and MAG due to the high sample variability, though an increasing trend in $Prnp^{0/0}$ OHC is still present (Figure 28A). Additional experiments are required to improve the statistics. Figure 28B shows representative images of WB bands obtained from one experiment (Exp.1), while Figure 28C reports quantification results of PLP, MBP and MAG represented as a ratio between $Prnp^{0/0}$ and $Prnp^{+/+}$ OHC in the same replicate. The amount of analyzed myelin proteins is visibly higher in $Prnp^{0/0}$ than in $Prnp^{+/+}$ OHC. Taken together, results show the correlation between PrP^C-null 28 DIV OHC and *in vivo* P30 mouse brains. Thus, OHC are a suitable *ex vivo* model to study PrP^C role in CNS myelination.

A

		Exp.1	Exp.2	Exp.3	Paired t-Test
PLP	*Prnp*$^{0/0}$/*Prnp*$^{+/+}$	2.547	5.528	1.618	0.014
	SD	0.435	1.699	0.376	
	t-Test	0.0030	0.0009	0.0264	
MBP	*Prnp*$^{0/0}$/*Prnp*$^{+/+}$	1.724	1.924	1.780	0.072
	SD	0.220	0.263	0.569	
	t-Test	0.0029	0.0007	0.0260	
MAG	*Prnp*$^{0/0}$/*Prnp*$^{+/+}$	1.241	2.142	1.483	0.176
	SD	0.142	0.263	0.218	
	t-Test	0.0497	0.0002	0.0026	

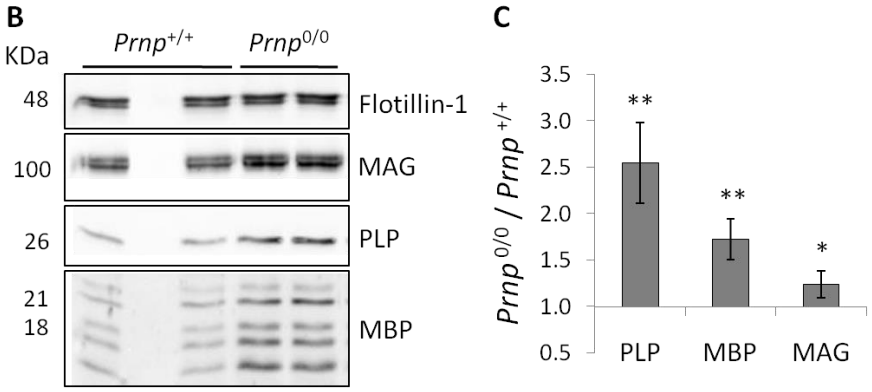

Figure 28. Myelin protein expression in 28 DIV *Prnp*$^{+/+}$ and *Prnp*$^{0/0}$ OHC. Membrane proteins were purified in order to get rid of the proteins composing the OHC covering clot. **(A)** Table representing PLP, MBP and MAG expression levels in three independent replicates of the experiment (Exp.1, Exp.2 and Exp.3). PLP, MBP and MAG optical density values were normalized *versus* Flotillin-1 and are reported as a ratio between *Prnp*$^{0/0}$ and *Prnp*$^{+/+}$ OHC. For each experimental replicate, SD derived from the technical replicates is shown. Furthermore, this table reports the p values calculated with the t-Test (for each individual experimental replica, in blue) or with the paired t-Test (considering all the replicates together). **(B)** Representative images of PLP, MBP and MAG WB bands obtained in Exp.1. The housekeeping protein Flotillin-1 is also reported. **(C)** PLP, MBP and MAG protein content represented as a ratio between *Prnp*$^{0/0}$ and *Prnp*$^{+/+}$ OHC in Exp.1. For each protein, the optical density value was normalized on the housekeeping protein. All error bars indicate SD. *p<0.05, **p<0.01.

TRANSCRIPTIONAL ANALYSIS OF MYELIN GENES IN OHC

To understand molecular mechanisms underlying myelin protein overexpression in *Prnp*$^{0/0}$ OHC, qRT-PCR experiments were performed on total RNA extracted from 28 DIV *Prnp*$^{+/+}$ and *Prnp*$^{0/0}$ OHC. The following transcripts were analyzed: Plp1, Dm20, Mbp, Mog, S-Mag and L-Mag. Four independent experiments were performed, each one comparing one set of around 20 or more *Prnp*$^{+/+}$ and *Prnp*$^{0/0}$ hippocampal slices. Table 5 reports the ΔCt values of WT and PrP^{C}-null OHC for each analyzed gene and for each experimental replicate. The results were normalized on two housekeeping genes (β-actin and Gapdh) whose expression levels are not different in *Prnp*$^{+/+}$ and *Prnp*$^{0/0}$ samples (data not shown). The NTC did not give any amplification result, as well as the RT- reactions. The resulting p value was calculated applying paired t-Test and it indicates that all transcripts are increased in *Prnp*$^{0/0}$ than in *Prnp*$^{+/+}$ OHC at 28 DIV when normalizing *versus* Gapdh. When normalizing *versus* β-actin, myelin genes show a tendency to increase in *Prnp*$^{0/0}$ OHC without being statistically significant. The correlation between protein overexpression and gene upregulation is also confirmed using OHC, as previously observed in mouse brains. Also in OHC Dm20 has the highest fold change (Figure 29A-B). This further confirms the suitability of OHC system as a model to study the role of PrP^{C} in CNS.

		Vs β-actin					Vs Gapdh				
		Exp.1	Exp.2	Exp.3	Exp.4	Paired t-Test	Exp.1	Exp.2	Exp.3	Exp.4	Paired t-Test
Plp1+ Dm20	ΔCT *Prnp*$^{+/+}$	-3.020	-0.849	-0.604	-0.903	0.076	0.648	0.942	0.427	0.582	0.001
	ΔCT *Prnp*$^{-/-}$	-4.174	-1.626	-2.605	-1.070		-0.827	-0.035	-0.804	-0.532	
Plp1	ΔCT *Prnp*$^{+/+}$	-2.029	0.105	0.454	0.373	0.138	1.639	1.896	1.485	1.858	0.005
	ΔCT *Prnp*$^{-/-}$	-2.790	-0.230	-1.175	0.327		0.557	1.360	0.627	0.865	
Dm20	ΔCT *Prnp*$^{+/+}$	-1.496	0.735	0.981	0.474	0.068	2.172	2.526	2.012	1.959	0.003
	ΔCT *Prnp*$^{-/-}$	-2.950	-0.293	-1.173	0.353		0.396	1.297	0.628	0.891	
Mbp	ΔCT *Prnp*$^{+/+}$	-4.107	-2.315	-1.497	-1.782	0.060	-0.439	-0.524	-0.466	-0.297	0.005
	ΔCT *Prnp*$^{-/-}$	-5.264	-2.927	-3.788	-2.395		-1.917	-1.336	-1.987	-1.857	
Mog	ΔCT *Prnp*$^{+/+}$	0.604	2.738	3.167	2.881	0.119	3.974	4.529	4.222	4.395	0.005
	ΔCT *Prnp*$^{-/-}$	-0.519	2.171	0.885	2.783		2.606	3.762	2.754	3.317	
S-Mag	ΔCT *Prnp*$^{+/+}$	1.872	2.433	3.426	3.068	0.127	5.541	4.224	4.457	4.553	0.013
	ΔCT *Prnp*$^{-/-}$	0.613	1.917	1.678	3.173		3.959	3.508	3.480	3.710	
L-Mag	ΔCT *Prnp*$^{+/+}$	3.619	4.538	6.276	6.235	0.081	7.287	6.330	7.307	7.720	0.018
	ΔCT *Prnp*$^{-/-}$	2.729	4.188	3.941	5.388		6.075	5.779	5.743	5.925	

Table 5. Transcriptional analysis of myelin genes in 28 DIV *Prnp*$^{+/+}$ and *Prnp*$^{0/0}$ OHC. Table reporting the ΔCt values of WT and PrP^{C}-null OHC for each analyzed gene (Plp1, Dm20, Mbp, Mog, S-Mag and L-Mag) and for each replicate of the experiment, normalized *versus* the housekeeping gene β-actin or Gapdh. The resulting p values calculated with the paired t-Test formula are also reported (blue). Sample size: in Exp.1, Exp.3 and Exp.4 a pull of around 20 *Prnp*$^{+/+}$ and 20 *Prnp*$^{0/0}$ OHC slices was used; in Exp.2 a pull of around 70 *Prnp*$^{+/+}$ and 70 *Prnp*$^{0/0}$ OHC slices was used.

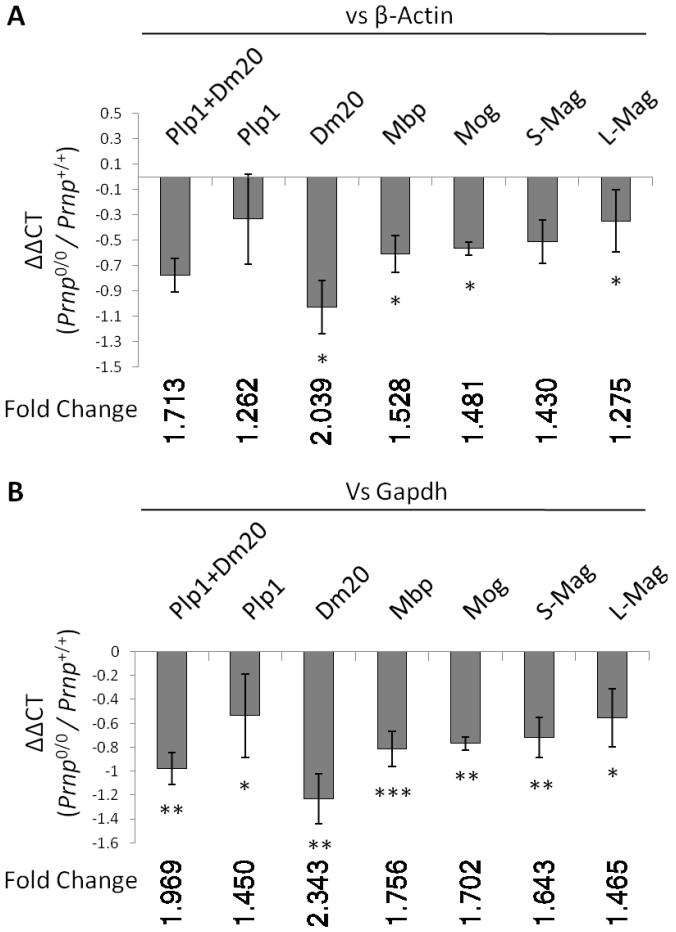

Figure 29. Example of myelin gene transcription results in *Prnp*$^{0/0}$ and *Prnp*$^{+/+}$ 28 DIV OHC measured by qRT-PCR in Exp.2 replicate. Plp1, Dm20, Mbp, Mog, S-Mag and L-Mag transcripts were analyzed and the results were normalized on the housekeeping gene β-actin **(A)** and Gapdh **(B)**. The graphs show the ΔΔCt relative quantification of *Prnp*$^{0/0}$ *versus* *Prnp*$^{+/+}$ samples. All error bars indicate SD derived from technical replicates. The fold change values, calculated by the formula $2^{-\Delta\Delta Ct}$, are reported in the lower part of each graph. Sample size: pull of around 70 *Prnp*$^{+/+}$ and 70 *Prnp*$^{0/0}$ OHC slices; *p<0.05, **p<0.01, ***p<0.001.

Since myelin protein overexpression in PrP^{C}-null OHC could be due to an increase of oligodendrocytes, qRT-PCR experiments on oligodendrocytic (NG2 and Sox10) and neuronal (Tubb3 and NeuN) markers

were performed. Table 6 reports ΔCt values of WT and PrP^C-null OHC, normalized on β-actin and Gapdh. For each considered gene, the p value was calculated with the paired t-Test. It indicates that no statistical significance was found between *Prnp*$^{+/+}$ and *Prnp*$^{0/0}$ OHC in the entire experimental set. The absence of oligodendrocyte transcriptional difference in OHC suggests that no alterations in oligodendrocyte proliferation occur in *Prnp*$^{0/0}$ OHC. Alternatively, oligodendrocyte proliferation could occur in PrP^C-null OHC without affecting gene transcription.

		Vs β-actin					Vs Gapdh				
		Exp.1	Exp.2	Exp.3	Exp.4	Paired t-Test	Exp.1	Exp.2	Exp.3	Exp.4	Paired t-Test
NG2	ΔCT *Prnp*$^{+/+}$	5.202	2.449	4.019	3.262	0.693	8.572	4.324	5.074	4.776	0.147
	ΔCT *Prnp*$^{-/-}$	5.480	2.474	2.475	3.709		8.605	4.187	4.345	4.243	
Sox10	ΔCT *Prnp*$^{+/+}$	7.114	1.382	3.159	2.335	0.352	10.484	3.257	4.214	3.849	0.100
	ΔCT *Prnp*$^{-/-}$	6.181	1.403	2.067	2.740		9.305	3.117	3.937	3.274	
Tubb3	ΔCT *Prnp*$^{+/+}$	-0.872	0.439	1.895	1.258	0.801	2.498	2.314	2.950	2.772	0.146
	ΔCT *Prnp*$^{-/-}$	-0.913	0.691	0.506	1.945		2.211	2.405	2.376	2.479	
NeuN	ΔCT *Prnp*$^{+/+}$	2.190	-0.291	1.037	0.376	0.961	5.559	1.584	2.092	1.890	0.179
	ΔCT *Prnp*$^{-/-}$	2.261	-0.402	0.121	1.416		5.386	1.312	1.990	1.950	

Table 6. Transcriptional analysis of oligodendrocytes and neuronal genes in 28 DIV *Prnp*$^{+/+}$ and *Prnp*$^{0/0}$ OHC. Table reporting the ΔCt values of WT and PrP^C-null OHC for each analyzed gene (NG2, Sox10, Tubb3, NeuN) and for each replicate of the experiment, normalized *versus* the housekeeping gene β-actin or Gapdh. The resulting p values calculated with the paired t-Test formula are also reported. Sample size: in Exp.1, Exp.3 and Exp.4 a pull of around 20 *Prnp*$^{+/+}$ and 20 *Prnp*$^{0/0}$ OHC slices was used; in Exp.2 a pull of around 70 *Prnp*$^{+/+}$ and 70 *Prnp*$^{0/0}$ OHC slices was used.

OHC TREATMENT WITH CUPRIZONE

Once validated the OHC system as a suitable tool for studying the role of PrP^C in CNS myelination, this *ex vivo* model was used to establish a myelination-demyelination-remyelination model. *Prnp*$^{+/+}$ and *Prnp*$^{0/0}$ OHC were exposed to the well-known demyelinating agent CZ. This copper chelating agent is widely used in myelin research to induce demyelination in animal models. No information are available on its use for *in vitro* and *ex vivo* purposes. After an initial period of myelination (14 DIV), *Prnp*$^{+/+}$ and *Prnp*$^{0/0}$ OHC were exposed to 1 mM CZ-containing medium for 7 days. At 21 DIV, the same treatment was

repeated with freshly prepared CZ-containing medium. Control and CZ-treated OHC were collected at 28 DIV and processed to analyze the effect of the treatment on myelin status.

Firstly, myelin protein expression analysis was performed using membranes extracted from around 40 *Prnp*$^{+/+}$ and 40 *Prnp*$^{0/0}$ OHC slices exposed to vehicle or CZ. OHC membrane proteins were processed through WB and PLP, MBP and MAG expression levels were quantified and normalized *versus* the housekeeping protein Flotillin-1. The results of one experimental replicate are reported in Figure 30A-C as the percentage of genotype-matched control. CZ-treated *Prnp*$^{+/+}$ OHC show a significant increase of PLP, MBP and MAG proteins compared to controls. Concerning *Prnp*$^{0/0}$ OHC, CZ treatment has a milder effect, triggering a significant increase in the expression level of PLP. Figure 30D shows representative images of PLP, MBP and MAG WB bands, together with the housekeeping protein Flotillin-1. A second replicate confirmed the results. These experiments show that CZ administration to OHC does not induce a decrease in the amount of myelin proteins. On the contrary this treatment induces myelin protein expression in WT OHC, while only a mild effect is observed in PrP^{C}-null samples.

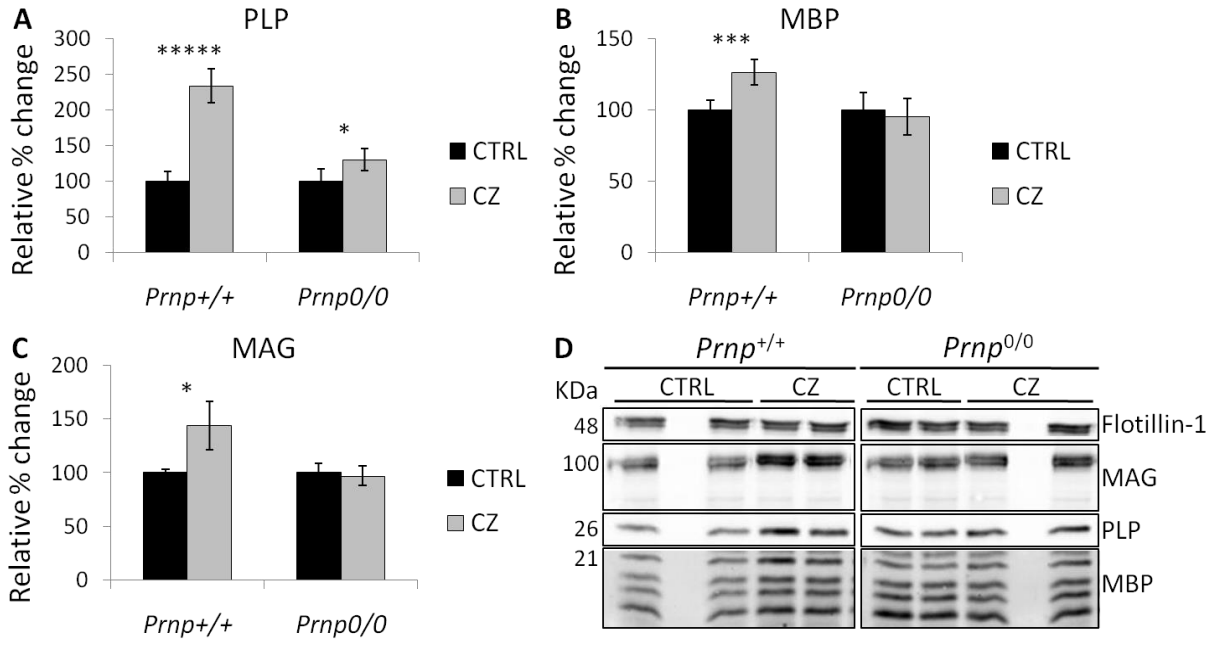

Figure 30. Myelin protein expression in CTRL and CZ treated *Prnp*$^{+/+}$ and *Prnp*$^{0/0}$ OHC. Membrane proteins were purified in order to get rid of the proteins composing the OHC covering clot. Western blots were performed and PLP, MBP and MAG optical densities were normalized *versus* the housekeeping protein Flotillin-1. **(A-C)** Graphs showing the results as the percentage of each myelin protein in CZ exposed *Prnp*$^{+/+}$ and *Prnp*$^{0/0}$ OHC compared to their genotype-matched control. These results come from one single experimental replicate; sample size: pull of about 40 OCH slices for each genotype and for each condition. All error bars represent SD derived from the technical replicates. *p<0.05, ***p<0.001; *****p<0.00001. **(A)** PLP. **(B)**

MBP. **(C)** MAG. **(D)** Representative images of PLP, MBP and MAG WB bands in CTRL and CZ-treated *Prnp*$^{+/+}$ and *Prnp*$^{0/0}$ OHC. The housekeeping protein Flotillin-1 is also reported.

To evaluate the effect of prolonged CZ treatment on cell viability, MTS assay was performed on *Prnp*$^{+/+}$ and *Prnp*$^{0/0}$ OHC after 14 days exposure to 1 mM CZ. Results reported in Figure 31 reveal that CZ treatment does not affect *Prnp*$^{0/0}$ OHC viability, while it increases viability in WT OHC.

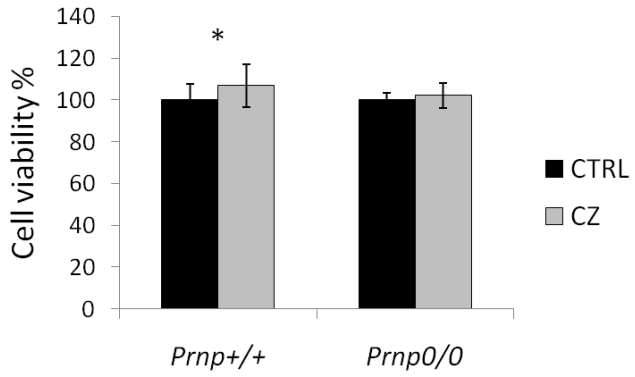

Figure 31. MTS assay on CTRL and CZ treated *Prnp*$^{+/+}$ and *Prnp*$^{0/0}$ OHC. The graph shows the cell viability percentage in *Prnp*$^{+/+}$ and *Prnp*$^{0/0}$ OHC treated and not treated with 1 mM CZ for 14 DIV; all error bars indicate SD; N=10-11; *p<0.05.

DISCUSSION

The cellular form of prion protein has been widely investigated since its misfolded isoform is the causative agent of prion disorders (Prusiner 1991). Although PrP^C localizes mainly in the nervous system and particularly in the synaptic compartments (Moya, Sales et al. 2000, Kanaani, Prusiner et al. 2005, Benvegnu, Poggiolini et al. 2010), PrP^C is expressed in most non-neuronal tissues, including blood lymphocytes, gastro-epithelial cells, heart, kidney, liver and muscles, prompting the involvement of this protein in various physiological processes (Horiuchi, Yamazaki et al. 1995, Fournier, Escaig-Haye et al. 1998). It is known that PrP^C structural features such as glycosylation sites, cysteines forming a disulfide bridge and a hydrophobic transmembrane region are perfectly conserved among different mammalian species. PrP^C sequences responsible for secondary structure elements, N- and C-terminal processing of the precursor protein and attachment of the GPI membrane anchor are highly conserved, suggesting that PrP^C may retain important physiological functions (van Rheede, Smolenaars et al. 2003, Colby and Prusiner 2011). Little is known about PrP^c normal cellular function and about the precise manner in which it exerts its pathogenicity. At a first look, PrP^c-deficient mice develop normally but they display minor defects imputable to a higher sensitivity to various stress stimuli. Many PrP^c functions rely on its ability to bind divalent cations and particularly copper with higher affinity (Stockel, Safar et al. 1998, Jackson, Murray et al. 2001, Singh, Das et al. 2010, Arena, La Mendola et al. 2012). Thus, PrP^c is involved in metal homeostasis, protecting neurons from possible Fenton reactions produced by metal unbalance (Brown 2003). PrP^c is a copper-binding protein that could protect neurons against oxidative damages through its superoxide dismutase activity, and contribute to synaptic homeostasis (Brown, Wong et al. 1999, Brown, Clive et al. 2001). PrP^c and copper cooperatively protect neurons from excitotoxicity by mediating NMDAR inhibition through S-nitrosylation (Gasperini, Meneghetti et al. 2015). Other studies report a PrP^c protective role against programmed cell death (Kuwahara, Takeuchi et al. 1999) and Bax-mediated apoptosis (Bounhar, Zhang et al. 2001, Didonna, Sussman et al. 2012). There is evidence that PrP^c is a cell-surface receptor for signal transduction, coupled to the tyrosine kinase Fyn (Mouillet-Richard, Ermonval et al. 2000). Considering the involvement of PrP^c in all these protective functions and in many other cellular processes, it is clear that a full understanding of PrP^c normal and physiological mode of action may help elucidating some of the pathological phenotypes observed in prion diseases. To date, the nature of the neurotoxicity observed in prion diseases is still an open debate. A first hypothesis concerns the gain of toxic function of the pathological isoform PrP^{Sc}. In this view, PrP^{Sc}

possesses novel toxic properties that are not related to the normal and physiological function of PrP^{C}. Since PrP^{Sc} alone is not sufficient to induce prion diseases (Bueler, Aguzzi et al. 1993, Brandner, Isenmann et al. 1996, Hill and Collinge 2003), it has been proposed that PrP^{C} protective activity may be lost upon conversion to or contact with PrP^{Sc}. This PrP^{C} loss-of-function would then cause neurodegeneration. This may explain some familial prion diseases, in which the effect of PrP mutations affects thermodynamic stability and biochemical properties of PrP, leading to the loss of its function. On the other hand, genetic ablation of *Prnp* expression has relatively little phenotypic effect and does not induce prion diseases by itself. Thus, it is possible that these two hypotheses work together, meaning that PrP^{Sc} toxicity may perturb PrP^{C} protective function, exacerbating the pathology. For instance, a PrP^{C} cytoprotective activity that is dispensable under normal conditions may become essential in the disease state due to cellular stress, but may be lost due to PrP^{Sc} presence (Harris and True 2006, Westergard, Christensen et al. 2007, Linden, Martins et al. 2008, Winklhofer, Tatzelt et al. 2008). Understanding the normal function of PrP^{C} may have important implications for possible future therapies of prion disorders. At present, most therapeutic approaches aim to inhibit PrP^{Sc} formation. Targeting the cellular pathways in which PrP^{C} exerts its protective function may be an alternative strategy to modulate the disease progression.

Among different physiological processes, PrP^{C} is involved also in the maintenance of PNS myelination (Bremer, Baumann et al. 2010, Benvegnu, Gasperini et al. 2011). PrP^{C}-null mice present an initial formation of morphologically normal PNS myelin, but long term myelin maintenance is disrupted as reported in Figure 10. In particular, neuronal PrP^{C} expression is sufficient to prevent peripheral myelin degeneration, possibly mediating axon to Schwann cells communication. Different hypotheses try to explain this late peripheral demyelination occurring in the absence of PrP^{C}. One is the age-related impairment in the correct PrP^{C} cleavage in late secretory compartments, which is necessary to preserve intact peripheral myelin (Bremer, Baumann et al. 2010). Secondly, the NRG1 and NRG3 processing is altered in PrP^{C} absence in the PNS of adult and aged mice (Benvegnu, Gasperini et al. 2011). PrP^{C} may influence NRG cleavage by modulating BACE1 (Parkin, Watt et al. 2007). Differently, PrP^{C} absence does not affect CNS myelin maintenance (Figure 11-12). Only the expression of PrP^{C} mutants lacking the HC domain (Figure5), but not the complete absence of the protein can trigger demyelination. The fact that PrP^{C} absence affects only PNS but not CNS myelin maintenance may rely on the different characteristics of these two myelin structures. Indeed PNS and CNS myelin differ one from the other in the kind of myelinating cells (Schwann cells or oligodendrocytes), lipid and protein composition, morphology (i.e.,

presence or absence of the basal lamina) and signaling (Baumann and Pham-Dinh 2001, Taveggia, Feltri et al. 2010). This may explain why the function that PrP^C fulfill is different from PNS to CNS myelin. However, the possibility that subliminal myelin pathologies might extend to central myelin in $Prnp^{0/0}$ mice has still not been excluded. Indeed, PrP^C is involved in many processes that may influence myelin formation and maintenance. Firstly, its absence increases OPC proliferation and delays their maturation (Bribián, Fontana et al. 2012). Secondly, PrP^C is involved in metal homeostasis and modulates oxidative stress. Both processes must be tightly regulated to prevent myelin structural or functional impairments (Zimmerman, Matthieu et al. 1976, Bongarzone, Pasquini et al. 1995, Matsushima and Morell 2001, Beard and Connor 2003, Bizzozero, DeJesus et al. 2004, Encinas, Manganas et al. 2005, Liu, Chen et al. 2005, Morelli, Ravera et al. 2012, Skjørringe, Møller et al. 2012, Aspli, Flaten et al. 2015).

In the first part of this work, the role of PrP^C in CNS myelination was deeper investigated. Taking advantage from *Prnp*$^{+/+}$ and *Prnp*$^{0/0}$ mice, myelin composition was evaluated in mouse brains at different developmental stages, from early postnatal days to aging: neonatal (P1), early postnatal (P7), young (P14), end of the development-early adulthood (P30), adulthood (P90), late adulthood (P180), early aging (P365) and late aging (P450). Furthermore, peripheral myelin status was also investigated in the SN in order to have a comparative analysis between the CNS and PNS myelin.

Myelin is composed of membranes with a peculiar lipid to protein composition. Differently from the other cellular membranes which present a higher amount of proteins respect to lipids, myelin is made of about 70-85% of lipids and only 15-30% of proteins (Baumann and Pham-Dinh 2001). As described above, myelin contains cholesterol, phospholipids and glycolipids in molar ratios ranging from 4:3:2 to 4:4:2. Cholesterol alone constitute about 30% of the total myelin lipids (Saher, Quintes et al. 2011). In the nervous system, the majority of brain cholesterol accumulates between the perinatal period and adolescence when neurons become myelinated. After this developmental period, cholesterol metabolism in the adult has a low turnover, but it continues to be active (Orth and Bellosta 2012, Zhang and Liu 2015). In this project, cholesterol content was investigated in *Prnp*$^{+/+}$ and *Prnp*$^{0/0}$ mice as a marker of myelin status. As reported in Figure 17, cholesterol is higher in *Prnp*$^{0/0}$ SN than in WT controls at early postnatal days P7 and P14. The higher SN cholesterol content at these developmental stages reflects either an increased rate of cholesterol synthesis or alterations during embryonic development. These changes are then compensated during the adulthood, when no differences in SN cholesterol content are observe between the two genotypes. During aging (P365 and P450), cholesterol content is

reduced in *Prnp*$^{0/0}$ SN of about 50% compared to *Prnp*$^{+/+}$ mice. This huge cholesterol depletion is consistent with PNS demyelination described in *Prnp*$^{0/0}$ mice. Conversely from PNS, cholesterol content is reduced in *Prnp*$^{0/0}$ brain at early postnatal stage P1. A non-statistically significant reduction is also visible at P7 (Figure 21). As for PNS, these changes may be caused by metabolic alterations during the embryo development. During embryonic development and in the early postnatal period, CNS undergoes an enormous cellular expansion. A sufficient availability of cholesterol as well as a correct ratio of cholesterol and phospholipids is crucial for the physicochemical properties of cells within the CNS (Orth and Bellosta 2012). Therefore, compensatory mechanisms may promptly re-establish the correct cholesterol content to guarantee the correct myelination of *Prnp*$^{0/0}$ brains. Similarly to PNS, a cholesterol decrease is observed during aging in *Prnp*$^{0/0}$ brains, with a significant 10% reduction at P365. During aging, cholesterol reduction in *Prnp*$^{0/0}$ brain appears subtle when compared to the 50% reduction observed in the SN. Since approximately 70% of brain cholesterol is associated to the myelin sheath, a slight decrease in cholesterol content may impair myelin functionality. Interestingly, PrP^{C} absence may impair PNS cholesterol more than CNS due to the higher metabolic activity of peripheral nerve myelin compared to CNS one (Rawlins and Smith 1971). Alternatively, higher cholesterol depletion in *Prnp*$^{0/0}$ SN might not be a cause, but simply the consequence of the peripheral myelin degenerative process. Concerning cholesterol and lipid metabolism, it is interesting to notice that iron is directly involved in cholesterol and other lipid biosynthesis, since it is a co-factor for many enzymes acting in these pathways (Connor and Menzies 1996). Since *Prnp*$^{0/0}$ brain presents an altered iron content and distribution, myelin production or maintenance may be affected (Singh, Kong et al. 2009, Pushie, Pickering et al. 2011).

Besides cholesterol measurement, the expression of myelin proteins was evaluated in the PNS and CNS of *Prnp*$^{+/+}$ and *Prnp*$^{0/0}$ mice from early postnatal days to aging. PLP and MBP have low expression levels in the PNS where they seem not essential for a correct myelin structure (Baumann and Pham-Dinh 2001). Compared to WT mice, in *Prnp*$^{0/0}$ SN PLP expression is lower at P30 and P365 (Figure19A) and MBP decreases in the first developmental stages (P7 and P30) and during the aging (P365 and P450) (Figure 19B). Although these proteins are not essential in the PNS, changes in their expression level during aging may correlate with the peripheral demyelination process. These results indicate an altered PNS myelin composition from postnatal stages up to the adulthood, before the appearance of morphological changes occurring during aging. In this work MAG was also analyzed in the SN. This protein is mostly found in its fully glycosylated form and it is involved in neuron-glia adhesion and in bi-directional

signaling. In PrP^C-null SN, the glycosylated form of MAG is quite constant throughout the development, while the non-glycosylated form of MAG is considerably increased starting from 3 months of age (Figure 19C). The absence of glycosylation may affect the interaction of the protein with myelin sheath or impair its signaling role. MPZ is the most important protein for PNS myelination, representing about 50% of total myelin proteins. It is essential for PNS myelination and it resembles PLP function in the CNS. MPZ expression is increased in aged *Prnp*$^{0/0}$ SN, with significant difference at P365 (Figure 19D). This result apparently contrasts with the demyelination affecting the PNS of aged *Prnp*$^{0/0}$ mice. It is possible that demyelination occurs without altering MPZ relative content in myelin, thus impeding a reduced detection in WB. Differently, its isoform L-MPZ is reduced in P7 *Prnp*$^{0/0}$ SN and a decreasing trend is visible also during the aging, with significant difference at P450. Since very little is known about the function of L-MPZ isoform, it is not possible to speculate on the biological meaning of its decrease in early postnatal and aged *Prnp*$^{0/0}$ SN (Yamaguchi, Hayashi et al. 2012). Moving to the CNS, myelin proteins show a general upregulation in *Prnp*$^{0/0}$ brain at all the ages, except at P90 (Figure 23). More in detail, in PrP^C-null brain membrane fractions, PLP is increased at all the ages (Figure 23A) and MBP is increased at P1 and P365 (Figure 23B). The level of MOG protein is higher at all ages except at P90 in PrP^C-null mice than in WT (Figure 23C). The expression of the main MAG glycosylated form is increased at all stages except at P90 (Figure 23D). Conversely from PNS, the non-glycosylated form of MAG is poorly detectable and it rises with the aging (P365 and P450) in a similar way between WT and *Prnp*$^{0/0}$ mice. Although the non-glycosylated MAG has a very low expression level, it shows an increment in P7 *Prnp*$^{0/0}$ mice compared to WT. It must be noticed that myelin protein expression changes between *Prnp*$^{+/+}$ and *Prnp*$^{0/0}$ brains occur only in enriched membrane fractions. No changes were observed in total brain homogenates, indicating that these are subtle differences. A possible reason for explaining different sample preparation used to appreciate changes in SN and brains relies on tissue composition. While SN is indeed principally made of myelinated and unmyelinated axons, brain homogenate include white and grey matter. Thus the presence of subtle differences may be hidden by the complexity of brain protein composition. To exclude the dependence of these results on the membrane extraction protocol, another method was applied and the same protein overexpression trend was confirmed in *Prnp*$^{0/0}$ brains (Figure 24). Myelin protein expression analysis does not allow a direct quantification of myelin content, but it indicates membrane composition of SN and brain. Taken together, these results show that PrP^C absence alters myelin protein composition differently in peripheral and central nervous system. Changes in PrP^C-null SN protein composition during aging are possibly related to myelin sheath degeneration, while subtle impairments are observed in *Prnp*$^{0/0}$ CNS throughout the whole lifetime, with

the only exception of P90. Many possible causes can justify the observed general myelin protein overexpression in *Prnp*$^{0/0}$ brain. Firstly, myelin protein increase may be related to alterations in the transcriptional regulation of related genes. Secondly, a different trafficking and tournover of myelin proteins can occur in *Prnp*$^{0/0}$ brain, storing or arranging them in different membrane compartments. Thirdly, an increased oligodendrocyte number can account for this observation.

In order to verify whether myelin protein amount correlates with the transcriptional level of the corresponding genes, a qRT-PCR analysis was performed on SN and brain total RNA extracted from P30, P180 and P365 *Prnp*$^{+/+}$ and *Prnp*$^{0/0}$ mice. At P365, *Prnp*$^{0/0}$ SN presents a significant decrease in the transcription level of myelin-related genes compared to WT mice. These results are consistent with the PNS demyelination affecting *Prnp*$^{0/0}$ mice. Concerning the CNS, a small but general increase of myelin gene expression was observed in *Prnp*$^{0/0}$ brain at all ages (Figure 25). These data correlate with the myelin protein increment described before (Figure 23). As reported in Figure 25, the differences are characterized by a low fold change increment, confirming that PrP^{C} absence induce subtle impairments in the CNS. Interestingly, in *Prnp*$^{0/0}$ brains Dm20 has the highest fold changes. Dm20 expression precedes that of PLP1 during development. Differently, in adult brain DM20 protein is present at much lower level compared to PLP1. In some reports, Dm20 gene expression has been associated to remyelinating conditions in adult brain (Mathisen, Kawczak et al. 2001). Considering that demyelination does not occur in *Prnp*$^{0/0}$ brains (Bremer, Baumann et al. 2010, Bribián, Fontana et al. 2012), Dm20 transcriptional upregulation cannot be implicated in remyelinating processes, but more likely in reparative processes. The myelin protein and gene increment in *Prnp*$^{0/0}$ brains could be due to an increment in oligodendrocyte number. To verify this hypothesis, qRT-PCR experiments were performed on the same brain RNA samples in order to investigate the oligodendrocyte and neuronal population. NG2 and Sox10 transcripts were analyzed as oligodendrocyte precursor cells and total oligodendrocyte marker, while Tubb3 and NeuN were used as neuronal markers. The transcription of these genes shows only some oscillations that were not maintained between different ages and that were not confirmed in both Gapdh and β-actin normalization (Figure 26). This hampered the possibility to clarify the contribution of oligodendrocyte proliferation on myelin protein increase in PrP^{C}-null mice. Other techniques such as WB or immunofluorescence could be applied to better elucidate this question.

To conclude the analysis of CNS myelin in *Prnp*$^{+/+}$ and *Prnp*$^{0/0}$ mice, an electron microscopy study was performed in the corpus callosum of P180 and P365 mice. Corpus callosum was chosen since it is the

myelin richest region in the brain. Evidence reported in literature showed that CNS myelin structure and morphology do not have alterations due to PrP^C absence (Bremer, Baumann et al. 2010, Bribián, Fontana et al. 2012). Transmission electron microscopy measurements were done in order to unveil subtle differences between *Prnp*$^{+/+}$ and *Prnp*$^{0/0}$ myelin. As shown in Figure 27, Prnp$^{0/0}$ mice exhibit normal CNS myelination. These qualitative observations indicate that the subtle changes observed in CNS myelin protein expression and gene transcription do not affect myelin structure and morphology in *Prnp*$^{0/0}$ mice. Taken together, these results suggest that myelin protein overexpression could be due to a compensatory mechanism for preventing functional abnormalities in CNS myelin. It would be useful to study the oligodendrocyte lineage and myelin protein distribution in different membrane compartments.

Once the characterization of peripheral and central nervous system myelin in *Prnp*$^{+/+}$ and *Prnp*$^{0/0}$ mice was completed, an *ex vivo* model based on OHC was established to better investigate PrP^C role in CNS myelin. The first report describing organotypic cultures myelination was dated 1956 (Hild 1956). Later, since organotypic cultures can be maintained *in vitro* for a prolonged period of time compared to other dissociated cultures and considered that they preserve a pool of active OPC, this *ex vivo* technique was adapted as a model to study myelination, demyelination and remyelination (Zhang, Jarjour et al. 2011). The organotypic cultures myelination process was reported to occur readily and to be extensive by 10 DIV (Zhang, Jarjour et al. 2011). Therefore, *Prnp*$^{+/+}$ and *Prnp*$^{0/0}$ OHC were prepared and let in culture for up to 28 DIV to reach a myelination rate similar to the *in vivo* P30 mouse brain. To confirm the occurrence of myelination in OHC and to verify whether this system reflects *in vivo* condition, myelin protein and gene expression was evaluated. A significant increase in PLP was observed in *Prnp*$^{0/0}$ OHC compared to *Prnp*$^{+/+}$ OHC (Figure 28). MBP and MAG expression level was also found increased in PrP^C-null OHC compared to WT ones. The transcriptional regulation of myelin related genes was analyzed by qRT-PCR on RNA extracted from 28 DIV *Prnp*$^{+/+}$ and *Prnp*$^{0/0}$ OHC. The statistical analysis of four experimental replicates (Table 5) indicates that the transcription of all the analyzed myelin genes is higher in *Prnp*$^{0/0}$ than in *Prnp*$^{+/+}$ OHC at 28 DIV when normalizing *versus* Gapdh. When normalizing *versus* β-actin, myelin genes show a tendency to increase in *Prnp*$^{0/0}$ OHC, without being statistically significant. Therefore, myelin protein increment in PrP^C-null OHC correlates with an increased gene expression, as it was previously observed in mouse brains. To verify the possibility that myelin protein over-expression observed in PrP^C-null OHC could be due to an increment in oligodendrocytes number, oligodendrocyte and neuronal genes were analyzed by qRT-PCR. As shown in Table 6, no difference was found in NG2, Sox10, Tubb3 and NeuN between *Prnp*$^{+/+}$ and *Prnp*$^{0/0}$ OHC in the entire experimental set. The absence of oligodendrocyte genes transcriptional difference in OHC suggests that an increase in oligodendrocyte

proliferation and number does not explain myelin protein over-expression in *Prnp*$^{0/0}$ OHC. Alternatively, oligodendrocyte proliferation could occur in PrP^{C}-null OHC without affecting gene transcription. Taken together, myelin protein and gene expression results concerning OHC are consistent with previous *in vivo* observations in mouse brains. Therefore, OHC are a suitable model to study PrP^{C} role in CNS, though large numbers of OHC are required to have reliable and confident results. Indeed, the variability among different sets of cultures is high and it can be overcome only by increasing sample size and experimental replicates.

Once the OHC model was established, the effect of the presence or absence of PrP^{C} on myelin was studied. Trying to establish a myelination-demyelination-remyelination model, *Prnp*$^{+/+}$ and *Prnp*$^{0/0}$ OHC were exposed to the copper chelator CZ, which is known to induce demyelination following oral administration in mice. However, no reports were already present concerning a similar use in *in vitro* or *ex vivo* cultures. Therefore, after 14 days in culture, necessary for the initial OHC myelination, *Prnp*$^{+/+}$ and *Prnp*$^{0/0}$ OHC were exposed to 1 mM CZ-containing medium for an overall period of 14 days. Myelin protein expression was analyzed by WB revealing that PLP, MBP and MAG protein percentage is significantly increased in *Prnp*$^{+/+}$ OHC exposed to CZ, compared to controls (Figure 30). Concerning *Prnp*$^{0/0}$ OHC, CZ treatment has a milder effect, triggering a significant increase in the expression level of PLP, but not of MBP and MAG. It is clear that CZ treatment does not induce a decrease in OHC myelin protein expression level as it would have been expected in case of demyelination (Praet, Guglielmetti et al. 2014). The effect of prolonged CZ treatment to cell viability was evaluated through the MTS assay. *Prnp*$^{+/+}$ and *Prnp*$^{0/0}$ OHC exposed to control and CZ conditions revealed that CZ treatment do not influence *Prnp*$^{0/0}$ OHC viability, while it increases the viability of WT OHC. Two different hypotheses can explain the increase in *Prnp*$^{0/0}$ OHC viability: firstly, CZ treatment may not be adequate to induce a sustained oligodendrocyte death and demyelination, thus promoting oligodendrocyte proliferation or reparative events following the toxic insult; secondly, the increase in viability percentage may be related to hormesis, a favorable biological response following low exposure to toxins or other stressors (Martins, Galluzzi et al. 2011). To discriminate between these two hypotheses, cell proliferation should be investigated during CZ exposure. One possible method could be the immunofluorescence-based detection of 5'-bromo-2'-deoxyuridine (BrdU) incorporation during CZ administration, in association with other neuronal and glial markers. The fact that CZ treatment is not inducing a decrease in OHC myelin protein expression, but an increase in myelin protein level, may have different reasons. First of all, it is possible that CZ does not act in culture. In fact, all the reports concerning CZ demyelinating role refer to *in vivo* experiments (Carlton 1967, Hoffmann, Lindner et al. 2008, Koutsoudaki, Skripuletz et al.

2009, Zendedel, Beyer et al. 2013). *In vivo*, CZ induces the death of mature myelinating oligodendrocytes, but its precise mechanism of action is still unclear (Norkute, Hieble et al. 2009, Bénardais, Kotsiari et al. 2013). Since no traces of CZ have ever been found in the brain of CZ-fed mice, CZ may exert its myelinotoxic effect by interfering with copper intestinal absorption, thus decreasing the content of this metal also in the brain (Venturini 1973, Benetti, Ventura et al. 2010). Therefore, it is not obvious that CZ action *in vitro* is the same as *in vivo*. It is also possible that the effects observed in this thesis are due to CZ ability to chelate copper. Given the strict interconnection between copper and the homeostasis of other metals such as iron, it is possible that copper decrease may trigger a general metal dysregulation which can be sufficient to alter myelin status. This could also explain why CZ treatment acts strongly in WT OHC by increasing the myelin protein amount, while its effect is milder in PrP^C-null samples. Since PrP^C-null mice present a lower level of brain copper content *per se*, chelation of this metal ion may influence $Prnp^{+/+}$ samples more than $Prnp^{0/0}$ ones. A second possibility is that the dose and timing of CZ administration is not suitable to induce demyelination. While in mice CZ administration lasts at least 5-6 weeks to induce demyelination, OHC are exposed to two consecutive CZ treatments of 7 days each. It is possible that CZ activity decreases during the 7 days in culture. Therefore, if CZ treatment is not enough strong or prolonged, OPC proliferation and myelin reparative processes may occur following the initial toxic stimulus. To better elucidate this point, it would be interesting to try other protocols for CZ administration to OHC. For example a daily OHC exposure to freshly dissolved CZ may give more insights concerning the suitability of the adopted protocol. Concluding, at the moment a suitable protocol to induce OHC demyelination has not yet been established. However, the observation of a different response of $Prnp^{+/+}$ and $Prnp^{0/0}$ OHC to CZ exposure denote a different CNS susceptibility to this kind of stimulus in the presence or absence of PrP^C.

CONCLUSIONS AND PERSPECTIVES

In this project, PrP^C role in CNS myelination was investigated, taking advantage from *Prnp*$^{+/+}$ and *Prnp*$^{0/0}$ mice. Myelin composition was examined in mouse brains at different developmental stages, from early postnatal days to aging, through cholesterol content measurement and through myelin protein and gene expression evaluation. Furthermore, peripheral myelin status was also investigated in the SN in order to have a comparative analysis between the CNS and PNS myelin. In the last part of the project, an *ex vivo* model based on OHC was established to better investigate PrP^C role in CNS myelin.

Concerning the PNS, most of our results are in line with the myelin degeneration observed in literature (Bremer, Baumann et al. 2010, Benvegnu, Gasperini et al. 2011). A 50% decrease in SN cholesterol content, a strong reduction of myelin genes transcription and an altered expression level of some myelin proteins were found during *Prnp*$^{0/0}$ mouse aging. Moreover, some changes in the early postnatal period were also observed and these may be triggered by some alterations during embryonic development. Considering the CNS, the results obtained in this work are not discordant with the previous literature (Bremer, Baumann et al. 2010, Benvegnu, Gasperini et al. 2011, Bribián, Fontana et al. 2012). Since the fold change increase in myelin gene expression in *Prnp*$^{0/0}$ brains is low and the increase in myelin protein level can be observed only in membrane-enriched fractions, it can be concluded that the differences induced by PrP^C absence are subtle. In literature, a similar analysis of myelin protein has never been performed in membrane- or myelin-enriched fractions. Thus, such small differences were not noticed before. According to the previous literature, electron microscopy on CNS myelinated corpus callosum did not show gross morphological changes between *Prnp*$^{+/+}$ and *Prnp*$^{0/0}$ mice. It is possible that myelin protein overexpression could be the result of a compensatory mechanism to prevent functional abnormalities. Since myelin must be finely regulated and even small changes can impair the normal function, myelin reparative processes can be established to guarantee the maintenance of a correct morphology. This hypothesis could also relate to the observation that among all the analyzed myelin genes, DM20 isoform of PLP presents the highest increasing rate in *Prnp*$^{0/0}$ brains. This isoform has been associated to remyelination. Further investigation of reparative mechanisms and signalling could elucidate this hypothesis. An increased number of oligodendrocyte may also account for the general myelin protein and genes overexpression in PrP^C-null brains. According to Bribián and colleagues (Bribián, Fontana et al. 2012), PrP^C absence increases OPC proliferation and delays their maturation, without affecting the final amount and quality of myelin. These authors hypothesize that

oligodendrocytes produced in excess undergo cell death to maintain a proper number of mature myelinating cells. However, their oligodendrocyte quantification is limited to 2-month-old mice, an age close to 3 months, when differences are scarcely detected also in this thesis. Therefore, it cannot be excluded with certainty that OPC increased proliferation may produce mature oligodendrocytes able to integrate themselves in the tissue cytoarchitecture being required for the maintenance of the correct myelin functionality. A quantitative and qualitative analysis of the oligodendrocyte lineage between *Prnp*$^{+/+}$ and *Prnp*$^{0/0}$ mice may be useful to confirm or exclude this hypothesis. Running against this hypothesis, an accurate electron microscopy analysis should be able to detect the occurrence of reparative phenomena. Furthermore, since the increase in myelin protein level in *Prnp*$^{0/0}$ brains does not correspond necessarily to a myelin increase, it would be interesting to evaluate the myelin protein trafficking and localization in various cell membrane compartments, even different from myelin sheath. For example, it has been reported that PLP overexpression triggers its accumulation in endosomes-lysosomes, together with cholesterol (Simons, Kramer et al. 2002). Therefore, immunofluorescence or WB on different cellular fractions may help investigating the localization of the myelin proteins, comparing *Prnp*$^{0/0}$ with *Prnp*$^{+/+}$ mice.

As already discussed, PrP^{C} plays numerous protective functions against different kind of stress conditions, such as oxidative and nitrosative stress and excitotoxicity. It is possible that PrP^{C} cytoprotecting activity may be dispensable under normal conditions, but may become essential in stressful conditions or even in the disease state. According to this hypothesis, differences in CNS myelin status between *Prnp*$^{0/0}$ and *Prnp*$^{+/+}$ mice may be exacerbated in stress conditions. The particular combination of some peculiar features (high rate of ATP production, high iron content) renders oligodendrocytes, and consequently also myelin sheaths, more susceptible to damage than other CNS cellular components. In PrP^{C}-null mice, and even more in prion diseases, PrP^{C} loss of protective function may facilitate demyelinating processes. Since PrP^{C} can modulate synaptic activity through its interaction with copper ions, its absence may increase excitotoxic effects, leading to cytosolic calcium accumulation. Calcium may be directly toxic for oligodendrocytes or may modulate different signalling pathways involved in myelination. The establishment of an *ex vivo* myelination model such as the OHC is important since it allows to investigate the CNS myelin response to different stimuli in the presence or absence of PrP^{C}. Since OHC allow to investigate myelination, demyelination and remyelination, the different rate of occurrence of these processes might be evaluated between *Prnp*$^{0/0}$ and *Prnp*$^{+/+}$ mice.

Understanding PrP^C physiological function in CNS myelin formation, maintenance and protection against toxic insults might be essential not only in the comprehension of some of the pathological phenotypes observed in prion diseases, but may also elucidate the PrP^C protective role in other neurodegenerative conditions sharing elevated levels of oxidative and metabolic stress.

ACKNOWLEDGEMENTS

At the end of these four years of Ph.D. I would like to thank Prof. Giuseppe Legname for giving me the possibility to work in his laboratory. I would like to thank him for the discussions, for trusting me and for allowing me to be completely independent in the project planning. During these years I had the opportunity to participate to courses, workshops and conferences where I learned new topics and presented my work. I really appreciated this great chance.

I would like to thank Dr. Federico Benetti for giving me the possibility to work on the nitrosylation and myelin projects. I appreciated in particular his presence, since he continued to follow me also after the initial discouraging results in the myelin project. I'm grateful to him for the precious suggestions, for finding the time to reason about my data and for all the discussions. It has been an enormous opportunity for me to learn from him.

I would like to thank all the present and past members of the Prion Biology Lab since they cheered up the time I spent here in SISSA, besides giving a contribution to my work. However, my deepest thanks are for Lisa, who fell in love with my hippocampus pictures and choose me to work with her. I have been her shadow during my first period here in SISSA and she taught me almost all what I know. I'm grateful to her for being always present, listening to my doubts, giving me suggestions and compensating for my poor memory. Sharing with her time and space in the lab has been a great experience and I appreciated our full collaboration. Beside the working reasons, I would like to thank Lisa for her friendship. I would like to thank the two halves, Irene and Lara, for the time we spent together in these years and for helping me to carry out my experiments during my absences and during this last period. I hope they can conclude with enthusiasm their Ph.D. and have a rewarding future. I'm grateful also to the ubiquitous Stefano, who gave me some precious suggestions concerning some experiments. I thank him also for eating salted codfish with me during his visits in Trieste.

I would like to thank all the members of the Common Molecular Biology Lab and in particular Roberta, the guardian of the lab and a precious guide for all the people working there. She has always been ready to help me and I thank her for being a good friend and also my personal chocolate pusher.

I'm grateful to all the SISSA staff and in particular to Bea, who helped me with the organotypic cultures. I thank her for her friendship and for the long and relaxing chats during culture preparations.

I would like to thank also Andrea, Gianluca and Dario for sharing with me part of this SISSA adventure and for cheering up my lunchtime.

I'm grateful also to external scientist who collaborated with me or contributed to my work with precious suggestions. In particular I would like to thank Dr. Roberto Furlan for the scientific discussion, Dr. Angelo Quattrini and Giorgia Dina for the electron microscopy experiments, Dr. Carla Taveggia and Dr. Sophie Mouillet-Richard for reading my thesis, providing comments and helpful suggestions.

Outside the spheres of work, I would like to thank the friends that I met during my sport activities. In particular I thank the guys of the Olympic Rock Climbing Team for having fun and suffering together during our trainings and days at the cliffs. The time we spent together was essential to free my mind from problems and fill the stomach with huge sandwiches. I thank also the guys of the Guru Team who gave me the possibility to play volleyball again after many years.

I would like to thank also my old friends, the ones who didn't get scared about the distance and continued to share some moments with me. In particular, I'm grateful to Chiara who never stopped asking me to meet us together.

However, my greatest thanks are for my big family since all the members have always been present and supported me during this period in Trieste. They are a point of reference on which I can rely in every moment.

I would like to thank Ale for his presence, patience and support. He was able to color the gray days and to make the sunny day shine. I'm grateful to him for the continuous coming and going and for the precious moments we spent together.

BIBLIOGRAPHY

Aarts, M., Y. Liu, L. Liu, S. Besshoh, M. Arundine, J. W. Gurd, Y. T. Wang, M. W. Salter and M. Tymianski (2002). "Treatment of ischemic brain damage by perturbing NMDA receptor- PSD-95 protein interactions." Science **298**(5594): 846-850.

Abo-Krysha, N. and L. Rashed (2008). "The role of iron dysregulation in the pathogenesis of multiple sclerosis: an Egyptian study." Multiple Sclerosis **14**(5): 602-608.

Aggarwal, S., L. Yurlova and M. Simons (2011). "Central nervous system myelin: structure, synthesis and assembly." Trends Cell Biol **21**(10): 585-593.

Aguzzi, A., F. Baumann and J. Bremer (2008). "The prion's elusive reason for being." Annu Rev Neurosci **31**: 439-477.

Aguzzi, A., M. Heikenwalder and G. Miele (2004). "Progress and problems in the biology, diagnostics, and therapeutics of prion diseases." J Clin Invest **114**(2): 153-160.

Alper, T., W. A. Cramp, D. A. Haig and M. C. Clarke (1967). "Does the Agent of Scrapie Replicate without Nucleic Acid ?" Nature **214**(5090): 764-766.

Arena, G., D. La Mendola, G. Pappalard, I. Sóvágód and E. Rizzarelli (2012). "Interactions of Cu2+ with prion family peptide fragments: Considerationson affinity, speciation and coordination." Coordination Chemistry Reviews **256**: 2202-2218.

Aspli, K. T., T. P. Flaten, P. M. Roos, T. Holmøy, J. H. Skogholt and J. Aaseth (2015). "Iron and copper in progressive demyelination – New lessons from Skogholt's disease." Journal of Trace Elements in Medicine and Biology **31**: 183-187.

Avery, S. V. (2001). "Metal toxicity in yeasts and the role of oxidative stress." Adv Appl Microbiol **49**: 111-142.

Bauer, J., M. Bradl, M. Klein, M. Leisser, T. L. Deckwerth, H. Wekerle and H. Lassmann (2002). "Endoplasmic reticulum stress in PLP-overexpressing transgenic rats: gray matter oligodendrocytes are more vulnerable than white matter oligodendrocytes." J Neuropathol Exp Neurol **61**(1): 12-22.

Baumann, F., J. Pahnke, I. Radovanovic, T. Rülicke, J. Bremer, M. Tolnay and A. Aguzzi (2009). "Functionally Relevant Domains of the Prion Protein Identified In Vivo." PLoS ONE **4**(9): e6707.

Baumann, F., M. Tolnay, C. Brabeck, J. Pahnke, U. Kloz, H. H. Niemann, M. Heikenwalder, T. Rulicke, A. Burkle and A. Aguzzi (2007). "Lethal recessive myelin toxicity of prion protein lacking its central domain." EMBO J **26**(2): 538-547.

Baumann, N. and D. Pham-Dinh (2001). "Biology of oligodendrocyte and myelin in the mammalian central nervous system." Physiol Rev **81**(2): 871-927.

Beard, J. L. and J. R. Connor (2003). "IRON STATUS AND NEURAL FUNCTIONING." Annual Review of Nutrition **23**(1): 41-58.

Beirowski, B. (2013). "Concepts for regulation of axon integrity by enwrapping glia." Frontiers in Cellular Neuroscience **7**: 256.

Bénardais, K., A. Kotsiari, J. Škuljec, P. Koutsoudaki, V. Gudi, V. Singh, F. Vulinović, T. Skripuletz and M. Stangel (2013). "Cuprizone [Bis(Cyclohexylidenehydrazide)] is Selectively Toxic for Mature Oligodendrocytes." Neurotoxicity Research **24**(2): 244-250.

Benetti, F. and G. Legname (2015). "New insights into structural determinants of prion protein folding and stability." Prion **9**(2): 119-124.

Benetti, F., M. Ventura, B. Salmini, S. Ceola, D. Carbonera, S. Mammi, A. Zitolo, P. D'Angelo, E. Urso, M. Maffia, B. Salvato and E. Spisni (2010). "Cuprizone neurotoxicity, copper deficiency and neurodegeneration." NeuroToxicology **31**(5): 509-517.

Benvegnu, S., L. Gasperini and G. Legname (2011). "Aged PrP null mice show defective processing of neuregulins in the peripheral nervous system." Mol Cell Neurosci **47**(1): 28-35.

Benvegnù, S., L. Gasperini and G. Legname (2011). "Aged PrP null mice show defective processing of neuregulins in the peripheral nervous system." Molecular and Cellular Neuroscience **47**(1): 28-35.

Benvegnu, S., I. Poggiolini and G. Legname (2010). "Neurodevelopmental expression and localization of the cellular prion protein in the central nervous system of the mouse." J Comp Neurol **518**(11): 1879-1891.

Bizzozero, O. A., G. DeJesus and T. A. Howard (2004). "Exposure of rat optic nerves to nitric oxide causes protein S-nitrosation and myelin decompaction." Neurochem Res **29**(9): 1675-1685.

Blakemore, W. F. and R. J. Franklin (2008). "Remyelination in experimental models of toxin-induced demyelination." Curr Top Microbiol Immunol **318**: 193-212.

Bolognin, S., L. Messori and P. Zatta (2009). "Metal Ion Physiopathology in Neurodegenerative Disorders." NeuroMolecular Medicine **11**(4): 223-238.

Bongarzone, E. R., J. M. Pasquini and E. F. Soto (1995). "Oxidative damage to proteins and lipids of CNS myelin produced by in vitro generated reactive oxygen species." J Neurosci Res **41**(2): 213-221.

Bonomo, R. P., G. Pappalardo, E. Rizzarelli, G. Tabbi and L. I. Vagliasindi (2008). "Studies of nitric oxide interaction with mono- and dinuclear copper(ii) complexes of prion protein bis-octarepeat fragments." Dalton Transactions(29): 3805-3816.

Bounhar, Y., Y. Zhang, C. G. Goodyer and A. LeBlanc (2001). "Prion Protein Protects Human Neurons against Bax-mediated Apoptosis." Journal of Biological Chemistry **276**(42): 39145-39149.

Bozzali, M. and L. Wrabetz (2004). "Axonal signals and oligodendrocyte differentiation." Neurochem Res **29**(5): 979-988.

Bradl, M. and H. Lassmann (2010). "Oligodendrocytes: biology and pathology." Acta Neuropathologica **119**(1): 37-53.

Brandner, S., S. Isenmann, A. Raeber, M. Fischer, A. Sailer, Y. Kobayashi, S. Marino, C. Weissmann and A. Aguzzi (1996). "Normal host prion protein necessary for scrapie-induced neurotoxicity." Nature **379**(6563): 339-343.

Bremer, J., F. Baumann, C. Tiberi, C. Wessig, H. Fischer, P. Schwarz, A. D. Steele, K. V. Toyka, K.-A. Nave, J. Weis and A. Aguzzi (2010). "Axonal prion protein is required for peripheral myelin maintenance." Nat Neurosci **13**(3): 310-318.

Bremer, J., F. Baumann, C. Tiberi, C. Wessig, H. Fischer, P. Schwarz, A. D. Steele, K. V. Toyka, K. A. Nave, J. Weis and A. Aguzzi (2010). "Axonal prion protein is required for peripheral myelin maintenance." Nat Neurosci **13**(3): 310-318.

Bribián, A., X. Fontana, F. Llorens, R. Gavín, M. Reina, J. M. García-Verdugo, J. M. Torres, F. de Castro and J. A. del Río (2012). "Role of the Cellular Prion Protein in Oligodendrocyte Precursor Cell Proliferation and Differentiation in the Developing and Adult Mouse CNS." PLoS ONE **7**(4): e33872.

Brown, D. and J. Sassoon (2002). "Copper-dependent functions for the prion protein." Molecular Biotechnology **22**(2): 165-178.

Brown, D. R. (2001). "Prion and prejudice: normal protein and the synapse." Trends Neurosci **24**(2): 85-90.

Brown, D. R. (2003). "Prion protein expression modulates neuronal copper content." J Neurochem **87**(2): 377-385.

Brown, D. R. and A. Besinger (1998). "Prion protein expression and superoxide dismutase activity." Biochem J **334 (Pt 2)**: 423-429.

Brown, D. R., C. Clive and S. J. Haswell (2001). "Antioxidant activity related to copper binding of native prion protein." J Neurochem **76**(1): 69-76.

Brown, D. R., R. S. Nicholas and L. Canevari (2002). "Lack of prion protein expression results in a neuronal phenotype sensitive to stress." J Neurosci Res **67**(2): 211-224.

Brown, D. R., K. Qin, J. W. Herms, A. Madlung, J. Manson, R. Strome, P. E. Fraser, T. Kruck, A. von Bohlen, W. Schulz-Schaeffer, A. Giese, D. Westaway and H. Kretzschmar (1997). "The cellular prion protein binds copper in vivo." Nature **390**(6661): 684-687.

Brown, D. R., B. Schmidt and H. A. Kretzschmar (1998). "Effects of copper on survival of prion protein knockout neurons and glia." J Neurochem **70**(4): 1686-1693.

Brown, D. R., W. J. Schulz-Schaeffer, B. Schmidt and H. A. Kretzschmar (1997). "Prion protein-deficient cells show altered response to oxidative stress due to decreased SOD-1 activity." Exp Neurol **146**(1): 104-112.

Brown, D. R., B. S. Wong, F. Hafiz, C. Clive, S. J. Haswell and I. M. Jones (1999). "Normal prion protein has an activity like that of superoxide dismutase." Biochem J **344 Pt 1**: 1-5.

Brown, L. R. and D. A. Harris (2003). "Copper and zinc cause delivery of the prion protein from the plasma membrane to a subset of early endosomes and the Golgi." J Neurochem **87**(2): 353-363.

Budka, H., M. W. Head, J. W. Ironside, P. Gambetti, P. Parchi and F. Tagliavini (2011). Sporadic Creutzfeldt–Jakob Disease. Neurodegeneration: The Molecular Pathology of Dementia and Movement Disorders, Wiley-Blackwell**:** 322-335.

Bueler, H., A. Aguzzi, A. Sailer, R. A. Greiner, P. Autenried, M. Aguet and C. Weissmann (1993). "Mice devoid of PrP are resistant to scrapie." Cell **73**(7): 1339-1347.

Bueler, H., M. Fischer, Y. Lang, H. Bluethmann, H. P. Lipp, S. J. DeArmond, S. B. Prusiner, M. Aguet and C. Weissmann (1992). "Normal development and behaviour of mice lacking the neuronal cell-surface PrP protein." Nature **356**(6370): 577-582.

Bush, A. I. (2000). "Metals and neuroscience." Curr Opin Chem Biol **4**(2): 184-191.

Bush, A. I. (2000). "Metals and neuroscience." Current Opinion in Chemical Biology **4**(2): 184-191.

Caiati, M. D., V. F. Safiulina, G. Fattorini, S. Sivakumaran, G. Legname and E. Cherubini (2013). "PrPC Controls via Protein Kinase A the Direction of Synaptic Plasticity in the Immature Hippocampus." The Journal of Neuroscience **33**(7): 2973-2983.

Campagnoni, A. T. (1988). "Molecular biology of myelin proteins from the central nervous system." J Neurochem **51**(1): 1-14.

Carleton, A., P. Tremblay, J. D. Vincent and P. M. Lledo (2001). "Dose-dependent, prion protein (PrP)-mediated facilitation of excitatory synaptic transmission in the mouse hippocampus." Pflugers Arch **442**(2): 223-229.

Carlton, W. W. (1967). "Studies on the induction of hydrocephalus and spongy degeneration by cuprizone feeding and attempts to antidote the toxicity." Life Sci **6**(1): 11-19.

Caughey, B. (2003). "Prion protein conversions: insight into mechanisms, TSE transmission barriers and strains." British Medical Bulletin **66**(1): 109-120.

Caughey, B. and G. S. Baron (2006). "Prions and their partners in crime." Nature **443**(7113): 803-810.

Caughey, B. and G. J. Raymond (1991). "The scrapie-associated form of PrP is made from a cell surface precursor that is both protease- and phospholipase-sensitive." J Biol Chem **266**(27): 18217-18223.

Caughey, B. W., A. Dong, K. S. Bhat, D. Ernst, S. F. Hayes and W. S. Caughey (1991). "Secondary structure analysis of the scrapie-associated protein PrP 27-30 in water by infrared spectroscopy." Biochemistry **30**(31): 7672-7680.

Chattopadhyay, M., E. D. Walter, D. J. Newell, P. J. Jackson, E. Aronoff-Spencer, J. Peisach, G. J. Gerfen, B. Bennett, W. E. Antholine and G. L. Millhauser (2005). "The octarepeat domain of the prion protein binds Cu(II) with three distinct coordination modes at pH 7.4." J Am Chem Soc **127**(36): 12647-12656.

Chesebro, B., M. Trifilo, R. Race, K. Meade-White, C. Teng, R. LaCasse, L. Raymond, C. Favara, G. Baron, S. Priola, B. Caughey, E. Masliah and M. Oldstone (2005). "Anchorless prion protein results in infectious amyloid disease without clinical scrapie." Science **308**(5727): 1435-1439.

Colby, D. W. and S. B. Prusiner (2011). "Prions." Cold Spring Harbor Perspectives in Biology **3**(1): a006833.

Colling, S. B., J. Collinge and J. G. Jefferys (1996). "Hippocampal slices from prion protein null mice: disrupted Ca(2+)-activated K+ currents." Neurosci Lett **209**(1): 49-52.

Collinge, J., M. A. Whittington, K. C. Sidle, C. J. Smith, M. S. Palmer, A. R. Clarke and J. G. Jefferys (1994). "Prion protein is necessary for normal synaptic function." Nature **370**(6487): 295-297.

Collingridge, G. (1987). "Synaptic plasticity. The role of NMDA receptors in learning and memory." Nature **330**(6149): 604-605.

Connor, J. R. and R. E. Fine (1987). "Development of transferrin-positive oligodendrocytes in the rat central nervous system." J Neurosci Res **17**(1): 51-59.

Connor, J. R. and S. L. Menzies (1996). "Relationship of iron to oligodendrocytes and myelination." Glia **17**(2): 83-93.

Criado, J. R., M. Sanchez-Alavez, B. Conti, J. L. Giacchino, D. N. Wills, S. J. Henriksen, R. Race, J. C. Manson, B. Chesebro and M. B. Oldstone (2005). "Mice devoid of prion protein have cognitive deficits that are rescued by reconstitution of PrP in neurons." Neurobiol Dis **19**(1-2): 255-265.

Cui, T., M. Daniels, B. S. Wong, R. Li, M. S. Sy, J. Sassoon and D. R. Brown (2003). "Mapping the functional domain of the prion protein." Eur J Biochem **270**(16): 3368-3376.

Cull-Candy, S., S. Brickley and M. Farrant (2001). "NMDA receptor subunits: diversity, development and disease." Curr Opin Neurobiol **11**(3): 327-335.

Das, S., Y. F. Sasaki, T. Rothe, L. S. Premkumar, M. Takasu, J. E. Crandall, P. Dikkes, D. A. Conner, P. V. Rayudu, W. Cheung, H. S. Chen, S. A. Lipton and N. Nakanishi (1998). "Increased NMDA current and spine density in mice lacking the NMDA receptor subunit NR3A." Nature **393**(6683): 377-381.

Dening, T. R. (1991). "The neuropsychiatry of Wilson's disease: a review." Int J Psychiatry Med **21**(2): 135-148.

Didonna, A. and F. Benetti (2015). "Post-translational modifications in neurodegeneration." AIMS Biophysics **3**(1): 27-49.

Didonna, A., J. Sussman, F. Benetti and G. Legname (2012). "The role of Bax and caspase-3 in doppel-induced apoptosis of cerebellar granule cells." Prion **6**(3): 309-316.

Dingledine, R., K. Borges, D. Bowie and S. F. Traynelis (1999). "The glutamate receptor ion channels." Pharmacol Rev **51**(1): 7-61.

Dong, Z., P. Saikumar, J. M. Weinberg and M. A. Venkatachalam (2006). "Calcium in cell injury and death." Annu Rev Pathol **1**: 405-434.

Encinas, J. M., L. Manganas and G. Enikolopov (2005). "Nitric oxide and multiple sclerosis." Curr Neurol Neurosci Rep **5**(3): 232-238.

Ford, M. J., L. J. Burton, H. Li, C. H. Graham, Y. Frobert, J. Grassi, S. M. Hall and R. J. Morris (2002). "A marked disparity between the expression of prion protein and its message by neurones of the CNS." Neuroscience **111**(3): 533-551.

Fournier, J. G., F. Escaig-Haye, T. Billette de Villemeur, O. Robain, C. I. Lasmezas, J. P. Deslys, D. Dormont and P. Brown (1998). "Distribution and submicroscopic immunogold localization of cellular prion protein (PrPc) in extracerebral tissues." Cell Tissue Res **292**(1): 77-84.

Franklin, R. J. and C. Ffrench-Constant (2008). "Remyelination in the CNS: from biology to therapy." Nat Rev Neurosci **9**(11): 839-855.

Friese, M. A., B. Schattling and L. Fugger (2014). "Mechanisms of neurodegeneration and axonal dysfunction in multiple sclerosis." Nat Rev Neurol **10**(4): 225-238.

Fruhbeis, C., D. Frohlich, W. P. Kuo, J. Amphornrat, S. Thilemann, A. S. Saab, F. Kirchhoff, W. Mobius, S. Goebbels, K. A. Nave, A. Schneider, M. Simons, M. Klugmann, J. Trotter and E. M. Kramer-Albers (2013). "Neurotransmitter-triggered transfer of exosomes mediates oligodendrocyte-neuron communication." PLoS Biol **11**(7): e1001604.

Fuhrmann, M., T. Bittner, G. Mitteregger, N. Haider, S. Moosmang, H. Kretzschmar and J. Herms (2006). "Loss of the cellular prion protein affects the Ca2+ homeostasis in hippocampal CA1 neurons." J Neurochem **98**(6): 1876-1885.

Funfschilling, U., L. M. Supplie, D. Mahad, S. Boretius, A. S. Saab, J. Edgar, B. G. Brinkmann, C. M. Kassmann, I. D. Tzvetanova, W. Mobius, F. Diaz, D. Meijer, U. Suter, B. Hamprecht, M. W. Sereda, C. T. Moraes, J. Frahm, S. Goebbels and K. A. Nave (2012). "Glycolytic oligodendrocytes maintain myelin and long-term axonal integrity." Nature **485**(7399): 517-521.

Furlan, R., C. Cuomo and G. Martino (2009). "Animal models of multiple sclerosis." Methods Mol Biol **549**: 157-173.

Gahwiler, B. H., M. Capogna, D. Debanne, R. A. McKinney and S. M. Thompson (1997). "Organotypic slice cultures: a technique has come of age." Trends Neurosci **20**(10): 471-477.

Gasperini, L., E. Meneghetti, B. Pastore, F. Benetti and G. Legname (2015). "Prion Protein and Copper Cooperatively Protect Neurons by Modulating NMDA Receptor Through S-nitrosylation." Antioxidants & Redox Signaling **22**(9): 772-784.

Gasset, M., M. A. Baldwin, R. J. Fletterick and S. B. Prusiner (1993). "Perturbation of the secondary structure of the scrapie prion protein under conditions that alter infectivity." Proc Natl Acad Sci U S A **90**(1): 1-5.

Giese, A., M. Buchholz, J. Herms and H. A. Kretzschmar (2005). "Mouse brain synaptosomes accumulate copper-67 efficiently by two distinct processes independent of cellular prion protein." J Mol Neurosci **27**(3): 347-354.

Gregson, N. A. (1989). "Lysolipids and membrane damage: lysolecithin and its interaction with myelin." Biochem Soc Trans **17**(2): 280-283.

Gudi, V., S. Gingele, T. Skripuletz and M. Stangel (2014). "Glial response during cuprizone-induced de- and remyelination in the CNS: lessons learned." Frontiers in Cellular Neuroscience **8**: 73.

Haeberle, A. M., C. Ribaut-Barassin, G. Bombarde, J. Mariani, G. Hunsmann, J. Grassi and Y. Bailly (2000). "Synaptic prion protein immuno-reactivity in the rodent cerebellum." Microsc Res Tech **50**(1): 66-75.

Halliday, M., H. Radford and G. R. Mallucci (2014). "Prions: Generation and Spread Versus Neurotoxicity." The Journal of Biological Chemistry **289**(29): 19862-19868.

Haraguchi, T., S. Fisher, S. Olofsson, T. Endo, D. Groth, A. Tarentino, D. R. Borchelt, D. Teplow, L. Hood, A. Burlingame and et al. (1989). "Asparagine-linked glycosylation of the scrapie and cellular prion proteins." Arch Biochem Biophys **274**(1): 1-13.

Harris, D. A. and H. L. True (2006). "New Insights into Prion Structure and Toxicity." Neuron **50**(3): 353-357.

Hartline, D. K. (2008). "What is myelin?" Neuron Glia Biology **4**(02): 153-163.

Hartter, D. E. and A. Barnea (1988). "Evidence for release of copper in the brain: depolarization-induced release of newly taken-up 67copper." Synapse **2**(4): 412-415.

Herms, J., T. Tings, S. Gall, A. Madlung, A. Giese, H. Siebert, P. Schurmann, O. Windl, N. Brose and H. Kretzschmar (1999). "Evidence of presynaptic location and function of the prion protein." J Neurosci **19**(20): 8866-8875.

Herms, J. W., T. Tings, S. Dunker and H. A. Kretzschmar (2001). "Prion protein affects Ca2+-activated K+ currents in cerebellar purkinje cells." Neurobiol Dis **8**(2): 324-330.

Hess, D. T., A. Matsumoto, S.-O. Kim, H. E. Marshall and J. S. Stamler (2005). "Protein S-nitrosylation: purview and parameters." Nat Rev Mol Cell Biol **6**(2): 150-166.

Hild, W. (1956). "[Myelin formation in central nervous system tissue cultures]." Verh Anat Ges **53**: 315-317.

Hill, A. F. and J. Collinge (2003). "Subclinical prion infection in humans and animals." British Medical Bulletin **66**(1): 161-170.

Hines, J. H., A. M. Ravanelli, R. Schwindt, E. K. Scott and B. Appel (2015). "Neuronal activity biases axon selection for myelination in vivo." Nat Neurosci **18**(5): 683-689.

Hoffmann, K., M. Lindner, I. Groticke, M. Stangel and W. Loscher (2008). "Epileptic seizures and hippocampal damage after cuprizone-induced demyelination in C57BL/6 mice." Exp Neurol **210**(2): 308-321.

Horiuchi, M., N. Yamazaki, T. Ikeda, N. Ishiguro and M. Shinagawa (1995). "A cellular form of prion protein (PrPC) exists in many non-neuronal tissues of sheep." J Gen Virol **76 (Pt 10)**: 2583-2587.

Hornshaw, M. P., J. R. McDermott, J. M. Candy and J. H. Lakey (1995). "Copper binding to the N-terminal tandem repeat region of mammalian and avian prion protein: structural studies using synthetic peptides." Biochem Biophys Res Commun **214**(3): 993-999.

Itoh, Y., M. Yamada, M. Hayakawa, T. Shozawa, J. Tanaka, M. Matsushita, T. Kitamoto, J. Tateishi and E. Otomo (1994). "A variant of Gerstmann-Straussler-Scheinker disease carrying codon 105 mutation with codon 129 polymorphism of the prion protein gene: a clinicopathological study." J Neurol Sci **127**(1): 77-86.

Jackson, G. S., I. Murray, L. L. Hosszu, N. Gibbs, J. P. Waltho, A. R. Clarke and J. Collinge (2001). "Location and properties of metal-binding sites on the human prion protein." Proc Natl Acad Sci U S A **98**(15): 8531-8535.

Jellinger, K. A. (2010). "Basic mechanisms of neurodegeneration: a critical update." Journal of Cellular and Molecular Medicine **14**(3): 457-487.

Jones, C. E., S. R. Abdelraheim, D. R. Brown and J. H. Viles (2004). "Preferential Cu2+ coordination by His96 and His111 induces beta-sheet formation in the unstructured amyloidogenic region of the prion protein." J Biol Chem **279**(31): 32018-32027.

Kanaani, J., S. B. Prusiner, J. Diacovo, S. Baekkeskov and G. Legname (2005). "Recombinant prion protein induces rapid polarization and development of synapses in embryonic rat hippocampal neurons in vitro." J Neurochem **95**(5): 1373-1386.

Khosravani, H., Y. Zhang, S. Tsutsui, S. Hameed, C. Altier, J. Hamid, L. Chen, M. Villemaire, Z. Ali, F. R. Jirik and G. W. Zamponi (2008). "Prion protein attenuates excitotoxicity by inhibiting NMDA receptors." J Cell Biol **181**(3): 551-565.

Koutsoudaki, P. N., T. Skripuletz, V. Gudi, D. Moharregh-Khiabani, H. Hildebrandt, C. Trebst and M. Stangel (2009). "Demyelination of the hippocampus is prominent in the cuprizone model." Neurosci Lett **451**(1): 83-88.

Kralovicova, S., S. N. Fontaine, A. Alderton, J. Alderman, K. V. Ragnarsdottir, S. J. Collins and D. R. Brown (2009). "The effects of prion protein expression on metal metabolism." Mol Cell Neurosci **41**(2): 135-147.

Kramer, M. L., H. D. Kratzin, B. Schmidt, A. Romer, O. Windl, S. Liemann, S. Hornemann and H. Kretzschmar (2001). "Prion protein binds copper within the physiological concentration range." J Biol Chem **276**(20): 16711-16719.

Krebs, B., A. Wiebelitz, B. Balitzki-Korte, N. Vassallo, S. Paluch, G. Mitteregger, T. Onodera, H. A. Kretzschmar and J. Herms (2007). "Cellular prion protein modulates the intracellular calcium response to hydrogen peroxide." J Neurochem **100**(2): 358-367.

Kuwahara, C., A. M. Takeuchi, T. Nishimura, K. Haraguchi, A. Kubosaki, Y. Matsumoto, K. Saeki, Y. Matsumoto, T. Yokoyama, S. Itohara and T. Onodera (1999). "Prions prevent neuronal cell-line death." Nature **400**(6741): 225-226.

Lazarini, F., J. P. Deslys and D. Dormont (1991). "Regulation of the glial fibrillary acidic protein, beta actin and prion protein mRNAs during brain development in mouse." Brain Res Mol Brain Res **10**(4): 343-346.

Lazzari, C., C. Peggion, R. Stella, M. L. Massimino, D. Lim, A. Bertoli and M. C. Sorgato (2011). "Cellular prion protein is implicated in the regulation of local Ca2+ movements in cerebellar granule neurons." J Neurochem **116**(5): 881-890.

Li, A., H. M. Christensen, L. R. Stewart, K. A. Roth, R. Chiesa and D. A. Harris (2007). "Neonatal lethality in transgenic mice expressing prion protein with a deletion of residues 105-125." EMBO J **26**(2): 548-558.

Linden, R., V. R. Martins, M. A. Prado, M. Cammarota, I. Izquierdo and R. R. Brentani (2008). "Physiology of the prion protein." Physiol Rev **88**(2): 673-728.

Lipton, S. A., Y. B. Choi, H. Takahashi, D. Zhang, W. Li, A. Godzik and L. A. Bankston (2002). "Cysteine regulation of protein function--as exemplified by NMDA-receptor modulation." Trends Neurosci **25**(9): 474-480.

Lipton, S. A. and P. A. Rosenberg (1994). "Excitatory amino acids as a final common pathway for neurologic disorders." N Engl J Med **330**(9): 613-622.

Liu, L., D. Jiang, A. McDonald, Y. Hao, G. L. Millhauser and F. Zhou (2011). "Copper redox cycling in the prion protein depends critically on binding mode." J Am Chem Soc **133**(31): 12229-12237.

Liu, P.-C., Y.-W. Chen, J. A. Centeno, M. Quezado, K. Lem and S. G. Kaler (2005). "Downregulation of myelination, energy, and translational genes in Menkes disease brain." Molecular Genetics and Metabolism **85**(4): 291-300.

Livak, K. J. and T. D. Schmittgen (2001). "Analysis of relative gene expression data using real-time quantitative PCR and the 2(-Delta Delta C(T)) Method." Methods **25**(4): 402-408.

Lledo, P. M., P. Tremblay, S. J. DeArmond, S. B. Prusiner and R. A. Nicoll (1996). "Mice deficient for prion protein exhibit normal neuronal excitability and synaptic transmission in the hippocampus." Proc Natl Acad Sci U S A **93**(6): 2403-2407.

Loftis, J. M. and A. Janowsky (2003). "The N-methyl-D-aspartate receptor subunit NR2B: localization, functional properties, regulation, and clinical implications." Pharmacol Ther **97**(1): 55-85.

Lovell, M. A. (2009). "A potential role for alterations of zinc and zinc transport proteins in the progression of Alzheimer's disease." J Alzheimers Dis **16**(3): 471-483.

Madsen, E. and J. D. Gitlin (2007). "Copper and iron disorders of the brain." Annu Rev Neurosci **30**: 317-337.

Maglio, L. E., M. F. Perez, V. R. Martins, R. R. Brentani and O. A. Ramirez (2004). "Hippocampal synaptic plasticity in mice devoid of cellular prion protein." Brain Res Mol Brain Res **131**(1-2): 58-64.

Mallucci, G., A. Dickinson, J. Linehan, P. C. Klohn, S. Brandner and J. Collinge (2003). "Depleting neuronal PrP in prion infection prevents disease and reverses spongiosis." Science **302**(5646): 871-874.

Mallucci, G. R., S. Ratte, E. A. Asante, J. Linehan, I. Gowland, J. G. Jefferys and J. Collinge (2002). "Post-natal knockout of prion protein alters hippocampal CA1 properties, but does not result in neurodegeneration." EMBO J **21**(3): 202-210.

Malone, M., D. Gary, I. H. Yang, A. Miglioretti, T. Houdayer, N. Thakor and J. McDonald (2013). "Neuronal activity promotes myelination via a cAMP pathway." Glia **61**(6): 843-854.

Mange, A., F. Beranger, K. Peoc'h, T. Onodera, Y. Frobert and S. Lehmann (2004). "Alpha- and beta-cleavages of the amino-terminus of the cellular prion protein." Biol Cell **96**(2): 125-132.

Manson, J., J. D. West, V. Thomson, P. McBride, M. H. Kaufman and J. Hope (1992). "The prion protein gene: a role in mouse embryogenesis?" Development **115**(1): 117-122.

Manson, J. C., A. R. Clarke, M. L. Hooper, L. Aitchison, I. McConnell and J. Hope (1994). "129/Ola mice carrying a null mutation in PrP that abolishes mRNA production are developmentally normal." Mol Neurobiol **8**(2-3): 121-127.

Manson, J. C., J. Hope, A. R. Clarke, A. Johnston, C. Black and N. MacLeod (1995). "PrP gene dosage and long term potentiation." Neurodegeneration **4**(1): 113-114.

Martins, I., L. Galluzzi and G. Kroemer (2011). "Hormesis, cell death and aging." Aging (Albany NY) **3**(9): 821-828.

Mathisen, P. M., J. A. Kawczak, M. Yu, J. M. Johnson and V. K. Tuohy (2001). "Differential DM20 mRNA expression distinguishes two distinct patterns of spontaneous recovery from murine autoimmune encephalomyelitis." J Neurosci Res **64**(5): 542-551.

Matsushima, G. K. and P. Morell (2001). "The Neurotoxicant, Cuprizone, as a Model to Study Demyelination and Remyelination in the Central Nervous System." Brain Pathology **11**(1): 107-116.

Matute, C., M. V. Sanchez-Gomez, L. Martinez-Millan and R. Miledi (1997). "Glutamate receptor-mediated toxicity in optic nerve oligodendrocytes." Proc Natl Acad Sci U S A **94**(16): 8830-8835.

Mayer, M. L., L. Vyklicky and J. Clements (1989). "Regulation of NMDA receptor desensitization in mouse hippocampal neurons by glycine." Nature **338**(6214): 425-427.

McDonald, J. W., S. P. Althomsons, K. L. Hyrc, D. W. Choi and M. P. Goldberg (1998). "Oligodendrocytes from forebrain are highly vulnerable to AMPA/kainate receptor-mediated excitotoxicity." Nat Med **4**(3): 291-297.

McLennan, N. F., P. M. Brennan, A. McNeill, I. Davies, A. Fotheringham, K. A. Rennison, D. Ritchie, F. Brannan, M. W. Head, J. W. Ironside, A. Williams and J. E. Bell (2004). "Prion protein accumulation and neuroprotection in hypoxic brain damage." Am J Pathol **165**(1): 227-235.

McTigue, D. M. and R. B. Tripathi (2008). "The life, death, and replacement of oligodendrocytes in the adult CNS." J Neurochem **107**(1): 1-19.

McTigue, D. M. and R. B. Tripathi (2008). "The life, death, and replacement of oligodendrocytes in the adult CNS." Journal of Neurochemistry **107**(1): 1-19.

Milhavet, O. and S. Lehmann (2002). "Oxidative stress and the prion protein in transmissible spongiform encephalopathies." Brain Research Reviews **38**(3): 328-339.

Mitsios, N., M. Saka, J. Krupinski, R. Pennucci, C. Sanfeliu, M. Miguel Turu, J. Gaffney, P. Kumar, S. Kumar, M. Sullivan and M. Slevin (2007). "Cellular prion protein is increased in the plasma and peri-infarcted brain tissue after acute stroke." J Neurosci Res **85**(3): 602-611.

Miura, T., S. Sasaki, A. Toyama and H. Takeuchi (2005). "Copper reduction by the octapeptide repeat region of prion protein: pH dependence and implications in cellular copper uptake." Biochemistry **44**(24): 8712-8720.

Mobley, W. C., R. L. Neve, S. B. Prusiner and M. P. McKinley (1988). "Nerve growth factor increases mRNA levels for the prion protein and the beta-amyloid protein precursor in developing hamster brain." Proc Natl Acad Sci U S A **85**(24): 9811-9815.

Moore, R. C., I. Y. Lee, G. L. Silverman, P. M. Harrison, R. Strome, C. Heinrich, A. Karunaratne, S. H. Pasternak, M. A. Chishti, Y. Liang, P. Mastrangelo, K. Wang, A. F. Smit, S. Katamine, G. A. Carlson, F. E. Cohen, S. B. Prusiner, D. W. Melton, P. Tremblay, L. E. Hood and D. Westaway (1999). "Ataxia in prion protein (PrP)-deficient mice is associated with upregulation of the novel PrP-like protein doppel." J Mol Biol **292**(4): 797-817.

Morelli, A., S. Ravera, D. Calzia and I. Panfoli (2012). "Impairment of heme synthesis in myelin as potential trigger of multiple sclerosis." Medical Hypotheses **78**(6): 707-710.

Moriyoshi, K., M. Masu, T. Ishii, R. Shigemoto, N. Mizuno and S. Nakanishi (1991). "Molecular cloning and characterization of the rat NMDA receptor." Nature **354**(6348): 31-37.

Mouillet-Richard, S., M. Ermonval, C. Chebassier, J. L. Laplanche, S. Lehmann, J. M. Launay and O. Kellermann (2000). "Signal Transduction Through Prion Protein." Science **289**(5486): 1925-1928.

Moya, K. L., N. Sales, R. Hassig, C. Creminon, J. Grassi and L. Di Giamberardino (2000). "Immunolocalization of the cellular prion protein in normal brain." Microsc Res Tech **50**(1): 58-65.

Nakamura, T. and S. A. Lipton (2011). "Redox modulation by S-nitrosylation contributes to protein misfolding, mitochondrial dynamics, and neuronal synaptic damage in neurodegenerative diseases." Cell Death Differ **18**(9): 1478-1486.

Naslavsky, N., R. Stein, A. Yanai, G. Friedlander and A. Taraboulos (1997). "Characterization of detergent-insoluble complexes containing the cellular prion protein and its scrapie isoform." J Biol Chem **272**(10): 6324-6331.

Nave, K.-A. (2010). "Myelination and support of axonal integrity by glia." Nature **468**(7321): 244-252.

Nazor, K. E., T. Seward and G. C. Telling (2007). "Motor behavioral and neuropathological deficits in mice deficient for normal prion protein expression." Biochim Biophys Acta **1772**(6): 645-653.

Nishida, N., P. Tremblay, T. Sugimoto, K. Shigematsu, S. Shirabe, C. Petromilli, S. P. Erpel, R. Nakaoke, R. Atarashi, T. Houtani, M. Torchia, S. Sakaguchi, S. J. DeArmond, S. B. Prusiner and S. Katamine (1999). "A mouse prion protein transgene rescues mice deficient for the prion protein gene from purkinje cell degeneration and demyelination." Lab Invest **79**(6): 689-697.

Norkute, A., A. Hieble, A. Braun, S. Johann, T. Clarner, W. Baumgartner, C. Beyer and M. Kipp (2009). "Cuprizone treatment induces demyelination and astrocytosis in the mouse hippocampus." J Neurosci Res **87**(6): 1343-1355.

Oder, W., G. Grimm, H. Kollegger, P. Ferenci, B. Schneider and L. Deecke (1991). "Neurological and neuropsychiatric spectrum of Wilson's disease: a prospective study of 45 cases." J Neurol **238**(5): 281-287.

Oesch, B., D. Westaway, M. Walchli, M. P. McKinley, S. B. Kent, R. Aebersold, R. A. Barry, P. Tempst, D. B. Teplow, L. E. Hood and et al. (1985). "A cellular gene encodes scrapie PrP 27-30 protein." Cell **40**(4): 735-746.

Orth, M. and S. Bellosta (2012). "Cholesterol: its regulation and role in central nervous system disorders." Cholesterol **2012**: 292598.

Parkin, E. T., N. T. Watt, I. Hussain, E. A. Eckman, C. B. Eckman, J. C. Manson, H. N. Baybutt, A. J. Turner and N. M. Hooper (2007). "Cellular prion protein regulates beta-secretase cleavage of the Alzheimer's amyloid precursor protein." Proc Natl Acad Sci U S A **104**(26): 11062-11067.

Pauly, P. C. and D. A. Harris (1998). "Copper stimulates endocytosis of the prion protein." J Biol Chem **273**(50): 33107-33110.

Perez-Otano, I., C. T. Schulteis, A. Contractor, S. A. Lipton, J. S. Trimmer, N. J. Sucher and S. F. Heinemann (2001). "Assembly with the NR1 subunit is required for surface expression of NR3A-containing NMDA receptors." J Neurosci **21**(4): 1228-1237.

Peters, S., J. Koh and D. Choi (1987). "Zinc selectively blocks the action of N-methyl-D-aspartate on cortical neurons." Science **236**(4801): 589-593.

Praet, J., C. Guglielmetti, Z. Berneman, A. Van der Linden and P. Ponsaerts (2014). "Cellular and molecular neuropathology of the cuprizone mouse model: Clinical relevance for multiple sclerosis." Neuroscience & Biobehavioral Reviews **47**: 485-505.

Prestori, F., P. Rossi, B. Bearzatto, J. Laine, D. Necchi, S. Diwakar, S. N. Schiffmann, H. Axelrad and E. D'Angelo (2008). "Altered neuron excitability and synaptic plasticity in the cerebellar granular layer of juvenile prion protein knock-out mice with impaired motor control." J Neurosci **28**(28): 7091-7103.

Prusiner, S. B. (1982). "Novel proteinaceous infectious particles cause scrapie." Science **216**(4542): 136-144.

Prusiner, S. B. (1991). "Molecular biology of prion diseases." Science **252**(5012): 1515-1522.

Prusiner, S. B. (1992). "Natural and experimental prion diseases of humans and animals." Curr Opin Neurobiol **2**(5): 638-647.

Prusiner, S. B. (1994). "Biology and genetics of prion diseases." Annu Rev Microbiol **48**: 655-686.

Prusiner, S. B. (2001). "Neurodegenerative Diseases and Prions." New England Journal of Medicine **344**(20): 1516-1526.

Prusiner, S. B. and S. J. DeArmond (1994). "Prion diseases and neurodegeneration." Annu Rev Neurosci **17**: 311-339.

Pushie, M. J., I. J. Pickering, G. R. Martin, S. Tsutsui, F. R. Jirik and G. N. George (2011). "Prion protein expression level alters regional copper, iron and zinc content in the mouse brain." Metallomics **3**(2): 206-214.

Quattrini, A., S. Previtali, M. L. Feltri, N. Canal, R. Nemni and L. Wrabetz (1996). "Beta 4 integrin and other Schwann cell markers in axonal neuropathy." Glia **17**(4): 294-306.

Rachidi, W., D. Vilette, P. Guiraud, M. Arlotto, J. Riondel, H. Laude, S. Lehmann and A. Favier (2003). "Expression of prion protein increases cellular copper binding and antioxidant enzyme activities but not copper delivery." J Biol Chem **278**(11): 9064-9072.

Radovanovic, I., N. Braun, O. T. Giger, K. Mertz, G. Miele, M. Prinz, B. Navarro and A. Aguzzi (2005). "Truncated prion protein and Doppel are myelinotoxic in the absence of oligodendrocytic PrPC." J Neurosci **25**(19): 4879-4888.

Radovanovic, I., N. Braun, O. T. Giger, K. Mertz, G. Miele, M. Prinz, B. Navarro and A. Aguzzi (2005). "Truncated Prion Protein and Doppel Are Myelinotoxic in the Absence of Oligodendrocytic PrPC." The Journal of Neuroscience **25**(19): 4879-4888.

Rangel, A., F. Burgaya, R. Gavin, E. Soriano, A. Aguzzi and J. A. Del Rio (2007). "Enhanced susceptibility of Prnp-deficient mice to kainate-induced seizures, neuronal apoptosis, and death: Role of AMPA/kainate receptors." J Neurosci Res **85**(12): 2741-2755.

Rawlins, F. A. and M. E. Smith (1971). "MYELIN SYNTHESIS IN VITRO: A COMPARATIVE STUDY OF CENTRAL AND PERIPHERAL NERVOUS TISSUE." Journal of Neurochemistry **18**(10): 1861-1870.

Rivera-Mancia, S., I. Perez-Neri, C. Rios, L. Tristan-Lopez, L. Rivera-Espinosa and S. Montes (2010). "The transition metals copper and iron in neurodegenerative diseases." Chem Biol Interact **186**(2): 184-199.

Rodolfo, K., R. Hassig, K. L. Moya, Y. Frobert, J. Grassi and L. Di Giamberardino (1999). "A novel cellular prion protein isoform present in rapid anterograde axonal transport." Neuroreport **10**(17): 3639-3644.

Rossi, D., A. Cozzio, E. Flechsig, M. A. Klein, T. Rulicke, A. Aguzzi and C. Weissmann (2001). "Onset of ataxia and Purkinje cell loss in PrP null mice inversely correlated with Dpl level in brain." EMBO J **20**(4): 694-702.

Saher, G., S. Quintes and K.-A. Nave (2011). "Cholesterol: A Novel Regulatory Role in Myelin Formation." The Neuroscientist **17**(1): 79-93.

Sakaguchi, S., S. Katamine, N. Nishida, R. Moriuchi, K. Shigematsu, T. Sugimoto, A. Nakatani, Y. Kataoka, T. Houtani, S. Shirabe, H. Okada, S. Hasegawa, T. Miyamoto and T. Noda (1996). "Loss of cerebellar Purkinje cells in aged mice homozygous for a disrupted PrP gene." Nature **380**(6574): 528-531.

Sales, N., R. Hassig, K. Rodolfo, L. Di Giamberardino, E. Traiffort, M. Ruat, P. Fretier and K. L. Moya (2002). "Developmental expression of the cellular prion protein in elongating axons." Eur J Neurosci **15**(7): 1163-1177.

Sales, N., K. Rodolfo, R. Hassig, B. Faucheux, L. Di Giamberardino and K. L. Moya (1998). "Cellular prion protein localization in rodent and primate brain." Eur J Neurosci **10**(7): 2464-2471.

Salzer, J. L., P. J. Brophy and E. Peles (2008). "Molecular domains of myelinated axons in the peripheral nervous system." Glia **56**(14): 1532-1540.

Schlief, M. L., A. M. Craig and J. D. Gitlin (2005). "NMDA receptor activation mediates copper homeostasis in hippocampal neurons." J Neurosci **25**(1): 239-246.

Schlief, M. L. and J. D. Gitlin (2006). "Copper homeostasis in the CNS: a novel link between the NMDA receptor and copper homeostasis in the hippocampus." Mol Neurobiol **33**(2): 81-90.

Schlief, M. L., T. West, A. M. Craig, D. M. Holtzman and J. D. Gitlin (2006). "Role of the Menkes copper-transporting ATPase in NMDA receptor-mediated neuronal toxicity." Proc Natl Acad Sci U S A **103**(40): 14919-14924.

Sebastiao, A. M., M. Colino-Oliveira, N. Assaife-Lopes, R. B. Dias and J. A. Ribeiro (2013). "Lipid rafts, synaptic transmission and plasticity: Impact in age-related neurodegenerative diseases." Neuropharmacology **64**(1): 97-107.

Shmerling, D., I. Hegyi, M. Fischer, T. Blattler, S. Brandner, J. Gotz, T. Rulicke, E. Flechsig, A. Cozzio, C. von Mering, C. Hangartner, A. Aguzzi and C. Weissmann (1998). "Expression of amino-terminally truncated PrP in the mouse leading to ataxia and specific cerebellar lesions." Cell **93**(2): 203-214.

Shyu, W. C., C. P. Chen, K. Saeki, A. Kubosaki, Y. Matusmoto, T. Onodera, D. C. Ding, M. F. Chiang, Y. J. Lee, S. Z. Lin and H. Li (2005). "Hypoglycemia enhances the expression of prion protein and heat-shock protein 70 in a mouse neuroblastoma cell line." J Neurosci Res **80**(6): 887-894.

Shyu, W. C., M. C. Kao, W. Y. Chou, Y. D. Hsu and B. W. Soong (2000). "Heat shock modulates prion protein expression in human NT-2 cells." Neuroreport **11**(4): 771-774.

Shyu, W. C., S. Z. Lin, K. Saeki, A. Kubosaki, Y. Matsumoto, T. Onodera, M. F. Chiang, P. Thajeb and H. Li (2004). "Hyperbaric oxygen enhances the expression of prion protein and heat shock protein 70 in a mouse neuroblastoma cell line." Cell Mol Neurobiol **24**(2): 257-268.

Simons, K. and E. Ikonen (1997). "Functional rafts in cell membranes." Nature **387**(6633): 569-572.

Simons, M., E. M. Kramer, P. Macchi, S. Rathke-Hartlieb, J. Trotter, K. A. Nave and J. B. Schulz (2002). "Overexpression of the myelin proteolipid protein leads to accumulation of cholesterol and proteolipid protein in endosomes/lysosomes: implications for Pelizaeus-Merzbacher disease." J Cell Biol **157**(2): 327-336.

Simons, M. and K. Trajkovic (2006). "Neuron-glia communication in the control of oligodendrocyte function and myelin biogenesis." J Cell Sci **119**(Pt 21): 4381-4389.

Singh, A., Q. Kong, X. Luo, R. B. Petersen, H. Meyerson and N. Singh (2009). "Prion protein (PrP) knock-out mice show altered iron metabolism: a functional role for PrP in iron uptake and transport." PLoS One **4**(7): e6115.

Singh, A., M. L. Mohan, A. O. Isaac, X. Luo, J. Petrak, D. Vyoral and N. Singh (2009). "Prion protein modulates cellular iron uptake: a novel function with implications for prion disease pathogenesis." PLoS One **4**(2): e4468.

Singh, N., D. Das, A. Singh and M. L. Mohan (2010). "Prion protein and metal interaction: physiological and pathological implications." Curr Issues Mol Biol **12**(2): 99-107.

Singh, N., A. Singh, D. Das and M. L. Mohan (2010). "Redox control of prion and disease pathogenesis." Antioxid Redox Signal **12**(11): 1271-1294.

Skjørringe, T., L. B. Møller and T. Moos (2012). "Impairment of interrelated iron- and copper homeostatic mechanisms in brain contributes to the pathogenesis of neurodegenerative disorders." Frontiers in Pharmacology **3**.

Sodero, A. O., J. Vriens, D. Ghosh, D. Stegner, A. Brachet, M. Pallotto, M. Sassoe-Pognetto, J. F. Brouwers, J. B. Helms, B. Nieswandt, T. Voets and C. G. Dotti (2012). "Cholesterol loss during glutamate-mediated excitotoxicity." Embo j **31**(7): 1764-1773.

Soto, C. and N. Satani (2011). "The intricate mechanisms of neurodegeneration in prion diseases." Trends in molecular medicine **17**(1): 14-24.

Spudich, A., R. Frigg, E. Kilic, U. Kilic, B. Oesch, A. Raeber, C. L. Bassetti and D. M. Hermann (2005). "Aggravation of ischemic brain injury by prion protein deficiency: role of ERK-1/-2 and STAT-1." Neurobiol Dis **20**(2): 442-449.

Stahl, N., D. R. Borchelt, K. Hsiao and S. B. Prusiner (1987). "Scrapie prion protein contains a phosphatidylinositol glycolipid." Cell **51**(2): 229-240.

Stahl, N., D. R. Borchelt and S. B. Prusiner (1990). "Differential release of cellular and scrapie prion proteins from cellular membranes by phosphatidylinositol-specific phospholipase C." Biochemistry **29**(22): 5405-5412.

Steele, A. D., J. G. Emsley, P. H. Özdinler, S. Lindquist and J. D. Macklis (2006). "Prion protein (PrP(c)) positively regulates neural precursor proliferation during developmental and adult mammalian neurogenesis." Proceedings of the National Academy of Sciences of the United States of America **103**(9): 3416-3421.

Steele, A. D., S. Lindquist and A. Aguzzi (2007). "The prion protein knockout mouse: a phenotype under challenge." Prion **1**(2): 83-93.

Stockel, J., J. Safar, A. C. Wallace, F. E. Cohen and S. B. Prusiner (1998). "Prion protein selectively binds copper(II) ions." Biochemistry **37**(20): 7185-7193.

Sugihara, H., K. Moriyoshi, T. Ishii, M. Masu and S. Nakanishi (1992). "Structures and properties of seven isoforms of the NMDA receptor generated by alternative splicing." Biochem Biophys Res Commun **185**(3): 826-832.

Sunyach, C., M. A. Cisse, C. A. da Costa, B. Vincent and F. Checler (2007). "The C-terminal products of cellular prion protein processing, C1 and C2, exert distinct influence on p53-dependent staurosporine-induced caspase-3 activation." J Biol Chem **282**(3): 1956-1963.

Tarohda, T., M. Yamamoto and R. Amamo (2004). "Regional distribution of manganese, iron, copper, and zinc in the rat brain during development." Analytical and Bioanalytical Chemistry **380**(2): 240-246.

Taveggia, C., M. L. Feltri and L. Wrabetz (2010). "Signals to promote myelin formation and repair." Nat Rev Neurol **6**(5): 276-287.

Thorburne, S. K. and B. H. Juurlink (1996). "Low glutathione and high iron govern the susceptibility of oligodendroglial precursors to oxidative stress." J Neurochem **67**(3): 1014-1022.

Tobler, I., S. E. Gaus, T. Deboer, P. Achermann, M. Fischer, T. Rulicke, M. Moser, B. Oesch, P. A. McBride and J. C. Manson (1996). "Altered circadian activity rhythms and sleep in mice devoid of prion protein." Nature **380**(6575): 639-642.

Treiber, C., R. Pipkorn, C. Weise, G. Holland and G. Multhaup (2007). "Copper is required for prion protein-associated superoxide dismutase-I activity in Pichia pastoris." FEBS J **274**(5): 1304-1311.

Valko, M., H. Morris and M. T. Cronin (2005). "Metals, toxicity and oxidative stress." Curr Med Chem **12**(10): 1161-1208.

van der Star, B. J., D. Y. Vogel, M. Kipp, F. Puentes, D. Baker and S. Amor (2012). "In vitro and in vivo models of multiple sclerosis." CNS Neurol Disord Drug Targets **11**(5): 570-588.

van Rheede, T., M. M. W. Smolenaars, O. Madsen and W. W. de Jong (2003). "Molecular Evolution of the Mammalian Prion Protein." Molecular Biology and Evolution **20**(1): 111-121.

Vassallo, N. and J. Herms (2003). "Cellular prion protein function in copper homeostasis and redox signalling at the synapse." J Neurochem **86**(3): 538-544.

Venturini, G. (1973). "Enzymic activities and sodium, potassium and copper concentrations in mouse brain and liver after cuprizone treatment in vivo." J Neurochem **21**(5): 1147-1151.

Vlachova, V., H. Zemkova and L. Vyklicky, Jr. (1996). "Copper modulation of NMDA responses in mouse and rat cultured hippocampal neurons." Eur J Neurosci **8**(11): 2257-2264.

Vulpe, C., B. Levinson, S. Whitney, S. Packman and J. Gitschier (1993). "Isolation of a candidate gene for Menkes disease and evidence that it encodes a copper-transporting ATPase." Nat Genet **3**(1): 7-13.

Vyklický, L., M. Benveniste and M. L. Mayer (1990). "Modulation of N-methyl-D-aspartic acid receptor desensitization by glycine in mouse cultured hippocampal neurones." The Journal of Physiology **428**: 313-331.

Waggoner, D. J., B. Drisaldi, T. B. Bartnikas, R. L. Casareno, J. R. Prohaska, J. D. Gitlin and D. A. Harris (2000). "Brain copper content and cuproenzyme activity do not vary with prion protein expression level." J Biol Chem **275**(11): 7455-7458.

Wake, H., P. R. Lee and R. D. Fields (2011). "Control of local protein synthesis and initial events in myelination by action potentials." Science **333**(6049): 1647-1651.

Waliś, A., J. Bratosiewicz, B. Sikorska, P. Brown, D. C. Gajdusek and P. P. Liberski (2003). "Ultrastructural Changes in the Optic Nerves of Rodents with Experimental Creutzfeldt–Jakob Disease (CJD), Gerstmann–Sträussler–Scheinker Disease (GSS) or Scrapie." Journal of Comparative Pathology **129**(2–3): 213-225.

Wang, Z., H. Colognato and C. Ffrench-Constant (2007). "Contrasting effects of mitogenic growth factors on myelination in neuron-oligodendrocyte co-cultures." Glia **55**(5): 537-545.

Watkins, T. A., B. Emery, S. Mulinyawe and B. A. Barres (2008). "Distinct stages of myelination regulated by gamma-secretase and astrocytes in a rapidly myelinating CNS coculture system." Neuron **60**(4): 555-569.

Watt, N. T., D. R. Taylor, A. Gillott, D. A. Thomas, W. S. Perera and N. M. Hooper (2005). "Reactive oxygen species-mediated beta-cleavage of the prion protein in the cellular response to oxidative stress." J Biol Chem **280**(43): 35914-35921.

Waxman, S. G. (1997). "Axon-glia interactions: Building a smart nerve fiber." Current Biology **7**(7): R406-R410.

Westaway, D., S. J. DeArmond, J. Cayetano-Canlas, D. Groth, D. Foster, S. L. Yang, M. Torchia, G. A. Carlson and S. B. Prusiner (1994). "Degeneration of skeletal muscle, peripheral nerves, and the central nervous system in transgenic mice overexpressing wild-type prion proteins." Cell **76**(1): 117-129.

Westergard, L., H. M. Christensen and D. A. Harris (2007). "The Cellular Prion Protein (PrP(C)): Its Physiological Function and Role in Disease." Biochimica et biophysica acta **1772**(6): 629-644.

White, A. R., S. J. Collins, F. Maher, M. F. Jobling, L. R. Stewart, J. M. Thyer, K. Beyreuther, C. L. Masters and R. Cappai (1999). "Prion Protein-Deficient Neurons Reveal Lower Glutathione Reductase Activity and Increased Susceptibility to Hydrogen Peroxide Toxicity." The American Journal of Pathology **155**(5): 1723-1730.

White, R. and E.-M. Krämer-Albers (2013). "Axon-glia interaction and membrane traffic in myelin formation." Frontiers in Cellular Neuroscience **7**: 284.

Whittal, R. M., H. L. Ball, F. E. Cohen, A. L. Burlingame, S. B. Prusiner and M. A. Baldwin (2000). "Copper binding to octarepeat peptides of the prion protein monitored by mass spectrometry." Protein Sci **9**(2): 332-343.

Wight, P. A. and A. Dobretsova (2004). "Where, when and how much: regulation of myelin proteolipid protein gene expression." Cell Mol Life Sci **61**(7-8): 810-821.

Wilkins, A., H. Majed, R. Layfield, A. Compston and S. Chandran (2003). "Oligodendrocytes Promote Neuronal Survival and Axonal Length by Distinct Intracellular Mechanisms: A Novel Role for Oligodendrocyte-Derived Glial Cell Line-Derived Neurotrophic Factor." The Journal of Neuroscience **23**(12): 4967-4974.

Winklhofer, K. F., J. Tatzelt and C. Haass (2008). "The two faces of protein misfolding: gain- and loss-of-function in neurodegenerative diseases." The EMBO Journal **27**(2): 336-349.

Wong, B. S., T. Liu, R. Li, T. Pan, R. B. Petersen, M. A. Smith, P. Gambetti, G. Perry, J. C. Manson, D. R. Brown and M. S. Sy (2001). "Increased levels of oxidative stress markers detected in the brains of mice devoid of prion protein." J Neurochem **76**(2): 565-572.

Yamaguchi, Y., A. Hayashi, C. W. Campagnoni, A. Kimura, T. Inuzuka and H. Baba (2012). "L-MPZ, a Novel Isoform of Myelin P0, Is Produced by Stop Codon Readthrough." The Journal of Biological Chemistry **287**(21): 17765-17776.

Yashiro, K. and B. D. Philpot (2008). "Regulation of NMDA receptor subunit expression and its implications for LTD, LTP, and metaplasticity." Neuropharmacology **55**(7): 1081-1094.

You, H., S. Tsutsui, S. Hameed, T. J. Kannanayakal, L. Chen, P. Xia, J. D. Engbers, S. A. Lipton, P. K. Stys and G. W. Zamponi (2012). "Abeta neurotoxicity depends on interactions between copper ions, prion protein, and N-methyl-D-aspartate receptors." Proc Natl Acad Sci U S A **109**(5): 1737-1742.

Zahn, R., A. Liu, T. Luhrs, R. Riek, C. von Schroetter, F. Lopez Garcia, M. Billeter, L. Calzolai, G. Wider and K. Wuthrich (2000). "NMR solution structure of the human prion protein." Proc Natl Acad Sci U S A **97**(1): 145-150.

Zendedel, A., C. Beyer and M. Kipp (2013). "Cuprizone-induced demyelination as a tool to study remyelination and axonal protection." J Mol Neurosci **51**(2): 567-572.

Zhang, H., A. A. Jarjour, A. Boyd and A. Williams (2011). "Central nervous system remyelination in culture — A tool for multiple sclerosis research." Experimental Neurology **230**(1-2): 138-148.

Zhang, J. and Q. Liu (2015). "Cholesterol metabolism and homeostasis in the brain." Protein & Cell **6**(4): 254-264.

Zimmerman, A. W., J. Matthieu, R. H. Quarles, R. O. Brady and J. M. Hsu (1976). "Hypomyelination in copper-deficient rats: Prenatal and postnatal copper replacement." Archives of Neurology **33**(2): 111-119.

APPENDIX

ANTIOXIDANTS & REDOX SIGNALING
Volume 22, Number 9, 2015
Mary Ann Liebert, Inc.
DOI: 10.1089/ars.2014.6032

ORIGINAL RESEARCH COMMUNICATION

Prion Protein and Copper Cooperatively Protect Neurons by Modulating NMDA Receptor Through S-nitrosylation

Lisa Gasperini,[1] Elisa Meneghetti,[1] Beatrice Pastore,[1] Federico Benetti,[1,*] and Giuseppe Legname[1,2]

Abstract

Aims: Several neurodegenerative disorders show alterations in glutamatergic synapses and increased susceptibility to excitotoxicity. Mounting evidence suggests a central role for the cellular prion protein (PrP^C) in neuroprotection. Therefore, the loss of PrP^C function occurring in prion disorders may contribute to the disease progression and neurodegeneration. Indeed, PrP^C modulates *N*-methyl-D-aspartate receptors (NMDAR), thus preventing cell death. In this study, we show that PrP^C and copper cooperatively inhibit NMDAR through S-nitrosylation, a post-translational modification resulting from the chemical reaction of nitric oxide (NO) with cysteines. ***Results:*** Comparing wild-type *Prnp* ($Prnp^{+/+}$) and PrP^C knockout ($Prnp^{0/0}$) mouse hippocampi, we found that GluN1 and GluN2A S-nitrosylation decrease in $Prnp^{0/0}$. Using organotypic hippocampal cultures, we found that copper chelation decreases NMDAR S-nitrosylation in $Prnp^{+/+}$ but not in $Prnp^{0/0}$. This suggests that PrP^C requires copper to support the chemical reaction between NO and thiols. We explored PrP^C-Cu neuroprotective role by evaluating neuron susceptibility to excitotoxicity in $Prnp^{+/+}$ and $Prnp^{0/0}$ cultures. We found that (i) PrP^C-Cu modulates GluN2A-containing NMDAR, those inhibited by S-nitrosylation; (ii) PrP^C and copper are interdependent to protect neurons from insults; (iii) neuronal NO synthase inhibition affects susceptibility in wild-type but not in $Prnp^{0/0}$, while (iv) the addition of a NO donor enhances $Prnp^{0/0}$ neurons survival. ***Innovation and Conclusions:*** Our results show that PrP^C and copper support NMDAR S-nitrosylation and cooperatively exert neuroprotection. In addition to NMDAR, PrP^C may also favor the S-nitrosylation of other proteins. Therefore, this mechanism may be investigated in the context of the different cellular processes in which PrP^C is involved. *Antioxid. Redox Signal.* 22, 772–784.

Introduction

THE CELLULAR PRION PROTEIN (PrP^C) has been extensively investigated since its isoform, the prion, was identified as the causative agent of prion disorders (33). PrP^C is widely expressed, reaching the highest levels in the nervous system (3, 12, 31). Comparing wild-type with PrP^C-null mice ($Prnp^{0/0}$) has revealed that PrP^C expression at synapses contributes to hippocampus synaptic function (6, 27, 28) and exerts neuroprotection by modulating neuronal excitability (21, 34, 38). In particular, PrP^C inhibits *N*-methyl-D-aspartate receptors (NMDAR) and requires copper for this effect (21, 40). Interestingly, Aβ oligomers induce neurotoxicity by blocking PrP^C-Cu modulation of NMDAR (40). Impairments in NMDAR regulation induce excitotoxicity, the neuronal cell death pathway triggered by massive calcium influx (10). Calcium ions enter the

Innovation

A major cause of neurodegeneration is the disruption of excitatory synapse regulation. Mounting evidence points to a central neuroprotective role for the cellular prion protein (PrP^C), a key player in prion disorders and Alzheimer disease (AD). Here, we describe a novel neuroprotective mechanism mediated by PrP^C, copper, and nitric oxide: copper-bound PrP^C modulates *N*-methyl-D-aspartate (NMDA)-type glutamate receptors by promoting S-nitrosylation, inhibiting the ionic channel. This mechanism is likely blocked in prion disorders and AD, thereby leading to neuron loss. PrP^C function in protein S-nitrosylation may also guide the study of the numerous cellular pathways in which PrP^C is involved.

[1]Laboratory of Prion Biology, Department of Neuroscience, Scuola Internazionale Superiore di Studi Avanzati (SISSA), Trieste, Italy.
[2]ELETTRA - Sincrotrone Trieste S.C.p.A, AREA Science Park, Trieste, Italy.
*Current affiliation: ECSIN-European Center for the Sustainable Impact of Nanotechnology, Veneto Nanotech S.C.p.A., Rovigo, Italy.

cell through the NMDAR channel and bind several interactors, for example, calmodulin (CaM). Calcium-bound CaM activates neuronal nitric oxide synthase (nNOS) and induces copper-transporting ATPase 1 (Atp7a) translocation, thus leading to nitric oxide (NO) production and copper release in the synaptic cleft (22, 36). Copper and NO modulate the NMDAR activity through a not clearly defined mechanism: NMDAR S-nitrosylation provides a link between copper and NO inhibitory roles (7, 23). S-nitrosylation is a chemical post-translational modification targeting protein cysteines. In NMDAR, S-nitrosylation is inhibitory and addresses two residues on GluN1 and three residues on GluN2A, including Cys399, which mediates the predominant inhibitory effect. Copper released in the synaptic cleft is bound by metal-binding proteins, such as PrP^C, which binds copper with high affinity and sustains Cu(II) redox cycling (5, 8, 24). *In vitro* results have shown that PrP^C-bound Cu(II) promotes NO oxidation and is consequently reduced to Cu(I) (4). As PrP^C-Cu is involved in glypican-1 heparan sulfate S-nitrosylation (29), the complex may also have a role in NMDAR S-nitrosylation.

Here, we show that PrP^C exerts copper-dependent neuroprotection by mediating NMDAR S-nitrosylation. We define PrP^C-Cu direct involvement in NMDAR S-nitrosylation comparing GluN2A and GluN1 S-nitrosylation levels in *Prnp*$^{+/+}$ and *Prnp*$^{0/0}$ hippocampi and cultures treated with a copper chelator. PrP^C neuroprotective function is characterized comparing excitotoxicity susceptibility in different *Prnp*$^{+/+}$ and *Prnp*$^{0/0}$ hippocampal areas. The copper/NO-dependence of PrP^C neuroprotective activity is assessed observing the effects of copper chelation, NOS inhibition, and NO donation on neuronal death in wild-type and *Prnp*$^{0/0}$ cultures. We propose a model for this molecular mechanism based on the results presented here.

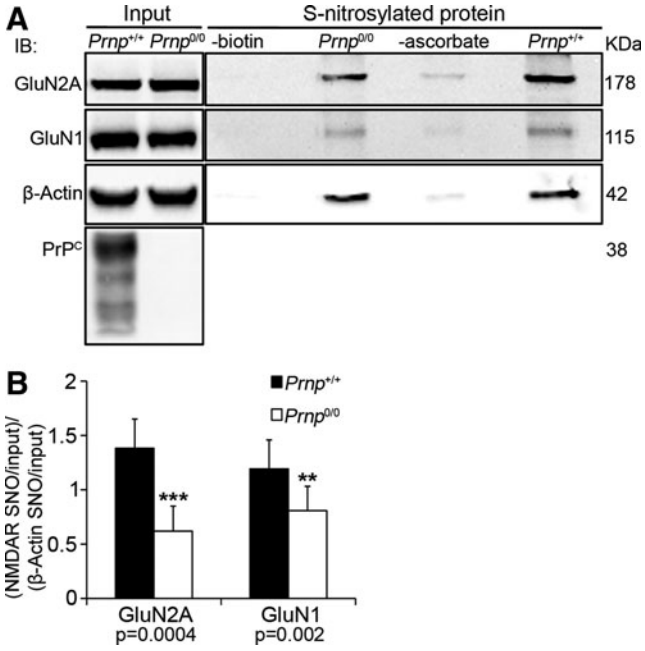

FIG. 1. In adult *Prnp*$^{0/0}$ hippocampus, the S-nitrosylation of GluN2A and GluN1 NMDAR subunits is lower compared to wild type. (A) Signals of S-nitrosylated fraction, controls without either biotin or ascorbate and corresponding input of GluN2A, GluN1, and β-actin resulting from the biotin switch assay of *Prnp*$^{+/+}$ and *Prnp*$^{0/0}$ hippocampus; controls without either biotin or ascorbate were done using *Prnp*$^{+/+}$ samples. **(B)** Statistical analysis of S-nitrosylated GluN2A and GluN1 signals normalized on the corresponding input and on β-actin; all error bars indicate SD; $^{**}p<0.01$; $^{***}p<0.001$. NMDAR, *N*-methyl-D-aspartate receptors.

Results

PrP^C is involved in NMDAR S-nitrosylation

The S-nitrosylation of NMDAR extracellular cysteines may be a mechanism by which the PrP^C-Cu complex inhibits ion gating. To test this hypothesis, we measured GluN2A and GluN1 S-nitrosylation levels in adult *Prnp*$^{+/+}$ and *Prnp*$^{0/0}$ hippocampi. To compare wild-type with PrP^C-null samples, the Western blotting signals corresponding to each S-nitrosylated protein (*i.e.,* GluN2A, GluN1 and β-Actin) were normalized against the respective input signals. Then, the obtained GluN2A and GluN1 ratio values were normalized against the corresponding β-actin ratio value, as an internal control. The resulting values for *Prnp*$^{+/+}$ and *Prnp*$^{0/0}$ hippocampi were compared by the Mann–Whitney test. In PrP^C-null hippocampus, we detected lower GluN2A ($n=9$, $p=0.0004$) and GluN1 ($n=9$, $p=0.00203$) S-nitrosylation levels compared with those in the wild type (Fig. 1A, B). These findings show that in PrP^C-null hippocampus NMDAR S-nitrosylation is reduced. We confirmed these results by using an additional S-nitrosylation-detection method (Supplementary Materials and Methods and Supplementary Fig. S1; Supplementary Data are available online at www.liebertpub.com/ars). This observation suggests that PrP^C is involved in GluN2A and GluN1 S-nitrosylation and, possibly through this mechanism, it can modulate the NMDAR activity.

To exclude that the results observed in *Prnp*$^{0/0}$ hippocampus are due to different levels of either GluN2A-containing NMDAR or nNOS at synapses, we performed a co-immunoprecipitation (coIP) with the postsynaptic density protein 95 (PSD95). The results revealed comparable GluN2A (direct PSD95 interactor), GluN1 (indirect PSD95 interactor), and nNOS levels in *Prnp*$^{+/+}$ and *Prnp*$^{0/0}$ hippocampal synapses (Supplementary Materials and Methods and Supplementary Fig. S2A–C). Furthermore, to exclude that the results observed in *Prnp*$^{0/0}$ hippocampus are due to altered NOS activity, first, we assessed the similarity of β-actin S-nitrosylation levels (Fig. 1A) and then measured both the consumption of NADPH, an essential cofactor for NO production, and the conversion of radiolabeled arginine to radiolabeled citrulline (Supplementary Materials and Methods). Adult *Prnp*$^{+/+}$ and *Prnp*$^{0/0}$ samples exhibited comparable kinetics for NADPH consumption and the same capability to convert arginine to citrulline (Supplementary Fig. S3A, C). Taken together, these results suggest that the decreased NMDAR S-nitrosylation in PrP^C-null hippocampus is not due to a reduction in the levels of NMDAR and nNOS at synapses or alterations in NO production.

In the absence of PrP^C, hippocampal neurons are more susceptible to NMDAR-mediated excitotoxicity

Since *Prnp*$^{0/0}$ hippocampus shows lower NMDAR S-nitrosylation (Fig. 1 and Supplementary Fig. S1) but the same protein level at synapses (Supplementary Fig. S2A, C), PrP^C-null neurons should be more susceptible to excitotoxic treatment. To investigate the neuroprotective role of PrP^C through glutamate receptor inhibition, we carried out excitotoxicity studies on *Prnp*$^{+/+}$ and *Prnp*$^{0/0}$ organotypic hippocampal

cultures (OHC) by analyzing specifically neuronal death in *Cornus Ammonis 1* (CA1), *Cornus Ammonis 3* (CA3), and dentate gyrus (DG). We exposed $Prnp^{+/+}$ and $Prnp^{0/0}$ OHC to two toxic treatments with NMDA as selective NMDAR agonist: 5 μM NMDA for 3 h (prolonged insult) and 10 μM NMDA for 10 min (acute insult). We chose these two protocols after observing that they induce low neuronal cell death levels in wild-type samples, hence they can clearly reveal a different susceptibility of $Prnp^{0/0}$ samples. Neuronal cell death was evaluated as pyknotic nuclei percentage over the total number of nuclei in CA1, CA3, and DG, respectively. The concomitant staining with the anti-neuronal nuclei marker antibody (NeuN) allowed us to localize the pyknotic event in neurons and clearly distinguished glia cells. Figure 2A–M shows the different

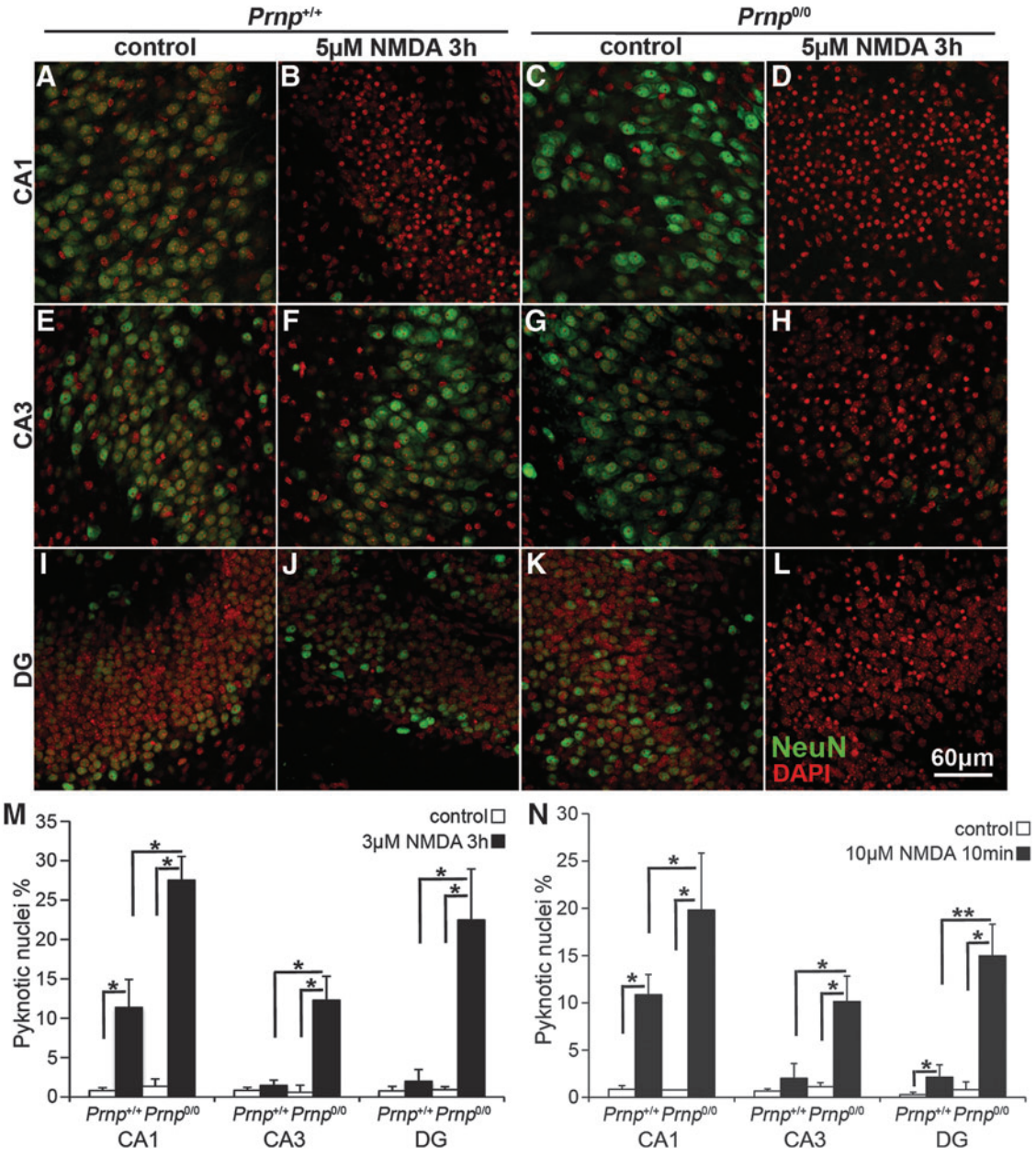

FIG. 2. Wild-type and PrP^C-null OHC show different regional susceptibility to NMDA treatment, under both prolonged and acute insult. Images from three hippocampal regions are reported in rows: **(A–D)** CA1, **(E–H)** CA3, and **(I–L)** DG. The four different combinations of treatment and samples are reported in columns: **(A, E, I)** $Prnp^{+/+}$ control, **(B, F, J)** $Prnp^{+/+}$ treated with 5 μM NMDA for 3 h, **(C, G, K)** $Prnp^{0/0}$ control, and **(D, H, L)** $Prnp^{0/0}$ treated with 5 μM NMDA for 3 h. NeuN staining is displayed in *green* and DAPI in *red*. Confocal microscope fluorescence images were acquired using a 40×/1.30 NA oil objective. Comparison of the neuronal pyknotic nuclei percentage induced by 5 μM NMDA for 3 h (**M**; $n = 4$ OHC, 5 slices per treatment in each culture) and by 10 μM NMDA for 10 min (**N**; $n = 5$ OHC, 5 slices per treatment in each culture), calculated over the total nuclei number, between $Prnp^{+/+}$ (*white bars*) and $Prnp^{0/0}$ (*black bars*) OHC in CA1, CA3, and DG; all error bars indicate SD; $*p < 0.05$, $**p < 0.01$. CA1, *Cornus Ammonis 1*; CA3, *Cornus Ammonis 3*; DAPI, 4′,6-diamidino-2-phenylindole; DG, dentate gyrus; OHC, organotypic hippocampal cultures. To see this illustration in color, the reader is referred to the web version of this article at www.liebertpub.com/ars

responses of *Prnp*$^{+/+}$ and *Prnp*$^{0/0}$ OHC to the prolonged treatment ($n=4$ OHC, 5 slices per treatment in each culture). In CA1, the NMDA exposure significantly induced neuronal cell death in both *Prnp*$^{+/+}$ ($p=0.03038$) and *Prnp*$^{0/0}$ ($p=0.03038$) OHC (Fig. 2A–D, M), but at the same time, it revealed a higher susceptibility of *Prnp*$^{0/0}$ OHC ($p=0.03038$). The NMDA treatment did not induce significant neuronal cell death in wild-type CA3 and DG, whereas it yielded high toxicity for both regions in PrP^C-null cultures (CA3, $p=0.03038$; DG, $p=0.03038$), highlighting a significant difference between *Prnp*$^{+/+}$ and *Prnp*$^{0/0}$ (CA3, $p=0.03038$; DG, $p=0.01996$) (Fig. 2E–M). The same quantitative differences between *Prnp*$^{+/+}$ and *Prnp*$^{0/0}$ OHC were observed following the acute treatment (Fig. 2N; $n=5$ OHC, 5 slices per treatment in each culture). In CA1, 10 μM NMDA for 10 min induced neuronal cell death in both *Prnp*$^{+/+}$ ($p=0.01996$) and *Prnp*$^{0/0}$ ($p=0.01996$) OHC, but it revealed a higher susceptibility of *Prnp*$^{0/0}$ compared with *Prnp*$^{+/+}$ ($p=0.02157$). In CA3, the acute treatment was toxic only for *Prnp*$^{0/0}$ OHC ($p=0.03038$), confirming their higher susceptibility compared with *Prnp*$^{+/+}$ ($p=0.01421$). The wild-type DG showed low levels of neuronal cell death in response to the acute insult ($p=0.02518$), whereas the same treatment caused a greater cell death percentage ($p=0.01421$) in *Prnp*$^{0/0}$ DG, leading to a higher damage compared to *Prnp*$^{+/+}$ ($p=0.00507$). The enhanced susceptibility of *Prnp*$^{0/0}$ neurons to the excitotoxic stimulus confirms findings previously reported in the literature, obtained by stimulating neurons with kainate (34) and NMDA (21).

To evaluate the early changes in neuronal cell viability, the MTT (thiazolyl blue tetrazolium bromide) mitochondrial toxicity assay was performed on *Prnp*$^{+/+}$ and *Prnp*$^{0/0}$ OHC after exposure to 5 μM NMDA for 3 h. Results revealed that *Prnp*$^{0/0}$ OHC are more susceptible to excitotoxicity also in the early phases after insult (Supplementary Materials and Methods and Supplementary Fig. S4).

The excitotoxic mechanism induced by NMDAR overactivation is triggered by calcium ion influx into the neuronal cell (10). To verify that the excitotoxicity observed was a calcium-mediated effect, the same treatments were performed adding a calcium chelator, ethylene glycol tetraacetic acid (EGTA; $n=3$ OHC, 4 slices per treatment in each culture). It should be noted that the treatment with 5 μM NMDA was shortened to 1.5 h since calcium deprivation for 3 h resulted to be toxic *per se*. As expected, adding EGTA to NMDA abolished neuronal cell death in all the analyzed regions and under both prolonged and acute insults (Fig. 3A–C and Supplementary Fig. S5A–I; *Prnp*$^{+/+}$ CA1: $p=0.03038$ and $p=0.03038$; *Prnp*$^{0/0}$ CA1: $p=0.01996$ and $p=0.03038$; *Prnp*$^{0/0}$ CA3: $p=0.01894$ and $p=0.0294$; *Prnp*$^{0/0}$ DG: $p=0.01945$ and $p=0.01996$). Shortening the exposure time

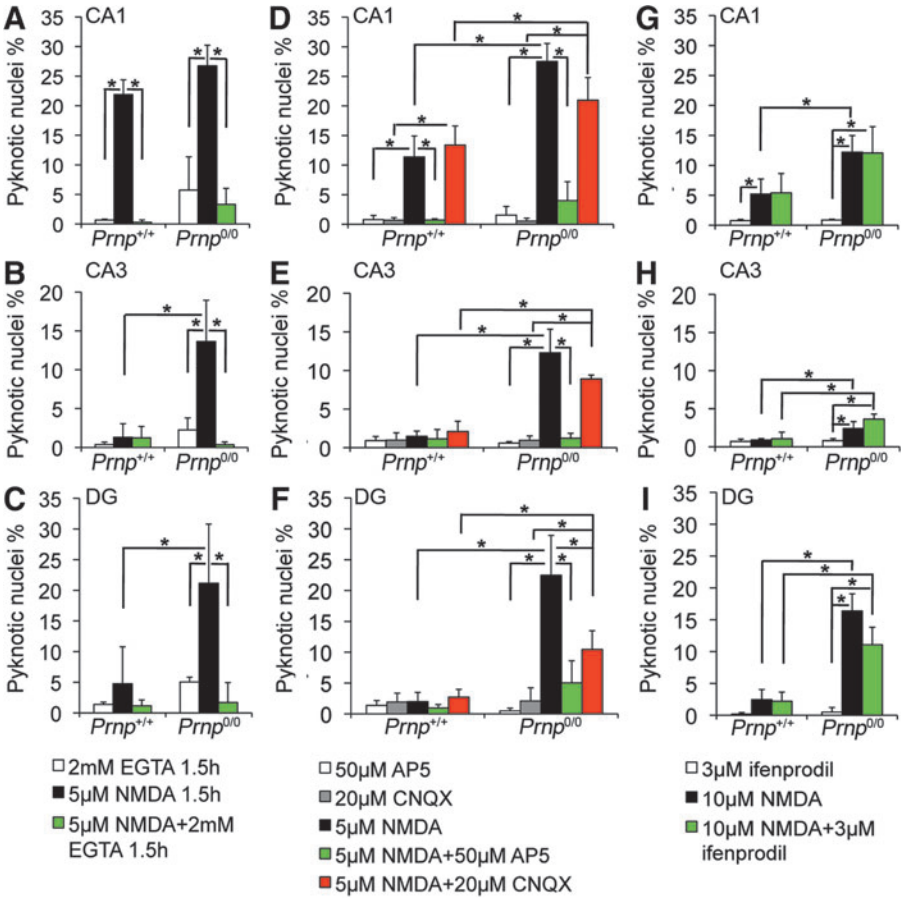

FIG. 3. Neuronal cell death induced by NMDA treatment is prevented by calcium chelation and NMDAR antagonist, unaltered by AMPA/kainate receptor and GluN2B-containing NMDAR antagonists. Comparison of NMDA-induced neuronal pyknotic nuclei percentages between EGTA-treated *Prnp*$^{+/+}$ and *Prnp*$^{0/0}$ OHC in the **(A)** CA1, **(B)** CA3, and **(C)** DG; $n=3$ OHC, 5 slices per treatment in each culture. Comparison of NMDA-induced neuronal pyknotic nuclei percentages between NMDAR inhibitors (AP5 and/or CNQX)-treated *Prnp*$^{+/+}$ and *Prnp*$^{0/0}$ OHC in the **(D)** CA1, **(E)** CA3, and **(F)** DG; $n=4$ OHC, 5 slices per treatment in each culture. Comparison of NMDA-induced neuronal pyknotic nuclei percentages between GluN2B inhibitor (ifenprodil)-treated *Prnp*$^{+/+}$ and *Prnp*$^{0/0}$ OHC in the **(G)** CA1, **(H)** CA3, and **(I)** DG; $n=4$ OHC, 5 slices per treatment in each culture. All error bars indicate SD; $*p<0.05$. AMPA, α-amino-3-hydroxy-5-methyl-4-isoxazolepropionic acid; AP5, (2*R*)-amino-5-phosphonovaleric acid; CNQX, 6-cyano-7-nitroquinoxaline-2,3-dione; EGTA, ethylene glycol tetraacetic acid. To see this illustration in color, the reader is referred to the web version of this article at www.liebertpub.com/ars

to 5 μM NMDA did not affect the differences between $Prnp^{+/+}$ and $Prnp^{0/0}$ OHC.

Next, we assessed the primary involvement of NMDAR in the neurotoxic mechanism ($n=4$ OHC, 5 slices per treatment in each culture). Adding the NMDAR blocker AP5 to 5 μM NMDA for 3 h abolished cell death (Fig. 3D–F and Supplementary Fig. S6A–F; $Prnp^{+/+}$ CA1: $p=0.03038$; $Prnp^{0/0}$ CA1: $p=0.03038$; $Prnp^{0/0}$ CA3: $p=0.03038$; $Prnp^{0/0}$ DG: $p=0.03038$). In contrast, adding the α-amino-3-hydroxy-5-methyl-4-isoxazolepropionic acid (AMPA)/kainate receptor blocker 6-cyano-7-nitroquinoxaline-2,3-dione (CNQX) to 5 μM NMDA for 3 h did not diminish cell death in $Prnp^{+/+}$ CA1, $Prnp^{0/0}$ CA1, and $Prnp^{0/0}$ CA3 (Fig. 3D, E and Supplementary Fig. S6A–D). However, adding CNQX to NMDA did reduce the pyknosis percentage in $Prnp^{0/0}$ DG ($p=0.03038$), suggesting a partial AMPA/kainate receptor involvement (Fig. 3F and Supplementary Fig. S6E, F). Overall, despite the AMPA/kainate receptor inhibition, the higher cell death levels in PrP^C-null were maintained, confirming a primary involvement of NMDAR. To assess whether the neurotoxic effect was mainly due to either GluN2A- or GluN2B-containig NMDAR, we used ifenprodil, a selective inhibitor of GluN2B. The excitotoxic condition applied was 10 μM NMDA for 10 min since ifenprodil has an aspecific toxic effect if added to lower NMDA concentrations (20). In both $Prnp^{+/+}$ and $Prnp^{0/0}$ OHC, ifenprodil did not reduce the cell death levels observed with NMDA alone, suggesting that the overactivation of GluN2B-containing receptor is not the leading cause for neuronal death (Fig. 3G–I and Supplementary Fig. S7). A major involvement of GluN2A-containing receptor is therefore a more likely hypothesis.

Copper ions are required for PrP^C to support NMDAR S-nitrosylation

Copper ions are fundamental in the S-nitrosylation reaction because their reduction from Cu(II) to Cu(I) allows for the oxidation of NO and its ensuing reaction with cysteine thiols (11, 17). Because PrP^C-bound Cu(II) promotes NO oxidation (4), PrP^C is likely to promote NMDAR S-nitrosylation through the copper ions it binds. To verify this mechanism, we measured GluN2A and GluN1 S-nitrosylation levels in $Prnp^{+/+}$ and $Prnp^{0/0}$ OHC upon treatment with cuprizone (CZ), a selective copper chelator that binds Cu^{2+}. Since Cu^{2+} promotes S-nitrosylation while Cu^{+} triggers denitrosylation, CZ treatment specifically blocks S-nitrosylation induction. CZ does not affect neuronal viability and cannot cross plasma membranes (2); hence, it should not affect cytoplasmic protein S-nitrosylation. Indeed, β-actin S-nitrosylation levels were comparable among control and CZ-treated wild-type and PrP^C-null OHC, providing us with a reliable internal control for the normalization of NMDAR S-nitrosylation signal. Moreover, we used serum-free medium to avoid copper content variability and thereby ensure uniform copper chelation. In serum-free medium, CZ binds copper ions released in the synaptic cleft (36), thus affecting the copper-mediated S-nitrosylation in the extracellular environment. $Prnp^{+/+}$ and $Prnp^{0/0}$ OHC were exposed to 20 μM CZ for 3 h, immediately frozen, and then processed for the detection of S-nitrosylated proteins. As already observed in the hippocampus, GluN2A and GluN1 S-nitrosylation was decreased in $Prnp^{0/0}$ samples (Fig. 4A, B; $n=4$ slice pools, $p=0.03038$ and $p=0.03038$, respectively). Consistent with the hypothesized mechanism, CZ addition reduced GluN2A and GluN1 S-nitrosylation in $Prnp^{+/+}$ OHC ($p=0.03038$ and $p=0.03038$, respectively) but not in $Prnp^{0/0}$ ones (Fig. 4A, B). Furthermore, NMDAR S-nitrosylation levels in CZ-treated wild-type OHC were not different from either control or CZ-treated $Prnp^{0/0}$ samples. This result shows that CZ addition affects NMDAR S-nitrosylation only in wild type but not in $Prnp^{0/0}$ OHC; hence, it strongly suggests that the lower S-nitrosylation of NMDAR subunits in $Prnp^{0/0}$ samples is due to the lack of the PrP^C-Cu complex and that PrP^C-bound copper ions favor the S-nitrosylation of NMDAR. Residual GluN1 and GluN2A S-nitrosylation is due to PrP^C-independent mechanisms.

To rule out that the results observed in $Prnp^{0/0}$ OHC are due to different levels of GluN2A-containing NMDAR and nNOS at synapses, we performed coIP assays with PSD95 using hippocampi from postnatal day 20 (P20) mice. This age was selected because it is close to the developmental stage of OHC

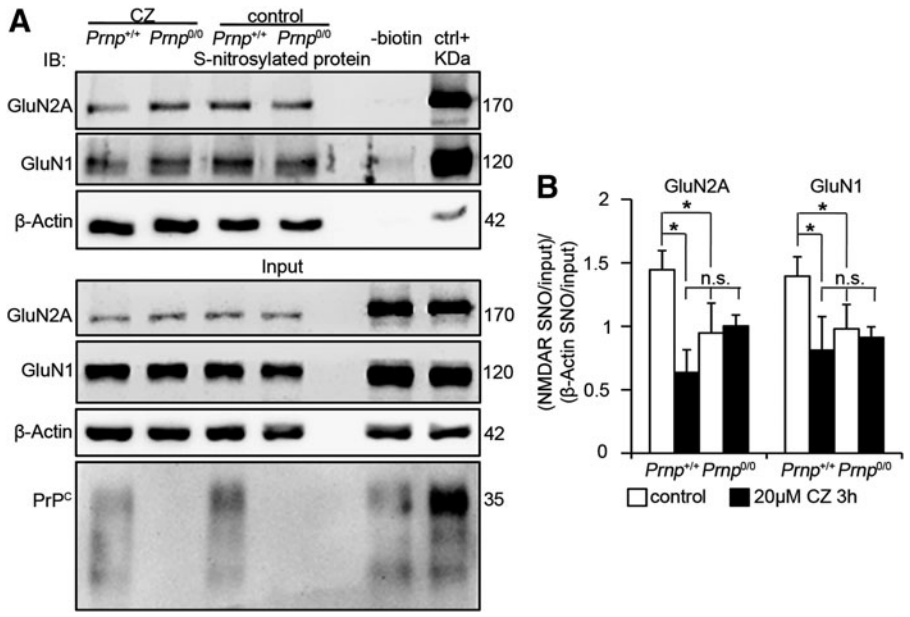

FIG. 4. Copper chelation decreases S-nitrosylation of GluN2A and GluN1 in wild type but not in $Prnp^{0/0}$ OHC. (A) Signals of S-nitrosylated fraction and corresponding input of GluN2A, GluN1, and β-actin resulting from the biotin switch assay of $Prnp^{+/+}$ and $Prnp^{0/0}$ OHC, treated and untreated with CZ; adult wild-type hippocampus was used as negative (−biotin) and positive control. **(B)** Statistical analysis of S-nitrosylated GluN2A and GluN1 signals normalized on the corresponding input and on β-actin; all error *bars* indicate SD; sample size $n=4$; $^*p<0.05$, n.s., not statistically significant difference. CZ, cuprizone.

at the time of the treatment. The results revealed comparable GluN2A, GluN1, and nNOS levels in P20 *Prnp*$^{+/+}$ and *Prnp*$^{0/0}$ hippocampal synapses (Supplementary Fig. S8A–C). Also, at this developmental stage, we reasoned to exclude that the results observed in *Prnp*$^{0/0}$ OHC were due to different levels of NOS activity. Like in the adult hippocampus, we observed that β-actin S-nitrosylation levels were similar in control and CZ-treated *Prnp*$^{+/+}$ and *Prnp*$^{0/0}$ OHC (Fig. 4A). Next, we measured the consumption of NADPH and the conversion of radiolabeled arginine to radiolabeled citrulline in P20 samples and found comparable results in *Prnp*$^{+/+}$ and *Prnp*$^{0/0}$ hippocampi (Supplementary Fig. S3B, C).

The neuroprotective function of PrP^C is copper-dependent

So far, we have shown that in *Prnp*$^{0/0}$ mouse OHC, NMDAR S-nitrosylation is not mediated by copper since it is not lowered by CZ addition. However, CZ treatment decreases NMDAR S-nitrosylation in *Prnp*$^{+/+}$ mouse OHC to the level detected in *Prnp*$^{0/0}$ mouse OHC (Fig. 4). Since extracellular cysteine S-nitrosylation inhibits NMDAR by lowering the frequency of channel opening (23), we measured intracellular calcium $[Ca^{2+}]_i$ waves in wild-type mouse hippocampal neurons upon treatment with 20 μM CZ, 5 μM NMDA, and 5 μM NMDA + 20 μM CZ (Supplementary Materials and Methods). We found that both CZ and NMDA triggered $[Ca^{2+}]_i$ waves, but the addition of CZ to NMDA induced a much higher $[Ca^{2+}]_i$ increase (Supplementary Fig. S9). These results indicate that copper chelation enhances NMDAR channel opening. Consistent with this finding, it has been reported that, upon copper chelation, wild-type hippocampal neurons exhibit nondesensitizing NMDAR currents comparable to those registered in *Prnp*$^{0/0}$ (40). Therefore, we studied the neurotoxic effects of NMDA exposure in *Prnp*$^{+/+}$ and *Prnp*$^{0/0}$ OHC in the presence of CZ ($n = 4$ OHC, 5 slices per treatment in each culture). CZ treatment without NMDA did not induce neuronal cell death in neither *Prnp*$^{+/+}$ nor *Prnp*$^{0/0}$ OHC (Supplementary Fig. S10A–F). Our results confirm the neuroprotective function of PrP^C through a copper-dependent inhibition of NMDAR (Fig. 5). In wild-type OHC CA1, copper chelation did not enhance significantly the pyknosis, but it abolished the difference with PrP^C-null OHC CA1 (Fig. 5A, G). In wild-type OHC CA3 and DG, CZ addition to NMDA significantly increased neuronal cell death (Fig. 5C, E, H, I; $p = 0.01219$, $p = 0.02157$). In contrast, in *Prnp*$^{0/0}$ CA1 and DG, the copper chelator did not alter the susceptibility of neurons to NMDA (Fig. 5 B, F, G, I), whereas in *Prnp*$^{0/0}$ CA3, it did decrease neuronal cell death (Fig. 5D, H; $p = 0.01219$). This partial neuroprotection exerted by CZ in *Prnp*$^{0/0}$ CA3 may be related to a toxic effect triggered by copper ions released after NMDAR activation in the absence of PrP^C. These results indicate that copper is neuroprotective in wild-type mouse OHC; on the contrary, this effect is greatly reduced in PrP^C-null OHC, thus suggesting that PrP^C and copper can contribute to neuroprotection only if simultaneously present.

The neuroprotective function of PrP^C is NO-dependent

Next, we verified the involvement of NO in PrP^C neuroprotective function. To this aim, we studied the neurotoxic effect of NMDA exposure in *Prnp*$^{+/+}$ and *Prnp*$^{0/0}$ OHC in the presence of either Nω-nitro-L-arginine (NNA), which blocks NO production by all NO synthase isoforms (*i.e.,* nNOS, endothelial NOS, and inducible NOS) or S-nitrosoglutathione (GSNO), a NO donor ($n = 4$ OHC, 5 slices per treatment in each culture). Both NNA and GSNO had no toxic effect (Supplementary Fig. S10A–F). NOS inhibition by NNA significantly enhanced cell death in all the analyzed regions in wild-type hippocampal cultures (Fig. 6A, C, E, G–I; $p = 0.03038$, $p = 0.03038$, $p = 0.03038$), while it had no effect in PrP^C-null OHC (Fig. 6B, D, F, G–I). GSNO addition to NMDA significantly increased neuronal cell survival in all the analyzed regions in PrP^C-null OHC (Fig. 6B, D, F, G–I; $p = 0.01996$, $p = 0.03038$, $p = 0.03038$) and also in wild-type CA1 region (Fig. 6A, G; $p = 0.03038$).

These results indicate that NOS production of NO is necessary to mediate PrP^C neuroprotective function.

Discussion

Determining the function of PrP^C is of utmost importance to understand different neurodegeneration mechanisms, in particular those underlying prion disorders and Alzheimer disease (AD). In prion disorders, the loss of PrP^C function upon protein aggregation may contribute to the pathology progression (1). PrP^C has been found to play a role also in AD (19), where it has been involved in pathological mechanisms together with copper and NMDAR. Recent results indicate that the interaction with Aβ oligomers prevents the PrP^C-Cu complex-mediated inhibition of NMDAR, leading to overactivation of the ion channel (40). Zamponi and colleagues propose that PrP^C bound to copper limits excessive NMDAR activity by reducing the receptor affinity for glycine. In the present work, we put forward an additional mechanism in which PrP^C-Cu modulates NMDAR together with NO. The novelty of this study is represented by the description of the functional interaction of PrP^C, copper, and NO. The relevance of copper, NO, and NMDAR overactivation in processes that lead to synapse loss in AD is widely accepted (15). In light of these premises, the mechanism we present here may help our understanding of the pathological processes involved in the progression of both AD and prion disorders.

Here, we argue that PrP^C protects glutamatergic synapses from excitotoxic insults by promoting NMDAR S-nitrosylation. Figure 7 shows the proposed model for NMDAR inhibition by PrP^C. Glutamate released from the presynaptic terminal activates NMDAR with ensuing calcium influx. In the intracellular compartment, calcium binds to CaM, and the Ca^{2+}/CaM complex activates, among others, nNOS and Atp7a (22, 36); NO and copper are thus released in the synaptic cleft. Because of PrP^C high affinity to copper ions (8) and high expression levels in hippocampal synapses (31, 35), it is likely to bind copper released in the synaptic cleft. In this milieu, PrP^C-bound Cu(II) can oxidize NO to NO^+ and be reduced to Cu(I) (4). This reaction enables the electrophilic attack of NO^+ on GluN2A and GluN1 extracellular cysteine thiol groups, resulting in the S-nitrosylation of NMDAR. coIP experiments of PrP^C with NMDAR subunits have yielded positive results (40), confirming the proximity of PrP^C and NMDAR subunits in lipid rafts (9, 32). The experimental evidence we present here supports this molecular mechanism.

NMDAR regulation operated by NO reduces significantly the neurotoxic effect induced by the overactivation of the

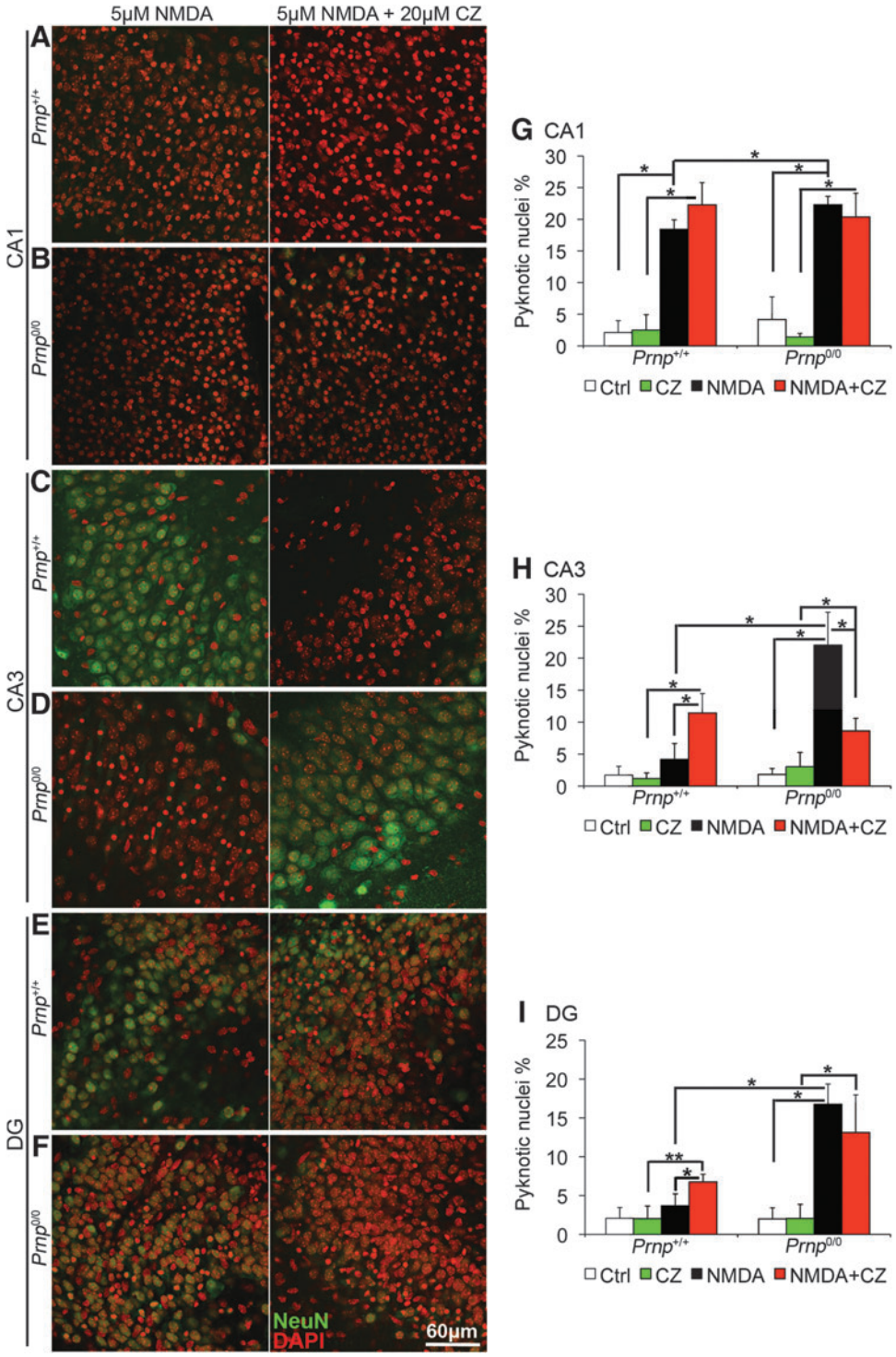

FIG. 5. Copper chelation increases neuronal cell death in *Prnp*$^{+/+}$ OHC but not in *Prnp*$^{0/0}$. Images from *Prnp*$^{+/+}$ and *Prnp*$^{0/0}$ OHC areas are reported in rows: **(A)** *Prnp*$^{+/+}$ CA1; **(B)** *Prnp*$^{0/0}$ CA1; **(C)** *Prnp*$^{+/+}$ CA3; **(D)** *Prnp*$^{0/0}$ CA3; **(E)** *Prnp*$^{+/+}$ DG; **(F)** *Prnp*$^{0/0}$ DG. The different treatments are reported in columns: 5 *μM* NMDA for 3 h, *left column*; 5 *μM* NMDA + 20 *μM* CZ for 3 h, *right column*. NeuN staining is displayed in *green* and DAPI in *red*. Confocal microscope fluorescence images were acquired using a 40×/1.30 NA oil objective. Graphs show the comparison of the neuronal pyknotic nuclei percentage, calculated over the total nuclei number, between *Prnp*$^{+/+}$ and *Prnp*$^{0/0}$ OHC in CA1 **(G)**, CA3 **(H),** and DG **(I)**; all error bars indicate SD; sample size $n = 4$ OHC, 5 slices per treatment in each culture; $*p < 0.05$, $**p < 0.01$. To see this illustration in color, the reader is referred to the web version of this article at www.liebertpub.com/ars

NMDAR-coupled ionic channel and the ensuing excessive calcium entry (30). S-nitrosylation diminishes the amplitude of NMDAR-evoked currents by reducing the number of channel openings (23). By comparing GluN2A and GluN1 S-nitrosylation levels in wild-type and PrP^{C}-null mouse hippocampi, we found that, in absence of PrP^{C}, NMDAR S-nitrosylation levels are decreased. S-nitrosylation can proceed through different routes not involving copper (14), and PrP^{C}-Cu is not the only complex able to support the copper-mediated reaction; otherwise, no S-nitrosylated NMDAR signal would be detectable in PrP^{C}-null samples. However, the extent of the reduction observed is remarkable, indicating that PrP^{C}-Cu is a key player in this post-translational modification on NMDAR.

Since S-nitrosylation limits NMDAR overactivation, thus staving off apoptosis, PrP^{C}-null neurons should be more susceptible to excitotoxicity. Consistent with this observation and with results reported in the literature (21), we found that PrP^{C} ablation strongly impairs neuronal survival upon toxic exposure to NMDA. By applying a pool of glutamate receptors antagonists, we found that GluN2A-containing NMDAR

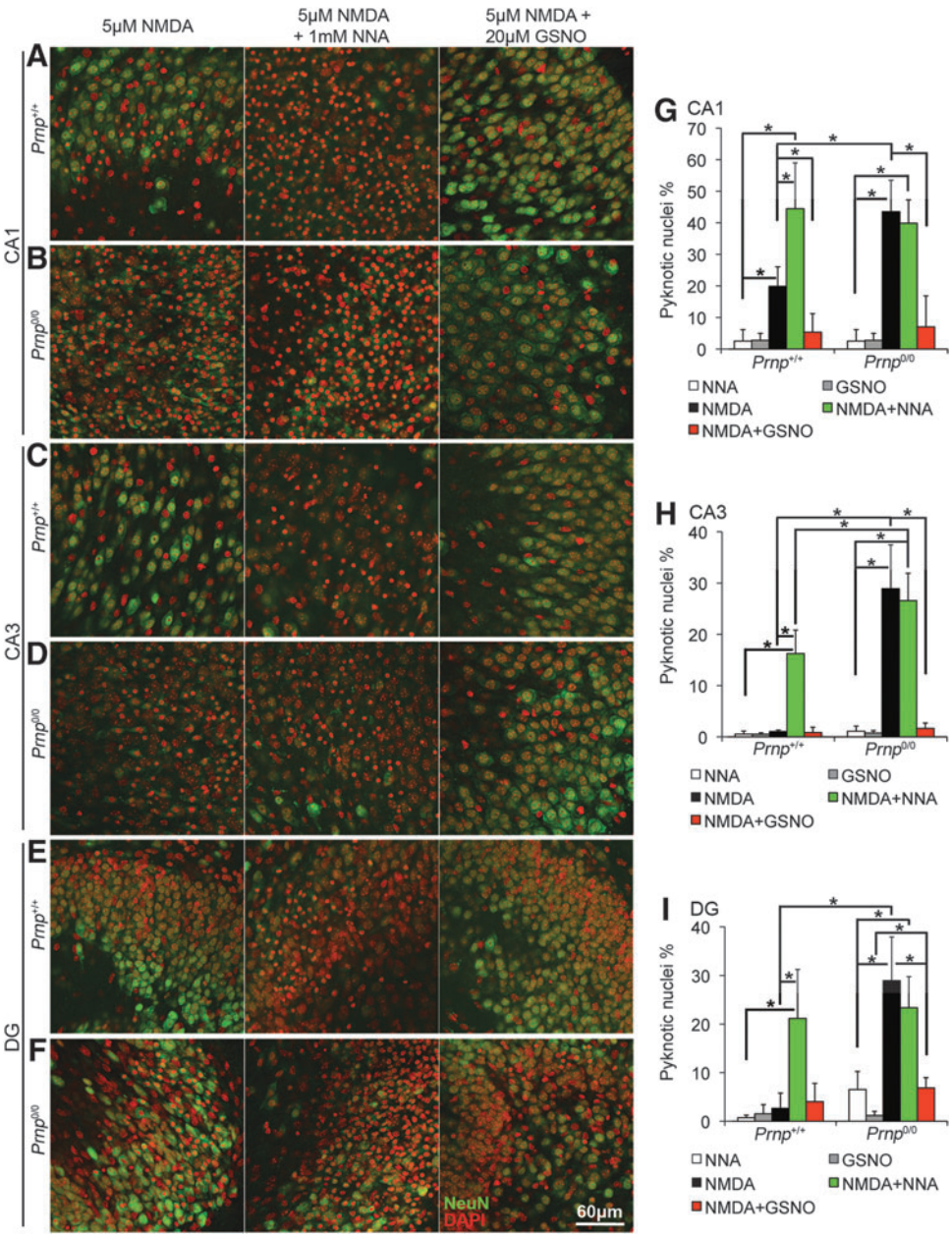

FIG. 6. NOS inhibition increases neuronal cell death in *Prnp*$^{+/+}$ OHC but not in *Prnp*$^{0/0}$, while NO addition enhances neuron survival upon NMDA exposure. Images from *Prnp*$^{+/+}$ and *Prnp*$^{0/0}$ OHC areas are reported in rows: **(A)** *Prnp*$^{+/+}$ CA1; **(B)** *Prnp*$^{0/0}$ CA1; **(C)** *Prnp*$^{+/+}$ CA3; **(D)** *Prnp*$^{0/0}$ CA3; **(E)** *Prnp*$^{+/+}$ DG; **(F)** *Prnp*$^{0/0}$ DG. The different treatments are reported in columns: 5 μM NMDA for 3 h, *left column*; 5 μM NMDA + 1 mM NNA for 3 h, *central column*; 5 μM NMDA + 20 μM GSNO for 3 h, *right column*. NeuN staining is displayed in *green* and DAPI in *red*. Confocal microscope fluorescence images were acquired using a 40×/1.30 NA oil objective. Graphs show the comparison of the neuronal pyknotic nuclei percentage, calculated over the total nuclei number, between *Prnp*$^{+/+}$ and *Prnp*$^{0/0}$ OHC in CA1 **(G)**, CA3 **(H)**, and DG **(I)**; all error bars indicate SD; sample size $n = 4$ OHC, 5 slices per treatment in each culture; $^*p < 0.05$. GSNO, S-nitrosoglutathione; NNA, Nω-nitro-L-arginine; NO, nitric oxide. To see this illustration in color, the reader is referred to the web version of this article at www.liebertpub.com/ars

were mainly responsible for increasing the cell death level in PrP^C-null neurons. These results contrast with the notion that GluN2B-enriched extrasynaptic receptors may be key mediators of neuron death (16). However, growing evidence supports an involvement of both GluN2A and GluN2B in synaptic and extrasynaptic NMDAR-mediated excitotoxicity (39, 41, 42). Therefore, it is plausible that a dysfunction in GluN2A inhibition causes higher neuron death in PrP^C-null mouse OHC. Interestingly, GluN2A is the subunit containing the cysteine residue that mediates the predominant inhibitory effect of NO (7, 23). This regulation provides a clear link between the increased neuron death level and the lower NMDAR S-nitrosylation detected in PrP^C-null mouse hippocampus. *In situ* hybridization experiments have shown that PrP^C knockout mouse hippocampus has higher GluN2A mRNA levels (27). However, we excluded the possibility that the higher susceptibility of PrP^C-null mouse OHC was due to an overexpression of NMDAR at synapses, as we revealed comparable levels of interaction between PSD95 and GluN2A, and indirectly with GluN1, in wild-type and PrP^C-null mouse hippocampi.

By measuring GluN2A and GluN1 S-nitrosylation levels in CZ-treated wild-type and PrP^C-null mouse OHC by CZ addition, we found that copper chelation lowers GluN2A and GluN1 S-nitrosylation in wild-type cultures but not in PrP^C-null ones. The residual signal detected in wild-type upon copper deprivation was not different from that in treated and untreated PrP^C knockout cultures.

In line with previously published electrophysiological recordings of NMDAR currents (40), our results on S-nitrosylation highlight that PrP^C regulation of NMDAR activity is copper dependent. Consistent with this fact, we found that also the neuroprotective effect of PrP^C requires copper. These results convincingly indicate that in glutamatergic synapses, the neuroprotective action of PrP^C depends on copper ions and that, *vice versa*, the neuroprotective action

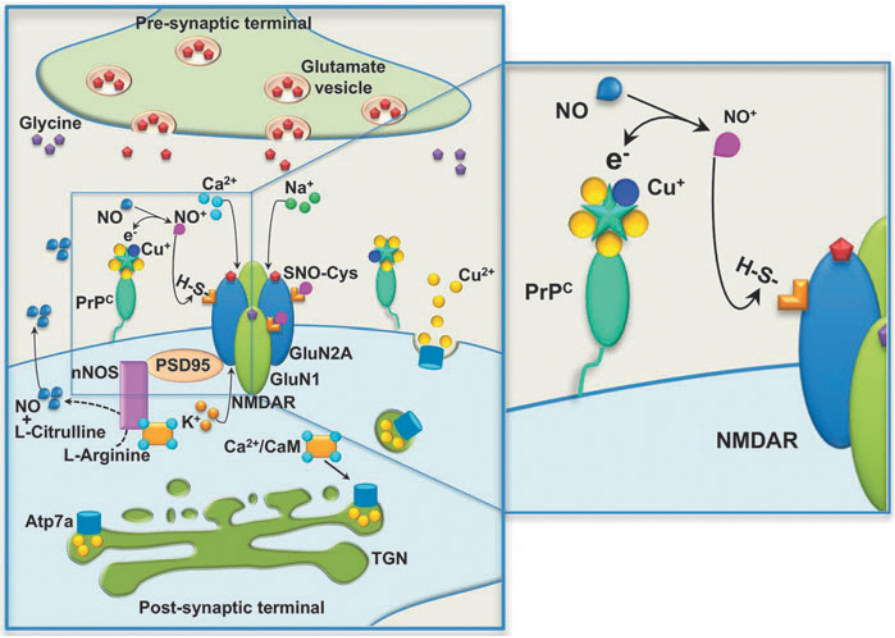

FIG. 7. Mechanism of PrP^C-mediated S-nitrosylation of NMDAR. Glutamate released from the presynaptic terminal activates NMDAR on the postsynaptic terminal. NMDAR activation triggers Na^+ and Ca^{2+} influx, together with K^+ efflux. In the intracellular compartment, Ca^{2+} ions bind different proteins, including calmodulin (CaM). The Ca^{2+}/CaM complex activates, among others, neuronal nitric oxide synthase (nNOS) and copper-transporting ATPase 1 (Atp7a): nNOS activation results in NO release in the synaptic cleft; Atp7a activation in the *trans*-Golgi network (TGN) results in Cu^{2+} release in the synaptic cleft. Released Cu^{2+} ions are immediately bound by copper-binding proteins: PrP^C is highly expressed in both presynaptic and postsynaptic terminals, and it can be included in lipid raft domains that also contain NMDARs, and it has high affintiy for both Cu^{2+} and Cu^+. Released NO can react with extracellular cysteines thiols of NMDAR subunits GluN1 and GluN2A, leading to cysteines S-nitrosylation (SNO-Cys). The S-nitrosylation inhibits NMDAR activation by closing the channel. The chemical reaction between NO and the cystein thiol requires the presence of an electron acceptor, often represented by Cu^{2+}. According to this model, PrP^C brings the Cu^{2+} ions that support the reaction of NO with thiols, leading to the S-nitrosylation of GluN1 and GluN2A, thus inhibiting NMDAR. To see this illustration in color, the reader is referred to the web version of this article at www.liebertpub.com/ars

of copper relies on PrP^C expression. This finding has relevant implications in defining copper-mediated modulation of NMDAR and the involvement of copper in neuroprotection, as these functions are impaired in both AD and prion diseases. Moreover, it is known that copper metabolism dysfunction is a primary cause of other pathologies, such as Menkes' disease (MD)—a disorder caused by a loss-of-function mutation in the Atp7a-encoding gene that results in altered copper trafficking (26). Indeed, hippocampal neurons derived from a MD murine model have shown altered NMDAR current and increased damage upon excitotoxic stimulus (37). Strikingly, this phenotype is very similar to that observed in PrP^C-null models (21, 34, 38).

Our findings indicate that PrP^C, copper, and NO regulate NMDAR and impart neuroprotection through a common mechanism that is likely to be lost in AD, MD, and prion diseases, thus leading to synapse degeneration. In this mechanism, PrP^C-bound copper ions act as electron acceptors in the reaction between NO and NMDAR cysteine thiols. The ensuing S-nitrosylation inhibits the receptor and reduces the neurotoxic effect caused by its overactivation. This mechanism is neuroprotective and crucial for normal synaptic functionality.

As in the case of NMDAR, PrP^C-Cu may also promote the S-nitrosylation of other membrane proteins. Indeed, inducing protein S-nitrosylation may be an overarching function of PrP^C. The novel mechanism presented here may provide a platform to investigate additional and previously unforeseen cellular processes in which PrP^C may be involved.

Materials and Methods

Animals

All experiments were performed in accordance with European regulations (European Community Council Directive, November 24, 1986 [86/609/EEC]). Experimental procedures were notified to and approved by the Italian Ministry of Health, Directorate General for Animal Health. All experiments were approved by the local authority veterinary service of Trieste, Italy, and by the Ethics Committee of the Scuola Internazionale Superiore di Studi Avanzati (SISSA), Trieste. All efforts were made to minimize animal suffering and to reduce the number of animals used. Inbred FVB/N (Friend virus B-type susceptibility-NIH) wild-type and FVB $Prnp^{0/0}$ mice were used in these experiments. The FVB $Prnp^{0/0}$ mice were obtained from George A. Carlson, McLaughlin Research Institute (Great Falls, MT) and were bred by backcrossing with the original $Prnp^{0/0}$ mice at least 20 times (25).

S-nitrosylated protein detection: biotin switch assay

The biotin switch assay was performed, as described by Jaffrey and Snyder (18) with a few modifications. Mouse

hippocampal samples (age-matched samples from 6-, 10-, and 12-month-old male animals) were dissected, immediately frozen in liquid nitrogen, and stored at −80°C. Each hippocampus was homogenized in 400 μl HEN buffer: 250 m*M* HEPES pH 7.5 (H3375; Sigma-Aldrich, St Louis, MO), 1 m*M* EDTA (E6758; Sigma-Aldrich), 0.1 m*M* neocuproine (N1501; Sigma-Aldrich), protease inhibitors cocktail (Roche Diagnostics Corp., Mannheim, Germany), and centrifuged at 2000 *g*, 10 min at 4°C. To evaluate the role of copper in NMDAR S-nitrosylation, *Prnp*$^{+/+}$ and *Prnp*$^{0/0}$ OHC were treated for 3 h with 20 μ*M* CZ (14690; Sigma-Aldrich) from the 4 m*M* stock in 50% ethanol, then immediately frozen. For each experiment, at least 60 slices per group were collected and homogenized in 100 μl HEN buffer by sonication. Protein concentration in the supernatant was determined by bicinchoninic acid assay and the same amount of proteins per sample was used for the further steps of the protocol (1 mg for hippocampal samples and 0.7–1 mg for OHC depending on the lowest sample concentration in each experiment). All the reagents were used proportionally. Samples were diluted to 0.8 μg/μl in HEN buffer + 0.04% CHAPS (C9426; Sigma-Aldrich) and incubated at 50°C for 1 h in 4 volumes of blocking solution: 9 volumes of HEN, 1 volume of 25% w/v SDS (L3771; Sigma-Aldrich) in ddH_2O, and 20 m*M* S-methyl thiomethanesulfonate (64306; Sigma-Aldrich) from the 2 *M* stock solution in dimethylformamide. S-methyl thiomethanesulfonate was removed by acetone precipitation and the protein pellet was resuspended in 100 μl of HENS buffer (HEN + 1% SDS) per mg of starting proteins. To selectively and efficiently reduce S-nitrosylated thiols, ascorbate (A4034; Sigma-Aldrich), prepared as 180 m*M* in ddH_2O, was added to 30 m*M* final concentration in the samples, and the reaction was carried out for 3 h at 25°C (14). A negative control without ascorbate was performed on *Prnp*$^{+/+}$ samples to check the efficiency of thiols blocking with S-methyl thiomethanesulfonate. Ascorbate was removed by acetone precipitation and the protein pellet was resuspended in 100 μl of HENS buffer per mg of starting proteins. EZ-Link HPDP-biotin (21341; Thermoscientific, Waltham, MA) was used to bind free thiols, corresponding to the previously S-nitrosylated residues. It was added 1:3 to the samples from the 4 m*M* stock in dimethylformamide. A negative control without biotin was performed on *Prnp*$^{+/+}$ samples to check the selective binding to the resin. After 1 h incubation at 25°C, HPDP-biotin was removed by dialysis in HENS buffer. To purify biotinylated proteins, 2 volumes of neutralization buffer (20 m*M* HEPES pH 7.5, 100 m*M* NaCl, 1 m*M* EDTA, 0.5% Triton X-100 [X100; Sigma-Aldrich]) and 50 μl of wet Immobilized NeutrAvidin Agarose (29200; Thermoscientific) were added to the samples and incubated for 2 h at room temperature (RT). Resin was washed 5 times with neutralization buffer adjusted to 600 m*M* NaCl; biotinylated proteins were eluted directly in SDS-PAGE sample buffer, boiled, and processed for Western blot detection. For each sample, 30 μg of protein extract were loaded as input. The following primary antibodies were used: anti-GluN1 1:500–1:2000 (G8913; Sigma-Aldrich); anti-GluN2A 1:500–1:2000 (G9038; Sigma-Aldrich); monoclonal anti-PrP SHA31 1 μg/ml (A03213; BertinPharma, Montigny le Bretonneux, France); anti-β-actin Peroxidase (AC-15) 1:10,000 (A3854; Sigma-Aldrich). After incubation with the secondary antibody, membranes were developed with the ECL detection reagent (GE Healthcare, Waukesha, WI) and recorded by the digital imaging system Alliance 4.7 (UVITEC, Cambridge, United Kingdom). Band quantification was performed with Uviband 15.0 software (UVITEC) obtaining an optical density (OD) value. To normalize OD values, the following formula was applied: (NMDAR subunit S-nitrosylation/input)/(β-actin S-nitrosylation/input). Basically, S-nitrosylation signals were normalized on the corresponding input. Then, NMDAR subunit values were normalized on β-actin value. *Prnp*$^{+/+}$ and *Prnp*$^{0/0}$ samples were compared by the Mann–Whitney test setting $F(x) <> G(x)$ as alternate hypothesis.

Organotypic hippocampal cultures preparation and treatments

OHC preparation protocol was set up based on Gahwiler's protocol (13). Briefly, in aseptic condition, P5 mouse hippocampus was dissected in the dissection medium (Gey's balanced salt solution, 5.6 m*M* D-glucose [G8270; Sigma-Aldrich], 1 m*M* kynurenic acid [K3375; Sigma-Aldrich]) and sliced by means of a tissue chopper into 300-μm-thick sections. After washing in the dissection medium for 40 min at 4°C, slices showing an intact hippocampal cytoarchitecture were selected, singularly attached to a coverslip by embedding in a chicken plasma (P3266; Sigma-Aldrich) and thrombin clot (112374; Merck KGaA, Darmstadt, Germany) and maintained at 10 rotations per hour at 37°C in Nunc cell culture tubes (156758; Thermoscientific) with a medium composed of 50% basal medium Eagle (41010026; Gibco, Carlsbad, CA), 25% horse serum (26050-088; Gibco), 25% Hank's balanced salt solution (24020141; Gibco), 5.6 m*M* D-glucose, 2 m*M* L-glutamine (25030-032; Gibco). After 13 days *in vitro*, OHC were treated in the serum-free medium, as described in Supplementary Table S1. The drug stock solutions were prepared as follows: 1 m*M* NMDA (0114; Tocris Biosciences, Missouri, United Kingdom) in ddH_2O stored at −20°C; 250 m*M* EGTA (E4378; Sigma-Aldrich) in phosphate-buffered saline (PBS), pH 7.4, stored at RT; 40 m*M* CNQX (C239; Sigma-Aldrich) in dimethyl sulfoxide (DMSO, D8418; Sigma-Aldrich) stored at −20°C; 10 m*M* (2*R*)-amino-5-phosphonovaleric acid (AP5, A5282; Sigma-Aldrich) in ddH_2O stored at −20°C; 5 m*M* threo ifenprodil hemitartrate (2892; Tocris Biosciences) in ddH_2O stored at −20°C; 10 m*M* GSNO (N4148; Sigma-Aldrich) in ddH_2O stored at −20°C; freshly prepared three NNA (N5501; Sigma-Aldrich) in serum-free medium; freshly prepared 4 m*M* CZ in 50% ethanol. To induce excitotoxicity, OHC were exposed either to 5 μ*M* NMDA for 3 h or to 10 μ*M* NMDA for 10 min. Experiments with EGTA were performed using 2 m*M* EGTA in combination with either 5 μ*M* NMDA for 1.5 h (EGTA treatment for 3 h was toxic for OHC) or 10 μ*M* NMDA for 10 min. Treatments with 5 μ*M* NMDA in combination with either 50 μ*M* AP5 or 20 μ*M* CNQX or 20 μ*M* GSNO or 1 m*M* NNA or 20 μ*M* CZ were incubated for 3 h. To obtain a more complete inhibition, AP5, CNQX, and NNA were preincubated for 30 min before adding NMDA. Treatments with NMDA and ifenprodil were carried out differently because of the toxic effect of ifenprodil when associated to low NMDA concentrations (20). For this reason, OHC were exposed to 10 μ*M* NMDA and 3 μ*M* ifenprodil for 10 min. To evaluate neuronal cell death, all the described treatments were followed by a 24 h washout before processing OHC for immunofluorescence.

Immunofluorescence

To evaluate neuronal cell death, slices were fixed in 4% paraformaldehyde (P6148; Sigma-Aldrich) in PBS, pH 7.4, O/N at 4°C. To improve the nuclear staining, slices were treated as follows: 3×5 min washes in PBS with 1% Triton X-100, 10 min in 0.1 N HCl at 4°C, 10 min in 0.2 N HCl at RT, 20 min in 0.2 N HCl at 37°C, 12 min in borate buffer pH 8.4 at RT, 3×5 min washes in PBS with 1% Triton X-100. Slices were incubated for 2 h at RT in the blocking solution (1 *M* glycin [G8898; Sigma-Aldrich], 5% normal goat serum [005-000-121; Jackson ImmunoResearch] in PBS with 1% Triton X-100) and O/N at 4°C with anti-neuronal nuclei (NeuN) clone A60 antibody 1:500 (mab377; Millipore, Billerica, MA) in the blocking solution. After washing with PBS and 1% Triton X-100, slices were incubated with Alexa fluorophore-conjugated secondary antibodies (1:500, R37120; Invitrogen, Carlsbad, CA) and 4′,6-diamidino-2-phenylindole (DAPI, 1:500) in the blocking solution for 2 h at RT. Slices were washed in PBS, rinsed in water, and mounted with VectaShield (Vector Laboratories, Burlingame, CA).

Confocal microscopy, image analysis, and statistics of OHC experiments

Immunofluorescence images were acquired on a Leica DMIRE2 confocal microscope (Leica Microsystem GmbH, Wetzlar, Germany) equipped with DIC and fluorescent optics, diode laser 405 nm, and Ar/ArKr 488 nm lasers. The fluorescence images (1024×1024 pixels) were acquired with a 40×/1.30 NA oil objective, additionally zoomed 1.5-fold, with 200 Hz acquisition speed. Stacks of z-sections with an interval of 3 μm were sequentially scanned. CA1, CA3, and DG were the regions selected for the analysis. A protocol for automatic count of the total amount of nuclei was set up for each hippocampal zone with the Volocity 5.4 3D imaging software (PerkinElmer, Coventry, United Kingdom). The same software was used to manually count the pyknotic nuclei. The dead cell count was performed as a blind analysis. The CA1, CA3, and DG regions were clearly distinguishable in OHC used in these experiments (Supplementary Fig. S11A) and the staining protocol allowed for the exact identification of neuronal pyknotic nuclei (Supplementary Fig. S11B). Pyknotic nuclei count results for $Prnp^{+/+}$ and $Prnp^{0/0}$ OHC were compared by performing the Mann–Whitney test setting $F(x) <> G(x)$ as alternate hypothesis. Each culture preparation (resulting from three to four mice dissection) was considered as one sample ($n=1$). In each culture, the average pyknotic nuclei percentage among the hippocampal slices (four to five slices) of the same treatment group was calculated, grouped with values obtained from other OHC of the same genotype with the same treatment for a final sample size of four ($n=4$) and compared with the other treatments and genotype by means of the Mann–Whitney test.

Acknowledgments

This work was supported by a grant from the Italian Ministry for Education, University and Research to G.L. (Grant MIUR-PRIN 2010/2011–A.AC.NSCI.780). F.B. gratefully acknowledges the International School for Advanced Studies (SISSA), Trieste, for partially supporting this work through the ''Young SISSA Scientists' Research Projects'' 2011–2012 scheme. The authors are grateful to Diego Favretto, Sara De Iudicibus, and Prof. Giuliana Decorti (Department of Life Sciences, University of Trieste) for their expertise in the analytical measurement of the NOS activity with radioactive substrate. The authors thank Prof. Enrico Cherubini for helpful scientific discussion and suggestions, Roberta Antonelli for her assistance in coIP experiments, and Erica Sarnataro for editing and proofreading the article.

Author Disclosure Statement

The authors declare no competing financial interests exist.

References

1. Aguzzi A, Baumann F, and Bremer J. The prion's elusive reason for being. *Annu Rev Neurosci* 31: 439–477, 2008.
2. Benetti F, Ventura M, Salmini B, Ceola S, Carbonera D, Mammi S, Zitolo A, D'Angelo P, Urso E, Maffia M, Salvato B, and Spisni E. Cuprizone neurotoxicity, copper deficiency and neurodegeneration. *Neurotoxicology* 31: 509–517, 2010.
3. Benvegnu S, Poggiolini I, and Legname G. Neurodevelopmental expression and localization of the cellular prion protein in the central nervous system of the mouse. *J Comp Neurol* 518: 1879–1891, 2010.
4. Bonomo RP, Pappalardo G, Rizzarelli E, Tabbi G, and Vagliasindi LI. Studies of nitric oxide interaction with mono- and dinuclear copper(II) complexes of prion protein bis-octarepeat fragments. *Dalton Trans* 3805–3816, 2008.
5. Brown DR, Qin K, Herms JW, Madlung A, Manson J, Strome R, Fraser PE, Kruck T, von Bohlen A, Schulz-Schaeffer W, Giese A, Westaway D, and Kretzschmar H. The cellular prion protein binds copper *in vivo*. *Nature* 390: 684–687, 1997.
6. Caiati MD, Safiulina VF, Fattorini G, Sivakumaran S, Legname G, and Cherubini E. PrPC controls via protein kinase A the direction of synaptic plasticity in the immature hippocampus. *J Neurosci* 33: 2973–2983, 2013.
7. Choi YB, Tenneti L, Le DA, Ortiz J, Bai G, Chen HS, and Lipton SA. Molecular basis of NMDA receptor-coupled ion channel modulation by S-nitrosylation. *Nat Neurosci* 3: 15–21, 2000.
8. D'Angelo P, Della Longa S, Arcovito A, Mancini G, Zitolo A, Chillemi G, Giachin G, Legname G, and Benetti F. Effects of the pathological Q212P mutation on human prion protein non-octarepeat copper-binding site. *Biochemistry* 51: 6068–6079, 2012.
9. Delint-Ramirez I, Fernandez E, Bayes A, Kicsi E, Komiyama NH, and Grant SG. *In vivo* composition of NMDA receptor signaling complexes differs between membrane subdomains and is modulated by PSD-95 and PSD-93. *J Neurosci* 30: 8162–8170, 2010.
10. Dong Z, Saikumar P, Weinberg JM, and Venkatachalam MA. Calcium in cell injury and death. *Annu Rev Pathol* 1: 405–434, 2006.
11. Foster MW, McMahon TJ, and Stamler JS. S-nitrosylation in health and disease. *Trends Mol Med* 9: 160–168, 2003.
12. Fournier JG, Escaig-Haye F, Billette de Villemeur T, Robain O, Lasmezas CI, Deslys JP, Dormont D, and Brown P. Distribution and submicroscopic immunogold localization of cellular prion protein (PrPc) in extracerebral tissues. *Cell Tissue Res* 292: 77–84, 1998.
13. Gahwiler BH, Capogna M, Debanne D, McKinney RA, and Thompson SM. Organotypic slice cultures: a technique has come of age. *Trends Neurosci* 20: 471–477, 1997.

14. Gow AJ and Ischiropoulos H. Nitric oxide chemistry and cellular signaling. *J Cell Physiol* 187: 277–282, 2001.
15. Greenough MA, Camakaris J, and Bush AI. Metal dyshomeostasis and oxidative stress in Alzheimer's disease. *Neurochem Int* 62: 540–555, 2013.
16. Hardingham GE and Bading H. Synaptic versus extrasynaptic NMDA receptor signalling: implications for neurodegenerative disorders. *Nat Rev Neurosci* 11: 682–696, 2010.
17. Hess DT, Matsumoto A, Kim SO, Marshall HE, and Stamler JS. Protein S-nitrosylation: purview and parameters. *Nat Rev Mol Cell Biol* 6: 150–166, 2005.
18. Jaffrey SR and Snyder SH. The biotin switch method for the detection of S-nitrosylated proteins. *Sci STKE* 2001: pl1, 2001.
19. Kellett KA and Hooper NM. Prion protein and Alzheimer disease. *Prion* 3: 190–194, 2009.
20. Kew JN, Trube G, and Kemp JA. A novel mechanism of activity-dependent NMDA receptor antagonism describes the effect of ifenprodil in rat cultured cortical neurones. *J Physiol* 497 (Pt 3): 761–772, 1996.
21. Khosravani H, Zhang Y, Tsutsui S, Hameed S, Altier C, Hamid J, Chen L, Villemaire M, Ali Z, Jirik FR, and Zamponi GW. Prion protein attenuates excitotoxicity by inhibiting NMDA receptors. *J Cell Biol* 181: 551–565, 2008.
22. Kone BC, Kuncewicz T, Zhang W, and Yu ZY. Protein interactions with nitric oxide synthases: controlling the right time, the right place, and the right amount of nitric oxide. *Am J Physiol Renal Physiol* 285: F178–F190, 2003.
23. Lipton SA, Choi YB, Takahashi H, Zhang D, Li W, Godzik A, and Bankston LA. Cysteine regulation of protein function—as exemplified by NMDA-receptor modulation. *Trends Neurosci* 25: 474–480, 2002.
24. Liu L, Jiang D, McDonald A, Hao Y, Millhauser GL, and Zhou F. Copper redox cycling in the prion protein depends critically on binding mode. *J Am Chem Soc* 133: 12229–12237, 2011.
25. Lledo PM, Tremblay P, DeArmond SJ, Prusiner SB, and Nicoll RA. Mice deficient for prion protein exhibit normal neuronal excitability and synaptic transmission in the hippocampus. *Proc Natl Acad Sci U S A* 93: 2403–2407, 1996.
26. Lutsenko S and Petris MJ. Function and regulation of the mammalian copper-transporting ATPases: insights from biochemical and cell biological approaches. *J Membr Biol* 191: 1–12, 2003.
27. Maglio LE, Perez MF, Martins VR, Brentani RR, and Ramirez OA. Hippocampal synaptic plasticity in mice devoid of cellular prion protein. *Brain Res Mol Brain Res* 131: 58–64, 2004.
28. Mallucci GR, Ratte S, Asante EA, Linehan J, Gowland I, Jefferys JG, and Collinge J. Post-natal knockout of prion protein alters hippocampal CA1 properties, but does not result in neurodegeneration. *EMBO J* 21: 202–210, 2002.
29. Mani L, Cheng F, Havsmark B, Jonsson M, Belting M, and Fransson L. Prion, amyloid-derived Cu(II) ions, or free Zn(II) ions support S-nitroso-dependent autocleavage of glypican-1 heparan sulfate. *J Biol Chem* 278: 38956–38965, 2003.
30. McBain CJ and Mayer ML. N-methyl-D-aspartic acid receptor structure and function. *Physiol Rev* 74: 723–760, 1994.
31. Moya KL, Sales N, Hassig R, Creminon C, Grassi J, and Di Giamberardino L. Immunolocalization of the cellular prion protein in normal brain. *Microsc Res Tech* 50: 58–65, 2000.
32. Naslavsky N, Stein R, Yanai A, Friedlander G, and Taraboulos A. Characterization of detergent-insoluble complexes containing the cellular prion protein and its scrapie isoform. *J Biol Chem* 272: 6324–6331, 1997.
33. Prusiner SB. Shattuck lecture—neurodegenerative diseases and prions. *N Engl J Med* 344: 1516–1526, 2001.
34. Rangel A, Burgaya F, Gavin R, Soriano E, Aguzzi A, and Del Rio JA. Enhanced susceptibility of Prnp-deficient mice to kainate-induced seizures, neuronal apoptosis, and death: Role of AMPA/kainate receptors. *J Neurosci Res* 85: 2741–2755, 2007.
35. Sales N, Rodolfo K, Hassig R, Faucheux B, Di Giamberardino L, and Moya KL. Cellular prion protein localization in rodent and primate brain. *Eur J Neurosci* 10: 2464–2471, 1998.
36. Schlief ML, Craig AM, and Gitlin JD. NMDA receptor activation mediates copper homeostasis in hippocampal neurons. *J Neurosci* 25: 239–246, 2005.
37. Schlief ML, West T, Craig AM, Holtzman DM, and Gitlin JD. Role of the Menkes copper-transporting ATPase in NMDA receptor-mediated neuronal toxicity. *Proc Natl Acad Sci U S A* 103: 14919–14924, 2006.
38. Spudich A, Frigg R, Kilic E, Kilic U, Oesch B, Raeber A, Bassetti CL, and Hermann DM. Aggravation of ischemic brain injury by prion protein deficiency: role of ERK-1/-2 and STAT-1. *Neurobiol Dis* 20: 442–449, 2005.
39. Wroge CM, Hogins J, Eisenman L, and Mennerick S. Synaptic NMDA receptors mediate hypoxic excitotoxic death. *J Neurosci* 32: 6732–6742, 2012.
40. You H, Tsutsui S, Hameed S, Kannanayakal TJ, Chen L, Xia P, Engbers JD, Lipton SA, Stys PK, and Zamponi GW. Abeta neurotoxicity depends on interactions between copper ions, prion protein, and N-methyl-D-aspartate receptors. *Proc Natl Acad Sci U S A* 109: 1737–1742, 2012.
41. Zhou X, Ding Q, Chen Z, Yun H, and Wang H. Involvement of the GluN2A and GluN2B subunits in synaptic and extrasynaptic N-methyl-D-aspartate receptor function and neuronal excitotoxicity. *J Biol Chem* 288: 24151–24159, 2013.
42. Zhou X, Hollern D, Liao J, Andrechek E, and Wang H. NMDA receptor-mediated excitotoxicity depends on the coactivation of synaptic and extrasynaptic receptors. *Cell Death Dis* 4: e560, 2013.

Address correspondence to:
Dr. Federico Benetti
ECSIN-European Center for the Sustainable Impact of Nanotechnology
Veneto Nanotech S.C.p.A.
Viale Porta Adige 45
Rovigo 45100
Italy

E-mail: benetti@sissa.it

Prof. Giuseppe Legname
Laboratory of Prion Biology
Department of Neuroscience
Scuola Internazionale Superiore di Studi Avanzati (SISSA)
Via Bonomea 265
Trieste 34136
Italy

E-mail: legname@sissa.it

Date of first submission to ARS Central, June 25, 2014; date of final revised submission, November 5, 2014; date of acceptance, December 8, 2014.

Abbreviations Used

AD = Alzheimer disease
AP5 = (2*R*)-amino-5-phosphonovaleric acid
Atp7a = copper-transporting ATPase 1
CA1 = *Cornus Ammonis 1*
CA3 = *Cornus Ammonis 3*
CaM = calmodulin
CNQX = 6-cyano-7-nitroquinoxaline-2,3-dione
coIP = co-immunoprecipitation
CZ = cuprizone
DAPI = 4′,6-diamidino-2-phenylindole
DG = dentate gyrus
DMSO = dimethyl sulfoxide
EGTA = ethylene glycol tetraacetic acid
GluN1 = NMDAR subunit GluN1
GluN2A = NMDAR subunit GluN2A
GSNO = S-nitrosoglutathione
MD = Menkes' disease
MTT = 3-(4,5-dimethylthiazol-2-yl)-2,5-diphenyltetrazolium bromide
NeuN = anti-neuronal nuclei marker antibody
NMDA = *N*-methyl-D-aspartate
NMDAR = *N*-methyl-D-aspartate receptors
NNA = Nω-nitro-L-arginine
nNOS = neuronal nitric oxide synthase
NO = nitric oxide
OD = optical density
OHC = organotypic hippocampal cultures
$Prnp^{+/+}$, $Prnp^{0/0}$ = PrP^C wild type, PrP^C knockout
PrP^C = cellular prion protein
PSD95 = postsynaptic density protein 95
SNO-Cys = cysteine S-nitrosylation

Supplementary Data

Supplementary Materials and Methods

Protein S-nitrosylation detection by SNOB1 reagent

To compare GluN2A and GluN1 S-nitrosylation levels in $Prnp^{+/+}$ and $Prnp^{0/0}$ hippocampi, we used the SNOB1 reagent (sc-361363; Santa Cruz Biotechnology, Dallas, TX). Two $Prnp^{+/+}$ and two $Prnp^{0/0}$ hippocampi were separately homogenized in 1 ml phosphate-buffered saline (PBS) + 0.5% Triton X-100 + protease inhibitors and centrifuged for 10 min at 5000 rpm at 4°C. Protein concentration in the supernatant was determined by bicinchoninic acid assay, and the same amount of protein was used as input for the following steps. Half of the protein extract was added to PBS + 0.5% Triton up to 1 ml and incubated with 0.5 m*M* SNOB1 for 30 min at 37°C in the dark according to the manufacturer's instructions. The second half of the sample was added to PBS + 0.5% Triton up to 1 ml and incubated with 0.5 m*M* biotin for 30 min at 37°C in the dark, as negative control. To purify SNOB1-bound proteins, 50 μl of wet Immobilized NeutrAvidin Agarose (29200; Thermoscientific, Waltham, MA) were added to the samples and incubated for 2 h at room temperature (RT). Resin was washed five times PBS + 0.5% Triton. Then, proteins were eluted directly in SDS-PAGE sample buffer, boiled, and processed for Western blot detection. For each sample, 30 μg of protein extract was loaded as input. The following primary antibodies were used: anti-GluN1 1:500–1:2000 (G8913; Sigma-Aldrich, St Louis, MO); anti-GluN2A 1:500–1:2000 (G9038; Sigma-Aldrich); anti-β-actin peroxidase (AC-15) 1:10,000 (A3854; Sigma-Aldrich). After incubation with the secondary antibody, membranes were developed with the ECL detection reagent (GE Healthcare, Waukesha, WI) and recorded by the digital imaging system Alliance 4.7 (UVITEC, Cambridge, United Kingdom). Band quantification was performed with Uviband 15.0 software (UVITEC) obtaining an optical density (OD) value. To normalize OD values, the following formula was applied: (SNOB1-NMDAR subunit/input)/(SNOB1-β-actin/input). Basically, S-nitrosylation signals were normalized on the corresponding input. Then, *N*-methyl-D-aspartate receptors (NMDAR) subunit values were normalized on β-actin value. $Prnp^{+/+}$ and $Prnp^{0/0}$ samples were compared by the Mann–Whitney test setting F(x) < > G(x) as alternate hypothesis.

Co-immunoprecipitation

To compare GluN2A, GluN1, and neuronal nitric oxide synthase (nNOS) synaptic levels in $Prnp^{+/+}$ and $Prnp^{0/0}$ hippocampi, we performed a co-immunoprecipitation (coIP) with postsynaptic density protein 95 (PSD95). Samples from 6-, 10-, and 12-month-old male mice were used to parallel the biotin switch assay experiments, while postnatal day 20 (P20) mouse hippocampi were used to parallel organotypic hippocampal cultures (OHC) excitotoxicity studies. Samples were homogenized in 50 m*M* Tris-HCl, pH 7.5, 150 m*M* NaCl, 1 m*M* EDTA, 0.5% CHAPS, 10% glycerol, protease inhibitor cocktail, 5 m*M* NaF (S7920; Sigma-Aldrich), 0.5 m*M* Na_3VO_4 (S6508; Sigma-Aldrich), protein concentration was evaluated by the BCA assay to use the same amount of proteins in each sample. For PSD95 coIP with GluN2A (direct interaction) and GluN1 (indirect interaction), hippocampal protein extracts were precleared by 30 min incubation at 4°C with protein A/G (1:2) resin (17-5138-01 and 17-0618-01; GE Healthcare, Waukesha, WI). Then, the samples were incubated for 2.5 h at 4°C with 2 μg/ml of either anti-PSD95 antibody (ab2723; Abcam, Cambridge, United Kingdom) or normal mouse IgG (mIgG, 12-371; Millipore, Billerica, MA), followed by 2 h incubation with protein A/G (1:2) resin. For nNOS coIP with PSD95, hippocampal protein extracts were incubated O/N at 4°C with 2 μg/ml of either anti-nNOS antibody (4234; Cell Signaling, Danvers, MA) or normal rabbit IgG (rIgG, 12-370; Millipore), followed by 2 h incubation with protein A/G (1:2) resin. Proteins eluted from the resin were processed for standard Western blot protocol and revealed with anti-GluN1 1:2000 (G8913; Sigma-Aldrich), anti-GluN2A 1:2000 (G9038; Sigma-Aldrich), anti-nNOS, anti-PrP SHA31 1 μg/ml (A03213; BertinPharma, Montigny le Bretonneux, France), and anti-PSD95 antibodies. After incubation with the secondary antibody, membranes were developed with the ECL detection reagent (GE Healthcare) and recorded by Alliance 4.7 digital imaging system (UVITEC). Band quantification was performed with Uviband 15.0 software (UVITEC) obtaining an OD value. To normalize OD values, the following formula was applied: (co-immunoprecipitated protein/input)/(immunoprecipitated protein/input), that is, [GluN2A (or GluN1) coIP/input]/[PSD95 IP/input] and (PSD95 coIP/input)/(nNOS IP/input). Then, $Prnp^{+/+}$ and $Prnp^{0/0}$ samples were compared by the Mann–Whitney test setting F(x) < > G(x) as alternate hypothesis.

NADPH consumption assay

To estimate $Prnp^{+/+}$ and $Prnp^{0/0}$ nNOS activity level, we evaluated the kinetics of NADPH consumption. Samples from 6-month-old and P20 male mice were used to parallel the biotin switch assay experiments and OHC excitotoxicity studies, respectively. Samples were homogenized in 30 m*M* Tris-HCl, pH 7.5, and protease inhibitor cocktail and centrifuged at 10,000 *g*; the supernatant was used for the assay. The protein concentration was evaluated by the BCA assay to use the same amount of proteins in each sample ($\sim$1 mg). Five m*M* NADPH (481973; Millipore) was prepared in ddH_2O and added to each sample to 0.5 m*M* final concentration. The kinetics of NADPH consumption was evaluated by measuring the absorbance at 340 nm each minute for 30 min. For each sample, the respective absorbance without NADPH addition was subtracted as blank to avoid differences in tissue scattering.

NOS activity assay

To measure $Prnp^{+/+}$ and $Prnp^{0/0}$ NOS activity level, we used the NOS activity assay kit (Item Number 781001; Cayman, Ann Arbor, MI). Samples from 6-month-old and P20 male mice were used to parallel the biotin switch assay experiments and OHC excitotoxicity studies, respectively. We used the radiolabeled substrate [^{3}H]Arginine monohydrochloride (40–70 Ci/mmol, 1 μCi/μl [Item

No. NET1123001MC; Perkin Elmer, Waltham, MA]). The assay was run according to the manufacturer's instructions. Results are reported as counts per minute (cpm) subtracted of the blank-corresponding cpm value. As control of the specificity of the assay for the NOS activity, we measured the conversion of radiolabeled arginine in radiolabeled citrulline in the presence of the NOS blocker Nω-nitro-L-arginine (NNA, N5501; Sigma-Aldrich).

MTT mitochondrial toxicity assay

To evaluate the early phase of change in neuronal cell viability, the MTT (Thiazolyl Blue Tetrazolium Bromide) mitochondrial toxicity assay was performed on OHC after exposure to an excitotoxic stimulus. The MTT assay was set up following the protocol by Mazzone (1) with a few modifications. A 5 mg/ml MTT (M5655; Sigma-Aldrich) stock solution was prepared in PBS, pH 7.4. After 13 days *in vitro*, $Prnp^{+/+}$ and $Prnp^{0/0}$ OHC were exposed to 5 μM NMDA in serum-free medium for 3 h. After one wash, OHC were incubated with 0.5 mg/ml MTT in serum-free medium for 2 h at 37°C. To dissolve formazan crystals, OHC were incubated overnight at 37°C with 1 ml of acidified isopropanol (0.04 N HCl in isopropanol). Absorbance values were measured at 570 and 690 nm. The 690 nm absorbance value was used as background, hence subtracted to the 570 nm signal. Cell viability was expressed as percentage of the control OHC value that was considered to be 100% viable and compared by the Mann–Whitney test setting $F(x) < > G(x)$ as alternate hypothesis.

Primary cell culture preparation and measurement of relative intracellular Ca^{2+} $[Ca^{2+}]_i$ changes after NMDA and cuprizone treatment

Primary cell cultures were prepared from wild-type mouse hippocampal neurons. Hippocampi were dissected from P1 rats in the presence of 100 μM kynurenic acid and 25 μM 2-amino-5-phosphonovaleric acid (Tocris Biosciences, Missouri, United Kingdom). The isolated tissue was quickly sliced and digested with trypsin in the presence of DNAse. After stopping the digestion with trypsin inhibitor, cells were triturated in the dissection medium containing DNAse. After centrifugation, the resuspended cell pellet was distributed to 24-well Nunc cell culture multidishes previously coated with polyornithine (0.5 mg/ml) and Matrigel (2% [w/v]; BD Biosciences, San Jose, CA), each one containing 0.5 ml of modified minimal essential medium supplemented with dialyzed fetal bovine serum (Gibco, Carlsbad, CA). Two days after plating, the culture medium was supplemented with 2.5 μM Arabinosylcytosine (Sigma), which inhibits the growth of glial cells. The culture medium was exchanged every 2–3 days. The experiments were performed after 15 days *in vitro*. Primary culture neurons were washed, exposed to Fluo-3 AM (F-1242; Life Technologies, Carlsbad, CA), the dye indicator, for 60 min at 37°C, washed two times, equilibrated for 30 min at 22°C, and washed. $[Ca^{2+}]_i$ levels were determined as described by Tauskela *et al.* with a few modifications (2) by using temperature-controlled plate reader (EnSpire; Perkin Elmer) to measure fluorescence intensity (excitation wavelength 488 nm; emission wavelength 526 nm). Fluorescence intensities were measured from 19 locations within each well before the treatment and 0, 5, 10, and 15 min after the treatment (control, 20 μM cuprizone [CZ], 5 μM NMDA, 5 μM NMDA + 20 μM CZ). The background intensity was measured in cell-free plate with dye-free buffer. The fold increase in $[Ca^{2+}]_i$ levels was calculated by subtracting the background intensity and normalizing on the resting conditions in each well.

Supplementary References

1. Mazzone GL, Margaryan G, Kuzhandaivel A, Nasrabady SE, Mladinic M, and Nistri A. Kainate-induced delayed onset of excitotoxicity with functional loss unrelated to the extent of neuronal damage in the *in vitro* spinal cord. *Neuroscience* 168: 451–462, 2010.
2. Tauskela JS, Brunette E, O'Reilly N, Mealing G, Comas T, Gendron TF, Monette R, and Morley P. An alternative Ca2+ −dependent mechanism of neuroprotection by the metalloporphyrin class of superoxide dismutase mimetics. *FASEB J* 19: 1734–1736, 2005.

Supplementary Table S1. Organotypic Hippocampal Culture Treatments

Drug	*Control*	*Pretreatment*	*Treatment*	*Washout (h)*
Excitotoxic stimulus				
5 μM NMDA	ddH_2O	—	10 min	24
10 μM NMDA	ddH_2O	—	3 h	24
Calcium chelation				
10 μM NMDA + 2 mM EGTA	10 μM NMDA; 2 mM EGTA; PBS pH 7.4	—	10 min	24
5 μM NMDA + 2 mM EGTA	5 μM NMDA; 2 mM EGTA; PBS pH 7.4	—	1.5 h	24
NMDA receptor inhibition				
5 μM NMDA + 50 μM AP5	5 μM NMDA; 50 μM AP5; ddH_2O	30 min AP5	3 h	24
AMPA/kainate receptor inhibition				
5 μM NMDA + 20 μM CNQX	5 μM NMDA; 20 μM CNQX; 0.002% DMSO	30 min CNQX; 30 min 0.002% DMSO	3 h	24
GluN2B-containing NMDA receptor inhibition				
10 μM NMDA + 3 μM ifenprodil	10 μM NMDA; 3 μM ifenprodil; ddH_2O	—	10 min	24
Copper chelation				
5 μM NMDA + 20 μM CZ	5 μM NMDA; 20 μM CZ; 50% EtOH	—	3 h	24
nNOS inhibition				
5 μM NMDA + 1 mM NNA	5 μM NMDA; 1 mM NNA	30 min 1 mM NNA	3 h	24
NO donor				
5 μM NMDA + 20 μM GSNO	5 μM NMDA; 20 μM GSNO; ddH2O	—	3 h	24

AMPA, α-amino-3-hydroxy-5-methyl-4-isoxazolepropionic acid; AP5, (2*R*)-amino-5-phosphonovaleric acid; CNQX, 6-cyano-7-nitroquinoxaline-2,3-dione; CZ, cuprizone; DMSO, dimethyl sulfoxide; EGTA, ethylene glycol tetraacetic acid; EtOH, ethanol; GSNO, S-nitrosoglutathione.; NMDA, *N*-methyl-D-aspartate; NNA, Nω-nitro-L-arginine; nNOS, neuronal nitric oxide synthase; NO, nitric oxide; PBS, phosphate-buffered saline.

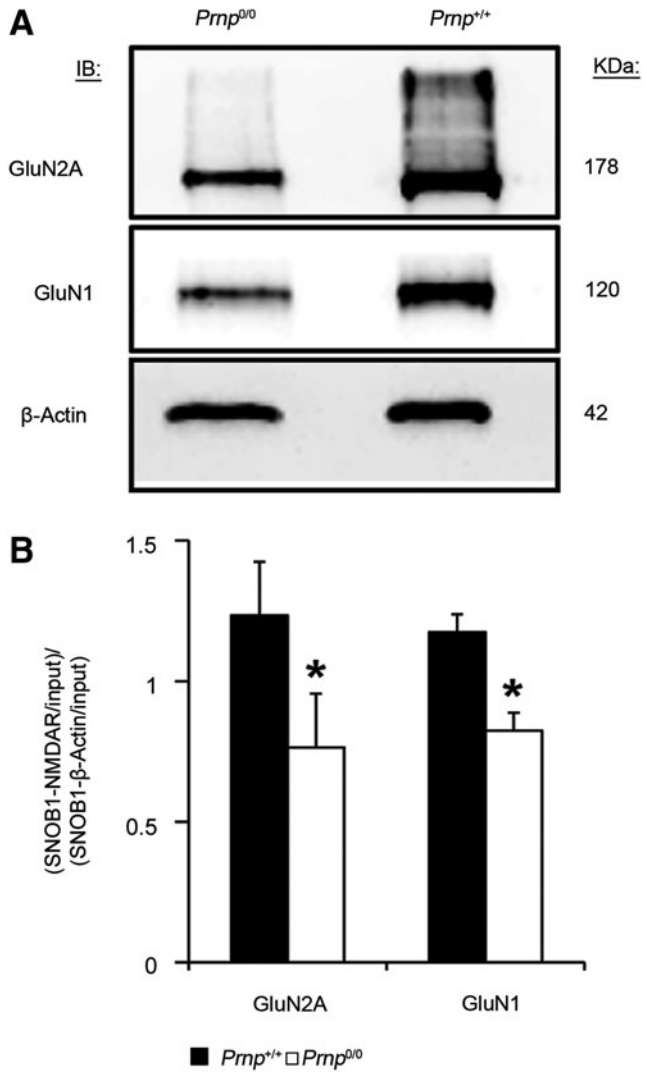

SUPPLEMENTARY FIG. S1. NMDAR subunit S-nitrosylation levels comparison in wild-type and PrP^{C} knockout hippocampi by SNOB1 reagent. (A) Immunoblot signals corresponding to SNOB1-bound GluN2A, GluN1, and β-actin in *Prnp*$^{+/+}$ and *Prnp*$^{0/0}$ hippocampi. **(B)** Graph showing the quantification of the immunoblot signals normalized according to the following formula: (SNOB1-NMDAR subunit/input)/(SNOB1-β-actin/input); all error bars indicate SD; $n=4$; $^{*}p<0.05$. NMDAR, *N*-methyl-D-aspartate receptors.

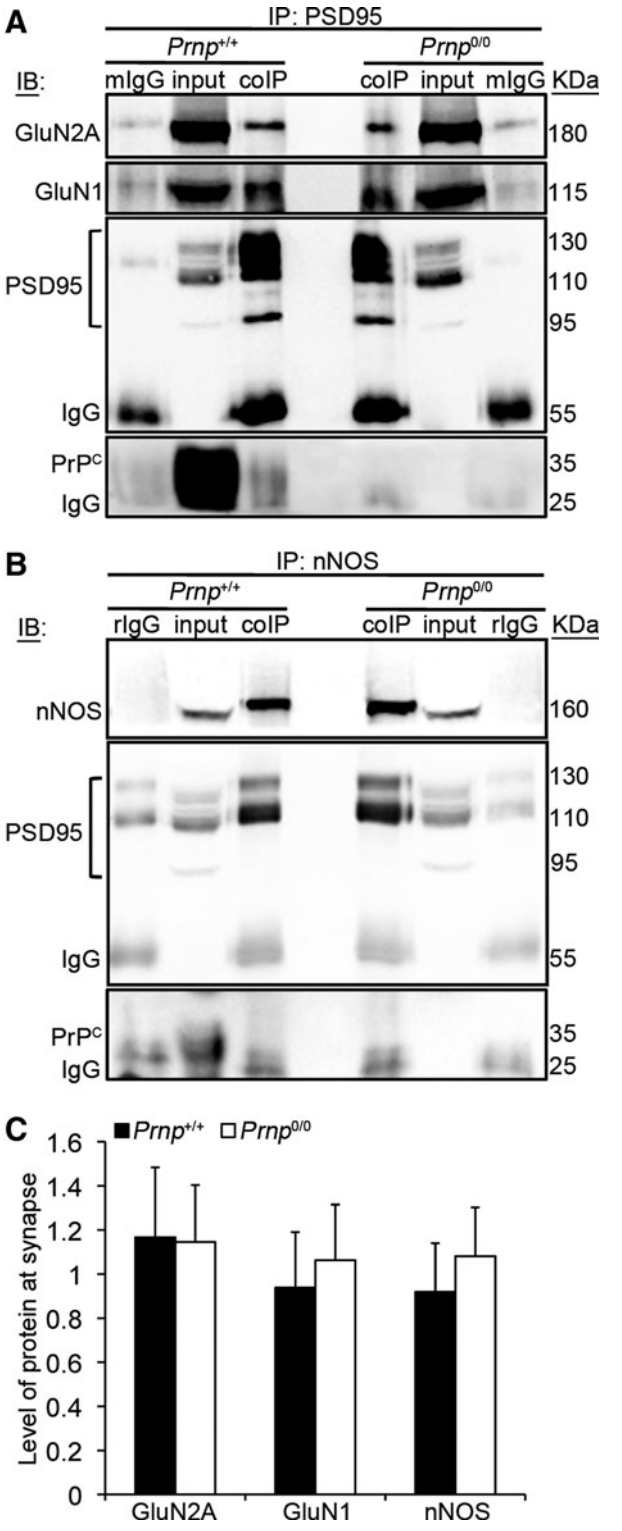

SUPPLEMENTARY FIG. S2. CoIP of GluN2A and GluN1 with PSD95 and coIP of PSD95 with nNOS show comparable levels in adult *Prnp*$^{+/+}$ and *Prnp*$^{0/0}$ hippocampi. (A) coIP of GluN2A and GluN1 with PSD95. **(B)** coIP of PSD95 with nNOS. **(C)** Graph showing the quantification of the coIP signals normalized according to the following formula: (co-immunoprecipitated protein/input)/(immunoprecipitated protein/input); all error bars indicate SD; $n=3$. coIP, co-immunoprecipitation; nNOS, neuronal nitric oxide synthase; PSD95, postsynaptic density protein 95.

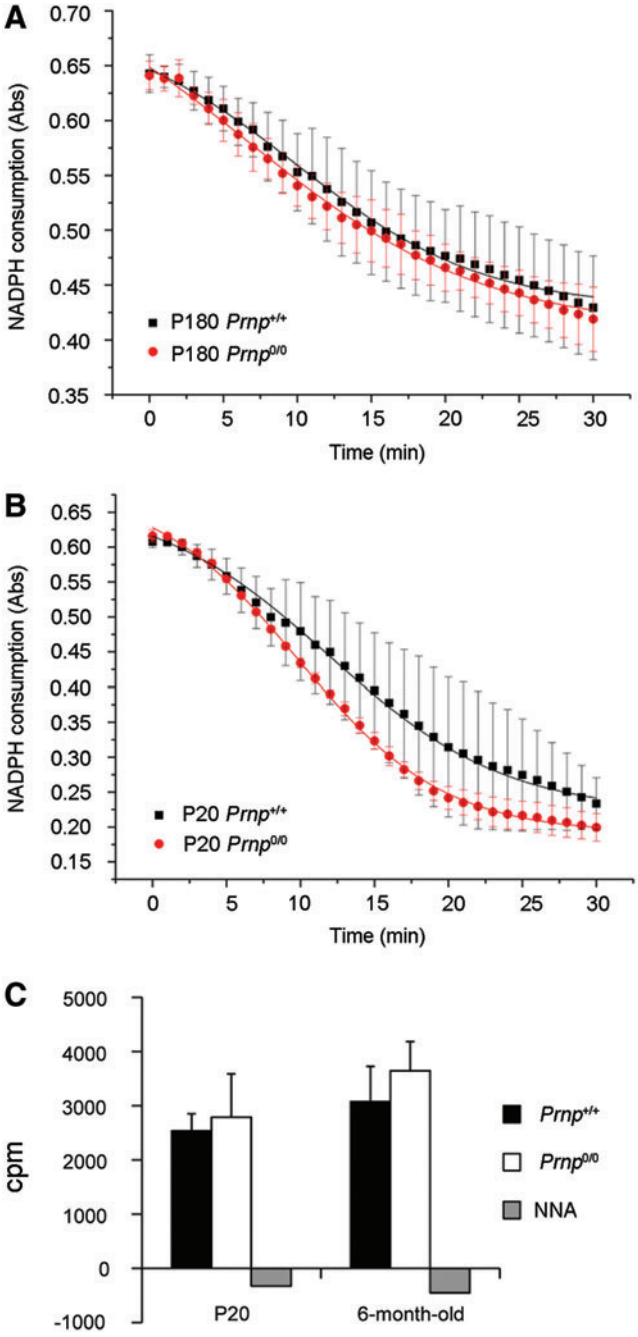

SUPPLEMENTARY FIG. S3. NADPH consumption assay and radiolabeled arginine conversion in citrulline shows comparable NOS activity levels in *Prnp*$^{+/+}$ and *Prnp*$^{0/0}$ mice. (A) NADPH consumption assay in P180 *Prnp*$^{+/+}$ and *Prnp*$^{0/0}$ samples; **(B)** NADPH consumption assay in P20 *Prnp*$^{+/+}$ and *Prnp*$^{0/0}$ samples; all error bars indicate SD; $n=3$; **(C)** radiolabeled citrulline level measurements in P20 and 6-month-old *Prnp*$^{+/+}$ and *Prnp*$^{0/0}$ mouse samples; all error bars indicate SD; $n=4$; *black columns* correspond to *Prnp*$^{+/+}$ mice, *white columns* correspond to *Prnp*$^{0/0}$ mice, *gray columns* correspond to the control with NNA. NNA, Nω-nitro-L-arginine.

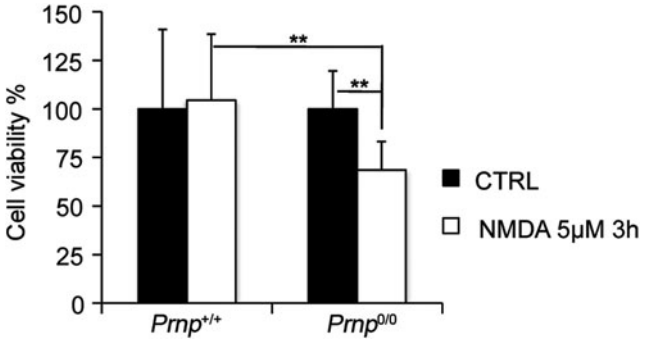

SUPPLEMENTARY FIG. S4. The MTT assay confirms PrP^{C}-null OHC higher susceptibility to excitotoxicity compared with wild-type OHC in the early phase after NMDA treatment. The graph shows the cell viability percentage in *Prnp*$^{+/+}$ and *Prnp*$^{0/0}$ OHC treated and not treated with 5 μM NMDA for 3 h; all bars indicate SD; $n=12$; $^{**}p<0.01$. OHC, organotypic hippocampal cultures.

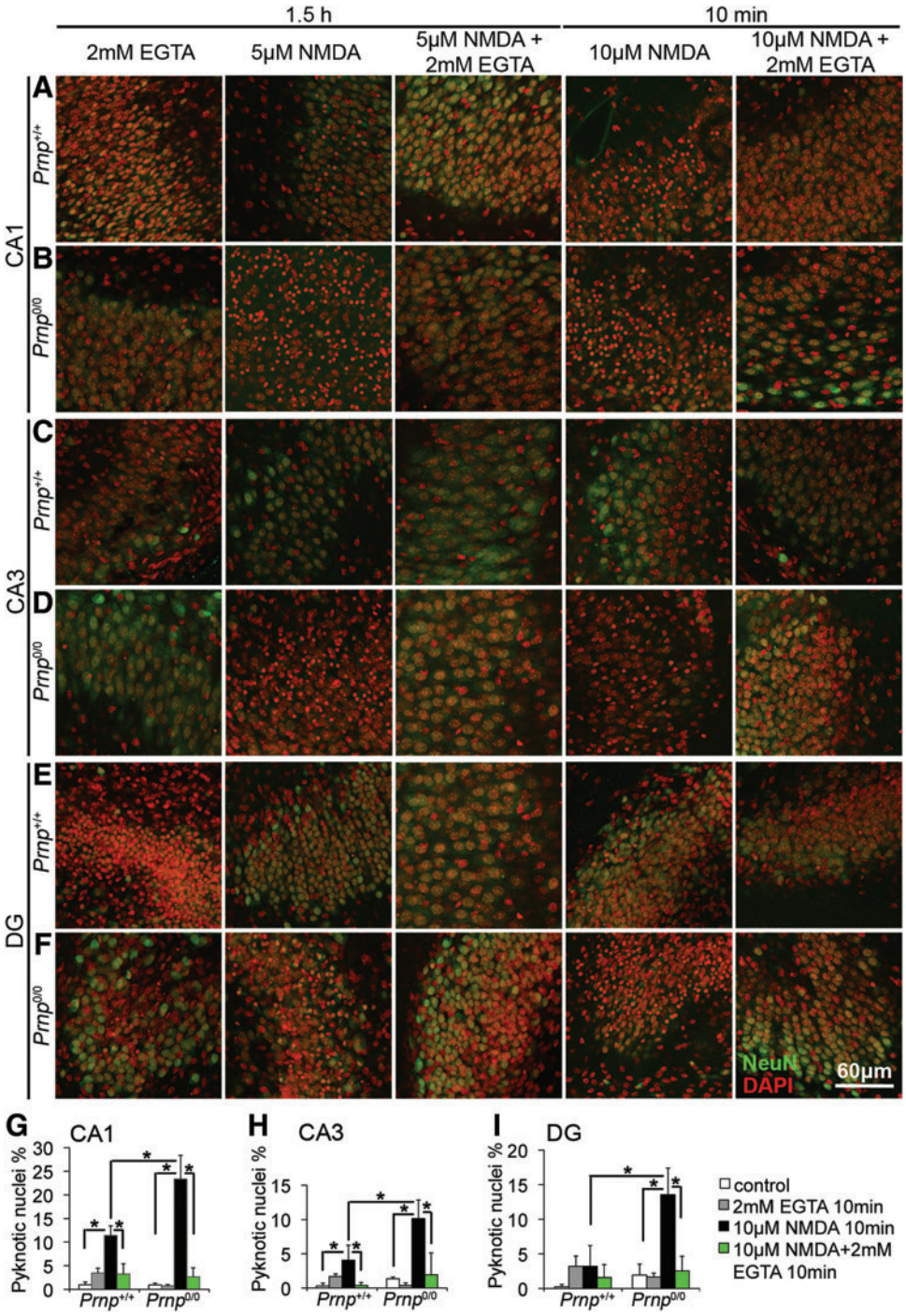

SUPPLEMENTARY FIG. S5. Neuronal cell death induced by NMDA treatment is prevented by calcium chelation. Images from $Prnp^{+/+}$ and $Prnp^{0/0}$ OHC areas are reported in rows: **(A)** $Prnp^{+/+}$ CA1; **(B)** $Prnp^{0/0}$ CA1; **(C)** $Prnp^{+/+}$ CA3; **(D)** $Prnp^{0/0}$ CA3; **(E)** $Prnp^{+/+}$ DG; **(F)** $Prnp^{0/0}$ DG. The different treatments are reported in columns: 2 m*M* EGTA for 1.5 h, *first column*; 5 μM NMDA for 1.5 h, *second column*; 5 μM NMDA + 2 m*M* EGTA for 1.5 h, *third column*; 10 μM NMDA for 10 min, *fourth column*; 10 μM NMDA + 2 m*M* EGTA for 10 min, *fifth column*. NeuN staining is displayed in *green* and DAPI in *red*. Confocal microscope fluorescence images were acquired using a 40×/1.30 NA oil objective. Comparison of neuronal pyknotic nuclei percentages induced by 10 μM NMDA for 10 min, between EGTA-treated $Prnp^{+/+}$ and $Prnp^{0/0}$ OHC in the **(G)** CA1, **(H)** CA3, and **(I)** DG; $n = 4$ OHC, 5 slices per treatment in each culture; all error bars indicate SD; $*p < 0.05$. CA1, *Cornus Ammonis 1*; CA3, *Cornus Ammonis 3*; DAPI, 4′,6-diamidino-2-phenylindole; DG, dentate gyrus; EGTA, ethylene glycol tetraacetic acid.

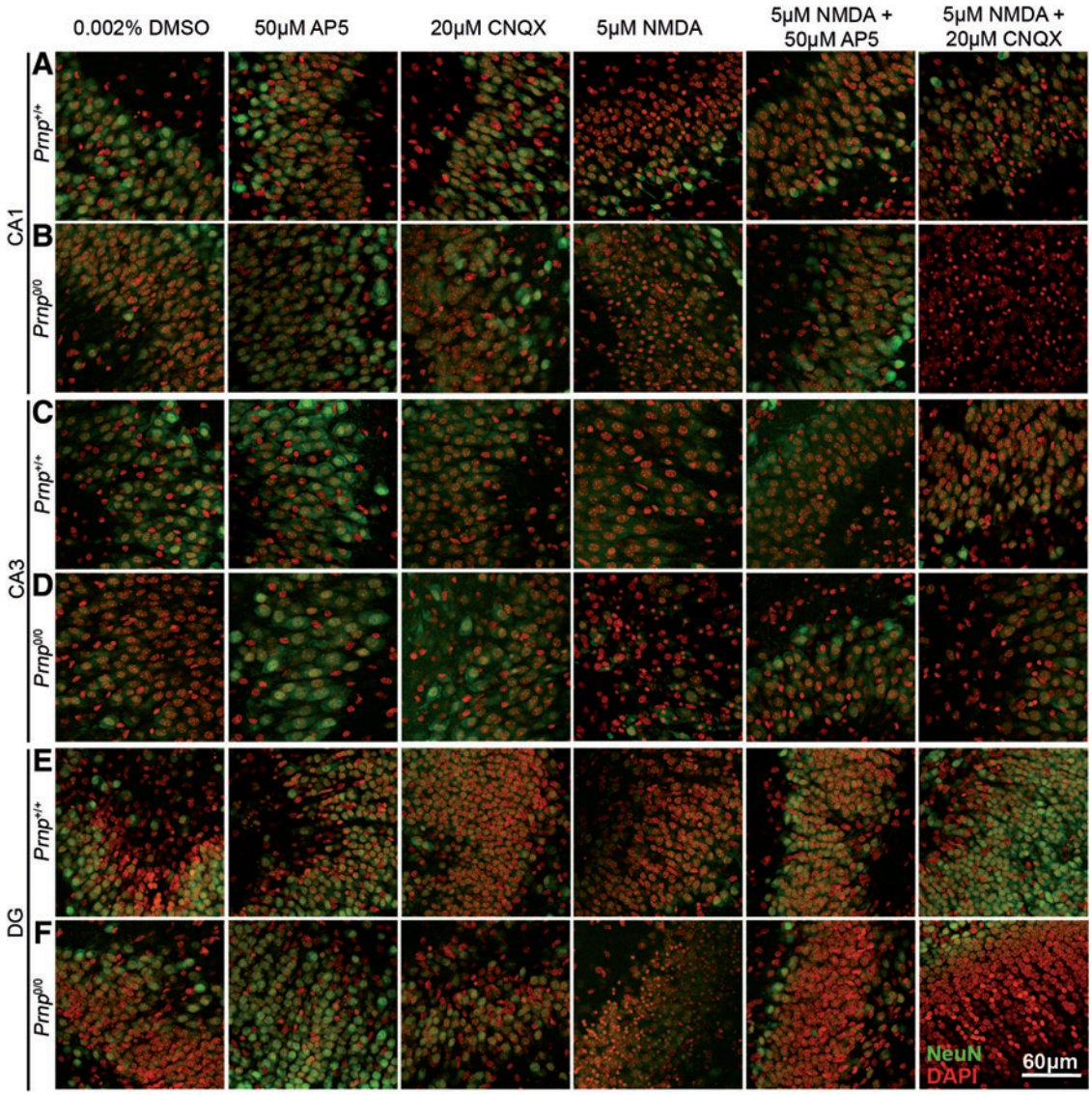

SUPPLEMENTARY FIG. S6. Neuronal cell death induced by NMDA treatment is prevented by NMDAR antagonist and unaltered by AMPA/kainate receptor antagonist. Images from $Prnp^{+/+}$ and $Prnp^{0/0}$ OHC areas are reported in rows: **(A)** $Prnp^{+/+}$ CA1; **(B)** $Prnp^{0/0}$ CA1; **(C)** $Prnp^{+/+}$ CA3; **(D)** $Prnp^{0/0}$ CA3; **(E)** $Prnp^{+/+}$ DG; **(F)** $Prnp^{0/0}$ DG. The different treatments are reported in columns: 0.002% DMSO for 3 h, *first column*; 50 *μM* AP5 for 3 h, *second column*; 20 *μM* CNQX for 3 h, *third column*; 5 *μM* NMDA for 3 h, *fourth column*; 5 *μM* NMDA + 50 *μM* AP5 for 3 h, *fifth column*; 5 *μM* NMDA + 20 *μM* CNQX for 3 h, *sixth column*. NeuN staining is displayed in *green* and DAPI in *red*. Confocal microscope fluorescence images were acquired using a 40×/1.30 NA oil objective. AMPA, α-amino-3-hydroxy-5-methyl-4-isoxazolepropionic acid; AP5, (2*R*)-amino-5-phosphonovaleric acid; CNQX, 6-cyano-7-nitroquinoxaline-2,3-dione; DMSO, dimethyl sulfoxide.

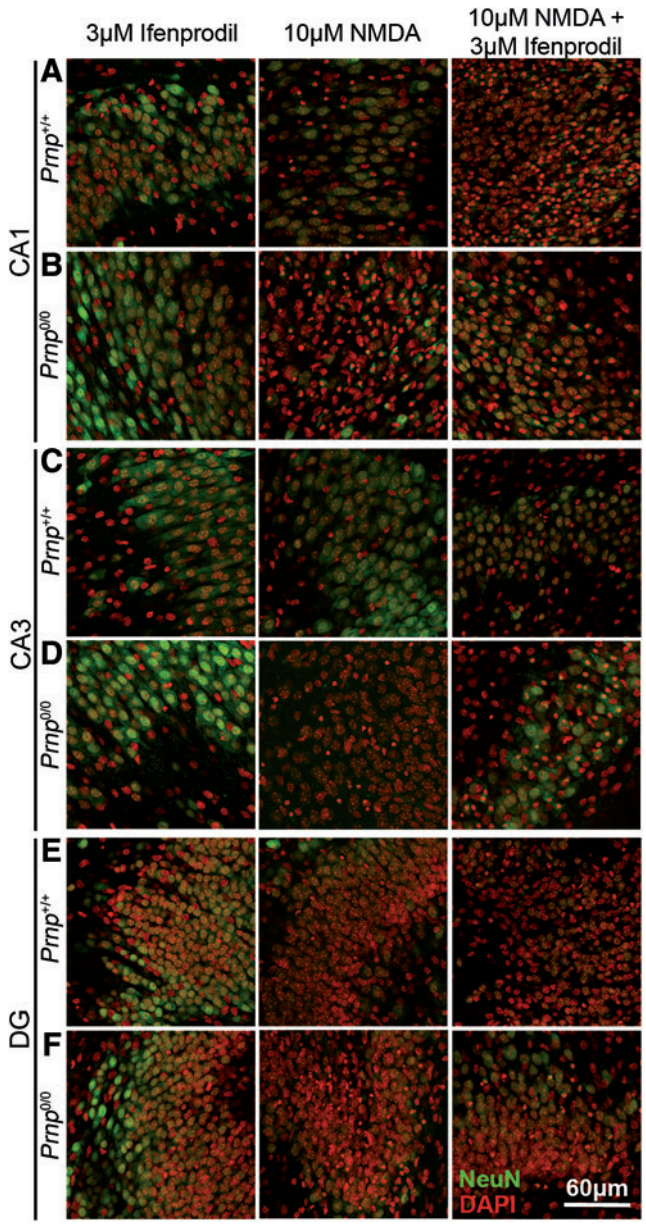

SUPPLEMENTARY FIG. S7. Neuronal cell death induced by NMDA treatment is unaltered by GluN2B-containing NMDAR antagonist. Images from *Prnp*$^{+/+}$ and *Prnp*$^{0/0}$ OHC areas are reported in rows: **(A)** *Prnp*$^{+/+}$ CA1; **(B)** *Prnp*$^{0/0}$ CA1; **(C)** *Prnp*$^{+/+}$ CA3; **(D)** *Prnp*$^{0/0}$ CA3; **(E)** *Prnp*$^{+/+}$ DG; **(F)** *Prnp*$^{0/0}$ DG. The different treatments are reported in columns: 3 *μM* Ifenprodil for 10 min, *left column*; 10 *μM* NMDA for 10 min, *central column*; 5 *μM* NMDA + 3 *μM* Ifenprodil for 10 min, *right column*. NeuN staining is displayed in *green* and DAPI in *red*. Confocal microscope fluorescence images were acquired using a 40×/1.30 NA oil objective.

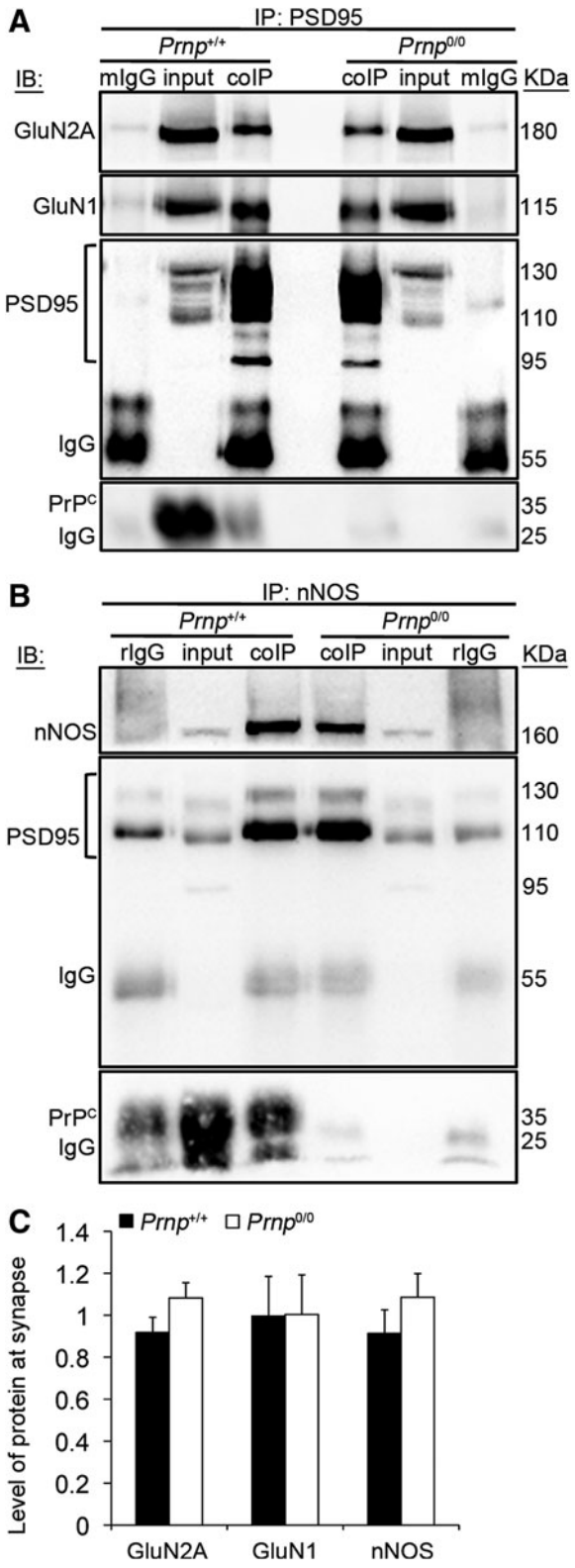

SUPPLEMENTARY FIG. S8. CoIP of GluN2A and GluN1 with PSD95 and coIP of PSD95 with nNOS show comparable levels in P20 *Prnp*$^{+/+}$ and *Prnp*$^{0/0}$ hippocampi. **(A)** coIP of GluN2A and GluN1 with PSD95. **(B)** coIP of PSD95 with nNOS. **(C)** Graph showing the quantification of the coIP signals normalized according to the following formula: (co-immunoprecipitated protein/input)/(immunoprecipitated protein/input); all error bars indicate SD; $n = 3$.

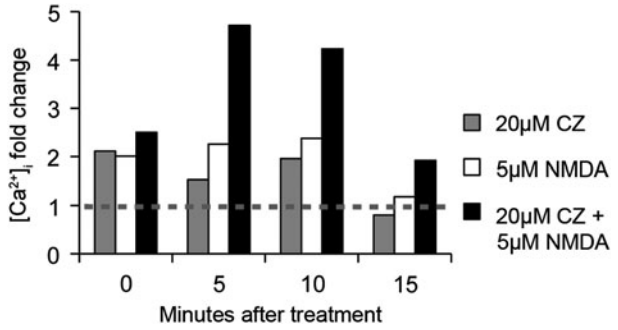

SUPPLEMENTARY FIG. S9. Copper chelation increases NMDA-induced $[Ca^{2+}]_i$ waves. The graph shows fluorescence intensity subtracted of the background intensity and normalized on resting condition measurements. The *dashed line* indicates the untreated cell fluorescence.

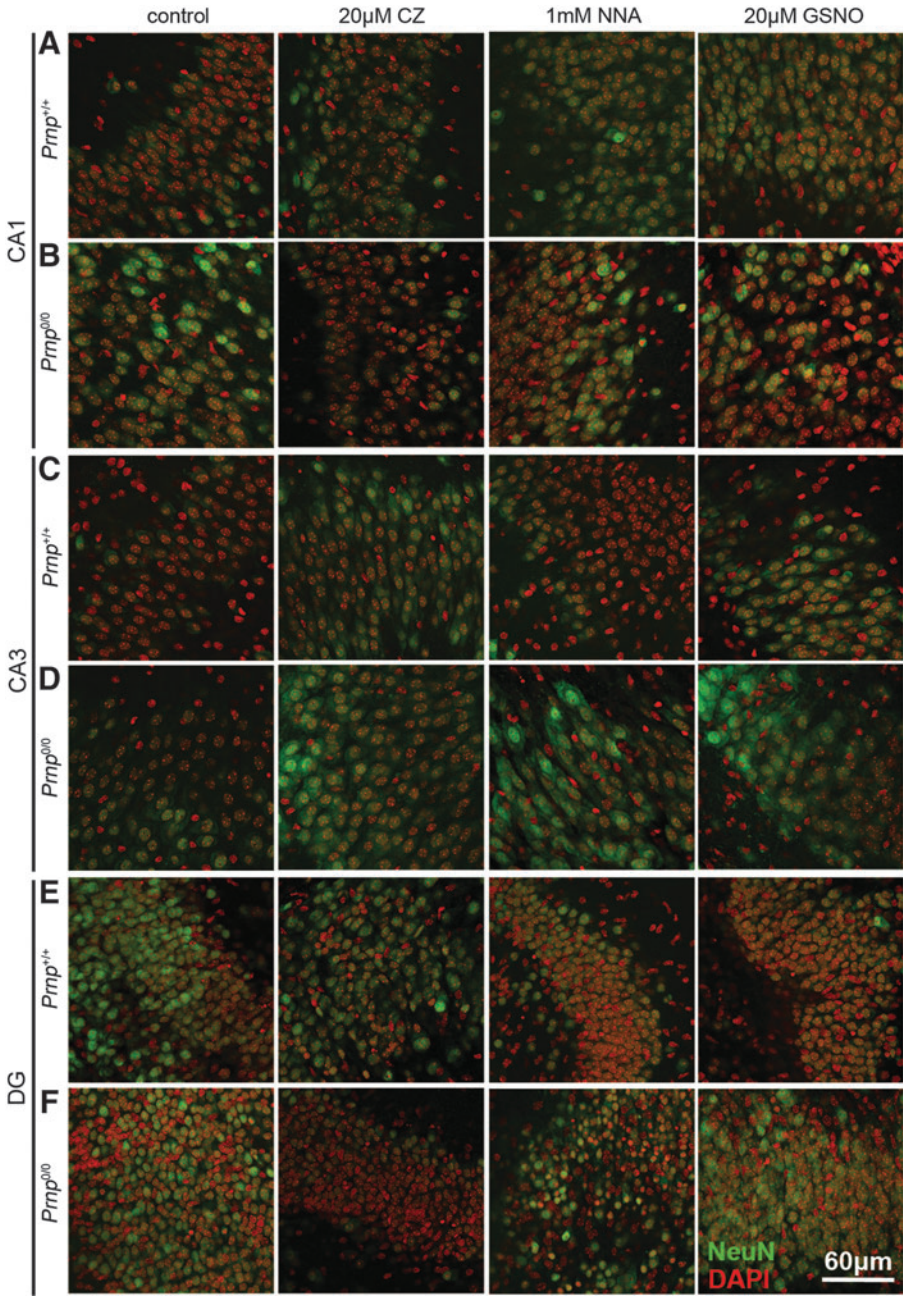

SUPPLEMENTARY FIG. S10. Treatments with CZ, NNA, and GSNO do not affect neuron health. Images from $Prnp^{+/+}$ and $Prnp^{0/0}$ OHC areas are reported in rows: **(A)** $Prnp^{+/+}$ CA1; **(B)** $Prnp^{0/0}$ CA1; **(C)** $Prnp^{+/+}$ CA3; **(D)** $Prnp^{0/0}$ CA3; **(E)** $Prnp^{+/+}$ DG; **(F)** $Prnp^{0/0}$ DG. The different treatments are reported in columns: control, *first column*; 20 μM CZ for 3 h, *second column*; 1 mM NNA for 3 h, *third column*; 20 μM GSNO for 3 h, *fourth column*. NeuN staining is displayed in *green* and DAPI in *red*. Confocal microscope fluorescence images were acquired using a 40×/1.30 NA oil objective. CZ, cuprizone; GSNO, S-nitrosoglutathione.

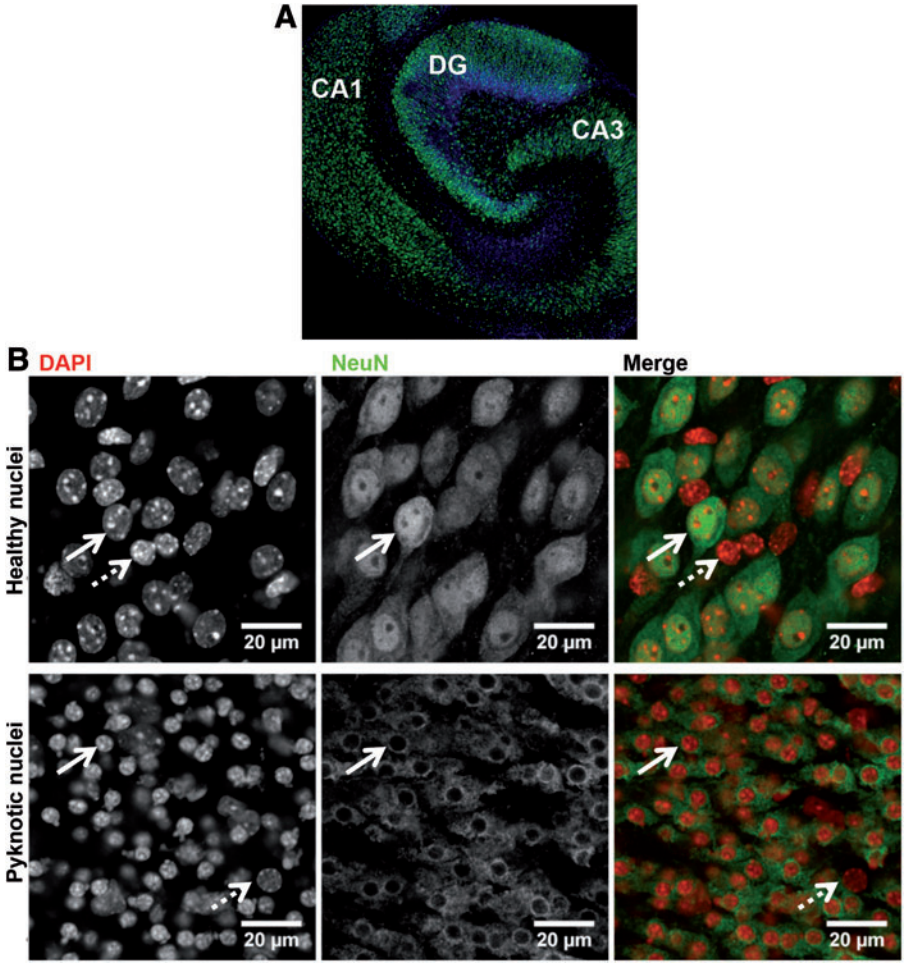

SUPPLEMENTARY FIG. S11. Description of the OHC system. (A) OHC staining with DAPI (in *red*) and anti-NeuN antibody (in *green*). Confocal microscope fluorescence images were acquired using a 10×/0.30 NA dry objective. **(B)** Example of discrimination between healthy and pyknotic neuronal nuclei. Neurons are indicated by *white arrows*, while glia cells are indicated by *dashed arrows*. DAPI is displayed in *red* and anti-NeuN antibody staining in *green*. Confocal microscope fluorescence images were acquired using a 63×/1.40 NA oil objective.